INCLUSION COMPOUNDS: STRUCTURE, REACTIVITY AND SELECTIVITY

Hong Su

(B.Sc., University of Hunan, People's Republic of China

M.Sc., University of Cape Town, South Africa)

Thesis Presented for the Degree of

DOCTOR OF PHILOSOPHY

In the Department of Chemistry

UNIVERSITY OF CAPE TOWN

2002, June

ACKNOWLEDGEMENTS

I would like to thank

Professor Luigi Nassimbeni for his guidance, enthusiasm and patience

Dr. Susan Bourne for her help in many ways

Professor Mino Caira for his expertise advice

All my colleagues, past or present, in the Supramolecular Chemistry Research Group, for their friendship and company

My family, especially my parents, Anmin and Lazhi, for their endless love and support.

PUBLICATIONS AND CONFERENCE PROCEEDINGS

Parts of this thesis have been published:

1. 'Inclusion Compounds of Alkaline-earth Metal *O,O'*-Dibenzoyl Tartrates: Structures and Thermal Stabilities', Luigi R. Nassimbeni and Hong Su, *J. Chem. Soc., Dalton Trans.,* 2000, 349-352.
2. 'Controlled Host:Guest Ratio In An Inclusion Compound', Luigi R. Nassimbeni and Hong Su, *J. Phys. Org. Chem.*, 2000, 13, 368-371.
3. 'Inclusion Compounds of Binaphthol with Picolines: Structures, Selectivity and Kinetics of Desolvation', Luigi R. Nassimbeni and Hong Su, *Acta Cryst.* B, 57, 2001, 394-396.
4. 'Inclusion Compounds of Binaphthol with Lutidines: Structures, Selectivity and Kinetics of Desolvation', Elise de Vries, Luigi R. Nassimbeni and Hong Su, *Eur. J. Org. Chem.*, 2001, 1887-1892.
5. 'Inclusion Compounds of A Diol Host with Xylidines: Controlled Stoichiometries', Luigi R. Nassimbeni and Hong Su, *Acta Cryst.* B58, 2002, 251-259.
6. 'Inclusion Compounds of Binaphthol with Xylidines: Structures, Selectivity and Kinetics of Desolvation', Luigi R. Nassimbeni and Hong Su, *J. Chem. Soc., Perkin Trans. 2*, 2002, 1-6.
7. 'Inclusion Compounds of Binaphthol with Volatile Guests: Structures, Selectivity and Kinetics of Desolvation', Luigi R. Nassimbeni and Hong Su, *New J. Chem.*, in press.

Parts of this thesis have been presented at the following conferences:

7th International Chemistry Conference in Africa (7th ICCA). Durban, South Africa. 6-10 July, 1998.

18th European Crystallographic Meeting. Prague, Czech Republic. 16-20 August 1998.

18th IUCr General Assembly and International Congress of Crystallography. Glasgow, Scotland, 4-13 August, 1999.

19th European Crystallographic Meeting. Nancy, France, 25-31 August 2000.

ABSTRACT

Title: **Inclusion Compounds: Structure, Reactivity and Selectivity**

Author: Hong Su

Date: 2002 June

This thesis is concerned with structure, thermodynamic and kinetic aspects of a variety of inclusion compounds which contain small organic guests. The host compounds studied are alkaline-earth metal salts of O,O'-dibenzoyl-(2R,3R)-tartranic acid (magnesium, calcium and strontium), 1,1'-bis-(4-hydroxyphenyl)cyclohexane (**DHPC**) and 2,2'-dihydroxy-1,1'-binaphthyl (**BINAP**).

The alkaline-earth metal salts form coordination complexes with 2-methoxyethanol, water or ethanol and the guests act as part of the coordination sphere of the metal ions. The diol host **DHPC** preferably forms layer type inclusion compounds with a number of isomers of xylidines. Another diol host **BINAP** forms inclusion compounds with the isomers of picoline, lutidine and xylidine, as well as a number of selected solvents including 1,4-dioxane, DMSO, morpholine, THF and acetone, preferably in channel type inclusion modes. In the latter two classes of inclusion compounds the inclusion is facilitated by the formation of hydrogen bonds from the host hydroxyl moieties to the guests.

Crystallisations were carried out at different temperatures and a number of inclusion compounds with differing host:guest ratio were obtained, *i.e.* **DHPC** with a number of isomers of xylidine, **BINAP** with 1,4-dioxane and DMSO. The host:guest ratio decreases as the crystallisation temperature increases. In addition, two polymorphic inclusion compounds were obtained between **BINAP** and morpholine at different temperatures.

The crystal structures of all these inclusion compounds were elucidated. Lattice energies were calculated for selected inclusion compounds to evaluate the stability of the host-guest system. Thermogravimetry, Differential Scanning Calorimetry, Hot Stage Microscopy, X-ray powder diffraction and IR spectra were employed to

characterise selected inclusion compounds. The kinetics of desolvation were studied using isothermal or programmed temperature thermogravimetry.

The selective inclusion properties of both the two diol host compounds in solution were investigated. Selectivity trends for a given group of guest compounds were established by carrying out series of two- or three-component competition experiments. These groups of guest compounds studied are isomers of xylidine by both the two hosts, isomers of picoline and lutidine, pairs of solvents such as 1,4-dioxane and morpholine, acetone and THF, all by the host **BINAP**. Attempts were made to correlate the selectivity with the structures and thermal properties of the appropriate inclusion compounds. In the case of the inclusion compounds formed having the same stoichiometries, good correlation between the selectivity trend and complementarity of the host and guest in the structure, lattice energies of the host-guest systems and thermal stability in term of onset temperature of guest desolvation were observed.

All the desolvation reactions of the inclusion compounds investigated showed Arrhenius behaviour. Attempts were made to describe the kinetic behaviour in terms of the crystal structures of these compounds. The Arrhenius parameters for the desolvation of the inclusion compounds containing the same host (**BINAP**) were found to show the compensation effect.

ABBREVIATIONS AND SYMBOLS USED IN THE THESIS

α		The angle between *b* and *c* unit cell axes
	or	Extent of reaction
	or	Unsolvated, non-porous phase of the host compound
β		The angle between *a* and *c* unit cell axes
	or	The phase of an inclusion compound
γ		The angle between *a* and *b* unit cell axes
	or	The intermediate phase of an inclusion compound
A		Arrhenius pre-exponential factor
bp		Boiling point
CSD		Cambridge Structural Database
Calc.		Calculated
DMSO		Dimethyl sulfoxide
DSC		Differential scanning calorimetry
E		Normalised structure factor
	or	Lattice energy
E_a		Activation energy
e.s.d.		Estimated standard deviation
$f(\alpha)$		Kinetic rate expression
G		Guest
GC		Gas chromatography
H		Host
ΔH		Enthalpy change
HSM		Hot Stage Microscopy
iso-		Isothermal
k		Rate constant
mp		Melting point
Obs.		Observed
RMS		Root-mean-squared deviation
s.o.f.		Site occupancy factor
T_{on}		Onset temperature
T_b		Boiling temperature
TG		Thermogravimetry
THF		Tetrahydrofuran
U		Isotropic or anisotropic displacement parameter
V		Unit cell volume
W		Water
XRD		X-ray powder diffraction
Z		Number of formula units per unit cell

ATOMIC COLOUR SCHEME

(M = Mg^{2+}, Ca^{2+}, Sr^{2+})

TABLE OF CONTENTS

Chapter 3 INCLUSION COMPLEXES OF ALKALINE-EARTH METAL O,O'-DIBENZOYL TARTRATES

Chapter 4 INCLUSION COMPOUNDS OF DHPC AND XYLIDINES WITH VARIOUS STOICHIOMETRIES

Chapter 5 SEPARATION OF CLOSE ISOMERS OF PICOLINE, LUTIDINE AND XYLIDINE BY THE HOST BINAP

"...dove la natura finisce di produrre le sue spezie, l' uomo quivi comincia con le cose naturali, con l'aiutorio di essa natura, a creare infinite spezie…".

" ...where nature finishes producing its own species, man begins, using natural things and with the help of this nature, to create an infinity of species…".

- Leonardo da Vinci

1 INTRODUCTION

Supramolecular Chemistry

In 1967, Charles J. Pedersen produced cyclic polyethers, which he named crown ethers. These compounds show binding selectivity with alkali metal ions of differing ionic radii. By building on Pedersen's fundamental discovery, Jean-Marie Lehn in 1969 developed bycyclic compounds of crown ether type which he called cryptands and which show even higher selectivity when forming complexes. Jean-Marie Lehn and Donald J. Cram have subsequently each developed increasingly sophisticated organic compounds which when forming complexes leave fissures and cavities where low molecular weight compounds with different types of geometry can be bound. With these works, Pedersen, Lehn and Cram were awarded The Nobel Prize in Chemistry in 1987. Their work laid the foundations of what is today one of the most active and expanding fields of chemical research, a field for which Cram has coined the term *host-guest chemistry*, while Lehn calls it *supramolecular chemistry*. Although the field was not conceived as such at that time, its root can be traced back to Alfred Werner's coordination theory (1893), Emil Fischer's *lock and key* concept (1894) and Paul Ehrlich's *receptor* idea (1906). In addition, in the middle of thirties K. L. Wolf even coined the term '*Übermoleküle*' (supermolecules) to describe organised entities arising from the association of coordinatively saturated species (*e.g.* the acetic acid dimer).

Within the last twenty years, Supramolecular Chemistry — chemistry beyond the *mo*lecule — has spanned a vast interdisciplinary field that has so far resisted all attempts to contain, and even fully define it. It is one of today's fastest growing disciplines, ranging from biological chemistry to materials science; synthesis to spectroscopy to diffraction and transcending traditional chemical subgroups, locating at the meeting point of chemistry, biology, physics and technology.

The pace of development of this field may be represented by the number of abstracts appearing under the keyword "Supramolecular" in Chemical Abstracts: there are about

1400 abstracts in the year of 2000, comparing to only about 100 abstracts twenty years ago (1980). Numerous books, monographs, journals and series have been dedicated to this field, to name a few: the five-volume series *Inclusion Compounds* (1984 and 1991)[1], the eleven-volume *Comprehensive Supramolecular Chemistry* (1996)[2], seven series of *Monographs in Supramolecular Chemistry* (2000)[3].

The very vigour and breadth of this topic has made it difficult to present a comprehensive review in this single chapter. Therefore only the topics of particular interests to this study are presented here. In the following sections, the basic concepts and principles relevant to this study are outlined, representative examples are accompanied if available, and the literature related to this study is briefly reviewed.

The classification of host-guest compounds

Host-guest compound or inclusion compound are all general terms that refer to a supermolecule. Two distinct categories of supermolecules are identified among host-guest compounds according to the relative topological relationship between host and guest, as proposed by Desiraju[4]: (1) those of which the host is a single molecule within which the whole guest molecule or molecules reside, and (2) those where several host molecules are assembled to form a host framework containing voids which can accommodate the guest molecule or molecules. The distinction between the two classes is schematically illustrated in **Figure 1.1**. The hosts from the first category possess intramolecular cavities and the complex formed can exist both in solution and in the solid state. Examples of these are crown ethers, cyclodextrins, corands, cavitands and cryptands. The hosts from the second category form host-guest aggregates called clathrates, the process is called lattice inclusion, which is of relevance only in the crystalline or solid state. Some of the early examples of this kind of host compounds include water, Dianin's compound, Urea and tri-o-thymotide.

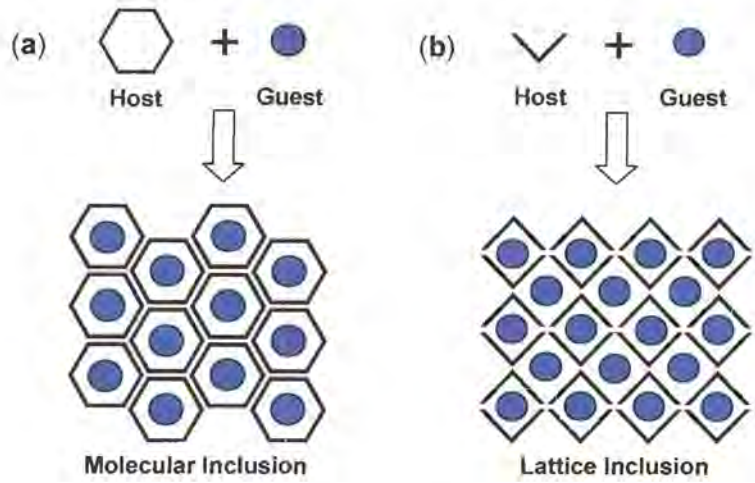

Figure 1.1 Schematic view of two types of inclusion compounds: (a) the host is a single molecule and encloses the guest; (b) the host network is itself composed of more than one molecule.

Supramolecular interactions, *e.g.* hydrogen bonding, ion-ion, dipole-dipole and π-stacking, are employed to stabilise the lattice network in clathrates. According to the interactions formed between the clathrating components, Weber[5] suggested a classification shown schematically in **Figure 1.2**.

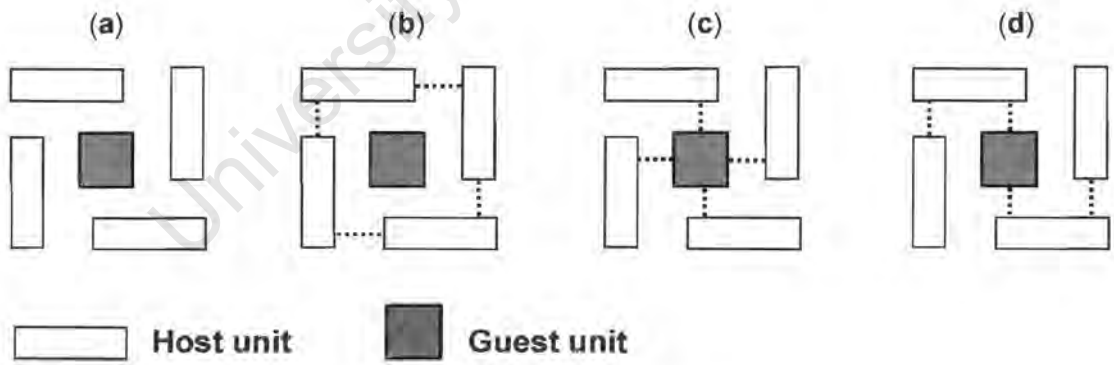

Figure 1.2 Representations of different lattice inclusions dependent on supramolecular interactions between host and guest: (a) no host-guest or host-host interactions, (b) host-host interactions only, (c) host-guest interactions only and (d) host-host and host-guest interactions.

The type **a** represents the so-called 'true clathrate', where the inclusion formation depends significantly on the steric compatibility between host and guest. In the type **b** the interactions between the host molecules are co-operative and stabilise the lattice

network. A survey of the literature indicates these two types dominate modes of lattice inclusion[6].

In the solid state crystalline host-guest structures, the host molecules pack in such a way to generate voids to accommodate the guest molecules. The clathrates can thus be classified according to the geometry of the cavities in which the guest species are encapsulated in the host framework: layers (intercalates), channels (tubulates) and cages (cryptates) or pockets (aediculates). Within these three broad categories a number of intermediates exist, to name a few of them: intersecting channels, interconnected cages, offset layers etc. A number of typical geometries of the cavities are shown in **Figure 1.3**[7].

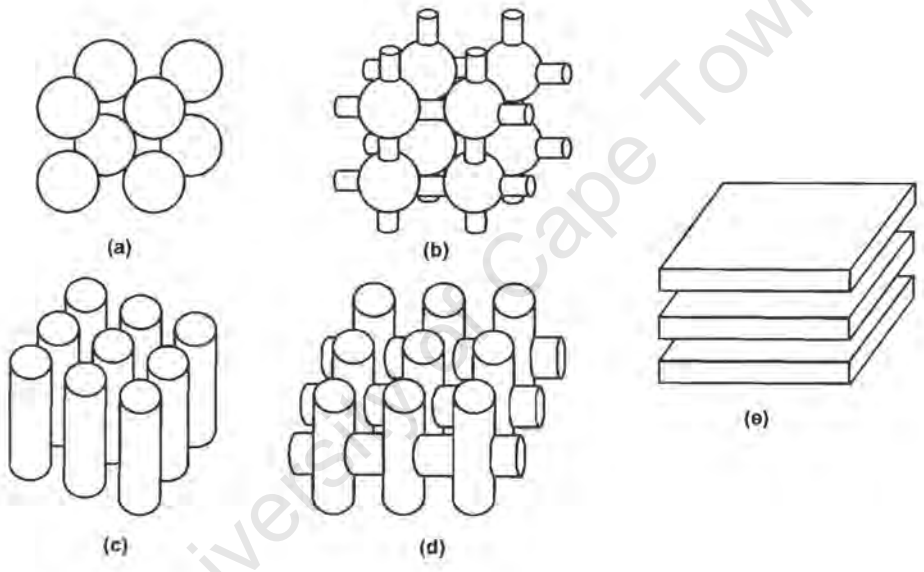

Figure 1.3 Typical topologies of the lattice inclusions: (a) isolated cages or cavities, (b) interconnected cages, (c) one-dimensional channels (d) intersecting channels and (e) two-dimensional layers.

Supramolecular glue

Supramolecular chemistry is the chemistry of intermolecular bonds, in Jean -Marie Lehn's words: 'supermolecules are to molecules and the intermolecular bond what molecules are to atoms and the covalent bond'[8]. Therefore knowledge of intermolecular interactions is very important in the study of supramolecular systems.

In general, intermolecular interactions concern all the non-covalent interactions. Steed and Atwood[9] give a list of these interactions, as well as effects, which interplay in the supramolecular system, together with an indication of their approximate energies:

- Ion - ion interactions (100 - 350 kJ mol^{-1})
- Ion - dipole interactions (50 - 200 kJ mol^{-1})
- Dipole - dipole interactions (5 - 50 kJ mol^{-1})
- Hydrogen bonding (4 - 120 kJ mol^{-1})
- Cation - π interactions (5 - 80kJ mol^{-1})
- π - π stacking (0 - 50 kJ mol^{-1})
- Van der Waals forces (< 5 kJ mol^{-1}, variable)
- Hydrophobic effects

Apart from the special case where metal ions are used as the 'glue', central to the supramolecular field is the use of a variety of weaker non-covalent interactions to hold the molecular components together[10]. These interactions are long range forces and can be either attractive or repulsive. The interactions between components must be maximised energetically and the ensuing crystalline complex represents a situation where all these forces are in balance and at an energy minimum.

Among these interactions, the hydrogen bond is particularly important in molecular assembly, molecular recognition and crystal engineering. Its properties have been extensively reviewed[11,12,13,14,15]. Hydrogen bonds come in a wide range of lengths, strengths and geometries. They may be strong enough to determine crystalline structure and exert a marked influence in the solution and gas phase. For example, the hydrogen bonds are responsible, though not entirely, for the overall shape of many proteins and the double helix structure of DNA. The relatively weak hydrogen bonds join with other intermolecular interactions such as Van der Waals forces in structure stabilisation, achieving complementarity in a supramolecular system.

The common hydrogen bond donor groups are C-H, N-H, O-H, F-H, P-H, S-H, Cl-H, Br-H and I-H, while acceptor groups include N, O, P, S, Cl, Br and I as well as alkenes, alkynes, aromatic π-systems and transition metals[16]. The acceptor groups are characterised by being associated with significant areas of electron density. It is only recently that the importance of weak hydrogen bonds of the type X-H···A, where X and A have low electron-negativity, have been recognised and their parameters reviewed[17]. Other relatively weak hydrogen bonds, involving π-facial interactions including π-π stacking[18,19,20,21], have also come into light, as illustrated in **Figure 1.4**.

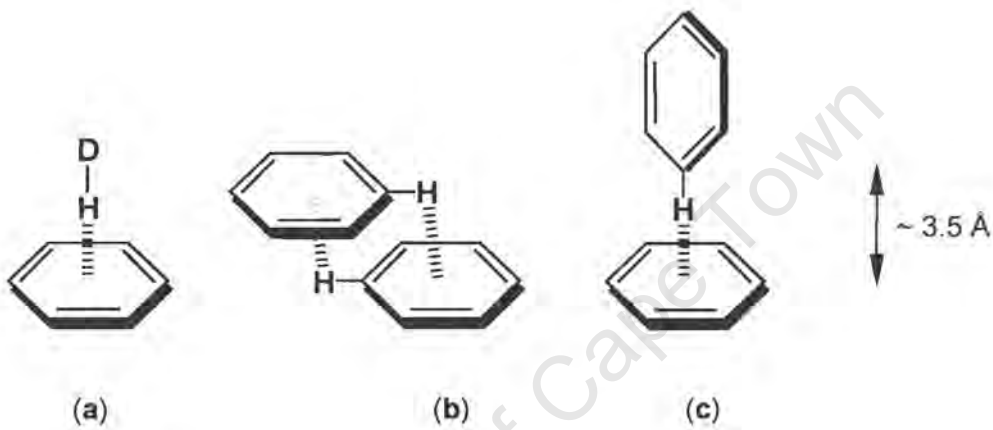

Figure 1.4 Weak hydrogen bonds: (a) analogue to classical (donor)D-H···A(acceptor) bonds, and π-π stacking in (b) face-to-face and (c) edge-to-face. Note the offset to the face-to-face mode (direct overlap is repulsive)[9,10].

The geometry of hydrogen bond donor-acceptor interactions is fairly well defined[22,23]. Statistical analysis of directionality in organic crystals gives an average angle of 167° for O-H···O bond and 161° for N-H···O bonds. A typical distance for an N-H···O bond is 1.80 to 2.00 Å, while O-H···O bonds are generally shorter (1.60 to 1.80 Å). The hydrogen bond with the shorter distance is considered to be stronger, but there is only an approximate (sigmoidal) correlation between distance and energy. It is widely accepted that linear hydrogen bonds are the strongest. The inherent directionality of hydrogen bonds dictates the orientation within a given supramolecular architecture. **Figure 1.5** shows a number of common hydrogen bonding arrangements.

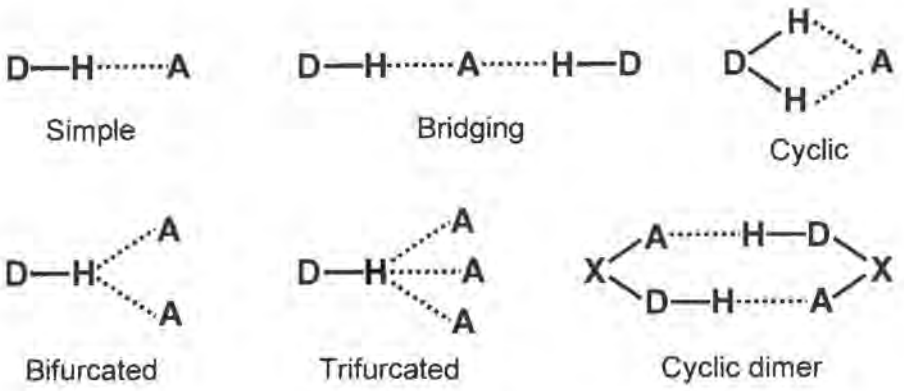

Figure 1.5 Common arrangements of hydrogen bond types. The *simple* hydrogen bond type is often bent rather than linear as shown[9,10].

It is noted that close packing is also an important driving force, particularly in the formation of solid state supramolecules[9]. Whenever molecules form a crystal, they try to pack as closely as their shape and functional complements permit. If the apohost is of such a shape that its packing leads to voids, the latter will be occupied by solvent molecules of a suitable shape, leading to the formation of the clathrate. For example in the Werner clathrates, large anions around a transition metal centre generate voids, which are filled with other molecules — the guest[24].

Host design

At the beginning of the last century, Sir Humphrey Davy discovered the first inclusion compound, chlorine hydrate ($Cl_2 \cdot 6H_2O$), by bubbling chlorine into water[25]. Since then numerous inclusion compounds and host compounds were discovered, most purely by chance. Among them are the graphite intercalations[26], hydroquinone[27], the Hofmann-type inclusion compounds[28], Dianin's compound[29], cyclodextrin inclusion compounds[30], the inclusion compounds of choleic acids[31], of phenols[32], of urea[33] and so on. Nowadays suitable host compounds and their corresponding inclusion compounds are often the products of rational design and synthesis. Initially new host compounds were created by simple modification of known hosts. An example of this is the modification of Dianin's compound (**1**)[34]. Upon substituting oxygen with sulphur, the resulting 4-*p*-hydrophenyl-2,2,4-trimethylchroman host compound (**2**) forms very similar shaped cavities to those of (**1**) upon crystallisation. The introduction of only one additional methyl group (**3**), however, leads to a significant change in the shape as well as size of

the host lattice cavity, as shown in **Figure 1.6**. Consequently, this change resulted in a modified selectivity.

Based on the knowledge obtained from the study of X-ray crystallographic structures of known host systems with various guests, an increasing number of new compounds, unrelated to known hosts, have been designed directly. The various concepts of efficient host molecule design have been reviewed and evaluated[1,6,35]. MacNicol pioneered the area of rational host design with the class of compounds called "hexahosts" (*e.g.* compound **4**)[36,37]. This group of compounds was designed by analogy to the host lattice formed by quinol or Dianin's compounds, as shown in **Figure 1.7**.

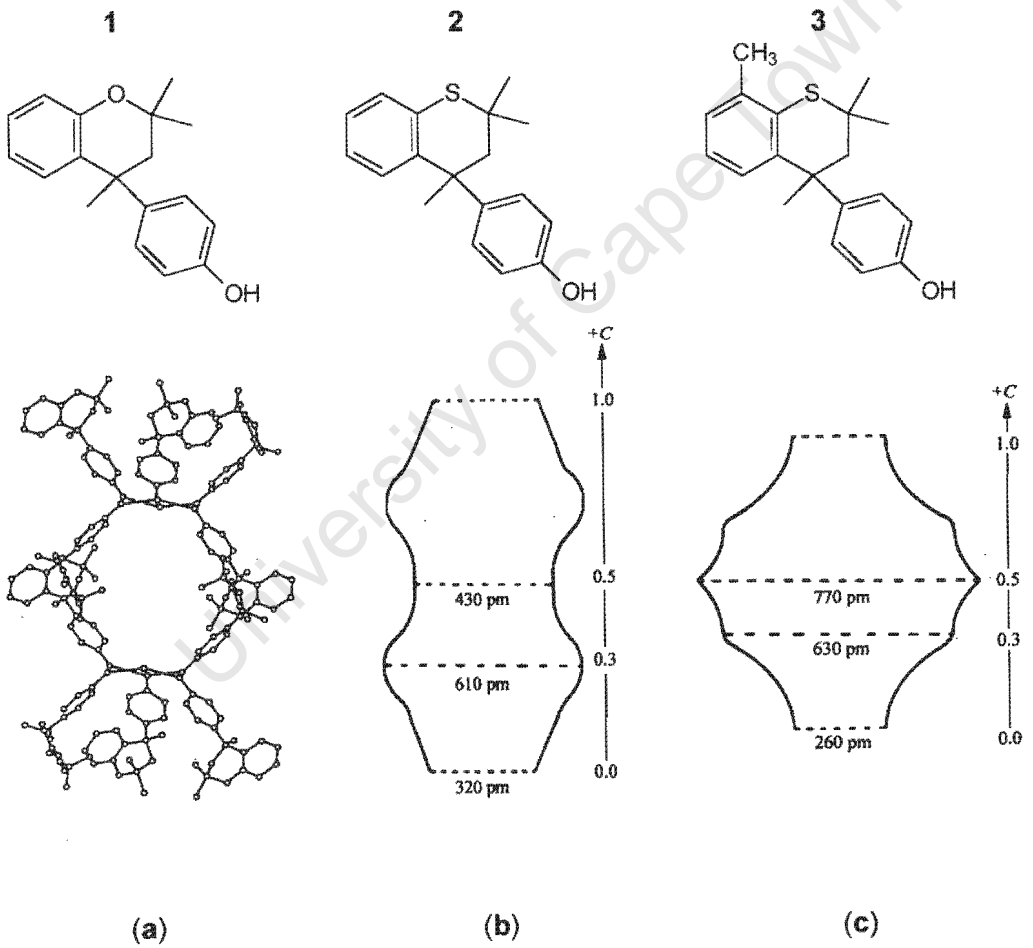

Figure 1.6 (a) The structure of unsolvated 4-*p*-hydroxyphenyl-2,2,4-trimethylchroman (**1**); The sections through the van der Waals surface of the cavity: (b) 4-*p*-hydrophenyl-2,2,4-trimethylthiachroman (**2**) and (b) 4-*p*-hydrophenyl-2,2,4,8-tetramethylthiachroman (**3**). Taken from reference 38.

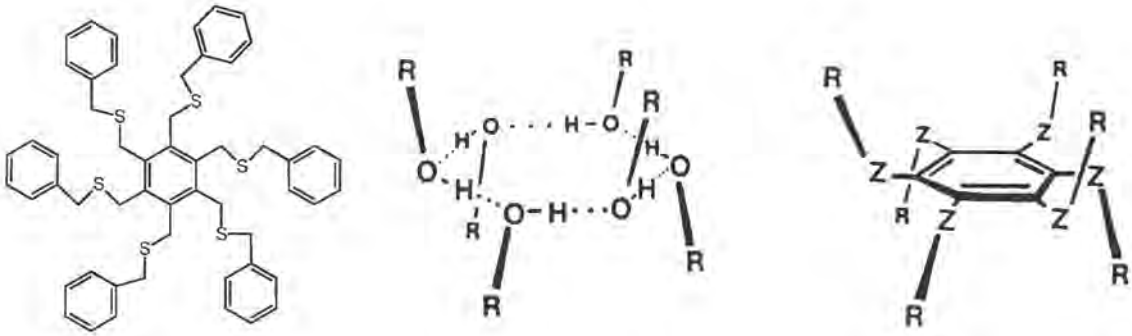

4 (a) (b)

Figure 1.7 Comparison of (a) hydrogen-bonded hexamer lattice unit with (b) hexasubstituted benzene analogue. Z is any bridging group or atoms (usually CH_2) attached directly to the central benzene ring. Taken from reference 39.

Weber[6] has summarised the basic features of an efficient host compound. It should possess molecular bulkiness, rigidity, functional groups and a degree of symmetry. A diagrammatic representation of such a host-guest system is illustrated in **Figure 1.8**. Bulkiness provides low-density packing so that a cavity can be generated to accommodate a guest molecule. Rigidity helps in maintaining the cavity and prevents collapse. The functional group in a suitable position may achieve specific and strong host-guest interactions for molecular recognition. A balance of these features is needed to stabilise the crystal packing. Using this strategy, a number of host compounds which are typically shaped as a pair of scissors (*e.g.* **5**), a roof (*e.g.* **6**), a dumb-bell (*e.g.* **7**) or a propeller, were synthesised, as schematically illustrated in **Figure 1.9**. 1,1'-binaphthyl-2,2'-dicarboxylic acid (**5**) provides for cavity formation due to its scissor shape between the orthogonal naphthyl units, and to hydrogen bonding both between the host and between host and guest. The diphenylhydroxy group of the propeller-shaped host **7** prevents dense self-packing in the crystal, providing a typical case for a void generation required to complex small neutral guest compounds.

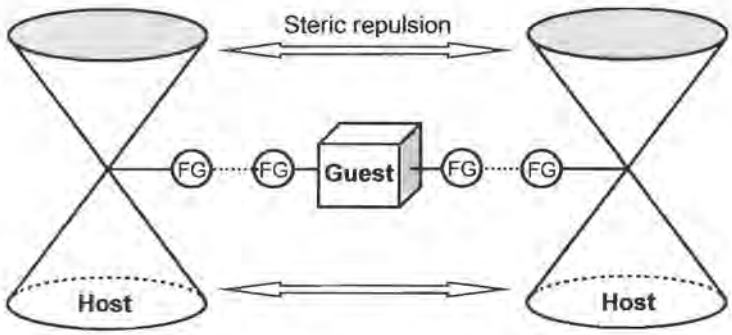

Figure 1.8 An efficient host-guest system. FG = functional group.

Based on the above principles, diol derivatives, which have a rigid molecule with hydroxyl moieties and sterically bulky groups (*e.g.* a hydrophobic group such as phenyl) may turn out to be good hosts. Toda[40], Weber[41] and Bishop[42] have specifically designed and synthesised diverse diol host compounds and found that they have a high inclusion affinity for a wide variety of organic solvent molecules, mostly due to the formation of hydrogen bonding between the host and guest. Some examples of diol host compounds are **7a**, **7b**, **7c**, **8**, **9** and **10**.

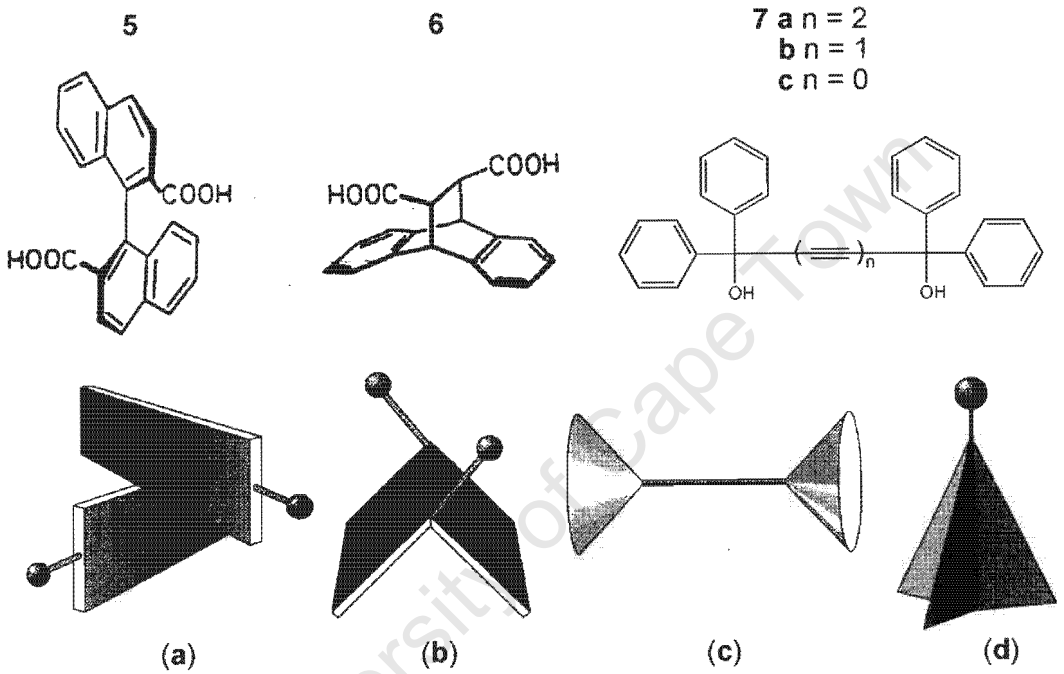

Figure 1.9 The typical overall shapes of the host molecules in host design: (a) a pair of scissors, (b) a roof, (c) a dumb-bell and (d) a propeller. The shaded balls represent functional group. Taken from reference 6.

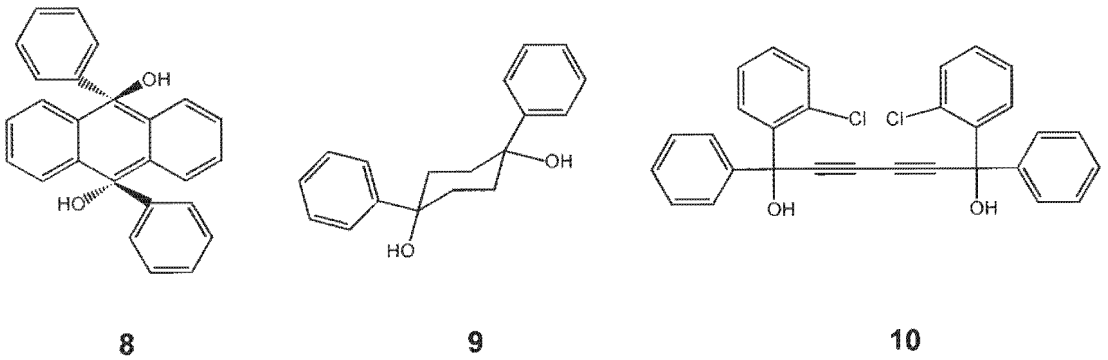

8 **9** **10**

Toda[43], who synthesised the hosts **7a**, **7b** and **7c**, found that larger substituents and longer alkyne linkage increased the inclusion capability of these related hosts. The rigidity of the linkage of these host compounds is also important in the formation of a stable crystalline lattice. Following these findings, the simplified host, *trans*-9,10-dihydroxy-9,10-diphenyl-9,10-dihydroanthracene (**8**) was developed. It is a very effective host compound for the inclusion of a wide range of aliphatic and aromatic guest substances[44,45,46]. However, the host (**8**) did not include alcohols except methanol and ethanol, while in contrast, the simpler host (**9**), with *cis*- conformation, tended to include various kinds of alcohols. X-ray structural analysis of a 1:2 inclusion compound of (**8**) with methanol showed that a four-member ring is formed through hydrogen bond formation, as schematically depicted in **Figure 1.10a**, while the host (**9**) includes alcohol through a linear hydrogen bond chain formation as depicted schematically in **Figure 1.10b**. Due to steric limitations, alcohols which are bulkier than ethanol cannot form the four-member ring, while sterically bulky alcohols can still be accommodated by (**9**). This implies that, beside the consideration of shape and symmetry, it is also important to identify hydrogen bonding motifs or other intermolecular interactions which will dominate in the supramolecular design of new inclusion systems.

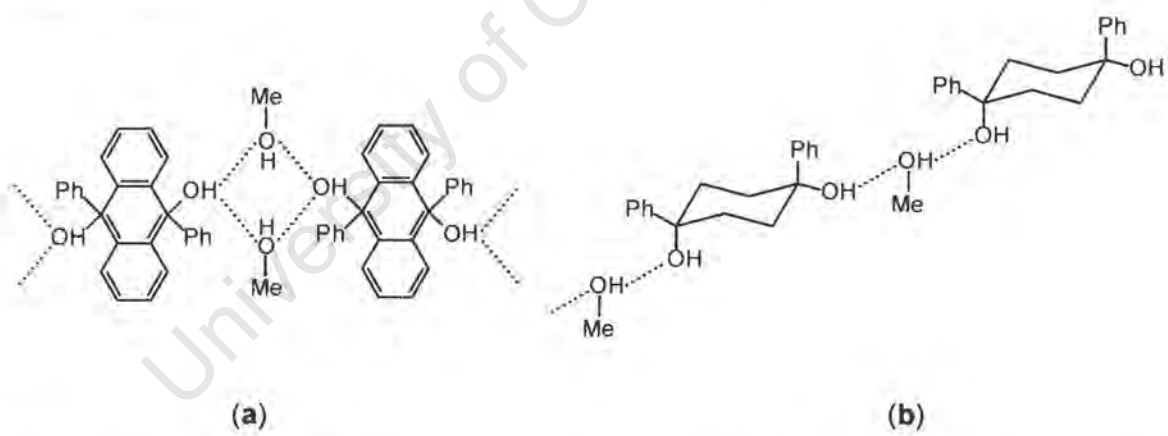

(**a**) (**b**)

Figure 1.10 Structures of (a) 1:2 inclusion complex of (**8**) and methanol, (b) 1:1 inclusion compound of (**9**) and methanol.

Some of the diol hosts are capable of separating isomers by enclathration. The achiral host (**7a**) was found to be effective for the separation of *o*- and *p*-isomers of di-substituted benzene, *e.g.* methylbenzaldehyde. Interestingly, in most cases, the *p*-isomers were preferentially included. Chiral diol hosts have been used to resolve guest substances into enantiomers. Toda used the chiral clathrate former ((+)**10**), derived from (**7a**), to successfully separate numerous racemic guests into enatiomers, *e.g.* cyclic ketones and lactones which constitute important synthetic building blocks.

Molecular recognition

The ultimate goal of supramolecular host design, both in nature (enzymes, transport proteins *etc.*) and in artificial systems, is the achievement of selectivity: the discrimination by a host molecule between a number of different guest molecules. It may be said that molecular recognition lies at the heart of supramolecular chemistry. The lock and key mechanism, formulated by Emil Fischer in 1894, is fundamental to the understanding of the recognition process in biological systems, for example the recognition of substrate by enzyme, antigen by antibody, neurotransmitter by neuroreceptor, DNA by protein[47]. The lock and key image is illustrated in **Figure 1.11**. By analogy to the lock and key image, the shape and size concept is applied in host-guest chemistry. The first example is the selective cation binding by crown ethers, as illustrated in **Figure 1.12**[48].

Figure 1.11 The lock and key mechanism, used to describe the enzyme and the substrate.

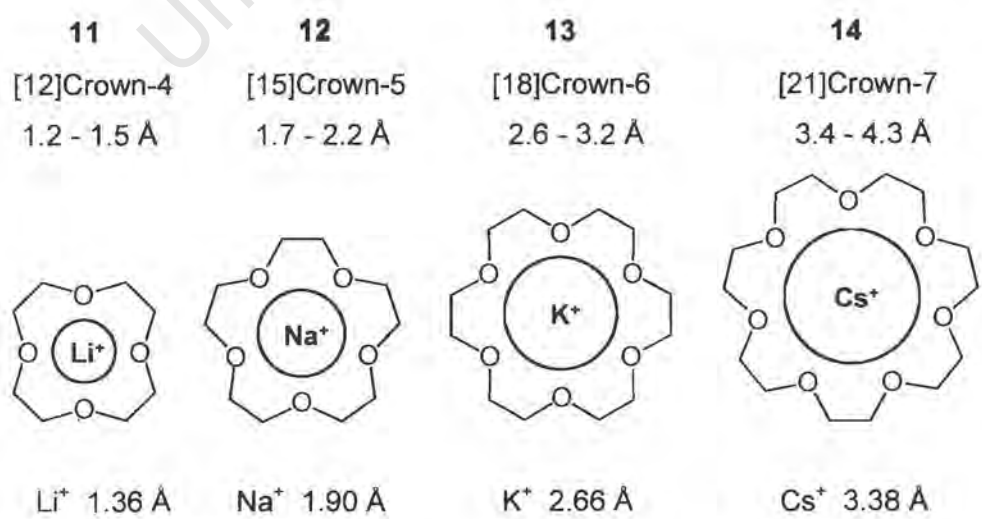

Figure 1.12 The hole and size concept: comparison of the diameters of different crown ethers and alkali metal cations.

Figure 1. 12 shows the relation between crown ethers and cations' size. Apparently the crown ethers select cations primarily by their sizes, and the most stable complexes are formed with the closest match between host cavity and cation size. The concept of optimal complementarity between guest size and host cavity (hole) is known as the 'ion-cavity' or, more frequently, as the 'hole-size' concept. However, this hole and size concept has some important limitations, especially for less rigid systems[49,50,51]. There are other factors that also influence the selective cation binding, including the degree of host preorganisation, the chelate and macrocyclic effects[52]. The host is said to be preorganised if it does not undergo a significant conformational change upon guest binding. The effects of preorganisation are startling and are illustrated by a comparison between the preorganised spherands (*e.g.* **15**) and the conformationally mobile corands (*e. g.* **11**, **12**, **13**, **14**)[9]. The affinities of the former compounds for alkali metal cations are significantly higher by factors of up to 10^{10}. The chelate effect is demonstrated by comparison between the macrocyclic polyamine (**16**) and the acyclic analogue (**17**)[53]. The macrocycle is about 10^9 times more stable than the acycle, mainly as a consequence of the additional operation of the macrocyclic effect. The dynamic process to reach selective binding is complicated, many other factors, for example solvent polarity, hydrogen bonding and coordinating ability, may also be involved.

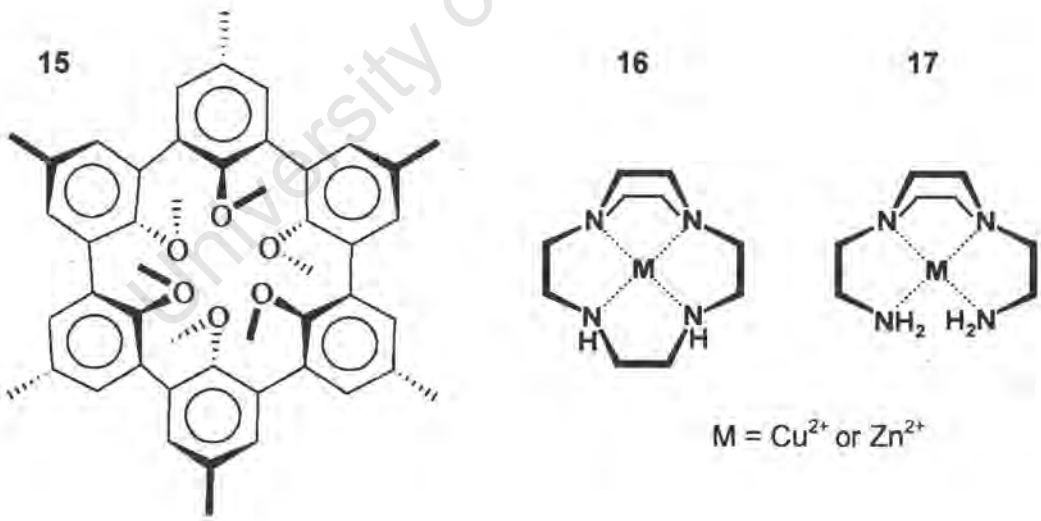

The remarkable selectivity of metal cation binding to macrocycles illustrates the principle of molecular recognition and is the basis for many applications. Another example illustrating the shape recognition is the urea clathrates[54], shown in **Figure 1.13**.

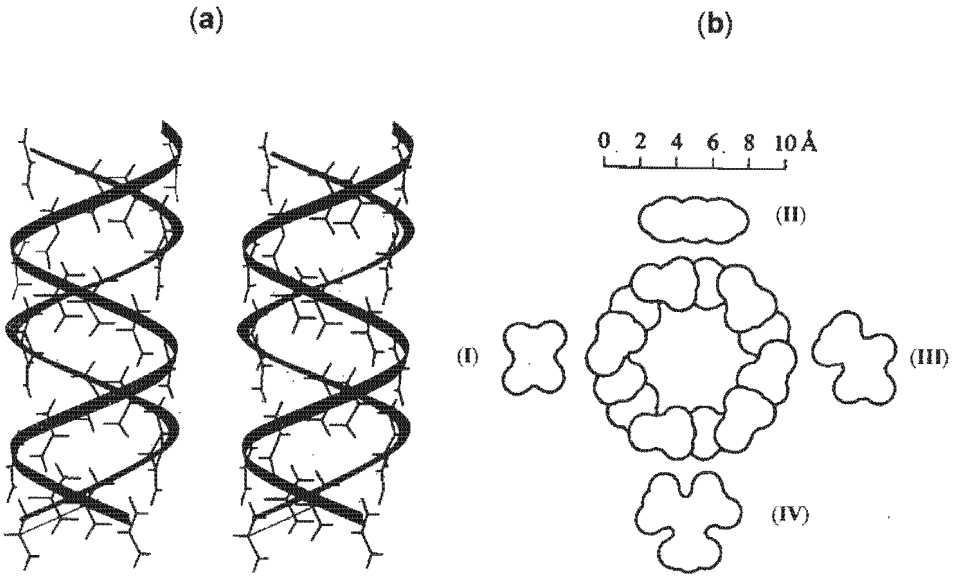

Figure 1.13 (a) Stereoview of one channel generated by urea host molecules, Taken from reference 55.
(b) Van der Waals cross-section of the cavity in the urea channel compared with the size of (**I**) n-octane (**II**) benzene (**III**) 3-methylhaptane (**IV**) 2,2,4-trimethylpentane, taken from reference 56.

The urea molecules hydrogen bond to one another forming long helical chains. This produces hollow channels in which the guests can be accommodated. The guest is weakly held in the channel mainly by van der Waals interaction, resulting in the formation of an inclusion compound which is often non-stoichiometric. The inclusion selectivity is simply assessed by inspecting the size of the guest. Benzene is found to be slightly wider than the channel and the inclusion is quite difficult. Interestingly, however, increasing chain lengths allow the toleration of larger endgroups, for example, 1-phenyloctane does not form a clathrate, but the much longer 1-phenyleicosane does, due to the enthalpy gain by about 10 kJ mol^{-1} for each $-CH_2-$ group added to the linear chain. It indicates that the additional stabilisation gained upon complexation of the longer chain outweights the unfavourable steric interactions with the channel wall.

For many host-guest systems, particularly those with both host and guest having limited flexibilities and irregular shapes, the molecular recognition is governed not only by complementary shape and size, but also, to a certain degree, by complementarity with respect to functionality. Such an example is given by the formation of carceplexes as shown below[57].

18

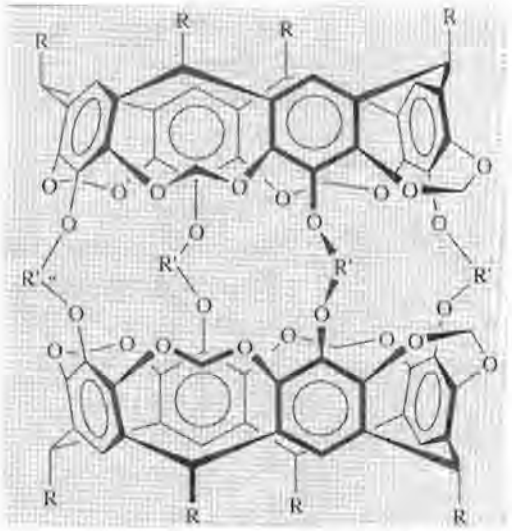

R = *n*-pentyl, CH_2CH_2Ph, *n*-undecyl etc.
R' = $(CH_2)_n$, n = 1 - 4

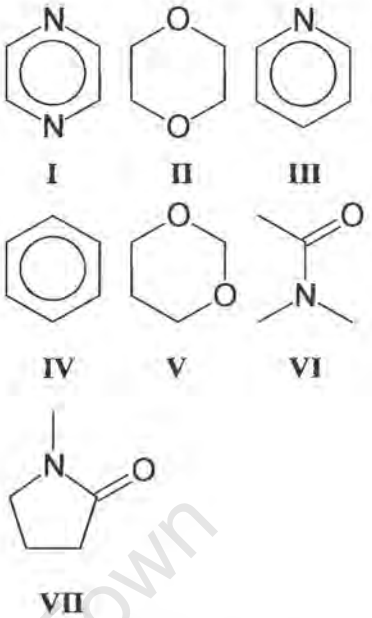

I **II** **III** **IV** **V** **VI** **VII**

Table 1.1 Template ratios for the formation of **18** (n = 1, R = CH_2CH_2Ph) by a variety of guest species, and relative stabilities (K_{rel}) of the resulting carceplexes in nitrobenzene-*d5*. Values normalised to N-methylpyrrolidinone (**VII**) = 1. Taken from reference 58.

Guest	Template ratio	K_{rel}
Pyrazene (**I**)	1 000 000	980 000
1,4-Dioxane (**II**)	290 000	240 000
Pyridine (**III**)	34 000	7100
Benzene (**VI**)	2400	540
1,3-Dioxane (**V**)	200	140
Dimethyl actamide (**VI**)	20	8.9
N-methylpyrrolidinone (**VII**)	1	1

In the synthesis of the host carcerand **18** (n=1, R = CH_2CH_2Ph), the guest solvent serves as template to fit in the cavity within the molecule of the host. Competition experiments conducted between a variety of guest solvents show that, the pyrazene is the most effective template in that it achieves the highest template ratio as well as highest yield (75%) (see **Table 1.1**). The x-ray crystal structure of the pyrazene carceplex, *i.e.* host-guest complex, of **18**, as illustrated in **Figure 1.14**, displays the excellent shape fit of the pyrazene guest. An analysis of its crystal structure revealed favourable host-guest interactions: C-H···N hydrogen bonds and C-H···π interactions from the host methylene bridges to the guest N atom and π-system respectively. It implies that suitable-sized guests that can achieve the maximum number of van der

Waals and specific directional intermolecular interactions with the cavity walls make the most effective templates.

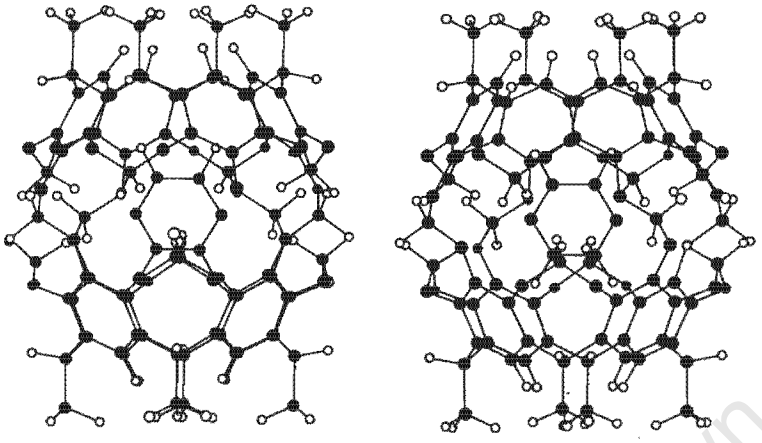

Figure 1.14 X-ray crystal structure (stereoview) of the pyrazene carceplex of 18. Taken from reference 59.

The selective incorporation of the guest molecules into the host frame work through intermolecular interactions is a matter of fine tuning. It requires the correct manipulation of the energetic and stereochemical features of the non-covalent, intermolecular forces within a defined molecular architecture.

Apart from the shape and size recognition and functionality selectivity, kinetic and thermodynamic aspects also contribute to the dynamic process of molecular recognition. In some case within the solid state supramolecular systems, the guest molecules that bind with host faster may well predominated over those that form most stable complex with host. In solution, the preorganisation effect as well as chelate effect is enhanced by means of guest binding kinetics and thermodynamic stability of host-guest complex[9].

Separation by enclathration

Selective enclathration is the quintessential example of molecular recognition, as it depends on the matching of steric and electronic features in host and guest molecules to optimise the strengths and directions of non-covalent intermolecular interactions formed between them. The design of host compounds which exhibit selective enclathration must take account of all of these intermolecular interactions.

Separation of close isomers by enclathration is one of the important applications of inclusion chemistry and has considerable industrial interest. This process generally follows the same simple methodology. A suitable host compound is recrystallised from the mixture of close isomers. The resulting clathrate crystals are filtered and heated gently to release the guest. A high purity of the required isomer can then be achieved after several cycles of recrystallisation. The host compound may be recovered and recycled during the process. This process may also be carried out in suspension and in the solid-solid state[60,61].

The process of selective enclathration has been studied in a varity of host-guest systems. Guanidium organodisulfonates have been employed to separate isomeric mixtures of xylenes and dimethylnaphthalenes by selective inclusion[62]. These hosts have been extensively studied and form the basis of crystal engineering of a range of lamellar structures[63,64,65]. α-Cyclodextrin and urea have been employed to separate mixtures of poly-(ethylene glycols) of different molecular weights[66]. Substituted resorcinarenes and calixarenes have been used to separate aromatic hydrocarbons[67]. A range of N,N'-ditritylurea and analogues have been synthesisted and their clathrating properties and selectivity with a variety of aliphalic guests have been established[68]. The inclusion properties of 1,4-(triorganostannyl and silyl) buta-1,3-diyne with chlorinated solvents and simple aromatic molecules have been studied[69]. These hosts mimic the noted Toda host 1,1,6,6-teta-phenylhexa-2,4-diyne-1,6-diol (**7a**) which has been studied extensively and has been employed in the separation of close isomers[70,71,72]. Gas chromatographic techniques are particularly useful in the study of guest selectivity, and these have been recently applied to test the inclusion preference of *p*-tert-butylcalix[4]arene and *p*-tert-butylcalix[8]arene towards positional isomers of xylenes, ethyltoluenes and diethylbenzenes[73].

Stoichiometry

Clathrates are mostly formed with stoichiometrically well defined host:guest ratio. The non-stoichiometric inclusion compounds often result from weak binding between host and guest. For example the Urea clathrates, because the urea molecules do not have 'spare' hydrogen bonding functionality for the guest, resulting in the guest being located in channels formed by urea molecules mainly with weak van der Waals forces[74]. The other well-known non-stoichiometric inclusion compounds include Werner clathrates[23], cyclodextrins with water etc.

A important parameter for controlling the host:guest ratio is the crystallisation temperature. Previous reports have appeared detailing the possibility of growing inclusion compounds with varying host-guest ratios by changing the crystallisation temperature. Reports of this phenomenon include the two compounds of trans-3,3'-bis(diphenylhydroxymethyl)azobenzene with acetone, which yields a host:guest ratio of 1:2 when crystallised at room temperature, but forms a different compound of 1:1 stoichiometry when the former compound is melted and cooled to 80°C under reduced pressure[75]. Varying the crystallisation temperature has been used to control the selectivity of xylene isomers by binaphthyl dicarboxylic acid[76], and to change the host:guest ratio of the inclusion compounds formed between an alicyclic diol and 1,2-dichlorobenzene[77]. In general the number of guest molecules entrapped by a host will decrease with increasing crystallisation temperature, but in the case of binaphthyldicarboxylic acid with DMSO, the host:guest ratio changes from 1:1 to 1:2 when the crystallisation temperature is raised from 50°C to 60°C. Disorder in both the host and guest molecules are apparent in these structures, and are important factors in the formation of the clathrates[78]. The general rules on how topology is likely to change with crystallisation temperature have been formulated[79].

Physical chemistry of inclusion compounds

The standard techniques, which are useful for characterising crystalline inclusion compounds, are summarised in **Figure 1.15**.

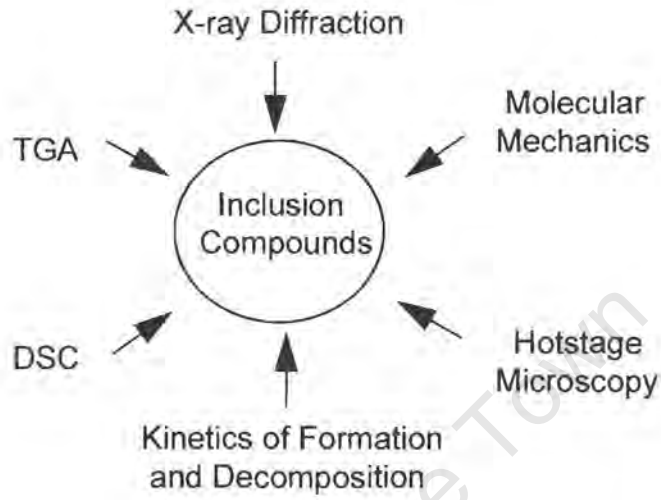

Figure 1.15 Techniques employed to study inclusion compounds.

The formation and stability of a particular inclusion compound depends on the strengths and directions of the intermolecular forces which act upon the host-guest system. Therefore accurate structure determination by single crystal X-ray diffraction is the most important tool, in that it yields not only detailed structural parameters of the individual host and guest molecules, but it also affords a description of their packing. Thus for a given inclusion compound it is possible to describe the topology of space in which the guests are encapsulated, which in turn impinges on its thermal stability, its guest selectivity, its ability to withstand guest exchange and its kinetics of formation and decomposition.

X-ray powder diffraction is also important technique as each crystalline inclusion compound has its own characteristic pattern and this method may be used as a mean of 'fingerprinting'[54]. The most widely use of the powder method is in the study of polymorphism, phase transitions and solid solutions. As this method of analysis does not give direct information about the chemical constitution, other analytical techniques should be employed in conjunction with it.

While the design, synthesis and structures of a large number of host molecules and their inclusion compounds have been extensively studied, their physical properties, such as thermal stability, kinetics of enclathration and desolvation, have received relatively little attention. Thermodynamics and kinetics in solid state clathrates have been reviewed recently[80,81,82]. Most of the thermal stability studies of inclusion compounds have employed techniques such as thermogravimetric analysis (TG) and differential scanning calorimetry (DSC), both of which are well-established[83,84]. For solid-solid reactions, X-ray powder diffraction, solid-state UV spectroscopy, solid state NMR and so on may be employed to investigate the kinetics; for solid-gas reaction, TG is the most convenient technique to study the kinetics of decomposition by isothermal or non-isothermal methods[85].

When a suitable host compound (H) is dissolved in a liquid guest (G) or is exposed to a guest vapour, an inclusion compound is formed.

$$H\,(s,\alpha) + nG\,(g) \rightarrow H{\cdot}G_n\,(s,\beta)$$

The crystal structure of the inclusion compound (β-phase) is different from the non-porous α-phase of the apohost. Under certain conditions of temperature and pressure of the guest, the inclusion compound may decompose in several possible ways, as schematically illustrated in **Figure 1.17**.

The inclusion compound may lose all the guests and revert back to the original non-porous α-phase. Alternatively, it may lose only part of the guests and form a metastable intermediate, γ-phase. Thirdly, it may lose all the guests without rearrangement of the host structure, resulting in the retention of the host framework, forming the so-called β_o-phase. Generally, the collapse of the β-phase back to the α-phase is most often encountered.

For the purpose of this study, TG has been used for the determination of host:guest ratios and in the investigations of kinetics of desolvation. DSC has been employed to measure the onset temperatures of guest desorption and the enthalpy changes accompanying the loss of guest, phase transformations and melting of guest-free host. In general, the onset temperature of the guest-loss process, when compared with the boiling point of the guest, is a crude measure of the stability of the inclusion compound. In the case when more than one species of the guest components may released from the inclusion compound, other analytical techniques, *i.e.* mass spectroscopy (MS) or infrared spectroscopy (IR), has also been used in combination with TG to determine the identity and amount of desolvated evolved gaseous products.

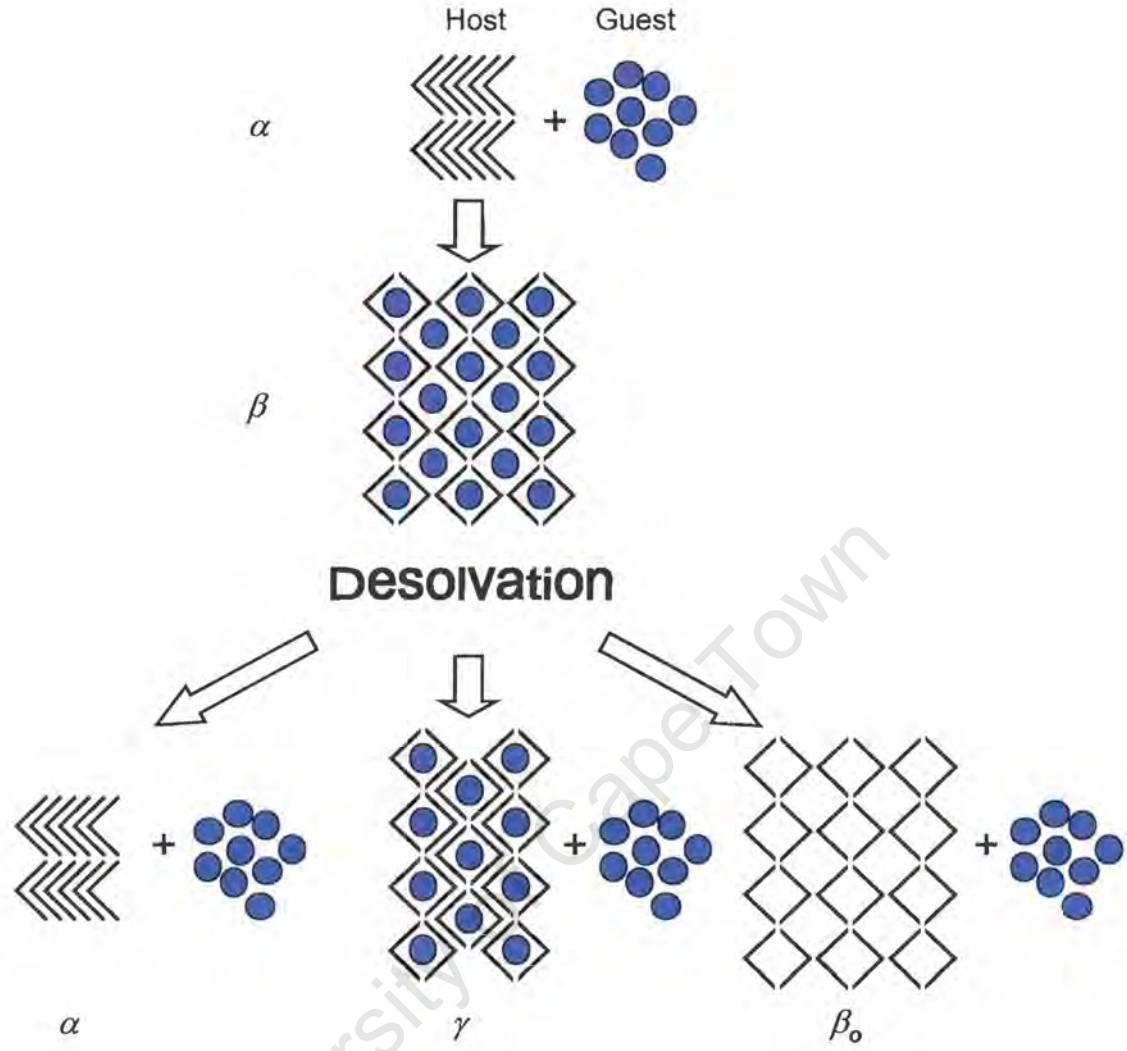

Figure 1.17 Schematic diagram showing the formation and possible desolvation pathways of the inclusion compound containing volatile guest.

Solid state kinetics

For a homogeneous reaction, the rate of reaction is conveniently measured by the decrease in concentration of reactants or the increase in concentration of products at constant temperature and can be expressed as

Rate = k f (concentration of reactants or products)

where *k* is the rate coefficient which is a function of temperature. The relationship between the rate constant and the absolute temperature

$k = A\, e^{-Ea/RT}$ or $\ln k = -E_a/RT + \ln A$

was first given quantitatively by Arrhenius[86], and is generally referred to as the Arrhenius law. Based on the theory of collisions, the Arrhenius parameters are defined as follows. E_a is identified as the activation energy which reactant molecules must have in order to react. While *A*, the pre-exponential factor or frequency factor refers to the number of collisions[87]. The Arrhenius law is one of the most important relationships in chemical kinetics, and one that provides much information as regards to mechanism.

For a heterogeneous reaction of the general form

$A\,(s) + nB\,(g) \Leftrightarrow AB_n\,(s)$

the concept of concentration no longer has the same significance as in the homogeneous reaction, so that the rate of reaction cannot be defined in the same way[88]. Since gas-solid reactions involve gas release or gas uptake, the rate of reaction can be measured by the loss or gain of mass of the sample during reaction. Usually, at time *t*, the extent of reaction, α, is defined as $\alpha = \left|\frac{m_t - m_o}{m_f - m_o}\right|$, where m_o is the initial mass of the reactant, m_f is the final mass of the product, and m_t is the mass of the sample at time *t*. The kinetic analysis of isothermal gas-solid reactions involves attempting to relate the experimentally measured α and *t* values with values predicted for a limited set of models based on processes of nucleation and growth, diffusion or geometrical progress of the reactant/product interfaces[85] The expressions derived from these ideal geometrical models can all be written in their integral forms: $f(\alpha) = kt$, at constant temperature *T*, as summarised in **Table 1.2**.

Table 1.2 Broad classification of solid state rate expressions[85].

	$f(\alpha) = kt$	$g(\alpha) = 1/k(d\alpha/dt)$
Acceleratory α-time curves		
P1 power law	$\alpha^{1/n}$	$n(\alpha)^{(n-1)/n}$
E1 exponential law	$ln\alpha$	α
Sigmoid α-time curves		
A2 Avrami-Erofe'ev	$[-ln(1-\alpha)]^{1/2}$	$2(1-\alpha)[-ln(1-\alpha)]^{1/2}$
A3 Avrami-Erofe'ev	$[-ln(1-\alpha)]^{1/3}$	$3(1-\alpha)[-ln(1-\alpha)]^{2/3}$
A4 Avrami-Erofe'ev	$[-ln(1-\alpha)]^{1/4}$	$4(1-\alpha)[-ln(1-\alpha)]^{3/4}$
B1 Prout-Tompkins	$ln[\alpha/(1-\alpha)]$	$\alpha(1-\alpha)$
Deceleratory α-time curves		
Geometrical models		
R2 contracting area	$1-(1-\alpha)^{1/2}$	$2(1-\alpha)^{1/2}$
R3 contracting sphere	$1-(1-\alpha)^{1/3}$	$3(1-\alpha)^{2/3}$
Diffusion controlled models		
D1 one-dimensional	α^2	$1/2\ \alpha$
D2 two-dimensional	$(1-\alpha)ln(1-\alpha)+\alpha$	$[-ln(1-\alpha)]^{-1}$
D3 three-dimensional	$[1-(1-\alpha)^{1/3}]^2$	$3/2\ (1-\alpha)^{2/3}[(1-\alpha)^{1/3}]^{-1}$
D4 Ginstling-Brounshtein	$(1-2\alpha/3)-(1-\alpha)^{2/3}$	$3/2\ [(1-\alpha)^{-1/3}-1]^{-1}$
"Order" of reaction		
F1 first order	$-ln(1-\alpha)$	$1-\alpha$
F2 second order	$1/(1-\alpha)$	$(1-\alpha)^2$
F3 third order	$[1/(1-\alpha)]^2$	$(1-\alpha)^3$
Fn n-th order	$[1/(1-\alpha)]^n$	$(1-\alpha)^n$

All above rate expressions can be summarised into the combined equation[83]:

$$d\alpha/dt = k\ \alpha^m\ (1-\alpha)^n\ [-ln(1-\alpha)]^p$$

In the general case, the experimental α-time curve under isothermal conditions has the features illustrated in **Figure 1.18**, though, any of these features except the maximum rate may be absent in specific cases[89]. From the typical α-time curve, we can get information about the mechanism of the reaction, which is often complex, as described below[89,90]:

1. Surface adsorption or desorption, yield initial section *a*,
2. The formation of nuclei, termed the induction period (section *b*), which is regarded as being terminated by the development of stable nuclei,
3. The growth of such nuclei, perhaps accompanied by further nucleation, extends to the maximum rate of reaction at *d*, yielding an acceleratory section *c*,
4. Thereafter, due to overlapping of nuclei and consumption of reactant, a deceleratory section *e* is yielded and continues until completion of reaction, *f*.

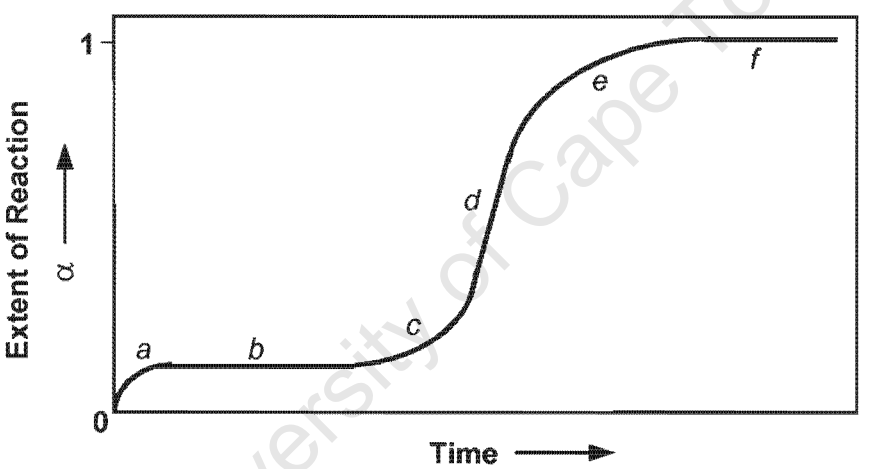

Figure 1.18 The generalised isothermal α-time curve for a solid state reaction

It is generally accepted that the nucleation and growth processes play an important role in the decomposition of a solid to yield a second product phase. The formation and growth of nuclei is depicted in **Figure 1.19**. The nuclei grow initially from "germ nuclei", which generally occurs at the defects existing in the crystalline reactant. Grains of product phase are formed in the reactant and these increase in size. The reactant/product interface advances and the growth of the product continues until no more reactant is left over.

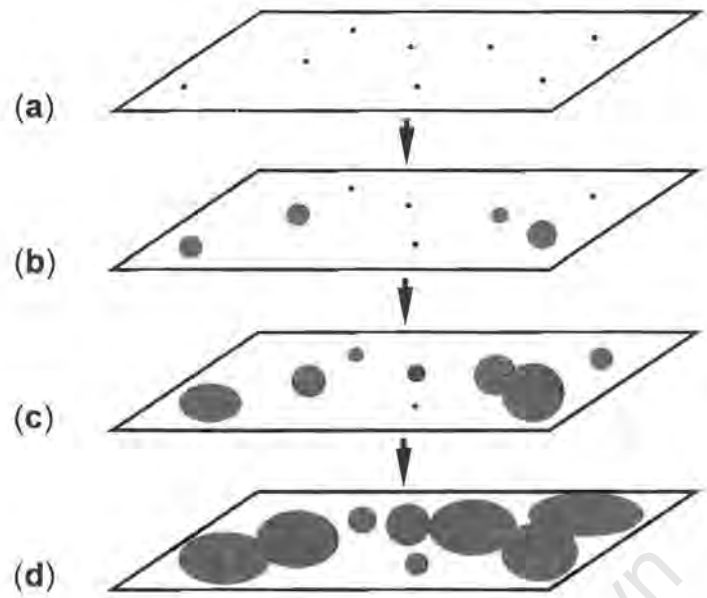

Figure 1.19 Formation and growth of nuclei in solid state decomposition. (a) nuclei site; (b) nuclei formed, grew and further nucleation; (c) overlap of nuclei and ingestion of nucleation site; (d) continued growth.

The rate-determining step in most solid phase reactions can be either diffusion, which is the migration of product away from or reactant towards a reaction interface, or chemical reaction which generally occurs at a reaction interface[91]. For diffusion-controlled reactions, based on the assumption that the diffusion coefficient is constant, one-dimensional diffusion on the reaction layer leads to kinetic equation D1, while D2 and D3 are derived from 2 or 3-dimensional diffusion in a cylinder and sphere respectively, and diffusion starting at the exterior of a spherical particle leads to equation D4. For a phase-boundary controlled reaction, which is controlled by movement of an interface at a constant velocity, the rate equations R2 and R3 are then derived simply for a circular disk reacting from the edge inward and for a sphere reacting from the surface inward respectively. Mainly for analytical convenience, the rate equations F1 - Fn based on the order of reaction has been applied to solid state reactions, being analogous to the homogeneous rate laws[91]. The α-time curves for decomposition of solids usually give rise to a sigmoidal shape, and are accounted for by the Prout-Tompkins model (B1) and Avrami-Erofe'ev models (A2 - A4). The Prout-Tompkins model was derived for symmetrically shaped sigmoid-curves based on a chain branching mechanism for nuclei. The Avrami-Erofe'ev equations can be written in the general form[90]:

$$[-ln(1-\alpha)]^{1/n} = kt$$

with the exponent $n = \beta + \lambda$, where β is the number of steps involved in nucleus formation and λ is the number of dimensions in which the nuclei grow.

In application of the rate equations contained in **Table 1.2**, caution must always be taken in giving geometrical interpretation to the mathematical models[92]. If, for a specific reaction, a given set of (α, t) values obeys a particular kinetic expression, it does not mean that the reaction follows the same mechanism from which that rate equation was derived. The different mechanistic models can lead to the same kinetic equation[86]. The converse is also true[90,93]. Other factors may also reduce the accuracy of interpretation of kinetic data, *e.g.* particle size effects, reactant pre-treatment or concentration of defects. The reaction rate can be inhomogeneous within the reaction mass, if for example, melting occurs[94]. It is also possible that the mechanism may change during reaction, or vary with the α. In view of these problems, geometric interpretations must be supported by independent evidence, *e.g.* microscopic observations or measurement of the nuclei.

The variation of the rate constant, k, with temperature is generally assumed to be governed by the Arrhenius equation, $ln\ k = -E_aR/T + ln\ A$, which was originally derived for homogeneous reactions based on well-established theories. Being analogous to the homogeneous reaction, the activation energy, E_a, is identified as the energy barrier which must be surmounted during transformation of reactants into products during the rate-limiting step. The frequency factor, A, was identified as a molecular encounter or as a specific vibration in the reaction co-ordinate. This assignment, as well as the concept of rate constants for solid state reactions have been challenged[95,96,97,98]. Some scientists prefer to regard both E_a and A as having empirical rather than theoretical significance and refer to them as "apparent kinetic parameters"[99,100,101]. However, the Arrhenius equation has been successfully applied to numerous reactions involving solids. The Arrhenius parameters do have practical value as suggested by Brown[85], even though there is still no satisfactory theoretical explanation.

About this study

1. Alkaline-earth metal complexes

This part of the work arose from a report by Mravik *et. al*[102], that a simple resolution of O,O'-dibenzoyltartaric acid can be achieved by the preferential crystallisation of its calcium salt with methoxyethanol. They formulated the reaction shown in **Scheme 1.1**.

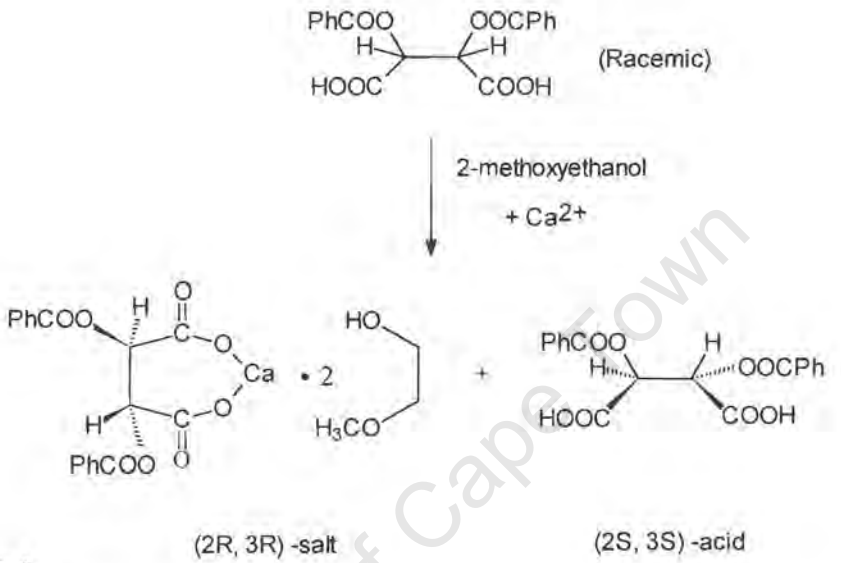

Scheme 1.1

Their procedure required the dissolution of the racemic acid in a mixture of ethanol and 2-methoxyethanol, adding calcium oxide, which was dissolved by heating, and allowing the crystallisation of the enantiomeric salt. The latter was induced by seeding with small quantities of the corresponding complex.

In previous reports, the structures of selected Grignard reagents have been elucidated[103,104,105], and the inclusion compounds of nitrogen base adducts of group 2 salts, which contain substituted pyridines as guest molecules, have been described[106]. The co-ordination geometry of Ca, Sr and Ba carbazoles has been studied[107], while the structural relations between alkoxides and aryloxides of Ca and Ba have been studied[108]. The inclusion compounds within organic system, their structures and thermal stabilities have been studied extensively in our laboratory; relatively little work, however, has been carried out on the structures of inclusion compounds containing alkaline-earth metals. In this study, the structures, thermal stabilities and kinetics of decomposition of three related inclusion compounds containing alkaline-earth metal salts of O,O'-dibenzoyltartaric acid (magnesium, calcium, strontium) as host were investigated. The results were compared with those of organic inclusion compounds.

2. The inclusion compounds of diol hosts

This part of the work is concerned with an exploratory investigation of structure/thermodynamic/selectivity relationships of the inclusion compounds of two diol hosts. Both the host 2,2'-dihydroxy-1,1'-binaphthyl (**BINAP**) and the host 1,1'-bis-(4-hydroxyphenyl)cyclohexane (**DHPC**) conform to the principles of directed host design[109], in that they are bulky, with a rigid backbone and contain hydroxyl moieties which facilitate the formation of coordinato-clathrates.

The host **BINAP** has been studied extensively in the literature. The structures of the non-porous α-phase, the apohost, have been elucidated for the racemic[110] and both enantiomerically pure forms[111,112]. The structures of its inclusion compounds with a variety of small guests have been solved. Of interest are the structures carried out with the resolved host with a chiral guest such as methyl *m*-tolyl-sulfoxide[113], dimethylphenylphosphinate[114], ethyl *m*-tolyl selenoxide[115], proline[116], ethylmethyl (*m*-tolyl) amine oxide[117] and 1,2-cyclohexane-diamine[118]. This host was employed in this study in an attempt to separate the close isomers of picoline, lutidine and xylidine. Its inclusion compounds formed with a number of volatile guest solvents were also investigated.

The host **DHPC** has been extensively employed previously in separating benzene-substituted organic compounds. The closely related isomers, which we have attempted to separate by this host in our laboratory, are listed in **Table 1.3**, together with the selectivity trend given as references. In this study the host **DHPC** was employed to selectively enclathrate close isomers of xylidine. The inclusion compounds formed were of different stoichiometries depending on crystallisation temperatures. The structure relationship of the inclusion compounds of various stoichiometries was studied.

Table 1.3 Separation results by employing the host **DHPC** from previous studies.

Separation of	Results	Reference
Isomers of phenylenediamine	4- > 2- ≈ 3-	119
Isomers of bezenediol	2- ≈ 3- > 4-	120
Isomers of picoline	3- ≈ 4- > 2-	121
Isomers of lutidine	3,5- > 2,4- > 2,6-	122
Isomers of xylenol	3,5- > 2,3- ≈ 2,6-	123
Phenol and isomers of cresol	3- > 4- > phenol > 2-	124

References

1. 'Inclusion Compounds' (1984, 1991). Editors: J. L. Atwood, J. E. D. Davies and D. D. MacNicol. 5 volumes, Oxford University Press, London.
2. 'Comprehensive Supramolecular Chemistry' (1996). Editors: Atwood, J. L., Davies, J. E. D., MacNicol, D. D. and Vögtle, F. 11 Volumes, Pergamon Press.
3. 'Monographs in Supramolecular Chemistry' (2000). Series Editor: Stoddart, J. F. FRS. 7 series, The Royal Society of Chemistry.
4. Desiraju, G. R. (1996). in 'Comprehensive Supramolecular Chemistry', Vol 6, 'Solid-state Supramolecular Chemistry: Crystal Engineering', MacNicol, D. D., Toda, F. and Bishop, R. (Volume Editors), Pergamon Press.
5. Weber, E. (1987). Editor of 'Molecular Inclusion and Molecular Recognition Clathrates I', Topics in Current Chemistry, Springer, Berlin, Vol. 140, pp1-20.
6 Weber, E. (1996). 'Comprehensive Supramolecular Chemistry', Vol 6, 'Solid-state Supramolecular Chemistry: Crystal Engineering', Volume Editors: MacNicol, D. D., Toda, F. and Bishop, R., Pergamon Press, Chapter 17.
7. Harris, K. D. M. (1992). *Chemistry in Britain*, 132.
8. Lehn, J. -M. (1988). *Angew. Chem., Int. Ed. Engl.* (Nobel Lecture), 27, 89.
9. Steed, J. W. and Atwood, J. L. (2000). 'Supramolecular Chemistry', John Wiley & Sons, Ltd. Baffins Lane, Chichester.
10. Lindoy, L. F. and Atkinson, I. M. (2000). 'Self-Assembly in Supramolecular Systems', Monographs in Supramolecular Chemistry, Series editor: J. Fraser Stoddart, FRS., University of California at Los Angeles, USA.
11. Jeffrey, G. A. (1997). 'An Introduction to Hydrogen Bonding', Oxford University Press: Oxford.
12. Desiraju, G. R. (1989). 'Crystal Engineering', Elsevier, Amsterdam, Chapter 5.
13. Bertolasi, V., Gilli, P., Ferretti, V. and Gilli, G. (1995). *Acta Cryst.*, B51, 1004.
14. Gilli, P., Bertolasi, V., Ferretti, V. and Gilli, G. (1994). *J. Am. Chem. Soc.*, 116, 909.
15. Etter, M. C. (1991). *J. Phys. Chem.*, 95, 4601.
16. Aakeröy, C. B. and Seddon, K. R. (1993). *Chem. Soc. Rev.*, 22, 397.
17. Desiraju, G. R. and Steiner, T. (1999). 'The Weak Hydrogen Bond', Oxford University Press, Oxford.
18. Hunter, C. A. and Sander, J. K. M. (1990). 'The Nature of π-π Interactions', *J. Am. Chem. Soc.*, 112, pp5525-5534.
19. Adams, H., Carver, F. J., Hunter, C. A. and Osborne, N. J. (1996). *Chem. Commun.*, 2529.
20. Adams, H., Harris, K. D. M., Hembury, G. A., Hunter, C. A., Livingstone, D. and McCabe, J. F. (1996). *Chem. Commun.*, 2531.

21. Hunter, C. A. (1994). *Chem. Soc. Rev.*, 23, 101.
22. Allen, F. H., Kennard, O. and Taylor, R. (1983). *Acc. Chem. Res.*, 16, 146.
23. Taylor, R. and Kennard, O. (1984). *Acc. Chem. Res.*, 17, 320.
24. Lipkowski, J. (1996). 'Werner Clathrates', in 'Comprehensive supramolecular Chemistry', Vol. 6, Editors: Atwood, L. J., Davies, J. E. D., MacNicol, D. D. and Vögtle, F. Pergamon: Oxford.
25. Davy, H. (1811). *Philos. Trans. R. Soc. London*, 101, 1.
26. Schöllhorn, R. (1984) 'Intercalation Compounds' in 'Inclusion Compounds', Vol. 1, Editors: Atwood, J. A., Davies, J. E. D. and MacNicol, D. D., Academic Press, London.
27. Vögtle, F. (1991). 'Supramolecular Chemistry', John Wiley & Sons, Chichester, reference 7-9.
28. Hoffmann K. A. and Küspert, F. A. (1897). *Z. Anorg. Allg. Chem.*, 15, 204.
29. Dianin, A. P. (1914). *J. Soc, Phys. Chem. Russe.*, 46, 1310.
30. Villiers, A., Hebd, C. R. (1891). *Sceances Acad. Sci.*, 112, 536.
31. Wieland, J. and Sorge, H. (1916). *Z. Physiol. Chem. Hoppe-Seyler's.*, 97, 1.
32. Terres, E. and Vollmer, W. (1935). *Z. Petroleum*, 31, 1.
33. Bengen, M. F. (1940). German Patent Application OZ 123438, March 18, 1940.
34. Hardy, A. D., McKendrick, J. J., MacNicol, D. D. (1979). *J. Chem. Soc., Perkin Trans 2*, 1072.
35. MacNicol, D. D. and Downing, G. R. (1996). 'Comprehensive Supramolecular Chemistry', Vol 6, 'Solid-state Supramolecular Chemistry: Crystal Engineering', Volume editors: MacNicol, D. D., Toda, F. and Bishop, R., Pergamon Press, Chapter 14.
36. MacNicol, D. D. and Wilson, D. R. (1976). *J. Chem. Soc. Chem. Commun.*, 494.
37. Hardy, A. D. U., MacNicol, D. D. and Wilson, D. R. (1979). *J. Chem. Soc. Perkin Trans. 2*, 1011.
38. MacNicol, D. D., Hardy, A. D. U. and Mckendrick, J. J. (1975). *Nature*, 256, 343.
39. MacNicol, D. D. (1984). 'Structure and Design of Inclusion Compounds: the Hexa-host and Symmetry Considerations' in 'Inclusion Compounds', Vol. 2, Editors: Arwood, J. L., Davies, J. E. D. and MacNicol, D. D., Academic Press, London.
40. Toda, F., Tanaka, K., Daumas, U. G. and Sanchez, C. (1983). *Chem. Lett.*, 1521.
41. Weber, E., Dõrpinghaus, N., Wimmer, C., Stein, Z., Krupitsky, H. and Goldberg, I. (1992). *J. Org. Chem.*, 57, 6825.
42. Bishop, R. (1996). 'Comprehensive Supramolecular Chemistry', Vol. 6, 'Solid-state Supramolecular Chemistry: Crystal Engineering', Volume editors: MacNicol, D. D., Toda, F. and Bishop, R., Pergamon Press, Chapter 4.

43. Toda, F. (1991). in 'Inclusion Compounds', Editors: Atwood, J. L., Davies, J. E. D. and MacNicol, D. D., Vol. 4, Oxford University Press, London, 126.
44. Toda, F., Tanaka, K. and Mak, T. C. W. (1984) *Tetrahedron Lett.*, 25, 1359. and (1985) *J. Inclu. Phen.*, 3, 225.
45. Bond, D. R., Nassimbeni, L. R. and Toda, F. (1989). *J. Crystallogr. Spectrosc. Res.*, 19, 847.
46. Toda, F. (1996). 'Comprehensive Supramolecular Chemistry', Vol. 6, 'Solid-state Supramolecular Chemistry: Crystal Engineering', Volume editors: MacNicol, D. D., Toda, F. and Bishop, R., Pergamon Press, Chapter15.
47. Behr, J. P. (1994). 'The Lock-and-Key Principle. The State of the Art-100 years on', J. Wiley & Sons: Chichester.
48. F. Vögtle (1991). 'Supramolecular Chemistry', John Wiley & Sons, Chichester, 38.
49. Schneider, Hans-Jörg and Yatsimirsky, A. K. (2000). 'Principles and methods In Supramolecular Chemistry' John Wiley & Sons, LTD.
50. Michaux, G and Reisse, J. (1982). *J. Am. Chem. Soc.*, 104, 6895.
51. Gokel, G. W., Goli, D. M., Minganti, C.and Echegoyen, L. (1983). *J. Am. Chem. Soc.*, 105, 6786.
52. Hancock, R. D. (1992). 'Chelate Ring Size and Metal Ion selection', *J. Chem. Ed.*, 69, pp615 - 621.
53. Martell, A. E., Hancock, R. D. and Motekaitis, R. J. (1994). *Coord. Hem. Rev.*, 133, 39.
54. Harris, K. D. M. (1993). *J. Solid State Chem.*, 106, 83.
55. Hollingsworth, M. D., Brown, M. E., Hillier, A. C. (1996). *Science*, 273, 1355.
56. Schlenk, W. (1949). *Justus Liebigs Ann.Chem.*, 565, 204.
57. Jasat, A. and Sherman, J. C. (1999). *Chem. Rev.*, 99, pp931-967.
58. Chapman, R. G., Olovsson, G., Trotter, J. and Sherman, J. C. (1998). *J. Am. Chem. Soc.*, 120, 6252.
59. Fraser, J. R., Borecka, B., Trotter, J. and Sherman, J. C. (1995). *J. Org. Chem.* 60, 1270.
60. Caira, M. R., Horne, A., Nassimbeni, L. R. and Toda, F. (1997). *J. Mater. Chem.*, 7, 2145; *J. Chem. Soc. Perkin Trans. 2*, 1717.
61. Caira, M. R., Horne, A., Nassimbeni, L. R., Okuda, K. and Toda, F. (1995). *J. Chem. Soc. Perkin Trans 2*, 1063.
62. Pivotar, A. M., Holman, K. T. and Ward, M. D. (2001). *Chem. Mater.*, 13, 3018.
63. Holman, K. T., Pivotar, A. M., Swift, J. A. and Ward, M. D.(2001). *Acc. Chem. Res.*, 34, 107.
64. Russell, V. A., Evans, C. C., Li, W. and Ward, M. D. (1997). *Science*, 276, 575.
65. Holman, K. and Ward, M. D. (2000). *Angew. Chem. Int. Ed.*, 39, 1653.

66. Rusa, C. C. and Tonelli, A. E. (2000). *Macromolecules*, 33, 1813.
67. Kalchenko, V. I., Solovov, A. V., Gladun, N. R., Shivanyuk, A. N., Atamas, L. I., Pirozhenko, V. V., Markovsky, L. N., Lipkowski, J. and Simonov, Y. A. (1997). *Supramol. Chem.*, 8, 269.
68. Ng, K. D. and Hart, H. (1995). *Tetrahedron,* 51, 7883.
69. Carré, F., Dutremez, S. G., Guériu, C., Henner, B. J. L., Jolivet, A., Tomberli, V. and Dahan, F. (1999). *Organometallics*, 18, 770.
70. Bacsa, J., Caira, M. R., Jacobs, A., Nassimbeni, L. R. and Toda, F. (2000). *Crystal Engineering*, 3, 251.
71. Caira, M. R., Nassimbeni, L. R., Toda, F. and Vujovic, D. (2001). *J. Chem. Soc. Perkin 2*, 2119.
72. Caira, M. R., Nassimbeni, L. R., Toda, F. and Vujovic, D. (2000). *J. Amer. Chem. Soc.*, 122, 9367.
73. Mñuk, P., Feltl, L. and Schuria, V. (1996). *J. Chromatogr. A.*, 732, 63.
74. Harris, K. D. M. (1993). *J. Solid State Chem.*, 106, 83.
75. Hamada, K., Oh-hira, M., Fujiwara, T. and Toda, F. (1992). *Acta Cryst.* C 48, pp1969-1971.
76. Beketov, K., Weber, E., Seidel, J., Köhnke, K., Makhkamov, K. and Ibragimov, B. (1999). *Chem. Commun.* pp91-92.
77. Ung, A. T., Bishop, R., Craig, D. C., Dance, I. G. and Scudder, M. L. (1993). *Tetrahedron*, Vol 109, no.3, pp639-348.
78. Makhkamov, K., Lbragimov, B. T., Weber, E. and Beketov, K. M. (1999). *J. Phys. Org. chem.* 12, pp157-164.
79. Ibragimov, B. (1999). *J. Incl. Phenom. And Macrocyclic Chemistry*, 34, pp345-353.
80. Nassimbeni, L. R. (1996). 'Crystallography of Supramolecular Compounds', p285, Kluwer Academic Publishers.
81. Caira, M. R. and Nassimbeni, L. R. (1996). 'Comprehensive Supramolecular Chemistry', Vol 6, 'Solid-state Supramolecular Chemistry: Crystal Engineering', Volume editors: D. D. MacNicol, F. Toda and R. Bishop, Pergamon Press, Chapter 25.
82. Nassimbeni, L. R. (2000). 'Useful Techniques in Host-guest Chemistry' in Supramolecular Chemistry, 12, pp161-167.
83. Haines, P. J. (1995). 'Thermal Methods of Analysis', Chapman and Hall. London.
84. Wunderlich, B. (1990). 'Thermal Analysis', Academic Press, Boston.
85. Brown, M. E. (1988). 'Introduction to Thermal Analysis - Techniques and Applications', Chapman and Hall, London.
86. Arrhenius, S. (1889). *Z. Phys. Chem. (Leipzig)* 4, 226.

87. Laidler, K. J. (1963). 'Reaction Kinetics', Vol.1, 'Homogeneous Gas Reactions', Vol.2, 'Homogeneous Reactions In Solution'. Pergamon press.
88. Laidler, K. J. (1965). 'Chemical Kinetics', McGraw-Hill, New York.
89. Young, D. A. (1966). 'Decomposition Of Solids', Pergamon press.
90. Brown, M. E., Dollimore, D. and Galwey, A. K. (1980). 'Comprehensive Chemical Kinetics', Vol. 22, 'Reaction In The Solid State', Elsevier, Amsterdam.
91. Sharp, J. H., Brindley, G. W. and Narahari, B. N. (1966). *Achar, J. Amer. Ceram. Soc.*, 7, 49, 379.
92. Barmford, C. H. and Tipper, C. F. H. (eds) (1980). 'Compreshensive Chemical Kinetics', Vol. 22, Elsevier, Aqmsterdam.
93. Dollimore, D. (1990). 'Thermal Analysis-Techniques and Applications', Editors: E. L. Charsley and S. B. Warrington.
94. Galwey, A. K. (1994). *J. Therm. Anal.*, 41, 267.
95. Galwey, A. K. and Brown, M. E. (1995). *Proc. R. Soc. Lond.* A450, 501.
96. Garn, P. D. (1972). *Crit. Rev. Anal. Chem.*, 3, 65; (1978). *J. Therm. Anal.*, 13, 581.
97. Arnold, M., Veress, G. E., Paulik, J. and Paulik, F. (1982). *Thermochim. Acta*, 52, 67; (1981) *Anal. Chim. Acta*, 124, 341
98. Gomes, W. (1961). *Nature*, 192, 865.
99. Pysiak, J. (1995). *J. Therm. Anal.*, 43, 9.
100. Wendlandt, W. W. M. (1964). 'Thermal Analysis', John Wiley and sons, New York.
101. Dollimore, D. (1992). *Thermochim. Acta.*, 203, 7.
102. Mravik, A., Lepp, Z. and Fogassy, E. (1996). *Tetrahedron Asymmetry*, 7, 2387.
103. Engelhardt, L. M., Harvey, S., Raston, C. L. and White, A. H. (1988). *J. Organometallic Chem.*, 341, 39.
104. Stucky, G. and Rundle, R. E. (1964). *J. Amer. Chem. Soc.*, 86, 4825.
105. Guggenberger, L. J. and Rundle, R. E. (1968). *J. Amer. Chem. Soc.*, 90, 5375.
106. Kepert, D. L., Skelton, B. W., Waters, A. F. and White, A. H. (1996). *Aust. J. Chem.*, 49, 47.
107. Mösges, G., Hampee, F., Kaupp, M. and vonRaguê Schleyer, P. (1992). *J. Amer. Chem. Soc.*, 114, 10880.
108. Tesh, K. F., Hanusa, T. P., Huffman, J. C. and Huffman, C. J. (1992). *Inorg. Chem.* 31, 5572.
109. Weber, E. (1991). in 'Inclusion Compounds', Editors: Atwood, J. L., Davies, J. E. D. and MacNicol, D. D., Oxford University Press, Oxford, Vol. 4, pp213-223.
110. Gridunova, G. V., Furmanova, V. E., Shklover, V. E., Struchkov, T. and Ezhkova, Z. I. (1982). *Kristallografiya* 27, pp477-484.
111. Mori, K. Masuda, Y. and Kashino, S. (1993). Acta Cryst. C49, pp1224-1227.

112. Toda, F., Tanaka, K., Miyamoto, H., Koshima, H., Miyahara, I. and Hirotsu, K. (1997). *J. Chem. Soc. Perkin Trans. 2*. pp1877-1885.
113. Toda, F., Tanaka, K. and Mak, T. C. W. (1984). *Chem. Lett*. pp2085-2088.
114. Toda, F., Mori, K., Stein, Z. and Goldberg, I. (1988). *J. Org. Chem. 53*, pp308-312.
115. Fujiwara, T., Tanaka, N., Ooshita, R., Hino, R., Mori, K. and Toda, F. (1990). *Bull. Chem. Soc. Jpn*. 63, pp249-251.
116. Periasamy, M., Venkatraman, L. and Thomas, K. R. J. (1997). *J. Org. Chem.* 62, pp4302-4306.
117. Toda, F., Mori, K., Stein, Z. and Goldberg, I. (1989). *Tetrahedron Lett*. 30, pp1841-1844.
118. Fukushima, S., Hosomi, H., Ohba, S. and Kawashima, M. (1999). *Acta Cryst.* C55, pp120-123.
119. Caira, M. R., Horne, A., Nassimbeni, L. R., Okuda, K. and Toda, F. (1995). *J. Chem. Soc., Perkin Trans. 2*, 1063.
120. Caira, M. R., Horne, A., Nassimbeni, L. R. and Toda, F. (1995). *J. Chem. Soc., Perkin Trans*. 2, 1717.
121. Caira, M. R., Horne, A., Nassimbeni, L. R. and Toda, F. (1997). *J. Mater. Chem.*, 7, pp2145-2149.
122. Caira, M. R., Horne, A., Nassimbeni, L. R. and Toda, F. (1998). *Supermol. Chem.*, 9, 231.
123. Caira, M. R., Nassimbeni, L. R., Toda, F. and Vujovic, D. (2000). *J. Phys. Org. Chem.*, 13, 75.
124. Goldberg, I., Stein, Z., Tanaka, K. and Toda, F. (1988). *J. Incl. Pheno.*, 6, 15.

2 EXPERIMENTAL AND COMPUTATION

Host compounds

The following host compounds were used in this study:

- (2R,3R)-(-)-di-*o*-benzoyl-tartaric acid (hereafter abbreviated **DBTA**, $C_{18}H_{14}O_8$, mol wt. 358.29, mp 149 - 152°C): It was purchased from Merck (Schuchardt).
- (1,1)-bis-(4-hydroxyphenyl)cyclohexane (hereafter abbreviated **DHPC**, $C_{18}H_{20}O_2$, mol wt. 268.34, mp 183 - 185°C): It was initially supplied by Professor Fumio Toda from Okayama University of Science, Japan and later synthesised by Dr. Alicia Horne, following the procedure described by McGreal *et al.* (1939). The melting point quoted by McGreal was 184°C.
- 2,2'-dihydroxy-1,1'-binaphthyl (hereafter abbreviated **BINAP**, $C_{20}H_{14}O_2$, mol wt. 286.33, mp 214 - 217°C): It was purchased from Aldrich-Chemical Co Gillingham-Dorset SP8 4JL.

The purity of the host compounds was confirmed by checking the melting points using Hotstage Microscopy. All host compounds were of sufficient purity when received and were used without further recrystallisation.

Guest compounds

The guest compounds were bought from various manufacturers, namely Sigma-Aldrich, Merck, Unilab, Orion and B & M Scientific Chemical Company. All of the guest compounds are of more than 99% chemical purity and were used as supplied without further distillation, purification or other preparative works. The volatile guest solvents, *e.g.* THF, actone, DMSO and 1,4-dioxane *etc.* were stored over dried molecular sieves. The relevant physical properties of the guest compounds are given in **Table 2.1**, together with their chemical formulae and molecular weights.

Table 2.1 Relevant physical properties of the guest compounds studied.

Guest compounds	Code	Structural formula	mol wt ($gmol^{-1}$)	bp* (^oC)	mp* (^oC)	Density# ($g\ cm^{-3}$)
2-Methoxyethanol	-	$HOCH_2CH_2OCH_3$	76.09	124.4	-85	0.9663
Ethanol	-	C_2H_5OH	46.07	78.5	-114.1	0.789
Water	-	H_2O	18.02	100	0	1.000
2,6-Xylidine	**26X**	$(CH_3)_2C_6H_3NH_2$	121.18	214	10	0.962
3,5-Xylidine	**35X**	$(CH_3)_2C_6H_3NH_2$	121.18	221	8	0.960
2,3-Xylidine	**23X**	$(CH_3)_2C_6H_3NH_2$	121.18	223	-15	0.993
3,4-Xylidine	**34X**	$(CH_3)_2C_6H_3NH_2$	121.18	225	49	1.134
2-Picoline	**2PIC**	$CH_3C_5H_4N$	93.12	128-129	-70	0.950
3-Picoline	**3PIC**	$CH_3C_5H_4N$	93.12	143-144	18	0.958
4-Picoline	**4PIC**	$CH_3C_5H_4N$	93.12	145	3.6	0.957
2,6-Lutidine	**26LUT**	$(CH_3)_2C_5H_3N$	107.15	144	-5.8	0.925
2,4-Lutidine	**24LUT**	$(CH_3)_2C_5H_3N$	107.15	159	-60	0.927
3,5-Lutidine	**35LUT**	$(CH_3)_2C_5H_3N$	107.15	169-170	-9	0.939
1,4-Dioxane	**DOX**	$C_4H_8O_2$	88.10	101.1	11.80	1.0329
Dimethylsulfoxide	**DMSO**	$(CH_3)_2OS$	78.13	189	18.45	1.100
Morpholine	**MOP**	C_4H_9NO	87.12	128.9	-4.9	1.007
Acetone	**ACT**	CH_3COCH_3	58.08	56.5	-94	0.788
Tetrahydrofuran	**THF**	C_4H_8O	72.10	66	-108.5	0.889

* bp and mp at 101.3kPa (760mmHg) are quoted either from The Merck Index (11^{th} Edition) if possible, or from The Chemist's Companion (Gordon & Ford, 1972).

Densities of solvents, measured at 25°C, are quoted from the reagent bottles.

Crystal growth

For the host **DHPC** and **BINAP**, crystals of the inclusion compounds were prepared using the following general methodology in the case of liquid guest: The host was dissolved in an excess amount of guest by gentle warming. The vial which containing the solution was closed with a lid with small holes and was left to stand at a certain temperature for crystals to appear by slow evaporation. In the case of the guest being solid at ambient temperature, an intermediate solvent was chosen based on its non-includable property by the appropriate host. The ratio of the amount of host used to that of guest is between 1:15 and 1:30. Full details of the preparation of individual inclusion compounds are given in the appropriate chapters.

Five different crystallisation temperatures were used in this study for preparing certain inclusion compounds, namely 1°C, 4°C, 25°C, 60°C and 80°C. Low temperature crystallisation experiments were carried out in refrigerators set at ±4°C and ±1°C respectively. The crystallisation temperature of 25°C is approximately assessed when the solutions were placed indoors, *i.e.* at room temperature. In the case of crystallisation experiments carried out at elevated temperatures, the vials containing the solutions were inserted in brass blocks maintained at 60°C and 80°C respectively in heated sand baths. These temperatures were controlled to ±1°C.

The preparations of the crystals of the alkaline-earth metal inclusion complexes with the host **DBTAM** ($M = Mg^{2+}$, Ca^{2+}, Sr^{2+}) are described in the appropriate chapter.

Infrared spectroscopy (IR)

IR spectra were obtained using a Perkin-Elmer 983 IR spectrophotometer. Percentage transmittance was recorded against frequency. Samples were ground with nujol into a mull and placed between two sodium chloride plates. Spectra were recorded in the 3000 - 3600cm^{-1} region, where the hydroxyl group stretching absorption occurs (Brown *et al.* 1998). This technique was applied for selected inclusion compounds with the diol host **BINAP**. Shifts in the frequency of the hydroxyl O-H group of the host were indicative of hydrogen-bond formation between the host and guest.

Thermal analysis (TG and DSC)

Thermogravimetry (TG) and Differential Scanning Calorimetry (DSC) were performed on a Perkin-Elmer PC-7 series thermal analysis system. The TG analyser was regularly calibrated using built-in procedures for furnace and weight calibration. A two-point standard temperature calibration was performed regularly by measuring the Curie points of Alum (163°C) and Nickel (354°C). The DSC instrument was calibrated using standard materials, *i.e.* Indium (ΔH = 28.5J/g, mp = 156.6°C) and Zinc (ΔH = 102.1J/g, mp = 419.5°C).

TG measures the mass loss of a sample as a function of temperature in the programmed temperature TG run, or time in the isothermal TG run, and was employed to establish the stoichiometries of the inclusion compounds as well as kinetic parameters. Mass losses observed in the TG traces are due to loss of guests from the inclusion complexes. The temperature ranges over which mass loss occurred were determined from the first derivative of the trace and are quoted together with the associated mass loss. The mass loss in percentage is compared with the calculated theoretical value and a host:guest ratio was assigned for the specific inclusion compound. The percentage mass loss has a precision of about 1%, yielding accurate host:guest ratios.

DSC was used to measure the enthalpy changes as well as onset temperatures associated with the desolvation, phase transformations, melting and other thermal events of the inclusion complexes during heating. There are two identical, crimped and vented aluminium pans, one for samples and the other, which is empty, is used as the reference. In power-compensated DSC the temperature of the sample and the reference are kept the same by supplying energy to them. The difference in the energy supplied is then plotted against temperature. Endothermic reactions within the sample result in more energy being supplied to the sample and are plotted as positive peaks. Exothermic reactions are represented by negative peaks. The DSC traces were analysed in terms of the onset temperature (determined from the first derivative of the peak) and the enthalpy change of the reaction, as measured by the area under the peak. The DSC results were interpreted in conjunction with TG and Hotstage Microscopy (HSM).

There are many factors or conditions that affect the TG and DSC results, *i.e.* the instrumental factors, including heating rate, furnace atmosphere, sample holder

geometry; the sample characteristics, including the sample mass, particle size, packing density and thermal conductivity. In order to ensure the reproducibility of the duplicated runs and to compare the results, the experimental conditions were kept constant and the samples were prepared in the same manner.

Both the programmed temperature TG and DSC analyses were carried out at a constant scanning rate of 10°C min^{-1} (unless otherwise stated) under a dry nitrogen gas purge with a flow rate of 30 cm^3 min^{-1}. The runs typically started at 30°C, and ended at temperatures chosen depending on the melting point, or the onset temperature of decomposition, of the host compound. Sample masses were typically between 2 and 8 mg. Samples were removed from the mother liquor, blotted dry on filter paper and crushed to a fine powder. The samples were held in an open platinum pan in TG and were placed in the crimped, vented aluminium pan with a lid in DSC.

Hotstage microscopy (HSM)

HSM was used as a visual method to observe the thermal behaviour of inclusion compounds during the heating process. It may be used to correlate thermal events measured using TG and DSC with the physical changes occurring in a crystal upon heating, such as polymorphic transitions, guest desorption, melting point, recrystallisation and so on. The guest desorption of the inclusion compounds may be detected by submerging the crystal in inert silicone oil and observing the evolution of the bubbles upon guest release. Another indication of guest loss is that a clear crystal turns opaque due to partial desolvation. The temperature at which any phenomenon is observed by the HSM may be correlated with the DSC onset temperature. The temperatures at which the changes were observed by HSM were often different from those measured in TG and DSC experiments. This is mainly due to particle size differences and the fact that the hot stage possesses an entirely different geometry from the TG and DSC. Generally large crystals were used (with diameters of 100 - 500 μm) as opposed to the powdered samples (10 - 100 μm).

The crystals of the inclusion compounds were subjected to heating on a Linkam TH600 hot stage mounted on a Nikon SMZ-10 microscope, on which a Sony Digital Hyper HAD colour video camera was mounted for simultaneous photography. The temperature was controlled by a Linkam CO600 temperature controller and can be raised at a linear rate. A heating rate of 10°C min^{-1} was used on all samples. The

photographs were captured and edited using program analySIS (Soft Imaging System GmbH, version 3.1).

Desolvation kinetic studies

Kinetics of desolvation of the inclusion compounds were studied using either isothermal methods or non-isothermal methods. Both methods employ TG techniques.

Isothermal TG was performed using the same Perkin Elmer PC series 7 system as the programmed TG under dry nitrogen gas purge with a flow rate of 30 cm^3min^{-1}. Samples were taken out from the mother liquor, dried between filter paper and crushed to very fine powder. A series of isothermal TG experiments were carried out at selected temperatures. The samples were rapidly heated to the selected temperature, which was then maintained until guest desorption was complete. The experiments were repeated at a series of different temperatures, which were chosen so that the total reaction time ranged typically from 0.5 to 18 hours and were usually lower than the onset temperature for the guest release, as obtained from the programmed TG experiments. Data obtained from these experiments were reduced to extent of reaction, α, versus time curves, and were fitted to various kinetic equations until appropriate models were determined (Brown, 1988). The extent of reaction, α, is described by $\alpha = (m_i - m_t) / (m_i - m_f)$, where m_i is the initial mass of the compound, m_f is the final mass and m_t is the mass at any time, t, during the mass loss process. Various kinetic models, of the form $f(\alpha) = kt$, were fitted to the α-time data using the program KINETIC, written by Barbour (1994). The kinetic model for which the function, $f(\alpha)$, was linear over the largest range of α was chosen as the best fit model. The judicious choice of the final equation should take into account both the correlation coefficient and the α range over which the model fitted (Byrn *et al.* 1999).

Details of the non-isothermal kinetic studies using programmed TG are described in the appropriate chapter.

X-ray powder diffraction (XRD)

XRD experiments were used in this study to monitor the phase changes during multiple desolvation of the inclusion compounds. They were carried out using a Philips vertical goniometer PW1050/80 with a Philips PW1394 motor control and PW1390 channel control. The X-rays were generated by a Philips PW1130/90 model operating at 40 kV and 20 mA. Using Nickel-filtered copper radiation (CuKα, λ = 1.5418Å), the powder patterns were collected over a 2θ range of 6 - 40°. The powdered samples were packed in an aluminium holder and step scans were recorded at 0.1° 2θ intervals and 1 second counts, unless otherwise specified in the text. Automatic receiving and divergence slits were used.

Experimental XRD patterns were compared with theoretically calculated XRD patterns to identify the crystalline phase. The calculated XRD patterns were produced using Lazy Pulverix (Yvon *et al.* 1977). In order to generate such an idealised X-ray powder pattern the cell parameters, space group symmetry, atomic scattering factors, atomic coordinates and thermal parameters of the appropriate crystal structure were used as input.

Competition experiment

Competition experiments were performed to determine the selectivity and tendency of the host to include various guests in a given set of guest mixtures. The compositions of guests were analysed using Gas Chromatography (GC).

All the competition experiments in this study were carried out in solution at room temperature. The total volume of guest solvents, which was used for each competition experiment, was kept to a minimum, so that crystals were obtained quickly without much evaporation of the mother liquor. An excess of all guests was always maintained. In general the host:guests mole ratio at values range from 1:15 to 1:30 were used.

In the case of the two-component competition experiments, a series of vials were made up of pairs of the liquid guests with mole fractions varying in steps of 10% or 20%. The appropriate host was added to the guest mixtures and warmed gently in order to dissolve the host. Slow cooling at room temperature produced crystals, usually after

one or two days. During the experimental process, the vials were always covered and sealed to prevent significant evaporation. The crystals were filtered, dried on filter paper and dissolved in chloroform in the case of the host **BINAP**, and in ethylacetate in the case of the host **DHPC**. These, as well as the mother liquors, were analysed by GC.

The results were plotted on a two-axis-chart. In this study three kinds of selectivity curves arose, as shown in **Figure 2.1**. X_{G1} is the mole fraction of guest **G1** in the liquid mixture and Z_{G1} that of guest **G1** which was enclathrated in the ensuing host-guest crystals. The diagonal line **a** represents null selectivity. The curve **b** ($\mathbf{b_1}$, $\mathbf{b_2}$, $\mathbf{b_3}$) occur when guest **G1** is preferentially selected over the other guest (**G2**) for the whole concentration range. Following Pivotar *et al.* (2001), a selectivity coefficient is defined as follow:

$$K_{G1:G2} = (K_{G2:G1})^{-1} = Z_{G1} / Z_{G2} * X_{G2} / X_{G1} \qquad (X_{G1} + X_{G2} = 1)$$

Thus $K_{G1:G2}$ = 1 yields line **a**, $K_{G1:G2}$ = 2, 8 and 32 yield curves $\mathbf{b_1}$, $\mathbf{b_2}$ and $\mathbf{b_3}$ respectively. The third kind of selectivity is represented by the sigmoidal curve **c** ($\mathbf{c_1}$, $\mathbf{c_2}$, $\mathbf{c_3}$), which results when the selectivity is concentration dependent. It was shown that the sigmoidal selectivity curve changed position depending on the extent of preference towards one of the guests by the host. The X_{G1} value of the point of intersection with the diagonal line is characteristic and is defined as the selectivity parameter, $Q_{G1:G2}$, for the specific sigmoidal curve. Thus curves $\mathbf{c_1}$, $\mathbf{c_2}$ and $\mathbf{c_3}$ have $Q_{G1:G2}$ = 0.3, 0.5 and 0.7 respectively. This parameter indicates that, when the initial starting mole fraction of **G1** is above this value ($Q_{G1:G2}$), **G1** is favoured otherwise **G2** is favoured.

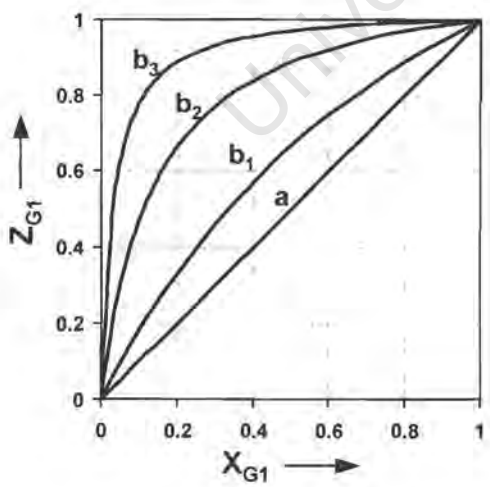

Curve	**a**	$\mathbf{b_1}$	$\mathbf{b_2}$	$\mathbf{b_3}$
$K_{G1:G2}$ =	1	2	8	32

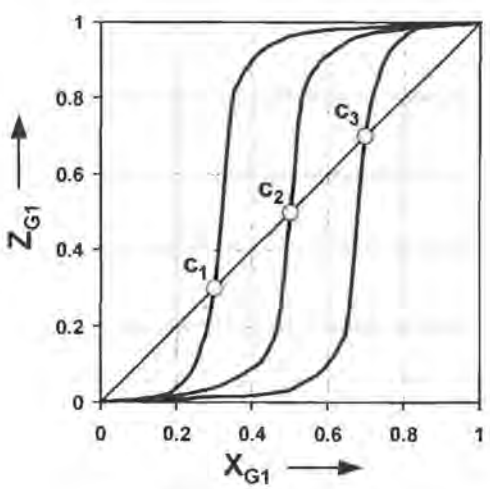

Curve	$\mathbf{c_1}$	$\mathbf{c_2}$	$\mathbf{c_3}$
$Q_{G1:G2}$ =	0.3	0.5	0.7

Figure 2.1 Two-component competition results between guests **G1** and **G2**. Curve **a** shows no selectivity. Curve **b** ($\mathbf{b_1}$, $\mathbf{b_2}$, $\mathbf{b_3}$) show preferential selectivity. Curve **c** ($\mathbf{c_1}$, $\mathbf{c_2}$, $\mathbf{c_3}$) show concentration dependent selectivity.

Nevertheless the experimental points sometimes deviated from the idealised curves shown in **Figure 2.1**. In such cases the selectivity coefficient K was averaged for all the points close to curve **b** and the selectivity parameter Q was calculated approximately for experimental results close to curve **c**.

In most cases, the two-component competition experiments were extended to analyse simultaneous competition by three guest components. The mole ratios of three components can be schematically shown on an equilateral triangle, as shown in **Figure 2.2**. The three apices represent 100% pure guest components **G1**, **G2** and **G3** respectively. The mole compositions of the starting mixtures are shown as dots within the inner triangle area and the results are shown by an arrow. In the example shown in the **Figure 2.2**, the dot shown is for a starting mixture with mole ratio 4:4:2 for **G1**:**G2**:**G3**, resulting in a final mixture with mole ratio 2:2:6 in the crystals. Representative experimental points of starting mixtures were chosen judicially, taking into account of the corresponding two-component competition results.

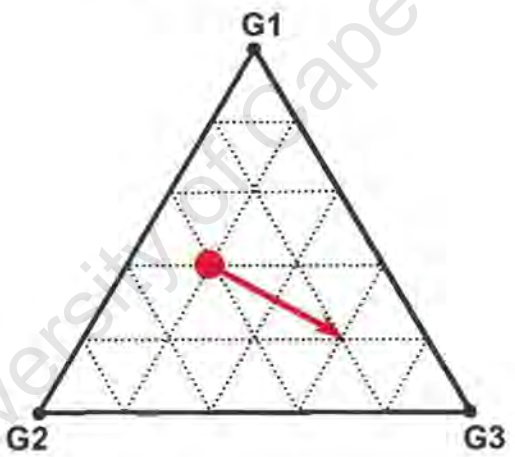

Figure 2.2 Three-component competition results between guests **G1**, **G2** and **G3**.

Gas chromatography (GC)

GC was employed in the competition experiments to analyse the relative percentages of various guests present in the mother liquor of the competition solutions and also in the ensuing inclusion crystals. Different Gas Chromatograph instruments and columns were used in this study. They are described as follows:

- Carlo Erba Fractovap 4200 instrument equipped with a Supelcowax Fused Silica Capillary Column (30 m, 0.20 mm LD, 0.20 μm film thickness), linked with a Spectra-Physics SP4290 integrator. This was used for the analyses of close isomers of xylidine.
- Varian 3400 Gas Chromatograph equipped with a polar carbowax capillary column (0.25mm in diameter, 25m in length) and linked to a Window98 computer system. The chromatograph was recorded and analysed using the program DELTA (version 5.0, 1998). This was used for the analysis of close isomers of picoline and lutidine.
- Philips PYE Unicam Series 304 Chromatograph equipped with a 10% OV101 on Chromosorp Packing Column (1m in length) and linked to a Waters 746 Data Module integrator. This was used in the competition experiments carried out between morpholine and 1,4-dioxane, THF and acetone.

For the analysis of the mother liquor from the competition experiments, a small amount of mother liquor was removed and diluted in an appropriate volatile solvent as described in the previous section and was injected into the GC column. For analysis of the guest components in the crystals, the crystals were removed from the mother liquor, thoroughly blotted dried on filter paper and dissolved in the same solvent used in the analysis of the mother liquor and then injected into the GC column. Each sample was analysed three times and the results averaged.

For each set of competition experiments, the GC column was calibrated by analysing a series of guest mixtures of known concentrations and the optimum operating condition was chosen so that the best separation was achieved.

The separation of 2,3-xylidine and 3,4-xylidine was not achieved on the columns available. Due to the close boiling points and polarities of the two components, a single peak appeared.

Lattice energy calculation

When interpreting the selectivity trend obtained from the competition experiments for a given set of guest compounds, lattice potential energies were evaluated for the appropriate host-guest systems. The lattice potential energy of a crystal structure is represented by a pairwise sum over atoms in different molecules. For all calculations, a representative of host and guest molecules was selected and appropriate summations were carried out for all intermolecular non-bonded interactions.

The empirical atom pair potentials were calculated using the program MPA (Williams, 1999), using a force field of the type

$$V(r) = \frac{ae^{-br}}{r^d} - \frac{c}{r^6}$$

where r is the interatomic distance and the coefficients a, b, c and d are those given by Gavezzotti (1998).

In addition a hydrogen bonding potential was incorporated into the calculations which is a simplified form of that given by Vedani and Dunitz (1985), and is expressed as

$$V_{hb} = \left(\frac{A}{R^{12}} - \frac{C}{R^{10}}\right)\cos^2\theta$$

where R is the distance between the hydrogen atom and the acceptor atom, θ is the donor–H···acceptor angle and the $\cos^2\theta$ term is the energy penalty paid by the bond for non-linearity. The constants A and C are related to the well-depth V_{min} and the equilibrium distance R_0 by $A = -5R_0^{12}V_{min}$ and $C = -6R_0^{10}V_{min}$.

In the case of the crystal structure being disordered, the potential energy contributions of each component of the disordered model was calculated separately, and the resultant energy was weighted according to the site occupancy factors refined in the structure solution and summed accordingly.

Crystal structure analysis

Preliminary unit cell parameters and space group symmetry were determined by X-ray photography for all inclusion compounds for which sufficiently good and relatively stable crystals had been grown. Oscillation and Weissenberg photographs were taken on a Stöe goniometers using nickel filtered Cu-K_α radiation (λ = 1.5418 Å).

For data collection, single crystals of suitable size (between 0.2 - 0.5mm in three dimensions) were selected based on their ability to extinguish plane polarised light uniformly. For the data collections carried out at room temperature (293K, 20°C), the crystals were mounted in Lindemann capillary tubes of internal diameter 0.3 or 0.5 mm, together with a drop of mother liquor to minimise deterioration of the crystal caused by guest desorption. Where the data collections were carried out at low temperature (173K, -100°C), the crystals were glued on glass fibres with Paratone N oil, bought from Exxon Chemical Co., TX, USA. If conditions permitted data collections were always carried out at low temperature. In the case of **BINAP** inclusion compounds with DMSO, the crystals cracked at low temperature, therefore the data collections were performed at room temperature.

For data collections at low temperature, the crystals were cooled and maintained at 173(2)K produced by a Cryostream cooler (Oxford Cryostreams) with a constant stream of nitrogen gas drawn up from a liquid nitrogen pool.

X-ray intensity data were collected on a Nonius Kappa-CCD diffractemeter using graphite-monochromated MoK_α radiation (λ = 0.7107 Å). The strategy for data collection was evaluated using the COLLECT software (1999). For all structures data were collected by the standard phi scan and omega scan techniques and were scaled and reduced using DENZO-SMN software (Otwinowski & Minor, 1997). Accurate unit cell parameters were refined on all data.

All structures were solved by direct methods using SHELXS-86 (Sheldrick, 1985) and refined employing full-matrix least-squares with the program SHELXL-97 refining on F^2 (Sheldrick, 1997). The program X-seed (Barbour, 1999a) was used as a graphical interface for structure solution and refinement using SHELX.

Direct methods yielded the positions of all non-hydrogen atoms in the asymmetric unit. Equivalent reflections were merged and those with $I < 2\sigma(I)$ were suppressed. Mean

$|E^2 - 1|$ (E is the normalised structure factor) were investigated to confirm the choice of space group determined from X-ray photography and intensity data, *i.e.* if $|E^2 - 1|$ is close to 0.968, the structure is centrosymmetric, and if $|E^2 - 1|$ is close to 0.736, the structure is acentric. Subsequent refinements by full-matrix least-squares were performed using SHELXL-97.

SHELXL-97 employs full-matrix least-squares refinement against F^2 for those reflections with $F > 4\sigma(F)$. Agreement between observed structure factors (F_o) and calculated structure factors (F_c) is expressed by the residual index, R. Since residual index for refinement against F^2, R_2, is larger than that for refinement against F, R_1, both the R-index factor based on F (R_1) and that based on F_2 (R_2) are quoted for comparison.

$$R_1 = \frac{\sum \| F_o | - | F_c \|}{\sum | F_o |}, \qquad wR_2 = \left[\frac{\sum w\left(F_o^2 - F_c^2\right)^2}{\sum w\left(F_o^2\right)^2} \right]^{1/2}$$

Where w is weighting scheme and was refined for each structure:

$$w = \frac{1}{\sigma^2\left(F^2\right)^2 + \left(aP\right)^2 + bP}$$

where $P = [\max(0, F_o^2) + 2F_c^2]/3$ and a, b were refined for each structure.

The Goodness of Fit (S) is based on F^2:

$$S = \left[\frac{\sum w(F_o^2 - F_c^2)^2}{n - p} \right]^{1/2}$$

where n is the number of reflections and p is the total number of parameters refined.

The program examines the analysis of variance and prints a warning that an extinction parameter, x, should be refined if S is significantly higher than unity. When necessary an extinction parameter x was refined by least-squares, where F_c is multiplied by:

$$[(1 + 0.001 \cdot x \cdot F_c^2 \cdot 3\chi) / \sin(2\theta)]^{-1/4}$$

The expression is empirical and covers both primary and secondary extinction.

Computing packages

Besides the program SHELXS for structure solution and SHELXL for structure refinement, a number of other programs are also included in the graphic interface software X-seed (Barbour, 1999a). Those of which were used in this study are listed here:

- Layer (Barbour, 1999b). This was used to investigate the systematic absences from the X-ray intensity data. It displays the intensity data as simulated procession photographs of all levels of the reciprocal lattice.
- XPrep (Version 5.1, 1997). This was used to determine or input the space group and set up SHELX input files. It was also used for unit cell transformations in the case of structures of both forms of **BINAP•1.5MOP**.
- Lazy Pulverix (Yvon *et al.* 1977). This was used to calculate the theoretical X-ray diffraction pattern following the procedure described in the previous section.
- Section (Barbour, 1999c). This was used to view the shapes and sizes of the voids in which the guest molecules were situated in the inclusion compound structure. After the guest molecules were removed from the crystal structure solution, the host molecules were viewed with atoms given their van der Waals radius. Using this program, a series of slices, which are all parallel to any chosen cell face, were presented by cutting the unit cell at selected intervals. This enables one to investigated the three dimensional shape of channels or cavities formed by the host molecules.
- PovRay. This was used to produce molecular structures and crystal packing diagrams for all the structures presented in this thesis.

In addition, the following programs, which are not included in X-seed, were also used for the analysis of crystal structures:

- Platon (Spek, version 10500) was used to calculate molecular parameters from results of crystal structure analyses.
- ConQuest (CCDC, version 1.3) was used to search the Cambridge Structural Database (CSD) for selected crystal structures which were used for comparison purposes.

3 INCLUSION COMPLEXES OF ALKALINE-EARTH METAL O,O'-DIBENZOYL TARTRATES

The inclusion complexes containing alkaline-earth metal salts of O,O'-dibenzoyl-(2R, 3R)-tartraric acid (magnesium, calcium and strontium) as host compounds (abbreviated as **DBTAM**), as shown in **Scheme 3.1**, are discussed in this chapter. For each inclusion complex, formed in the presence of 2-methoxyethanol, ethanol and water, results of the crystal structure in terms of structure solution, refinement and analysis, thermal analysis in terms of TG and DSC, and kinetics of desolvation, where applicable, are presented.

The crystal data, data collection and final refinement parameters are tabulated in **Table 3.7**, appearing at the end of this chapter. Final fractional atomic co-ordinates, temperature factors, table of bond length and angles, torsion angles and table of observed and calculated structure factors are contained in **Appendices**.

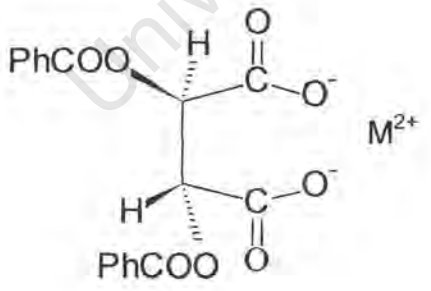

Scheme 3.1 The host **DBTAM**, M = Mg, Ca, Sr.

Preparation of the inclusion compounds

Magnesium (2R,3R)-(-)-di-o-benzoyl tartrate•2-methoxyethanol•ethanol•trihydrate (code: **MGDAME**):

(2R, 3R)-(-)-di-o-benzoyl tartaric acid (**DBTA**) was dissolved in 85 - 90% ethanol. Magnesium oxide was dissolved in the above solution by heating, followed by the addition of large excess of 2-methoxyethanol. The solution was cooled down to room temperature and allowed to stand. Colourless crystals appeared within a period of 24 hours.

Calcium (2R,3R)-(-)-di-o-benzoyl tartrate•di-2-methoxyethanol•monohydrate (code: **CADAME**) and Strontium (2R, 3R)-(-)-di-o-benzoyl tartrate•di-2-methoxyethanol•monohydrate (code: **SRDAME**):

Single crystals of the two inclusion complexes were prepared following a similar procedure described above, except calcium oxide and strontium oxide were substituted for magnesium oxide respectively.

Crystal structures

The preliminary cell parameters for each structure were determined by x-ray oscillation and Weissenberg photography. It was revealed that **MGDAME** belongs to the monoclinic crystal system (2/*m* Laue symmetry). The reflection condition *0k0: k = 2n* was observed, indicating the space group was either $P2_1$ or P2/m. Since the magnesium salt host molecule is chiral, the former space group $P2_1$ was chosen. This choice was vindicated by the successful refinement of the structure.

Oscillation and Weinssenberg photography showed that **CADAME**, as well as **SRDAME** belong to the orthorhombic crystal system (*mmm* Laue symmetry). For both structures, the reflection conditions

hkl:	*h+k = 2n*	*0kl:*	*k = 2n; (l = 2n)*
h0l:	*h = 2n; (l = 2n)*	*hk0:*	*h+k = 2n*
h00:	*h = 2n*	*0k0:*	*k = 2n*
00l:	*l = 2n*		

were observed, indicating the space group is $C222_1$. This choice was vindicated by the successful refinement for each structure.

The crystal structures are discussed in terms of structure solution, refinement and structure analysis. The molecular formula, space group, cell parameters, host:guest ratio and other crystallographic information are summarised at the beginning of the discussion of each inclusion compound. The structures of **CADAME** and **SRDAME** are isostructural and are discussed together.

MGDAME

$C_{18}H_{12}MgO_8 \cdot C_3H_8O_2 \cdot C_2H_6O \cdot 3H_2O$	
Guest: 2-methoxyethanol, ethanol and water	
Space group: $P2_1$	
a = 10.9056(5) Å	$\alpha = 90^o$
b = 11.4855(3) Å	$\beta = 105.09(3)^o$
c = 11.3693(5) Å	$\gamma = 90^o$
Volume = 1374.9(1) $Å^3$	
Z = 2	

Solution and refinement

Direct methods yielded the positions of all the non-hydrogen atoms of the magnesium salt host molecule. The guest non-hydrogen atoms were located in the difference electron density maps upon subsequent refinement, with the O atoms placed at the location of the highest peaks. The atomic numbering scheme is shown in **Figure 3.1**. The H atoms are numbered according to their parent atoms to which they are bonded, *e.g.* H(2) is bonded to C(2), H(1G) is bonded to O(1G), H(1G1) and H(1G2) are bonded to C(1G), H(1W1) and H(1W2) are bonded to O(1W) (of water molecule), and so on. The asymmetric unit contains one magnesium salt host molecule, one 2-methoxylethanol molecule, one ethanol molecule and three water molecules. They are all in general positions. This yields a host:guest ratio of 1:1:1:3, which was confirmed by the TG analysis (discussed in next section).

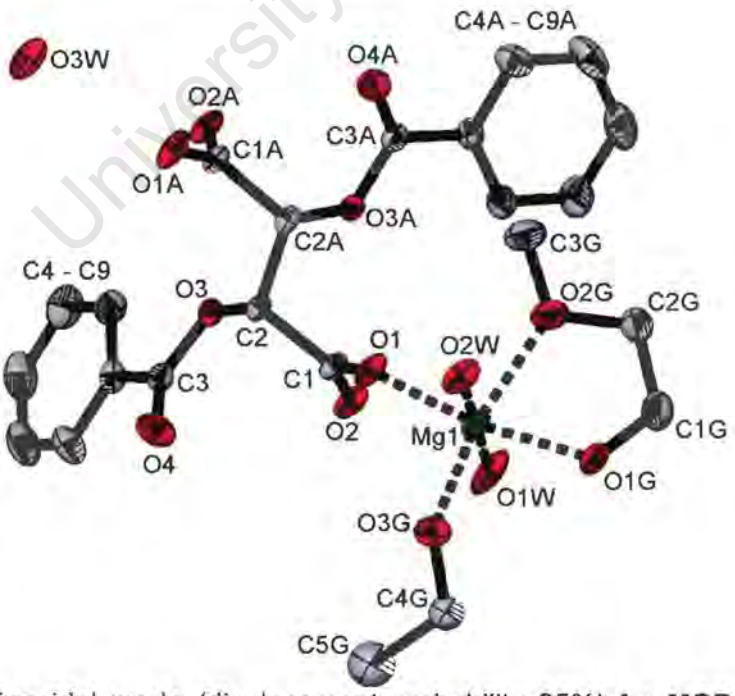

Figure 3.1 Ellipsoidal mode (displacement probability 35%) for **MGDAME**, showing the asymmetric unit and the atomic labelling scheme. The 2-methoxyethanol and ethanol guest molecules are shown without the disorder model. The H atoms are omitted for clarity.

Refinement was carried out with all of the non-hydrogen atoms treated anisotropically. The H atoms of water molecules and the hydroxyl hydrogen atoms of ethanol and 2-methoxyethanol molecules were independently located in the difference electron density maps, and refined with simple bond length constrains and individual temperature factors. The H atoms of the water molecules were confined with bond length d(O-H) = 0.97Å. The hydroxyl hydrogen atoms of ethanol and 2-methoxyethanol were restrained at a value of d(O-H) = 0.97 and 1.00Å respectively. These O-H bond lengths were obtained by extrapolation from a plot of O-H versus O···O distances for a large number of crystal structures (Olovsson & Jönsson, 1975). The rest of the H atoms were placed in geometrically constrained positions and refined with isotropic temperature factors assigned at 1.2 times the U_{eq} of the parent atoms, except those of the methyl hydrogen atoms which had U 1.5 times the U_{eq} of their parent atoms. Careful analysis of difference electron density maps showed that 2-methoxyethanol and ethanol molecules were partially disordered. Thus the final refinement employed the disorder model shown in **Figure 3.2**. The C(2G) atom of 2-methoxyethanol was disordered over two positions [C(2G) and C(2GA) with the fractional site occupancy factors of 0.75 and 0.25 respectively]. The disorder in the ethanol molecule was modelled with the two carbon atoms placed over two sites for each, with C(4G) and C(5G) at fractional site occupancies of 0.45, and C(4GA) and C(5GA) at 0.55. The site occupancy factors for these disordered atoms were linked and allowed to refine. The C atoms of ethanol molecule exhibit high thermal motion and were refined isotropically in the final refinement. The resultant bond lengths for the disordered molecules were as follows:

O(1G)-C(1G)	1.403(4) Å	C(1G)-C(2G)	1.434(6) Å
C(1G)-C(2GA)	1.58(2) Å	C(2G)-O(2G)	1.505(6) Å
C(2GA)-O(2G)	1.32(2) Å	O(2G)-C(3G)	1.411(4) Å
O(3G)-C(4G)	1.432(8) Å	C(4G)-C(5G)	1.49(2) Å
O(3G)-C(4GA)	1.41(1) Å	C(4GA)-C(5GA)	1.57(2) Å

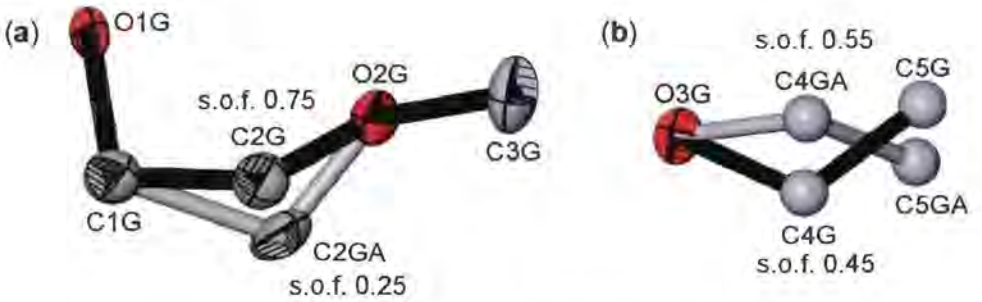

Figure 3.2 Disorder modelled in (a) 2-methoxyethanol and (b) ethanol guest molecule in **MGDAME**. All the H atoms are omitted for clarity. Ellipsoidal displacements are drawn at 35% probability level.

The **MGDAME** structure refined successfully to R_1 = 0.0366. All bond lengths and angles are in acceptable ranges (Allen *et al.* 1992).

Structure analysis

In the crystal structure of **MGDAME**, the magnesium ion is surrounded by six oxygen atoms: two from water molecules, two from the 2-methoxyethanol, one from ethanol and one from the ionised carboxyl group of a neighbouring host molecule. The coordinated oxygen atoms form an irregular octahedron, shown in **Figure 3.3**, and the parameters describing the coordination geometry, of bond lengths and angles, are given in **Table 3.1**. The Mg^{2+}-O bond between Mg^{2+} and the ionised carboxyl group of the tartrate host molecule is 2.013(2)Å in length, while the rest of Mg^{2+}-O bonds lie in the range 2.029(2)Å to 2.189(3)Å. These values compare well with those of similar hexa-coordinated Mg^{2+} complexes contained in CSD (2001, version 5.22).

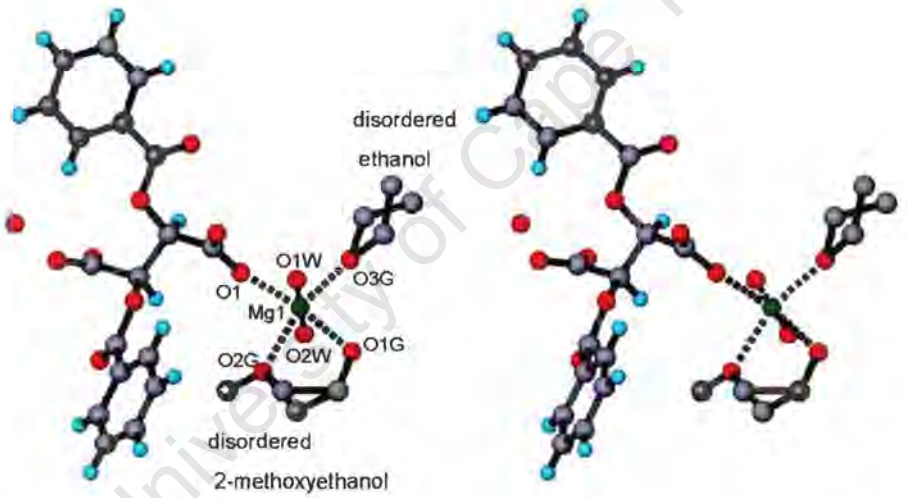

Figure 3.3 Stereoscopic view of **MGDAME**, showing molecular structure and coordination geometry. The coordination bonds are shown as broken lines. Only H atoms of the host molecule are shown.

Table 3.1 Parameters describing the Mg^{2+}-O coordination geometry.

Mg(1) -	Distance (Å)	Angles (°)				
O(1)	2.013(2)					
O(1W)	2.029(2)	89.27(9)				
O(2W)	2.035(2)	90.97(9)	179.1(1)			
O(1G)	2.054(2)	168.6(1)	89.0(1)	90.9(1)		
O(3G)	2.059(2)	101.6(1)	93.5(1)	85.7(1)	89.73(9)	
O(2G)	2.189(2)	93.24(9)	93.6(1)	87.2(1)	75.67(9)	163.7(1)
	Mg(1) -	O(1)	O(1W)	O(2W)	O(1G)	O(3G)

Note: A ideal octahedral geometry has twelve 90° and three 180° in bond angles <O-M-O.

CADAME

$C_{18}H_{12}CaO_8 \cdot 2C_3H_8O_2 \cdot H_2O$	
Guest: 2-methoxyethanol and water	
Space group: $C222_1$	
a = 9.1946(2) Å	$\alpha = 90^\circ$
b = 14.0300(3) Å	$\beta = 90^\circ$
c = 20.8925(5) Å	$\gamma = 90^\circ$
Volume = 2695.1(1) Å^3	
Z = 4	

SRDAME

$C_{18}H_{12}SrO_8 \cdot 2C_3H_8O_2 \cdot H_2O$	
Guest: 2-methoxyethanol and water	
Space group: $C222_1$	
a = 9.2324(1) Å	$\alpha = 90^\circ$
b = 14.3012(2) Å	$\beta = 90^\circ$
c = 20.9313(3) Å	$\gamma = 90^\circ$
Volume = 2763.7(1) Å^3	
Z = 4	

Solution and refinement

Direct methods yielded all the non-hydrogen atoms in the asymmetric unit. The atomic numbering scheme is shown in **Figure 3.7**. The asymmetric unit comprises half a Ca/Sr metal salt host molecule, one 2-methoxyethanol and half a water molecule. The host molecule exhibits two-fold symmetry and was placed with the central C-C bond of the tartrate molecule and the metal ion on a special position, located on a diad at Wyckoff position *b* [(0,y,¼) and (0,-y,¾)]. The water molecule was also placed with the oxygen atom on a diad at Wyckoff position *b*. Thus each unit cell has four metal salt host molecules, eight 2-methoxyethanol and four water guest molecules. It yields a host:guest ratio of 1:2:1, which was confirmed by the TG analysis (discussed below). Refinement was carried out with all the non-hydrogen atoms treated anisotropically. The aromatic and -CH group hydrogen atoms on the tartrate host molecule and the methylenic and methyl hydrogen atoms on the 2-methoxyethanol guest molecule were geometrically constrained and assigned common isotropic temperature factors for similar groups. The H atoms of water molecule and the hydroxyl hydrogen atoms of 2-methoxyethanol molecules were independently located in the difference electron density maps and refined with simple bond length constraints and individual temperature factors. The final R factors are 0.0363 and 0.0229 for **CADAME** and **SRDAME** respectively.

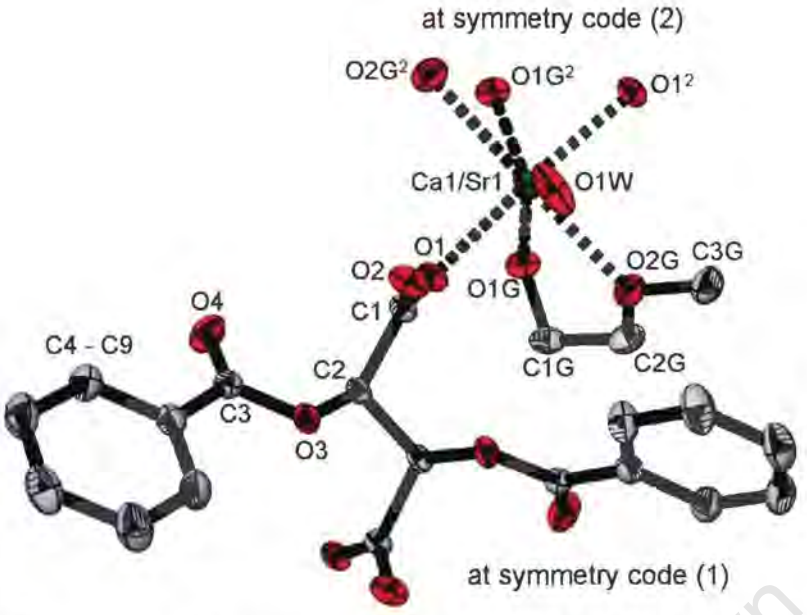

Figure 3.7 The asymmetric unit in **CADAME** and **SRDAME**, showing the atomic labelling scheme. Ellipsoidal displacements are drown at 40% probability level. The symmetry codes are (1) 3-x, y, 1/2-z and (2) 2-x, y, 1/2-z. The picture is extracted from **CADAME**.

Structure analysis

The structures of **CADAME** and **SRDAME** are isostructural. In the structures, the Ca^{2+}/Sr^{2+} metal ion is surrounded by seven oxygen atoms and is best described as having the geometry of a capped trigonal prism (**Figure 3.8**). Each Ca^{2+}/Sr^{2+} ion, located on a diad, is bonded to four oxygens from two 2-methoxyethanol molecules which are symmetry related, one oxygen of water molecule which lies on the diad and two oxygens from the ionised carboxyl moieties derived from adjacent host molecules. The two carboxyl groups on the host act as bridging ligands linking the metal centre running along the direction [100] (**Figure 3.9**). The Ca^{2+}/Sr^{2+}-O bond lengths are given in **Table 3.3**. The Ca^{2+}-O bond lengths vary from 2.337(1)Å to 2.514(1)Å, similar to those found in the structure of O,O'-dibenzoyl tartaric acid with Ca^{2+} and tetrahydrofurane carboxylate (Mravik *et al.* 1997). In the latter structure, however, the Ca^{2+} ion is described as exhibiting pentagonal bipyramidal coordination geometry. The Sr^{2+}-O bond lengths lie in the range 2.460(1)Å to 2.625(1)Å.

Table 3.3 Ca/Sr-O (M-O) bond lengths (Å) for **CADAME** and **SRDAME**.

	M-O(1) / M-O(1)[1]	M-(O1G) / M-O(1G)[1]	M-O(2G) / M-O(2G)[1]	M-O1W
CADAME	2.337(1)	2.432(1)	2.514(1)	2.356(2)
SRDAME	2.460(1)	2.562(2)	2.625(1)	2.511(2)

Symmetry code: (1) *-x+2, y, -z+1/2*

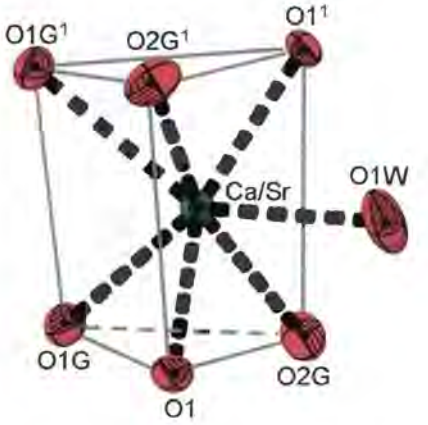

Figure 3.8 The capped trigonal prismatic coordination geometry of Ca^{2+}/Sr^{2+} in **CADAME** and **SRDAME**. The picture is extracted from **CADAME**.

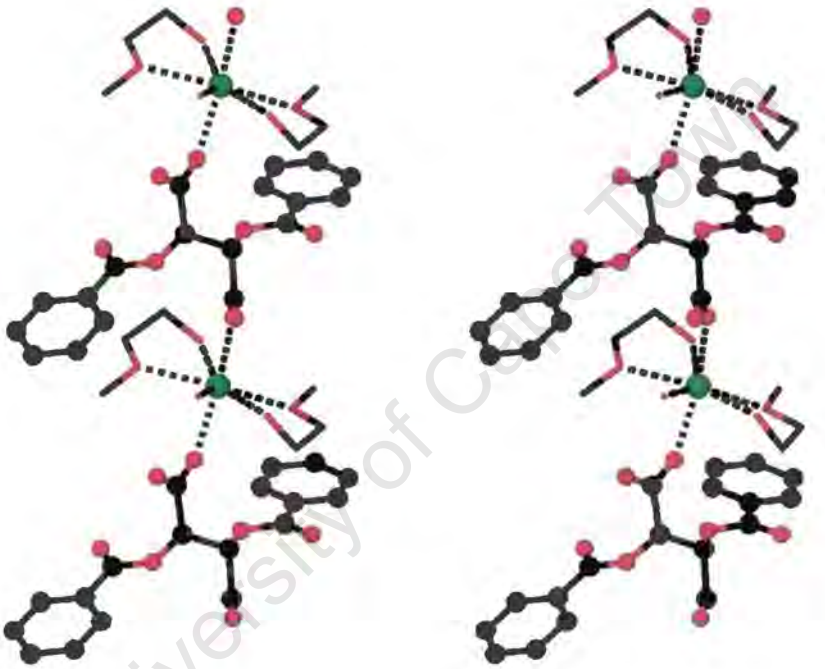

Figure 3.9 Stereoscopic view for **CADAME**, showing that a chain of host (in ball-and-stick representation) and guest (in stick representation) molecules formed via coordination bonds are running along [100]. All hydrogen atoms are omitted for clarity.

Intermolecular hydrogen bonds of O-H···O exist between the 2-methoxyethanol-water guest molecules and the tartrate host molecules. Details of the hydrogen bonding interactions are given in **Table 3.4**. The hydroxyl group of 2-methoxyethanol is hydrogen bonded to the carboxylic oxygen O(2) [d(O···O) = 2.651(2)Å] and to the ester oxygen O(3) [d(O···O) = 3.209(2)Å] within the same host molecule. The hydrogen bonds link the coordinated metal centre in the directions of [100] and [010], resulting in the formation of two-dimensional network of host and guest molecules that lie parallel to the (001) plane. The two-dimensional networks, which cut at the c axis at 0.25 and

0.75, are related by rotation through 180°, followed by translation of half a unit cell length along c. The projection down [001] of the network at c = 0.25 are shown in **Figure 3.10a**. The tartrate host molecules stack along [001] in multiple hydrogen bonding networks in such a way that generate channels running along [001] in which the 2-methoxyethanol-water guest molecules as well as the Ca^{2+}/Sr^{2+} ions are situated (**Figure 3.10b**). More crystal packing diagrams are shown in **Figure 3.11** and **3.12**.

Table 3.4. Hydrogen bonding details for **CADAME** and **SRDAME**.

	O-H···O	d(O-H) /Å	d(O···H) /Å	<OHO (°)	d(O···O) /Å
CADAME	O(1W)-H(1W)···O(2)	0.91(2)	1.96(2)	148(2)	2.766(1)
	O(1G)-H(1G)···O(2)^{1}	0.95(2)	1.80(2)	154(2)	2.691(2)
	O(1G)-H(1G)···O(3)^{1}	0.95(2)	2.62(2)	122(3)	3.233(2)
SRDAME	O(1W)-H(1W)···O(2)	0.91(2)	2.05(2)	141(2)	2.825(2)
	O(1G)-H(1G)···O(2)^{1}	0.93(1)	1.76(1)	158(2)	2.651(2)
	O(1G)-H(1G)···O(3)^{1}	0.93(1)	2.64(3)	120(2)	3.209(2)

Symmetry code: (1) *-x+5/2, y-1/2, -z+1/2*.

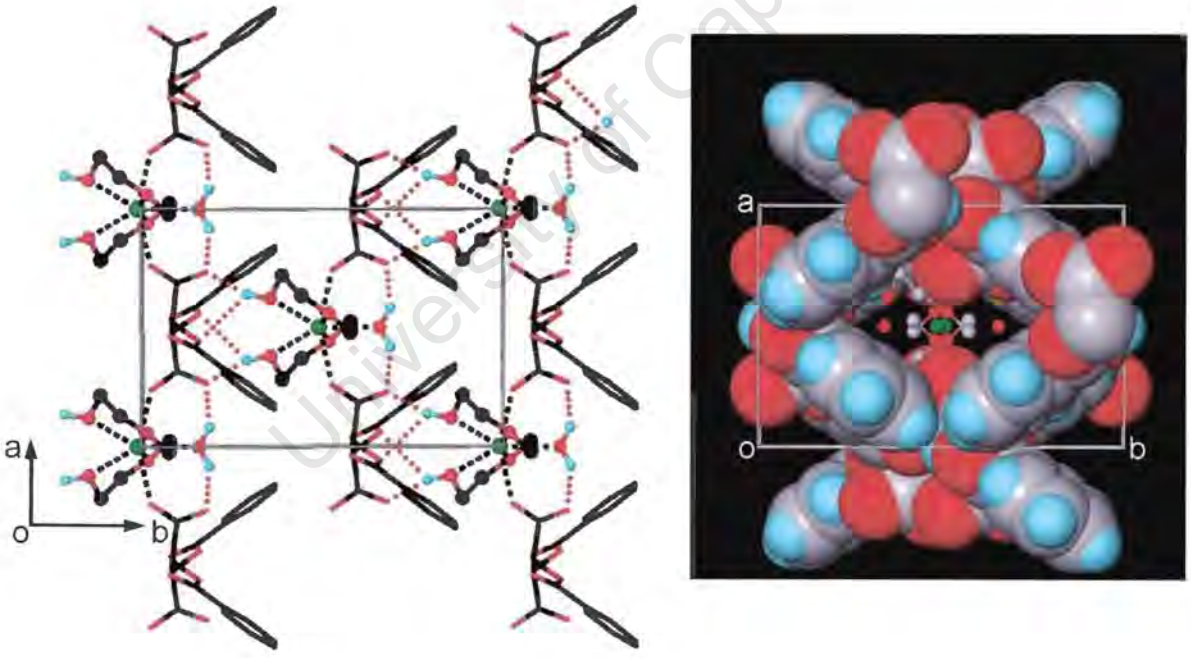

(**a**) (**b**)

Figure 3.10 CADAME viewed along [001]. (a) Single layer at c = 0.25 showing the two-dimensional hydrogen bonding network. The tartrate host atoms are in stick representation. The guest atoms and Ca^{2+} ion are shown as balls. Only hydrogen atoms involving in hydrogen bonds are shown. (b) Space-filling representation with multiple layers, showing the top view of the channel. The tartrate host molecules are shown in van der Waals radii. The guest and Ca^{2+} ion are in ball-and-stick representation with H atoms omitted.

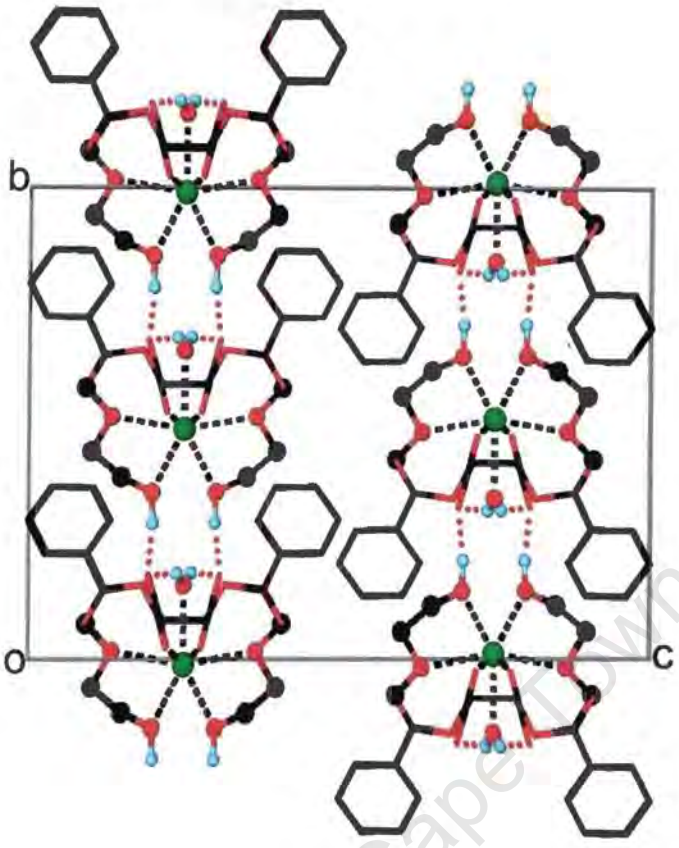

Figure 3.11 Projection viewed down [100] extracted from structure **SRDAME**. The hydrogen bond O(1G)-H(1G)···O(3) is not indicated since it overlaps with O(1G)-H(1G)···O(2). Other picture drawing details as in **Figure 3.10a**.

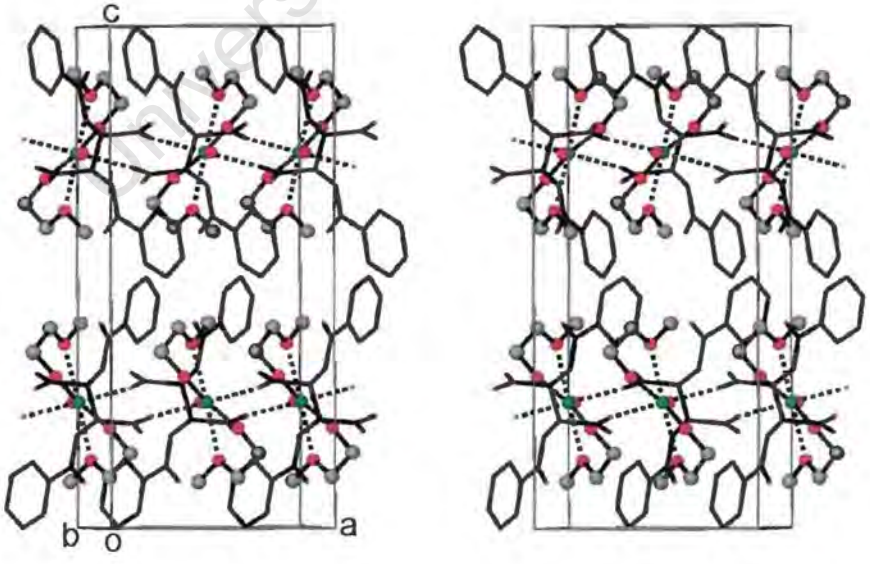

Figure 3.12 Stereo view along [010], extracted from **CADAME**. All H atoms are omitted for clarity. Other details as in **Figure 3.11**.

Thermal analysis and Evolved Gas Analysis

Thermal analysis results of **MGDAME**, **CADAME** and **SRDAME** are shown in **Figure 3.13**. The TG and DSC traces showed similar features for all of the three inclusion compounds. The TG shows a two-step decomposition. The percentage mass loss of the first step corresponds to the first endothermic peak of the DSC curve, and is associated with the total mass loss of guest molecules. The second decomposition step, however, corresponds to an exothermic peak in the DSC, and could not, at first, be interpreted. Therefore Evolved Gas Analysis (EGA) for **CADAME** was carried out. The sample was send to Professor M. E. Brown's laboratory at Rhodes University, South Africa, and thermal analysis was done under the same condition as in the TG run, but recorded the IR spectrum of the gases evolved during the decomposition. The IR spectrum corresponding with the first decomposition step is shown in **Figure 3.14a**, and that corresponding with the second step is shown in **Figure 3.14b**. The first spectrum clearly shows all the features of the 2-methoxyethanol guest, in that the stretching modes, ν(O-H), ν(C-H) and ν(C-O), as well as the bending δ(C-H) are clearly present (Pouchert, 1990). In the second spectrum, the bands for CO_2 stretch and CO_2 bend are clearly identified (Atkins, 1998), showing that CO_2 is a decomposition product of the host. This explains the presence of the exotherm on the DSC, and the mass loss of the second step. The decomposition of **CADAME** was followed by hot stage microscopy, with similar results observed for **MGDAME** and **SRDAME**. This is shown in **Photo 3.1**. During the first step the translucent crystal evolves gas bubbles between 150°C and 190°C and turns opaque white. The bubbling is resumed in the second step at about 200°C and the crystal turns brown. This second decomposition step of host proceeds up to 550°C and produces a dark brown residue. The relevant TG and DSC data are given in **Table 3.5**.

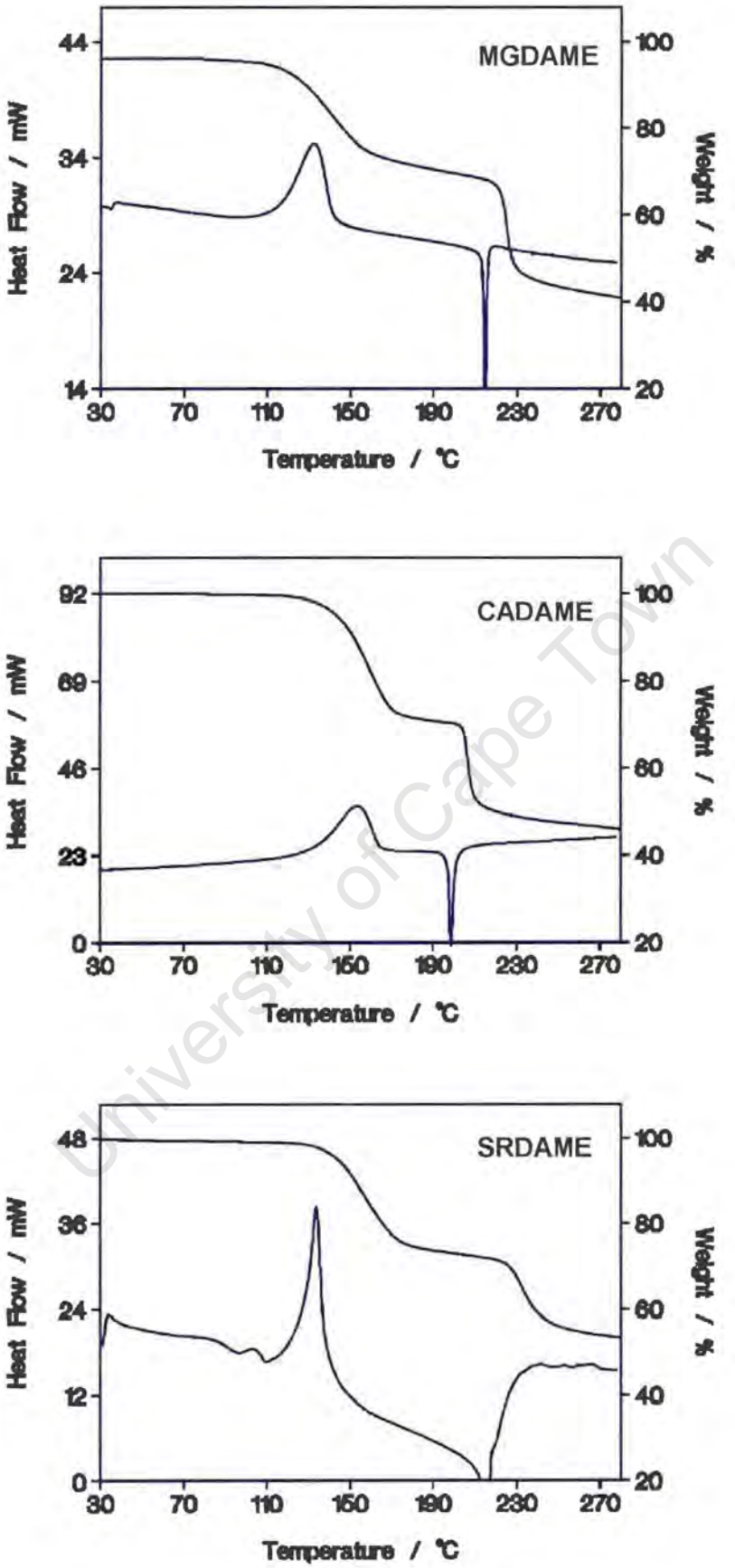

Figure 3.13 TG and DSC traces.

Table 3.5 TG and DSC results for the inclusion compounds of earth-metal tartrate.

Reaction*		TG			DSC	
		Temp. range (°C)	Exp. mass loss (%)	Calc. mass loss (%)	Onset temp. T_{on} (°C)[&]	ΔH (kJ mol^{-1})
1st step	**MGDAME** → $C_{18}H_{12}MgO_8$ + $C_3H_8O_2\uparrow$ + $C_2H_5O\uparrow$ + $3H_2O\uparrow$	100 - 209	30.5	31.65	117.2	159.2
2nd step	Decomposition of $C_{18}H_{12}MgO_8$	-	-	-	211.5	-48.3
1st step	**CADAME** → $C_{18}H_{12}CaO_8$ + $2C_3H_8O_2\uparrow$ + $H_2O\uparrow$	110 - 200	29.5	30.04	139.2	146.3
2nd step	Decomposition of $C_{18}H_{12}CaO_8$	-	-	-	202.8	-44.3
1st step	**SRDAME** → $C_{18}H_{12}CaO_8$ + $2C_3H_8O_2\uparrow$ + $H_2O\uparrow$	110 - 210	27.2	27.72	127.4	132.4
2nd step	Decomposition of $C_{18}H_{12}SrO_8$	-	-	-	214.6	-41.3

* $C_{18}H_{12}MO_8$: Metal salt of O, O'-dibenzoyl tartaric acid (Mg, Ca, Sr)
$C_3H_8O_2$: 2-Methoxyethanol
C_2H_5O: Ethanol
H_2O: Water

& For comparison purpose, the boiling points (T_b) of the pure guest solvents are quoted here as follows:
2-methoxyethanol: T_b = 124.4°C
ethanol: T_b = 78.5°C
water: T_b = 100°C

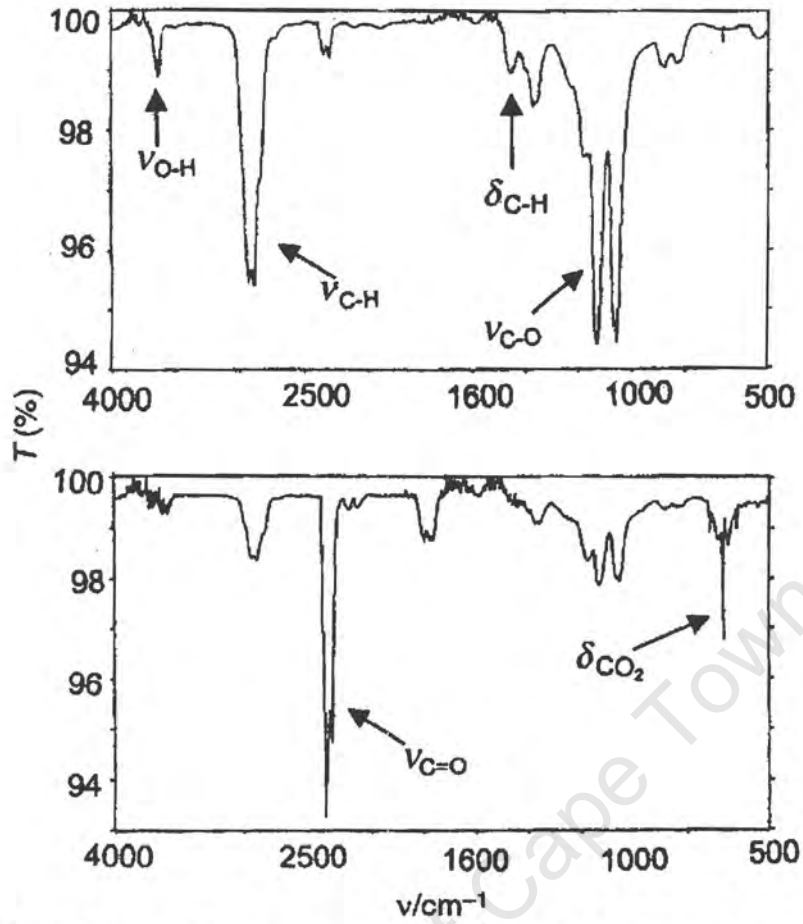

Figure 3.14 IR spectra recorded for the first (a) and second (b) decomposition steps for **CADAME**.

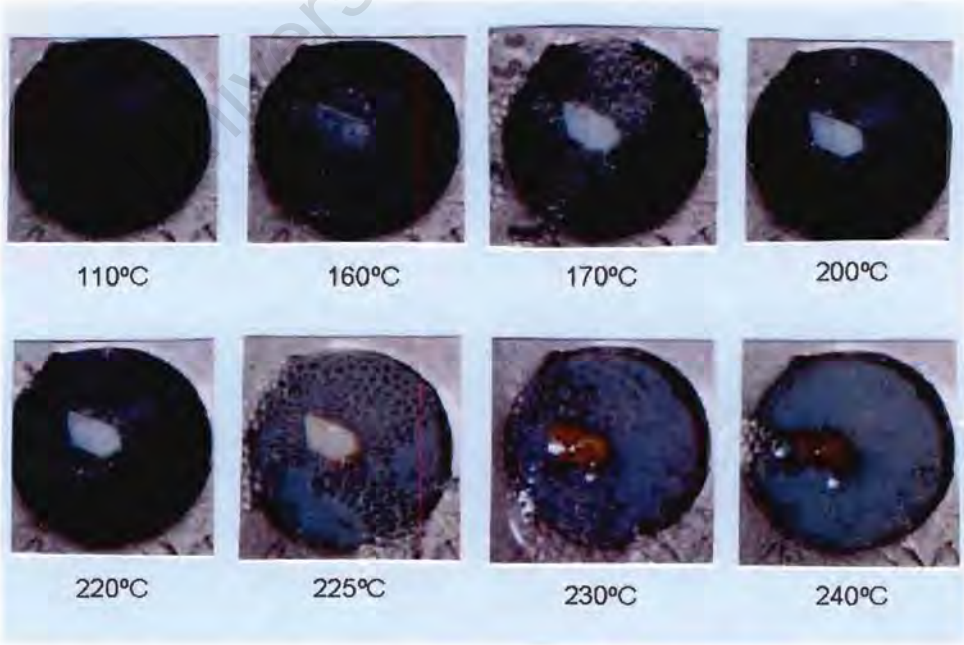

Photo 3.1 HSM photographs of a crystal of **CADAME** immersed in silicon oil at a constant heating rate of 10°C min^{-1}. The size of the crystal is about 0.5 x 0.4 x 0.1mm.

Kinetics of desolvation

The kinetics of the first step decomposition reaction, which corresponding to the release of the guest molecules from the metal salts of dibenzoyl tartaric acid host molecules, for complexes **MGDAME** and **CADAME** were investigated. The data were obtained from a series of isothermal TG experiments over a temperature range of 95°C to 135°C. The mass loss versus time curves were converted to the extent of reaction, α, versus time curves. The typical α-time curves for both compounds are illustrated in **Figure 3. 15**. For **MGDAME**, the α-time curves were best described by the first order kinetic law F1: $-\ln(1-\alpha) = kt$, over an α range of 0.10 to 0.90. The Arrhenius plot of ln *k versus* 1/T yields 128(10)kJ mol^{-1} as the activation energy (E_a) and 38(4) as the logarithm of pre-exponential factor (ln A) over the temperature range of 95°C to 130°C. For **CADAME**, the α-time curves show the desolvation process to be deceleratory and the data at an α range of 0.10 to 0.90 best fitted the equation corresponding to the contracting volume mechanism (R3): $1-(1-\alpha)^{1/3} = kt$. The plot of ln *k versus* 1/T yields E_a = 133 (6) kJ mol^{-1} and ln A = 35.9(2) over the temperature range of 95°C to 135°C. The Arrhenius plots for the first step decomposition reactions for **MGDAME** and **CADAME** are shown in **Figure 3.16**.

Table 3.6 Kinetic parameters for the first step desolvations of **MGDAME** and **CADAME**.

Reaction*	Temp. range (°C)	α range	Kinetic model	E_a (kJ mol^{-1})	ln A
MGDAME → $C_{18}H_{12}MgO_8$ + $C_3H_8O_2\uparrow$ + $C_2H_5O\uparrow$ + $3H_2O\uparrow$	95 - 130	0.1 - 0.9	F1	128(10)	38(4)
MGDAME → $C_{18}H_{12}MgO_8$ + $2C_3H_8O_2\uparrow$ + $H_2O\uparrow$	90 - 135	0.1 - 0.9	R3	133(6)	35.9(2)

* $C_{18}H_{12}MO_8$: Metal salt of O, O'-dibenzoyl tartaric acid (Mg, Ca, Sr)
$C_3H_8O_2$: 2-Methoxyethanol
C_2H_5O: Ethanol
H_2O: Water

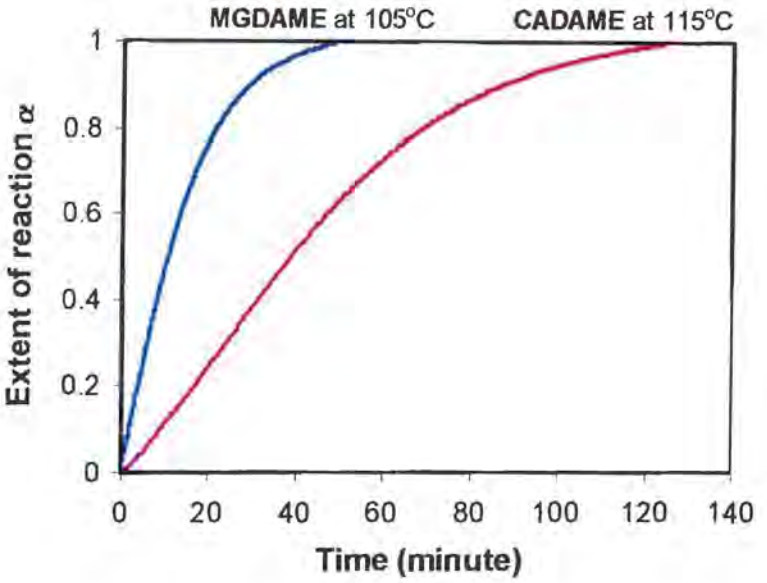

Figure 3.15 α-time curves of the first step desolvation of **MGDAME** at 105°C and **CADAME** at 115°C.

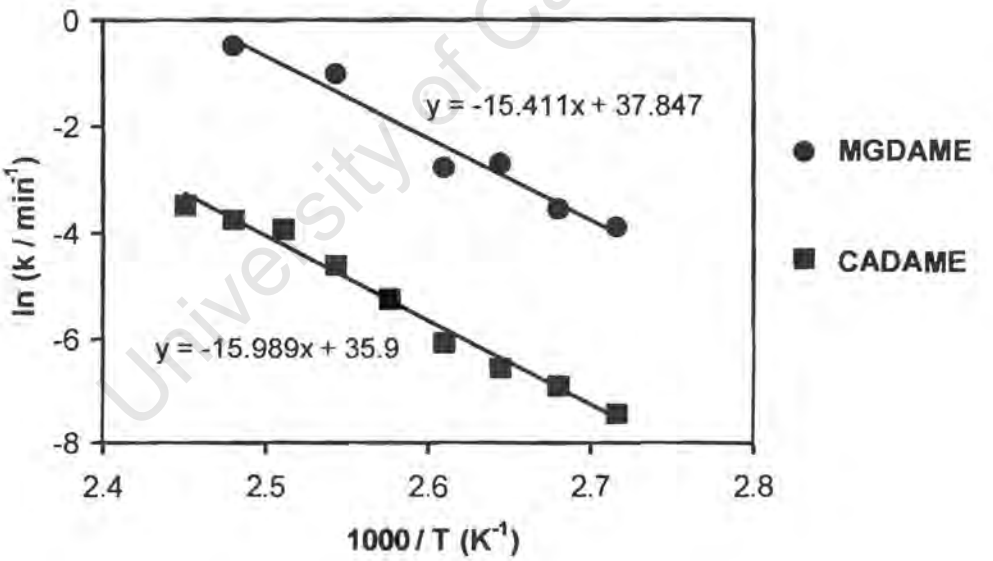

Figure 3.16 Arrhenius plots of ln *k versus 1/T* for the first step desolvation reactions of **MGDAME** and **CADAME**.

Discussion

The coordination complexes with guests, such as 2-methoxyethanol, water or ethanol which contain oxygen atoms with a lone pair of electrons, were discussed in this chapter. Despite being crystallised under virtually identical conditions, the calcium and strontium salt of O,O'-dibenzoyl tartaric acid, the so-called host molecules, coordinated to 2-methoxyethanol and water guest molecules, whereas the magnesium salt coordinated to ethanol, 2-methoxyethanol and water. In the structure of **MGDAME**, the Mg^{2+} ion forms an irregular octahedral coordination with 6 oxygens. This is the most favoured coordination geometry by Mg^{2+} ion, with approximately 90% of the 245 magnesium complexes retrieved from the CSD (Version 5.22, 2001) found in this geometry. In both structures of **CADAME** and **SRDAME**, the Ca^{2+}/Sr^{2+} ion coordinates to 7 oxygens with capped trigonal prismatic geometry. The factors that affect the natural coordination preferences of the metal are complicated, but it is noted that the increased coordination number in the Ca^{2+} / Sr^{2+} salts correlates with their larger ionic radii.

MGDAME crystallise in the space group $P2_1$ with Z = 2. Extensive hydrogen bonds, which form between the carboxyl moiety of the host and hydroxyl group of water/ethanol molecules, link the Mg^{2+} metal centre, resulting in the formation of two dimensional network perpendicular to the c axis. The structures of **CADAME** and **SRDAME** are isostructural. They both crystallise in the orthorhombic space group $C222_1$ with Z = 4. Their cell dimensions are all similar with the c axis of **SRDAME** being about 0.27Å longer which renders the volume of unit cell of **SRDAME** 68.5Å^3 larger. This is mainly due to the ionic radius of Sr^{2+} being larger than that of Ca^{2+}. In both structures, the carboxyl moieties of the host molecules act as bridging ligands linking the coordination metal centre along the direction [100]. The coordination bonds, as well as the hydrogen bonds that formed between the host and methoxyethanol/water molecules generate two two-dimensional networks perpendicular to [001]. All of the three structures are characterised by columns of guest molecules and metal ions located in channels, running parallel to one of the cell axes, as a result of the stacking of the dibenzoyl tartrate moiety of host molecules around the metal centre.

Thermal analysis (TG and DSC) and EGA results show that the three complexes lose all their guest species in an single endothermic step, followed by the exothermic decomposition of metal salts, which give rise to CO_2 as product. The desolvation of guests began at a higher temperature than the boiling points of the pure guests, with

MGDAME being an exception with regard to the 2-methoxyethanol guest (T_{on} - T_b = -7.2°C, see **Table 3.5**). The onset temperatures of guests release obtained form DSC run are also indicative of the relative thermal stabilities for the three complexes, where the guests desorb at about 94.3°C, 63.6°C and 87.2°C before the onset of decomposition of the metal salt host, for **MGDAME**, **CAMADE** and **SRDAME** respectively.

The desolvation of **MGDAME** follows the first order F1 mechanism. There is no physical explanation for reactions based on order with respect to α, since concentration is not usually a meaningful term in solid state reaction (Brown *et al.* 1980). The desolvation of **CADAME**, on the other hand, follows the contracting sphere kinetic model R3. Activation energies were calculated to be 128(10) and 133(6) kJ mol^{-1} for the desolvation of **MGDAME** and **CADAME** respectively. From the crystal structure analysis, we know that the guest molecules are all located in channels in both structures. This channel topology implies no severe physical barriers to the escape of the gaseous guest molecules, except for coordination bonds and hydrogen bonds. These values also compare well with activation energies obtained for the decomposition reactions of various metal-ligand complexes (Coetzee, 1996; Bourne *et al.* 2001).

Table 3.7 Crystal data, data collection and final refinement parameters.

Inclusion compound	**MGDAME**	**CADAME**	**SRDAME**
Molecular formula	$C_{18}H_{12}MgO_8$• $C_3H_8O_2$•C_2H_6O•$3H_2O$	$C_{18}H_{12}CaO_8$• $2C_3H_8O_2$•H_2O	$C_{18}H_{12}SrO_8$• $2C_3H_8O_2$•H_2O
Guest	2-Methoxyethanol Ethanol and water	2-Methoxyethanol Water	2-Methoxyethanol water
Formula weight (g mol^{-1})	556.80	566.65	614.10
Crystal Data			
Crystal system	Monoclinic	Orthorhombic	Orthorhombic
Space group	$P2_1$	$C222_1$	$C222_1$
a (Å)	10.9056(5)	9.1946(2)	9.2324(1)
b (Å)	11.4855(3)	14.0300(3)	14.3012(2)
c (Å)	11.3693(5)	20.8925(5)	20.9313(3)
α (°)	90	90	90
β (°)	105.09(3)	90	90
γ (°)	90	90	90
Volume ($Å^3$)	1374.9(1)	2695.1(1)	2763.7(1)
Z	2	4	4
Calculated density D_c (gcm^{-3})	1.345	1.396	1.476
μ (mm^{-1})	0.132	0.298	2.014
F(000)	588	1192	1264
Data collection			
Temperature (K)	293 (2)	293 (2)	293 (2)
Range scanned, θ (°)	3.01 – 26.40	2.82 - 28.26	2.03 - 25.94
Range of indices, *h*, *k*, *l*	0,13/0,14/-14,13	±12/±18/±27	±12 / ±18 / ±27
No. of measured reflections	7977	12412	10946
No. of unique reflections	2948	3341	3299
No. of reflections observed with $I > 2\sigma(I)$	2465	2775	3114
R_{int}	0.033	0.033	0.023
Structure refinement			
Data / restraints / parameters	2948 / 11 / 388	3341 / 4 / 186	3299 / 4 / 186
R indices R_1 / wR_2 [$I > 2\sigma(I)$]	0.0366 / 0.0914	0.0363 / 0.0732	0.0229 / 0.0541
R_1 / wR_2 (all data)	0.0470 / 0.0949	0.0516 / 0.0780	0.0256 / 0.0552
Goodness of fit on F^2, S	1.008	1.042	1.080
Weighting scheme [where $P = (F_o^2+2F_c^2)/3$]	$W = 1/[\sigma^2(F_o^2)+(0.0666P)^2+0.0000\ P]$	$w = 1/[\sigma^2(F_o^2)+(0.0351P)^2+0.2884P]$	$w = 1/[\sigma^2(F_o^2)+(0.025P)^2+1.1496P]$
Max. / Mean shift (esd)	0.086 / 0.005	0.001 / 0.000	0.001 / 0.000
Flack x parameter	0.1(3)	-0.01(3)	0.010(6)
Extinction coefficient	0.001(4)	0.0006(5)	0.0000(3)
Max./Min. height in difference electron density map (e $Å^{-3}$)	0.185 / -0.221	0.207 / -0.167	0.205 / -0.278

4 INCLUSION COMPOUNDS OF DHPC AND XYLIDINES WITH VARIOUS STOICHIOMETRIES

The inclusion compounds, formed between the host **DHPC** and a number of close isomers of xylidine (see **Scheme 4.1**) at various crystallisation temperatures, gave rise to differing stiochiometries. Their thermal characteristics, crystal structures, selectivities of enclathration, lattice energy calculation and kinetics of desolvation are discussed in this chapter.

The crystal data, data collection experimental and final refinement parameters are contained in **Table 4.13** appearing at the end of this chapter. Final fractional atomic co-ordinates, temperature factors, table of bond length and angles, torsion angles and table of observed and calculated structure factors are contained in **Appendices**.

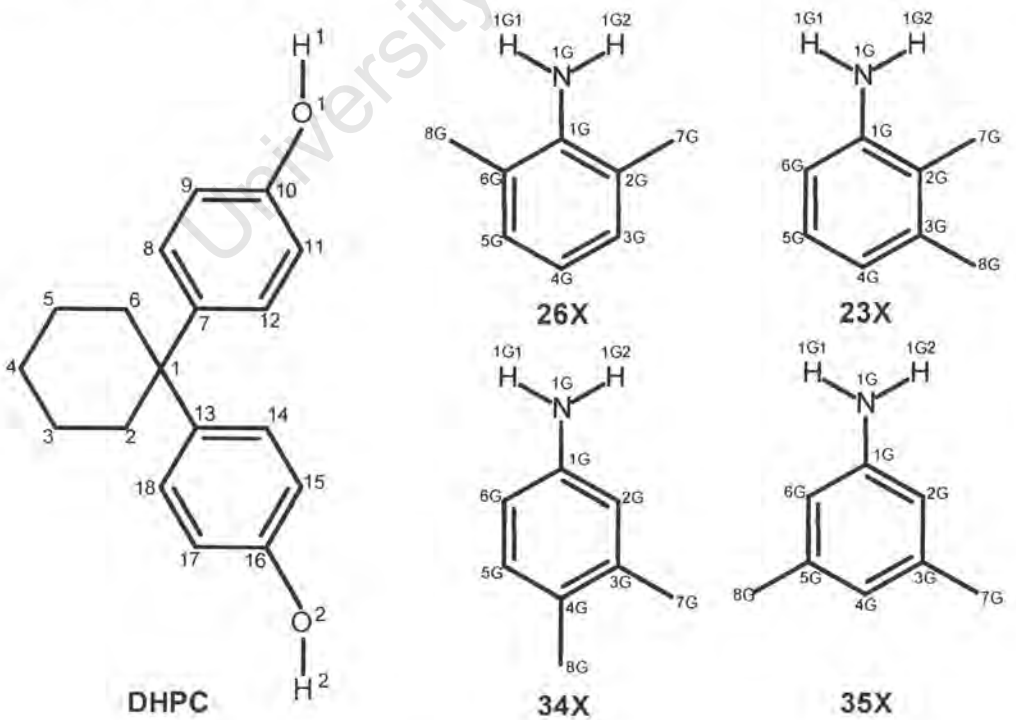

Scheme 4.1

Preparation of the inclusion compounds

The inclusion compounds were obtained by dissolving the host **DHPC** in excess amount of guest xylidines by warming and allowing the solution to crystallise at different controlled temperatures by concentration. The mole ratio of host to total guest used was about 1:15 in both crystallisation experiments and competition experiments. Crystals appeared within periods varying from 24 hours to 7 days. In the case of the guest 3,4-xylidine, which is solid at ambient temperature, toluene was used as a non-competitive solvent when crystallisation was carried out at room temperature (~25°C) and inclusion of water occurred from the wet toluene solvent. The crystallisation temperatures at 1°C, 4°C, 60°C and 80°C could be controlled about ±1°C. The inclusion compounds obtained are listed in **Table 4.1**, together with the host:guest ratios, crystallisation temperatures and compound code names.

Table 4.1 List of the inclusion compounds obtained.

Code name of inclusion compound	Guest	Host:guest	Crystallisation temperature
DHPC•26X	2,6-Xylidine	1:1	80°C
DHPC•1.5(26X)	**(26X)**	1:1.5	~25°C / 60°C
DHPC•2.5(26X)		1:2.5	4°C
DHPC•3(26X)		1:3	1°C
DHPC•0.5(23X)	2,3-Xylidine	1:0.5	80°C
DHPC•2(23X)	**(23X)**	1:2	~25°C
DHPC•0.5(34X)•H_2O	3,4-Xylidine	1:0.5:1H_2O	~25°C (in toluene)
DHPC•34X	**(34X)**	1:1	80°C
DHPC•35X	3,5-Xylidine	1:1	~25°C
	(35X)		

Thermal analysis

The TG and DSC experiments for the desolvation of the inclusion compounds were carried out on finely crushed microcrystalline samples at a constant heating rate of 10°C/min, unless otherwise stated. The results are shown in combined TG/DSC diagrams for each inclusion compound, followed by a brief description.

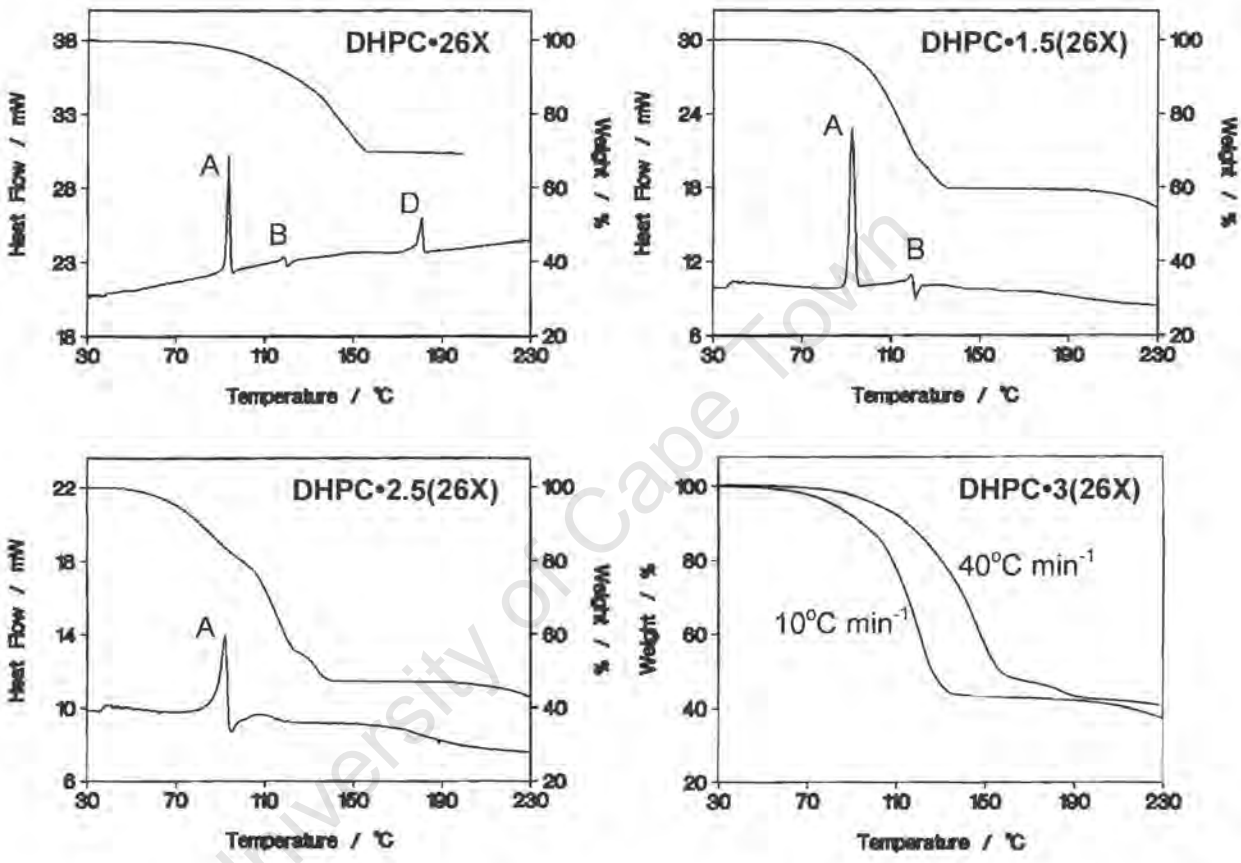

The TG trace for the desorption of **DHPC•26X** indicates one non-smooth mass loss step of weight loss 30.2%, corresponding to the loss of one mole of 2,6-xylidine (calc. 31.1%), confirming a host:guest ratio of 1:1. The DSC trace is characterised mainly by two sharp endothermic peaks A and C. The first peak A having an onset temperature of 92.4°C is attributed to the onset of guest loss reaction. The second sharp endothermic peak D with onset temperature of 181.7°C corresponds to the melt of guest-free host and is confirmed by the melting point of the non-porous α-phase host. A small step B in the baseline is observed between peak A and D at 117.5°C and is probably attributed to the uneven guest release process.

For **DHPC•1.5(26X)**, apparently the guess loss takes place in two overlapping steps, with a total mass loss of 40.4%, corresponding to the loss of one and half 2,6-xylidine molecules per host molecule (calc. 40.4%). The DSC trace shows a sharp endotherm A with an onset temperature of 90.5°C and a small step B at 119.8°C, both of which corresponding to the overlapping desolvation processes. No peak in the DSC trace is associated with the melt of the host alone, though the melting was observed on a single crystal sample by Hot Stage Microscopy.

Similar to **DHPC•1.5(26X)**, the desolvation of **DHPC•2.5(26X)** follows multiple steps. The TG trace exhibits three steps with no stable intermediates. The mass loss for each step could not be assigned with simple stoichiometry, however the total mass loss of 52.9% is in good agreement with the requirement of host:guest ratio of 1:3 (calc. 53.03%). Only one sharp endothermic peak, A, is observed in the DSC trace, corresponding to the overlapping desolvation processes. No melt endotherm is present for the melting of the desolvated host.

The TG results for the desolvation of **DHPC•3(26X)**, carried out at different heating rates, are shown. The TG trace resulting from the TG run at a standard heating rate of 10°C min^{-1} exhibits a single, but slightly uneven mass loss step. The TG trace at a increased heating rate, 40°C min^{-1}, shows two steps but with no simple stoichiometry being associated with each mass loss step. The total mass losses observed are in good agreement with the host:guest ratio of 1:3 requirement (see **Table 4.2**).

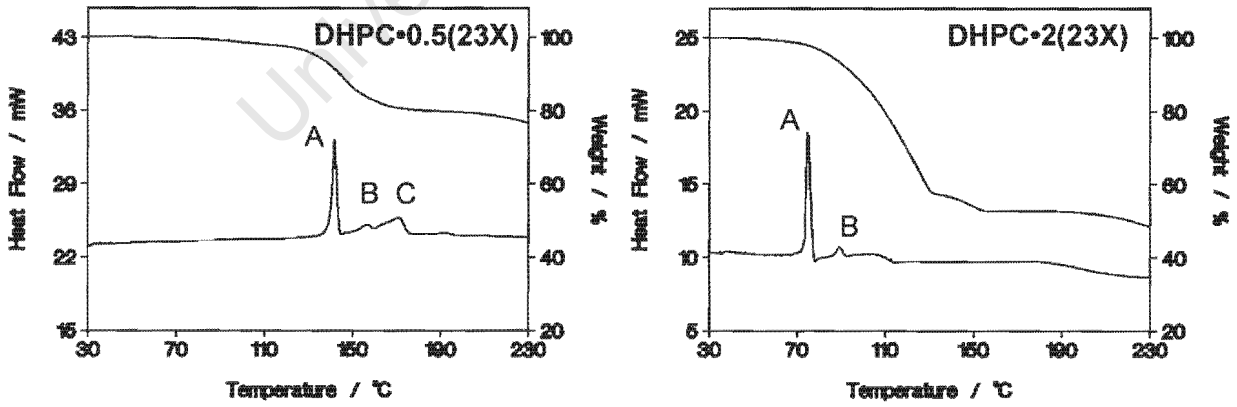

The TG for **DHPC•0.5(23X)** indicates a one-step desolvation reaction. While the DSC exhibits one sharp endothermic peak (A) and two broad peaks (B and C), corresponding to the desorption process. No endotherm corresponds to the melt of apohost.

The desorption of **DHPC•2(23X)** takes place in two overlapping steps with no simple stoichiometry being associated with each step by mean of mass loss percentage. The desolvation process gives rise to two endotherms A (large) and B (small) in the DSC trace.

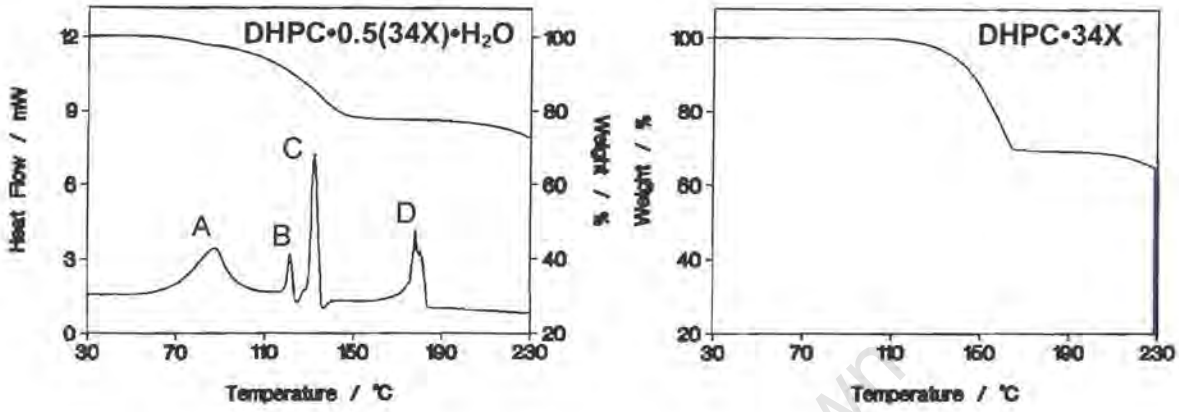

The TG and DSC traces for **DHPC•0.5(34X)•H_2O** are slightly different from the other compounds. The guests loss occurs in two steps, with the first 4.9% mass loss corresponding to the desorption of water and is associated with endotherm A. The 3,4-xylidine desorption (17.6% weight loss) corresponds to two endotherms B and C in the DSC, while endotherm D is associated with the melt of the host compound. The TG trace of **DHPC•34X** indicates a well-defined single step guest desorption step with onset temperature of 130.8°C and percentage mass loss of 30.8 (calc. 31.11) which confirms the 1:1 host:guest ratio.

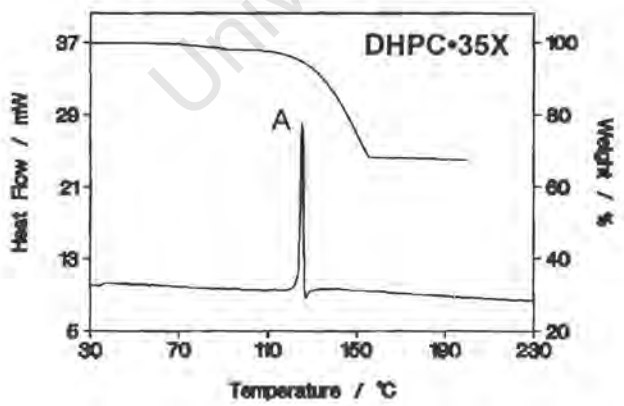

The TG trace for desolvation of **DHPC•35X** indicates a first step of desorption of solvent from the surface, followed by a definite single-step guest loss step, which corresponds to a sharp endotherm A in the DSC.

In most cases, endothermic peaks representing the melt of the host in the DSC traces are not observed. The hot stage microscopy investigation was followed for each inclusion compound using a single crystal sample. Similar thermal events were observed when heating the crystals. The transparent crystal turns opaque white during the guest release step, with the crystal shape retained, and the guest-free host melts in the temperature range of 180°C – 182°C (see **Photo 4.1**). The reason for the melting endothermic peak not being present in the DSC, is possibly due to differences in particle size and the fact that the hot stage possesses an entirely different geometry from the DSC. Fairly large crystals (0.2 - 0.5mm^3) were used at a relatively open environment on hot stage microscope, as opposed to the powdered samples (10 - 100μm) in closed, but vented pans used in DSC. The powdered sample, obtained from finely crushed crystals, decomposes and sublimes upon melting.

To show the general thermal behaviour of these inclusion compounds when heated on hot stage, the HSM photographs of a single crystal of **DHPC•35X** are shown in **Photo 4.1**, as a typical example. The crystal was placed on a glass slide and heated at a constant heating rate of 10°C min^{-1}. At 30°C, the crystal is clearly transparent. At approximately 90°C the surface of crystal becomes opaque. At 110°C, the outer part of the crystal is almost white completely while the inner part of the inclusion compound is still visible, indicating that the guest loss proceeds from the edge of the crystal inwards. By 150°C, the whole crystal is completely white with its original shape retained. At about 182°C, the apohost melts.

Photo 4.1 HSM photographs for a crystal of **DHPC•35X**. The crystal dimensions are approximately 0.5 x 0.2 x 0.07 mm^3.

All of the TG analyses for the inclusion compounds show that the total mass losses observed are in good agreement with the stoichiometrically calculated guest weight losses. The exact values are reported in **Table 4.2** for all of the inclusion compounds discussed, together with the relevant thermal data from DSC. The determined

host:guest ratios were confirmed by X-ray crystal structure analysis, which is discussed in the 'crystal structure' section.

Table 4.2 Summarisation of thermal analysis (TG/DSC) results.

Inclusion compound	TG			DSC		
	Guest loss temp. ranges (°C)	Obs. total mass loss (%)	Calc. total mass loss (%)	guest loss onset temp. (peak A) T_{on} (°C)	$T_{on} - T_b$[&] (°C)	Host melt Onset temp. (Peak D) (°C)
DHPC•26X	66 - 158	30.2	31.11	92.4	-121.6	181.7
DHPC•1.5(26X)	70 - 140	40.4	40.38	90.5	-123.5	/
DHPC•2.5(26X)	46 - 146	52.9	53.03	88.0	-126	/
DHPC•3(26X)	48 - 142	56.8	57.53	84.3*	-129.7	N/A
DHPC•0.5(23X)	110 - 186	18.1	18.42	139.8	-83.2	/
DHPC•2(23X)	74 - 162	47.2	47.46	73.4	-149.6	/
DHPC•0.5(34X)•H_2O	47 - 162	22.5	22.66	86.2 (A1) 119.6 (A2) 130.2 (A3)	-	180.1
DHPC•34X	104 - 166	30.8	31.11	130.2*	-94.8	N/A
DHPC•35X	98 - 161	30.3	31.11	124.2	-96.8	/

* The T_{on} value is obtained from TG trace run at 10°C min^{-1}.

& $T_{on} - T_b$ is the difference between guest desorb onset temperature and bp of the pure guest compound.

N/A means no experiment was carried out due to lack of available compound.

/ means not observed.

Crystal structures

Preliminary X-ray photography reveals that, all of the inclusion compounds, except **DHPC•3(26X)**, **DHPC•0.5(23X)** and **DHPC•34X**, belong to the triclinic crystal system; therefore the possible space groups are P1 or P $\bar{1}$. The centrosymmetric space group P $\bar{1}$ was chosen, in each case, based on the mean $|E^2-1|$ values obtained from direct methods for the zonal reflections, i.e. 0kl, h0l, hk0, and the reminder of the reflections.

The structures of **DHPC•3(26X)**, **DHPC•0.5(23X)** and **DHPC•34X** were found to belong to the monoclinic crystal system (2/m Laue symmetry). For **DHPC•3(26X)**, the conditions limiting reflections

h0l: $h + l = 2n$
0k0: $k = 2n$
h00: $(h = 2n)$
00l: $(l = 2n)$

were observed and the centrosymmetric space group $P2_1/n$ is chosen. $P2_1/n$ is equivalent to the space group $P2_1/c$, but refers to a different cell choice, which results in the c-glide plane being converted into an n-glide plane. For **DHPC•0.5(23X)** and **DHPC•34X**, the conditions limiting possible reflections

hkl: $h + k = 2n$
h0l: $l = 2n$; $(h = 2n)$
0k0: $(k = 2n)$

were observed, implying that the space group was either Cc or C2/c. The centrosymmetric space group C2/c was chosen, based on the intensity statistics obtained from the direct methods run. The choice of the centrosymmetric space group in each case was always vindicated by the successful final refinement of the structure.

The crystal structure for each inclusion compound is discussed in terms of refinement and structure analysis. The structures with the same guest isomer are discussed together. The space group, cell parameters, host:guest ratio and other crystallographic information are summarised at the beginning of the discussion for each inclusion compound. The atomic numbering scheme used for the host **DHPC** for all the structure solutions and the guest xylidines are shown in **Scheme 4.1**. In case of more than one host or guest molecules present in the asymmetric unit, the crystallographically independent molecules are assigned suffixes "X", "Y" etc for the host molecules and "A", "B" etc for the guest molecules. The hydrogen atoms of the guest are labelled according to the parent atoms to which they are bonded. For example H(7G1, H(7G2)

and H(7G3) bond to C(7G); H(8A1), H(8A2) an H(8A3) bond to C(8GA); H(1G1) and H(1G2) bond to N(1G); H(1A1) and H(1A2) bond to N(1GA); etc.

For all nine of the inclusion compounds, their crystal structures were solved by direct methods, which calculated the positions of all the non-hydrogen atoms for both of the host and the guest molecules in the asymmetric unit. For the guest molecules, the electron densities of the amino nitrogen atoms N(1G) were similar to those of the methylic carbon atoms C(7G) and C(8G). In case of ambiguity, N(1G) atoms were placed by means of their hydrogen bonding distances from the hydroxyl oxygen atoms of the host, or the oxygen atom of water molecule in case of **DHPC•0.5(34X)•H_2O**. In the structure refinements, the aromatic and methylenic hydrogen atoms on the host molecule were placed with geometric constraints and refined with isotropic temperature factors assigned as 1.2 times the value of the U_{eq} of their parent atoms. The aromatic and methyl hydrogen atoms on the guest molecules were also placed with geometrical constraints, but assigned isotropic temperature factors 1.2 and 1.5 times the U_{eq} of their parent atoms respectively. The hydroxyl hydrogen atoms on the host and the amino hydrogen atoms on the guests were located in difference electron density maps, where possible. The hydroxyl hydrogens were refined with simple bond length constraint according to a function of O-H *versus* O···O distances (Olovsson & Jönsson, 1975) where applicable and individual isotropic temperature factors. The amino hydrogens were refined with simple bond length at a value of d(N-H) = 0.97Å. Other details regarding structure refinements are discussed for each structure. The host conformation data obtained from all the structure solutions in this chapter will be discussed in more detail collectively in **Chapter 7**. The crystal data and final refinement parameters are contained in **Table 4.13** appearing at the end of this chapter.

DHPC•n(26X)

Guest: 2,6-xylidine (**26X**)

DHPC•26X ($C_{18}H_{20}O_2$•$C_8H_{11}N$)
Space group: P $\bar{1}$
a = 6.234(1) Å α = 84.98(1)°
b = 10.934(2) Å β = 81.29(2)°
c = 16.974(2) Å γ = 77.10(2)°
Volume = 1113.1(3) Å^3
Z = 2

DHPC•1.5(26X) ($C_{18}H_{20}O_2$•1.5$C_8H_{11}N$)
Space group: P $\bar{1}$
a = 7.859(1) Å α = 78.909(2)°
b = 10.015(1) Å β = 85.161(1)°
c = 17.169(1) Å γ = 71.238(1)°
Volume = 1255.3(2) Å^3
Z = 2

DHPC•2.5(26X) ($C_{18}H_{20}O_2$•2.5$C_8H_{11}N$)
Space group: P $\bar{1}$
a = 7.885 (1) Å α = 94.661(1)°
b = 10.026(1) Å β = 91.539(2)°
c = 43.761(3) Å γ = 109.020(1)°
Volume = 3254.6(6) Å^3
Z = 4

DHPC•3(26X) ($C_{18}H_{20}O_2$•3$C_8H_{11}N$)
Space group: $P2_1/n$
a = 9.807(1) Å α = 90°
b = 25.464(2) Å β = 98.28(1)°
c = 29.842(3) Å γ = 90°
Volume = 7374.62( ) Å^3
Z = 8

Refinement

The **DHPC•26X** structure was refined in P $\bar{1}$. There are one host molecule and one guest molecule in the asymmetric unit, both located in general positions. All the non-hydrogen atoms were refined with anisotropic temperature factors. The whole 2,6-xylidine guest molecule was found disordered over two positions. The two disordered guest molecules (**Figure 4.1**), assigned with suffixes A and B, have s.o.f. of 0.479 and 0.521 respectively with the two phenyl planes having bisection angle of 49.5(5)°. The fractional site occupancies for the two arrangements were determined by their relative heights of the electron densities and were linked during refinements. The aromatic rings of the disordered guest molecules were refined with simple bond-length constraints at a value of d(C_{ar}-H) = 1.39Å. The hydroxyl hydrogen atoms on the host molecule and amino hydrogen atoms on the guest molecule were located in difference

electron density maps and refined with bond length constraints at values of d(O-H) = 0.97Å and d(N-H) = 0.97Å. The rest of hydrogen atoms on the host molecule and guest molecule A were placed in geometrically constrained positions, using the built-in features in SHELXL-97 (Sheldrick, 1997). The structure refined to R_1 = 0.0557.

N(1GA)-C(1GA)	1.43(1)Å	N(1GB)-C(1GB)	1.43(1)Å
C(1GA)-C(2GA)	1.45(1)Å	C(1GB)-C(2GB)	1.41(1)Å
C(2GA)-C(3GA)	1.30(1)Å	C(2GB)-C(3GB)	1.53(1)Å
C(3GA)-C(4GA)	1.36(1)Å	C(3GB)-C(4GB)	1.37(1)Å
C(4GA)-C(5GA)	1.40(1)Å	C(4GB)-C(5GB)	1.34(1)Å
C(5GA)-C(6GA)	1.38(1)Å	C(5GB)-C(6GB)	1.39(1)Å
C(6GA)-C(1GA)	1.36(2)Å	C(6GB)-C(1GB)	1.34(2)Å
C(2GA)-C(7GA)	1.49(1)Å	C(2GB)-C(7GB)	1.51(1)Å
C(6GA)-C(8GA)	1.51(1)Å	C(7GB)-C(8GB)	1.49(1)Å

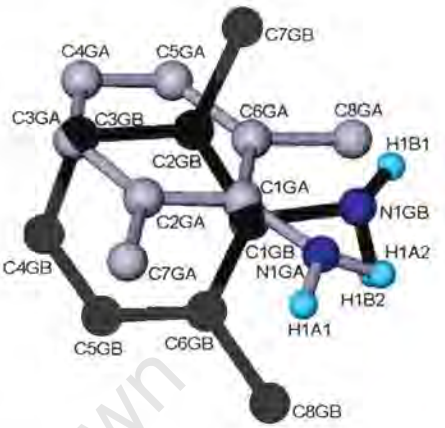

Figure 4.1 Disorder modelled for guest molecule 2,6-xylidine in **DHPC•26X** and the resultant bond lengths. Only the amino H atoms are shown.

DHPC•1.5(26X) crystallises in P $\bar{1}$ with Z = 2. There are two host molecules and three guest molecules in the unit cell. Therefore symmetry requires one guest molecule, B, to be located at a special position, on a centre of symmetry at Wyckoff position *e* (½,½,0). This guest molecule B is disordered via the centre of inversion, as shown in **Figure 4.2**. Refinements were carried out with the non-hydrogen atoms of both the host and guest treated anisotropically. The hydroxyl hydrogen atoms on the host molecule and the amino hydrogen atoms on the guest molecule A, which is on general position, were independently located in difference density maps and constrained with simple bond length. The rest of the hydrogen atoms on the host and the guest molecule A were geometrically constrained and assigned isotropic temperature factors related to their parent atoms. The hydrogen atoms on the disordered guest molecule B were omitted in the final model due to disorder. The structure refined successfully to R_1 = 0.0560.

N(1GB)-C(1GB)	1.448(5)Å
C(1GB)-C(2GB)	1.339(5)Å
C(2GB)-C(3GB)	1.446(5)Å
C(3GB)-C(4GB)	1.421(6)Å
C(4GB)-C(5GB)	1.319(9)Å
C(5GB)-C(6GB)	1.465(6)Å
C(2GB)-C(7GB)	1.562(6)Å
C(6GB)-C(8GB)	1.462(6)Å

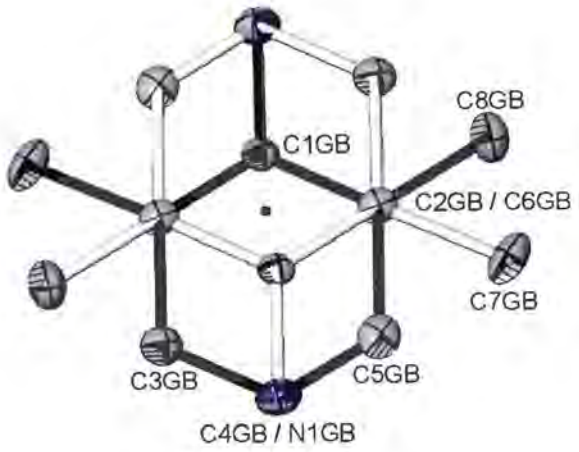

Figure 4.2 Disorder modelled for the guest molecule 2,6-xylidine in **DHPC•1.5(26X)**. The centre of inversion is indicated as a black dot lying on the plane of phenyl ring. Displacement ellipsoids are drawn at the 35% probability level. The labelled atoms are in the asymmetric unit and are placed with s.o.f of 0.50 for each. C(4GB) and N(1GB), as well as C(2GB) and C(6GB) are at the same positions.

DHPC•2.5(26X) crystallises in P $\bar{1}$ with Z = 4. There are two host molecules (X and Y) and five guest molecules (A, B, C, D and E) in the asymmetric unit and are all located in general positions. One of the phenol moieties on the host molecule Y and the phenyl rings of the two guest molecules D and E yielded unsatisfactory geometries. These phenyl ring systems were thus geometrically constrained to fit a regular hexagon, and the atoms were refined with isotropic temperature factors. U_{iso} for these atoms at the end of refinement are typically high (in range 0.078Å^2 to 0.36Å^2), thus their hydrogen atoms were omitted from the final model. The other hydroxyl hydrogen atoms were located in the maps and refined with simple bond length constraints. Not all of the amino hydrogen atoms of the guest could be located and they were thus omitted from the model. The rest of the hydrogen atoms that have not been mentioned were all placed with geometric constraints. The final R index for this model was R_1 = 0.1885. This is clearly unsatisfactory.

The data-collection experiment was therefore repeated and three complete data collections have since been carried out at low temperature on different crystals. On each attempt, the refinement yielded sensible positions for most of the atoms of the host molecules and three of the five guest molecules in the asymmetry unit. However the remaining two guest molecules proved intractable and gave unreasonable geometries.

DHPC•3(26X) crystallises in $P2_1/n$ with Z = 8. There are two host molecules (X and Y) and six guest molecules (A, B, C, D, E and F) in the asymmetric unit and thus no crystallographic symmetry is imposed on either host or guest molecules. All non-hydrogen atoms were refined anisotropically. The hydroxyl hydrogen atoms on the host molecules were found in the electron difference density maps and refined with simple bond length constraint at a value of d(O-H) = 0.96Å and independent isotropic temperature factors. The temperature factor for one of the four hydroxyl hydrogen atoms, H(1X), were relatively high (U_{iso} > 0.38Å^2), therefore it was assigned a fixed isotropic temperature factor of 1.2 times the value of U_{eq} of O(1X) to which it bonds. All of the amino hydrogen atoms on the guest molecules, except H(1C2) which bonds to N(1GC), were located in the electron difference density maps and refined with simple bond length constraint at a value of d(N-H) = 0.97Å and independent isotropic temperature factors. The position of H(1C2) was calculated based on an idealised linear hydrogen bond N(1GC)-H(1C2)···O(2Y) and then refined with isotropic temperature factor fixed at 1.2 times the value of U_{eq} of N(1GC). The rest of the hydrogen atoms were geometrically constrained. A residual electron density of 0.916 eÅ^{-3} was observed in the region of the host molecule Y, but could not be modelled sensibly. The final R factor for this structure is R_1 = 0.0973.

Structure analysis

DHPC•26X

The structure of **DHPC•26X** is stabilised by hydrogen bonds formed between host and host [(host)O-H···O(host)], host and guest [(host)O-H···N(guest) and (guest)N-H···O(host)]. The hydroxyl group on the host and the amino group on the guest act as both proton donors and proton acceptors. Adjacent host molecules are hydrogen bonded to each other through their hydroxyl groups, and form double ribbons running along direction [010]. A two-dimensional hydrogen bonding network is observed (**Figure 4.3**). Columns of host···host molecules run along [010], stabilised by O-H···O hydrogen bonds and the second columns of host···guest···host molecules run along [100], displaying O-H···N-H···O-H hydrogen bonds. Geometries of the hydrogen bonding interactions are listed in **Table 4.3**. The crystal packing, viewed along [010] and [100], is shown in **Figures 4.4** and **4.5a** respectively.

The clathrate mode of the structure is characterised by alternative layers of host and guest molecules perpendicular to [001], illustrated as a space-filling diagram in **Figure**

4.5b, in which the host atoms are presented with van der Waals radii and the guest molecules are shown as sticks. The space between layers of host molecules, which sandwich guest molecules, is approximately 6 Å across c in the narrowest part and 9 Å in the widest part.

Table 4.3 Details of hydrogen bonding in **DHPC•26X**.

Donor(D)-H···Acceptor(A)	D-H /Å	H···A /Å	D···A /Å	<DHA /°
O(1)-H(1)···N(1GA)	0.97(3)	1.96(3)	2.895(7)	160(4)
O(1)-H(1)···N(1GB)	0.97(3)	1.77(4)	2.642(6)	148(4)
N(1GA)-H1A2)···O(2)[1]	0.96(3)	2.28(6)	3.209(7)	162(5)
N(1GB)-H(1B2)···O(2)[1]	0.97(3)	2.29(4)	3.061(6)	136(4)
O(2)-H(2)···O(1)[2]	0.99(3)	1.78(3)	2.757(3)	172(5)

Symmetry code: (1) x+1, y-1, z (2) x, y+1, z

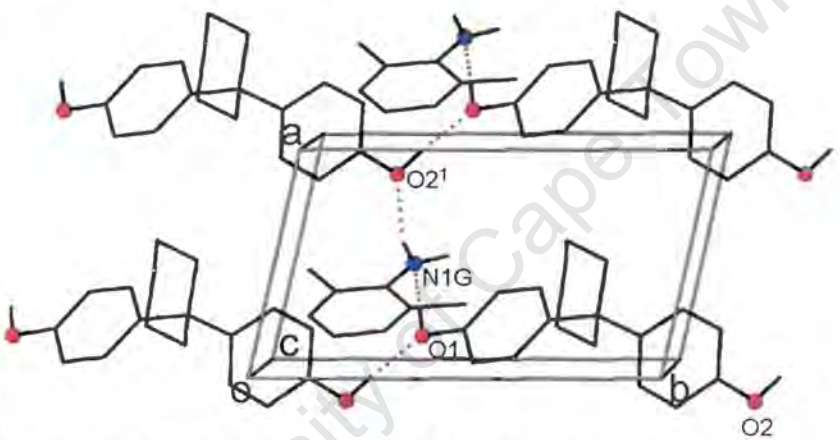

Figure 4.3 Part of the crystal structure of **DHPC•26X**, showing the hydrogen-bonding scheme. Only the hydroxyl and amino H atoms are shown. One orientation of the guest molecule is present. The H-bonds are indicated as dotted lines.

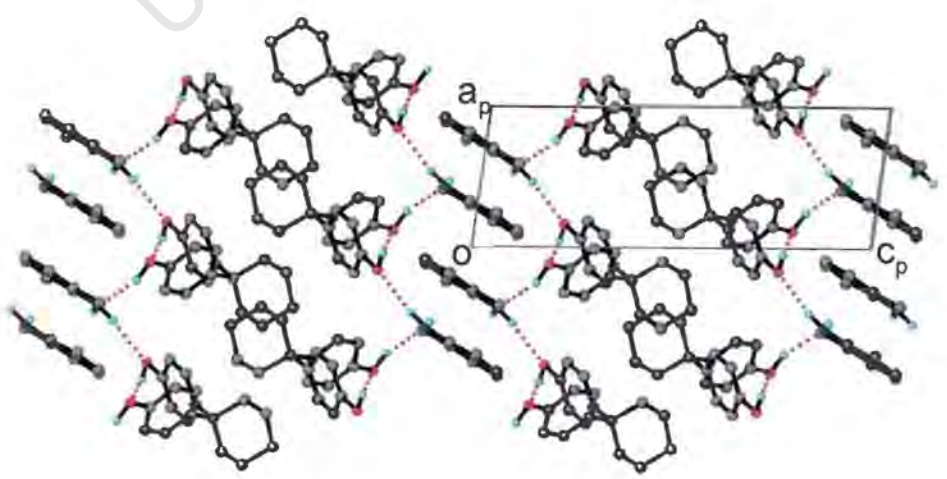

Figure 4.4 A projection down [010] showing the crystal packing of **DHPC•26X**. The picture drawing details as in **Figure 4.3**.

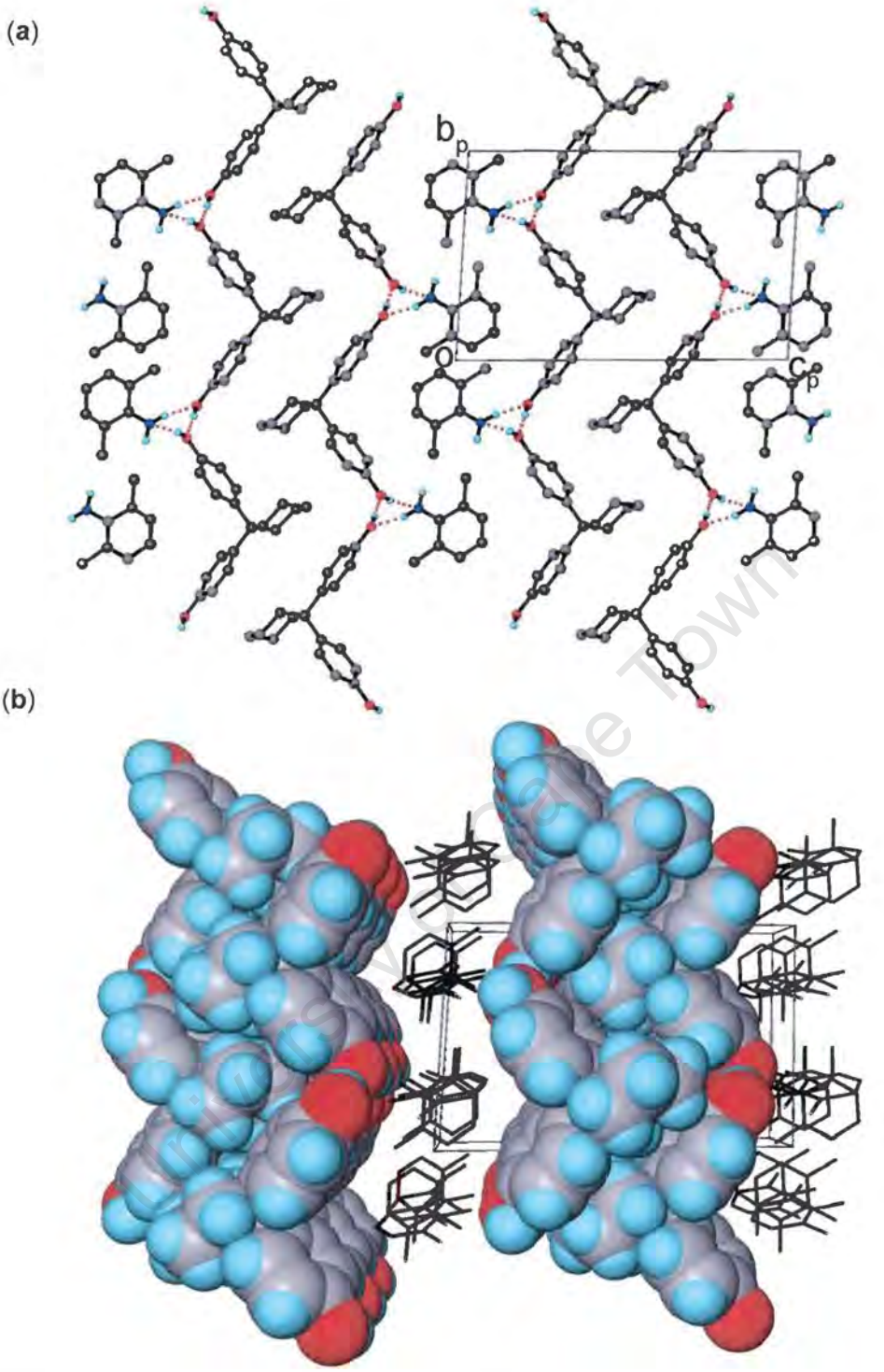

Figure 4.5 View along [100] for **DHPC•26X**. (a) Projection shows double ribbons of host molecules running along [010] and the hydrogen bonding links the host and guest spiral along [100]. Picture drawing details as in **Figure 4.4**. (b) Perspective view shows the layers of host (in van der Waals radii representation) sandwich the guest molecules (in stick representation). The two orientations of disordered guest molecules are shown with H atoms omitted.

DHPC•1.5(26X)

In this structure, the hydrogen bonding is such that two host molecules form a dimer about a centre of inversion via (host)O-H···O(host) interactions and, in addition are hydrogen bonded to the guest molecules (**Figure 4.6a**). A one-dimensional hydrogen bonding network formed via (host)O-H···N(guest), (guest)N-H···N(guest) and (guest)N-H···O(host) intermolecular interactions is observed running along the direction [10 $\bar{1}$]. This can be seen in the crystal packing projection down [010] (**Figure 4.6b**). The details of hydrogen bonds are listed in **Table 4.4**. Both the host and the guest molecules pack to form alternative layers perpendicular to the c axis with the guest layers centred at c = 0. The space for the guest molecules, which is between layers of host, is in an approximate range of 4.5Å - 9Å across c in width. This is shown as a space-filling diagram in **Figure 4.7**.

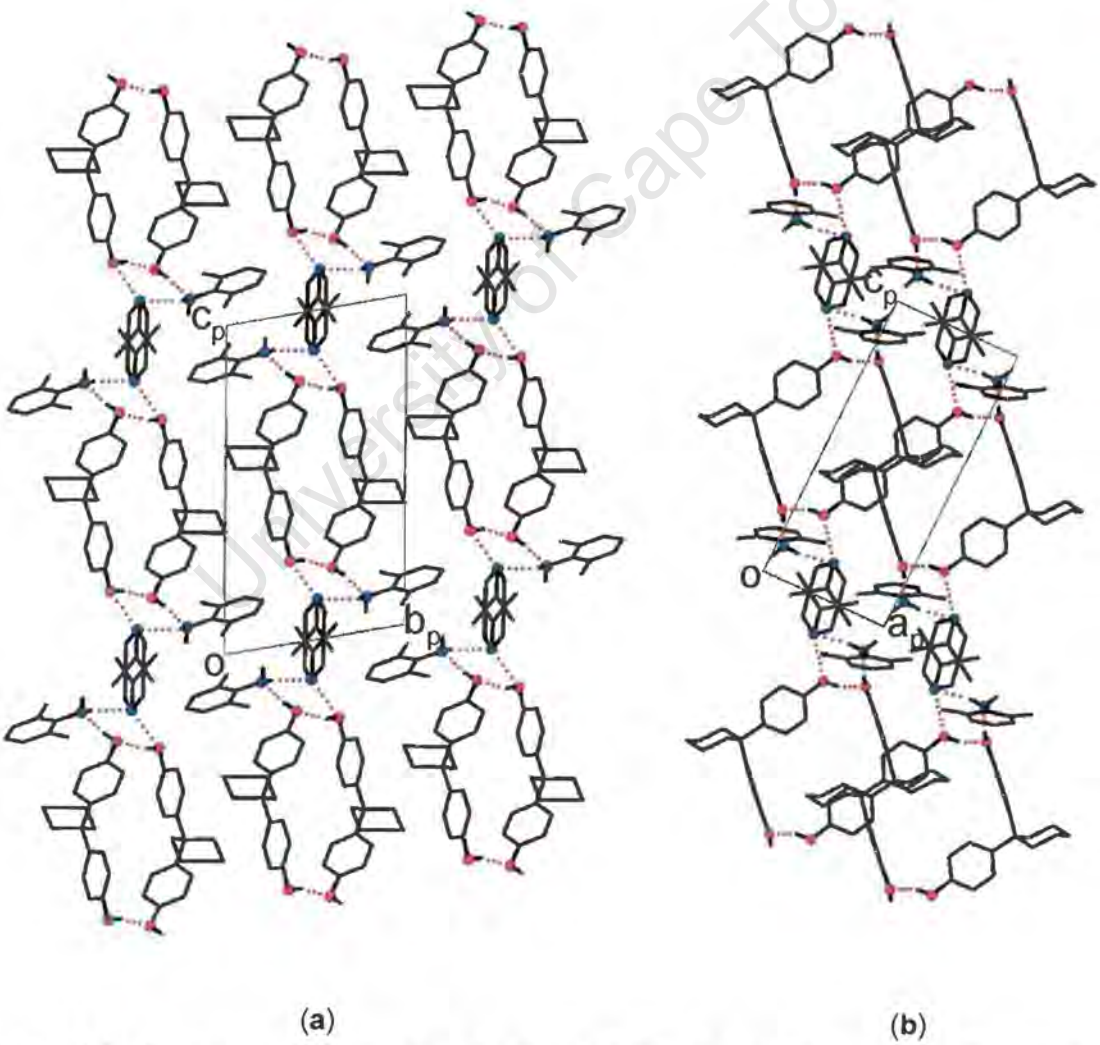

(**a**) (**b**)

Figure 4.6 Projections viewed along (a) [100] and (b) [010], showing the crystal packing in **DHPC•1.5(26X)**. All hydrogen atoms except the hydroxyl and amino hydrogen atoms were omitted. The hydrogen bonds are shown as dotted lines. The N and O atoms are highlighted as solid circles.

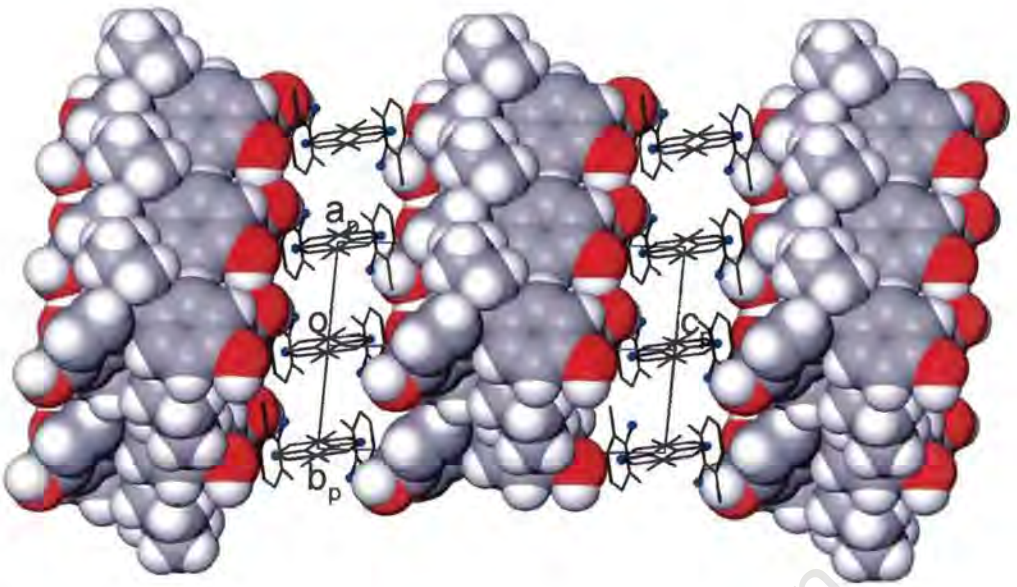

Figure 4.7 Space-filling diagram for **DHPC•1.5(26X)** viewed along [1 $\bar{1}$0]. The host atoms are shown with van der Waals radii and guest molecules shown as sticks with disordered model. All of the hydrogen atoms on the guest are omitted. The N atoms are shown as solid circles.

Table 4.4 Details of hydrogen bonding in **DHPC•1.5(26X)**.

Donor(D)-H···Acceptor(A)	D-H /Å	H···A /Å	D···A /Å	<DHA /°
O(1)-H(1)···N(1GA)	0.96(1)	1.85(1)	2.804(3)	170(3)
O(2)-H(2)···O(1)[1]	0.99(1)	1.81(2)	2.759(2)	163(3)
N(1GA)-H(1A1)···N(1GB)	0.95(2)	2.52(2)	3.392(3)	154(2)
*N(1GB)···O(2)[1]	/	/	3.191(3)	/

Symmetry code: (1) -x+2, -y+1, -z+1
*The amino hydrogen atom could not be located on the electron density maps due to disorder, this interaction is thus inferred from the N···O distance.

DHPC•2.5(26X)

The structure solution of **DHPC•2.5(26X)** is not totally satisfactory, but allows one to gain some insights into the overall molecular packing and the relative stability of the complex. The crystal packing diagrams are shown in **Figure 4.8a** and **4.9** as viewed along [100] and [010] respectively. The structure is stabilised by hydrogen bonds, of which metrics are shown in **Table 4.5**. The host molecule X forms a dimer about a centre of inversion via (host)O-H···O(host) interactions and, in addition are hydrogen bonded to the guest molecules B and C, which are then bonded to each other. This

hydrogen bonding motif is similar to that observed in **DHPC•1.5(26X)**. The host molecule Y is hydrogen bonded to two guest molecules A and D via its two hydroxyl groups. The guest molecule E does not participate in hydrogen bonding. The host molecule X packs to generate a layer perpendicular to [001] with centre at c = 0.5. The stacking of the host molecule Y results in the formation of a sandwich structure, in which columns of guest molecule E run along [100] and layers of guest D perpendicular to [001] at c = 0 with narrowest space about 1.5Å across c. The rest of guest molecules (A, B and C) are located in the second layer between the layer of host X and columns of host Y, of which the narrowest part is approximately 4.5Å across c. The column of guest E interconnects the first and second layers (**Figure 4.8b**).

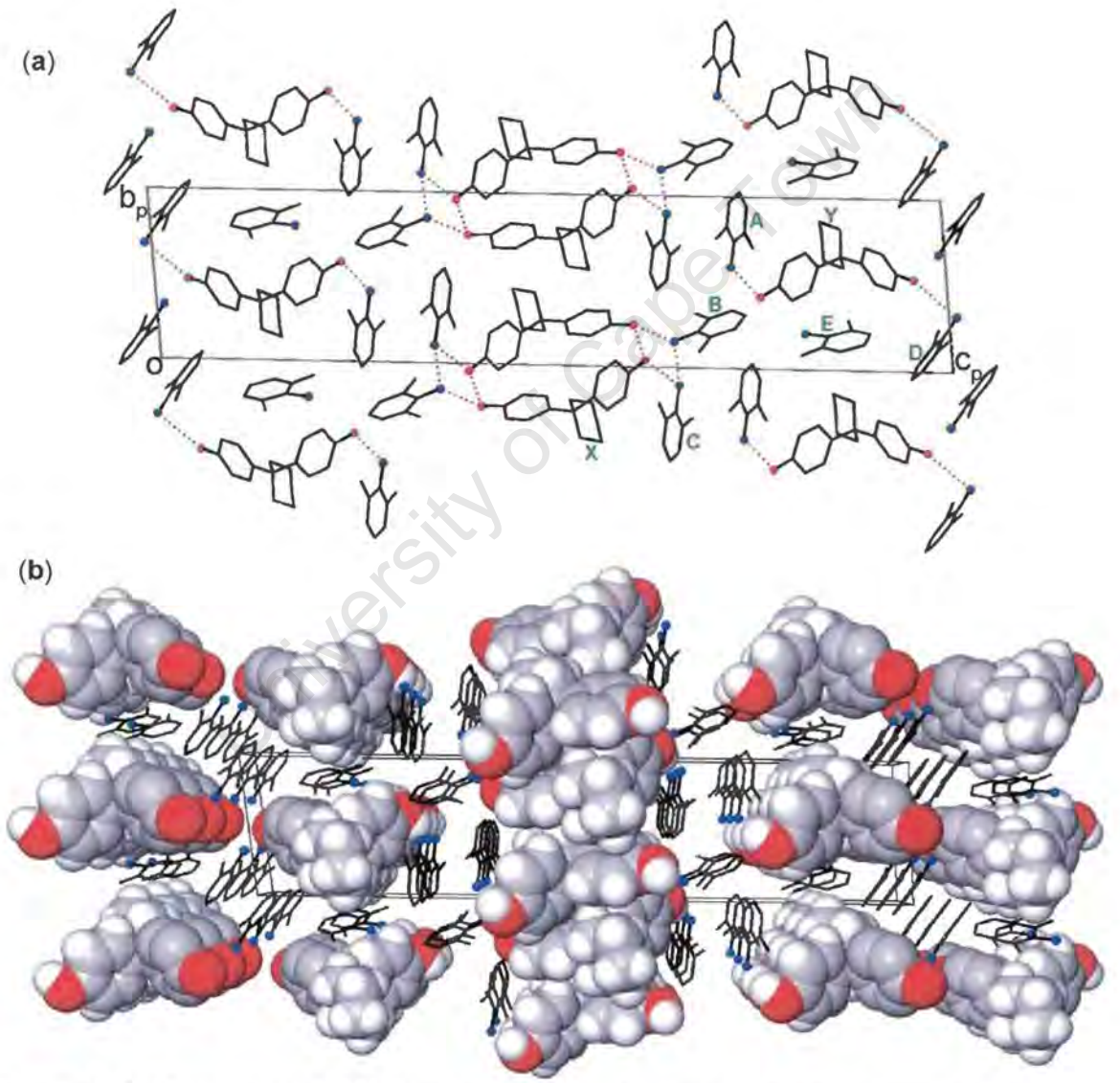

Figure 4.8 View along [100] for **DHPC•2.5(26X)**. (a) Projection shows the crystal packing. All H atoms are omitted. The hydrogen bonding contacts are indicated as dotted lines. The crystallographiclly independent molecules are marked. (b) Perspective view shows the clathrate mode. The host atoms are shown with van der Waals radii and guest in stick representation with H atoms omitted.

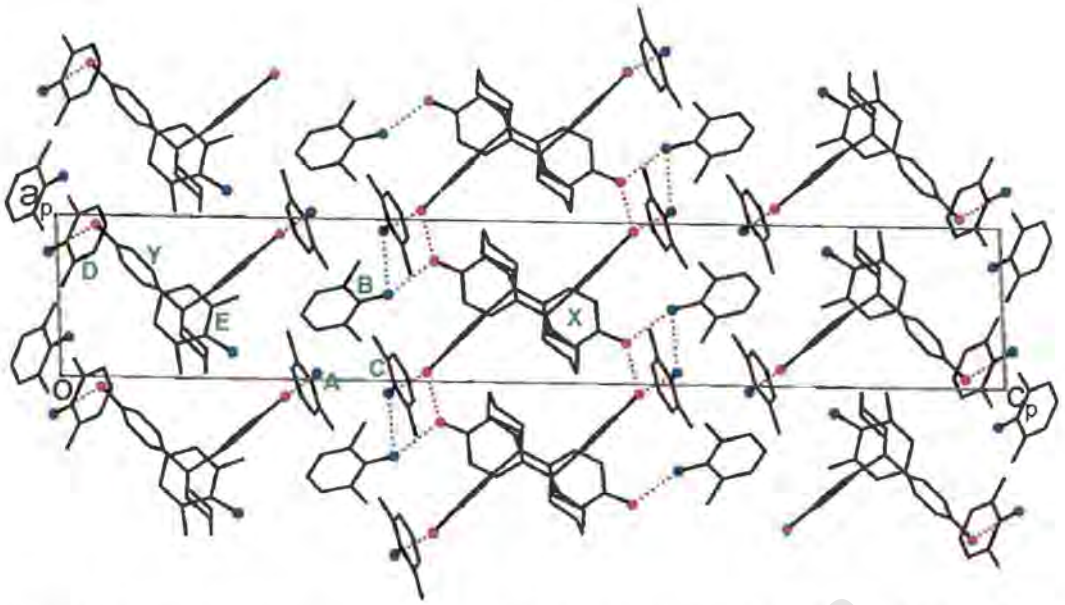

Figure 4.9 Projection down [010] showing the crystal packing in **DHPC•2.5(26X)**. The picture drawing details as in **Figure 4.8a**.

Table 4.5 Details of hydrogen bonding in **DHPC•2.5(26X)**.

Donor(D)-H···Acceptor(A)	D-H /Å	H···A /Å	D···A /Å	<DHA /°
O(1X)-H(1X)···O(2X)[1]	0.97(3)	1.92(6)	2.752(7)	142(7)
O(2X)-H(2X)···N(1GC)	0.98(3)	1.85(6)	2.783(8)	159(12)
O(2Y)-H(2Y)···N(1GA)[2]	0.97(3)	2.01(12)	2.837(10)	141(16)
*N(1GD)···O(1Y)	/	/	3.692(8)	/
*N(1GB)···O(1X)[3]	/	/	3.112(9)	/
*N(1GC)···N(1GB)[4]	/	/	3.327(8)	/

Symmetry code: (1) -x, -y+2, -z+1 (2) 1+x, y, z (3) -x+1, -y+2, -z+1 (4) x-1, y, z.
*The distances are longer than the sum of the van der Waals radii for the two heavy atoms (3.07Å for O···N and 3.10Å for N···N). Due to fairly poor solution of the structure, these interactions are indicative as possible hydrogen bonds.

DHPC•3(26X)

The structure is stabilised by a number of hydrogen bonds formed between host and guest, exhibiting (host)O-H···N(guest) and (guest)N-H···O(host) interactions. Two of the six crystallographically independent guest molecules, B and D, are not hydrogen bonded. The host molecule and four of the guest molecules, A, C, E and F, act as both proton donors and proton acceptors. These guest molecules act as double hydrogen bonding bridges between host molecules and the hydrogen bonds link chains of host and guest molecules zigzagging along [010] (**Figure 4.10**). **Table 4.6** lists all the details of the hydrogen bonds present in the structure. The crystal packing, viewed down the plane (010) and along [100], is shown in **Figure 4.11a** and **4.11b** respectively. The

structure can be best described by columns of guest molecules (A, C, E and F) running parallel to the direction [$\bar{1}$01] at y = 0 and 1/2, and other columns (guest B and D) running along the same direction at y = 1/4 and 3/4. This is illustrated in **Figure 4.12a**, **b**, **c**, in which the representative cross section planes cut through axis b are shown. The cross sections cut at y = 0 and 1/8 show topology of the void generated by the host, where the column of guest molecules A, C, E and F are located. The cross section cut at y = 1/4 shows the column of guests B and D. All these columns are interconnected with each other (see **Figure 4.12d**).

Table 4.6 Details of hydrogen bonding in **DHPC•3(26X)**.

Donor(D)-H···Acceptor(A)	D-H /Å	H···A /Å	D···A /Å	<DHA /°
O(1X)-H(1X)···N(1GA)[1]	0.95(2)	1.84(2)	2.783(4)	172(4)
O(2X)-H(2X)···N(1GE)	0.92(2)	1.94(2)	2.835(4)	164(5)
O(1Y)-H(1Y)···N(1GC)[2]	0.94(2)	1.92(2)	2.820(4)	159(4)
O(2Y)-H(2Y)···N(1GF)[2]	0.95(2)	1.88(2)	2.804(4)	165(5)
N(1GA)-H(1A2)···O(1X)[3]	0.93(3)	2.12(3)	3.025(4)	163(4)
N(1GC)-H(1C2)···O(2Y)[4]	1.00(2)	2.10(2)	3.041(4)	156(3)
N(1GE)-H(1E2)···O(2X)[5]	0.93(3)	2.24(3)	3.116(5)	156(3)
N(1GF)-H(1F2)···O(1Y)[6]	0.93(2)	2.24(3)	3.149(4)	166(3)

Symmetry code: (1) x-1, y, z (2) x-1, y+1, z (3) -x+1, -y+1, -z
(4) -x+0.5, y-0.5, -z+0.5 (5) -x, -y+2, -z (6) -x+0.5, y-1.5, -z+0.5

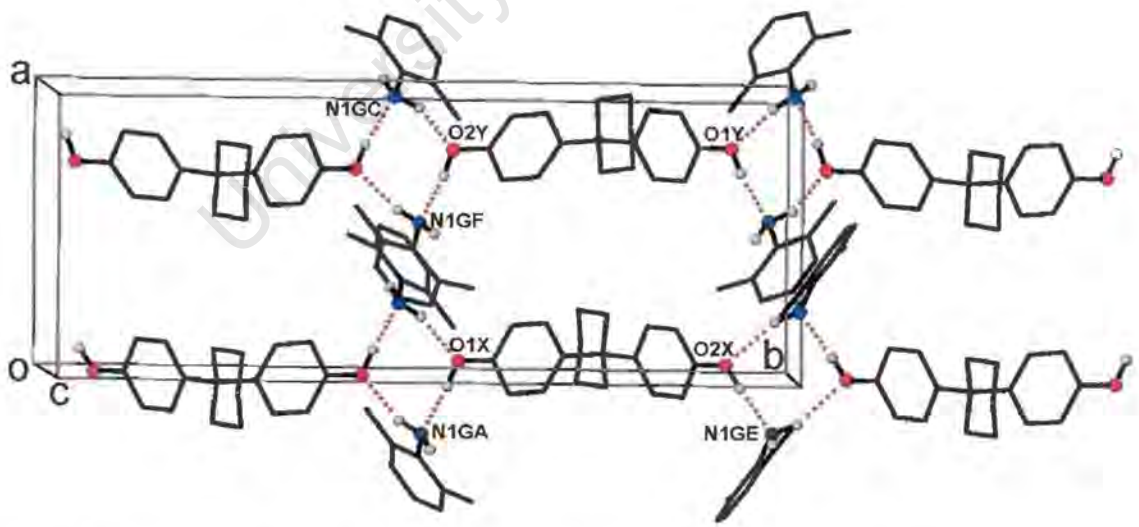

Figure 4.10 Part of the crystal structure of **DHPC•3(26X)** shows the hydrogen bonding scheme. Only the hydroxyl and amino hydrogens are shown. The O, H and N atoms are shown as solid circles.

(a)

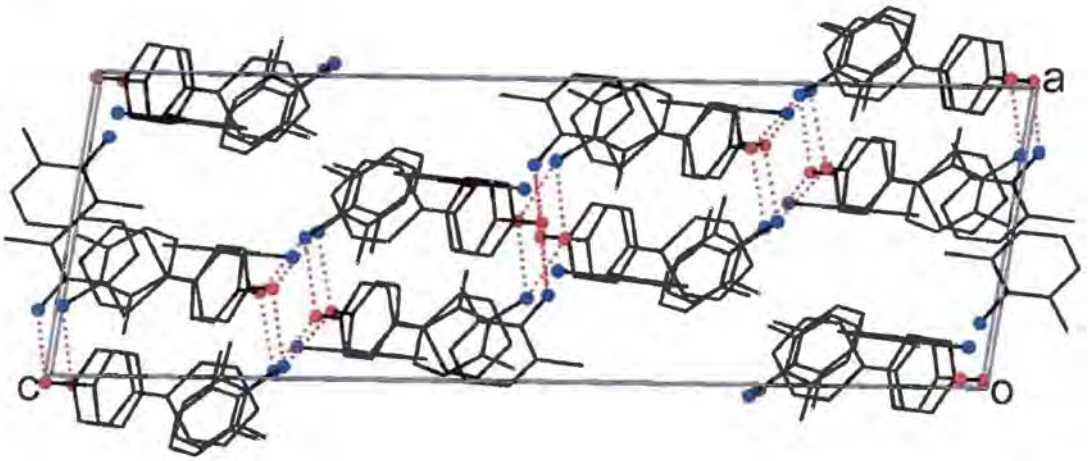

(b)

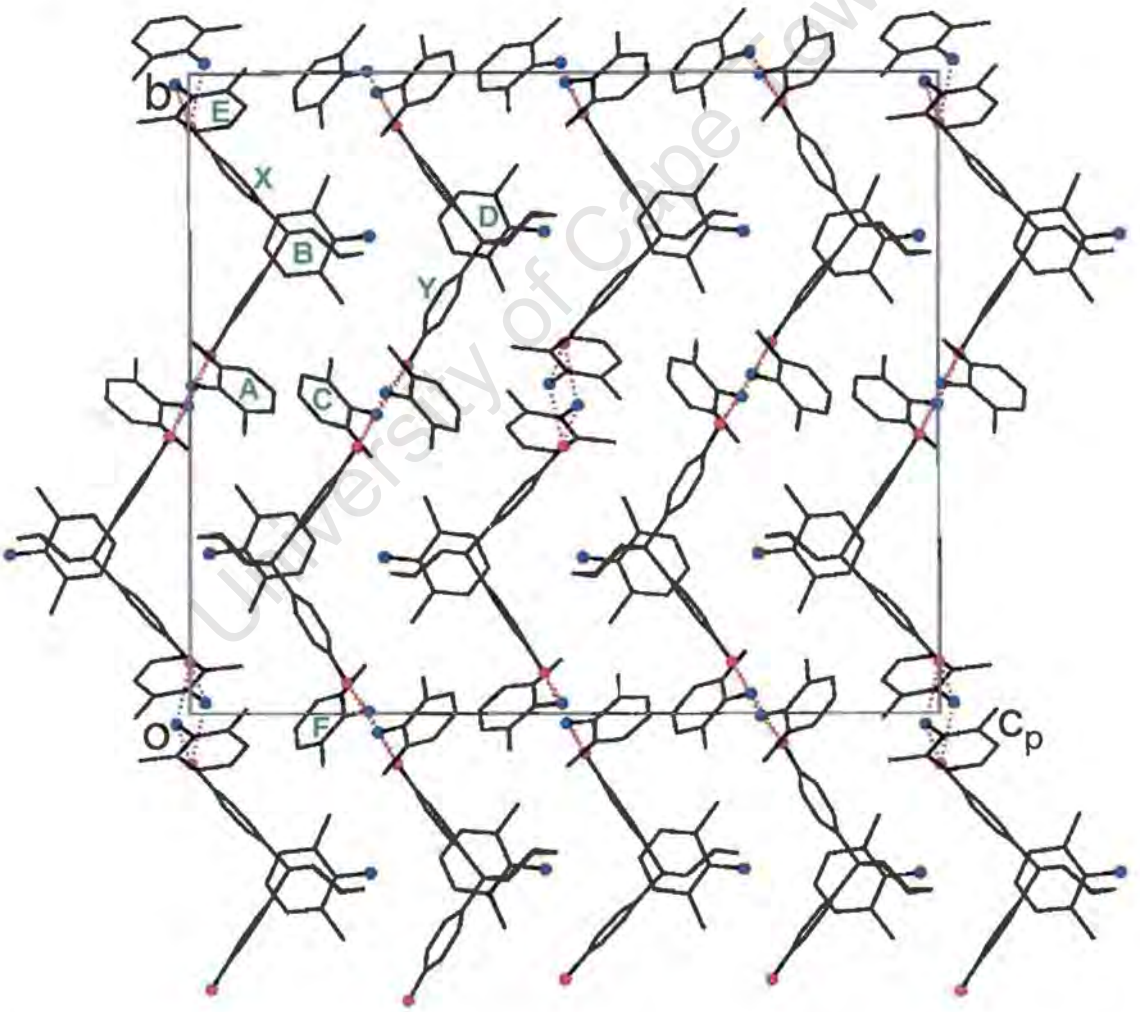

Figure 4.11 Projections of **DHPC•3(26X)** viewed (a) down the plane (010) and (b) along [100], showing the crystal packing. All H atoms are omitted. The hydrogen bonding contacts are indicated as dotted lines.

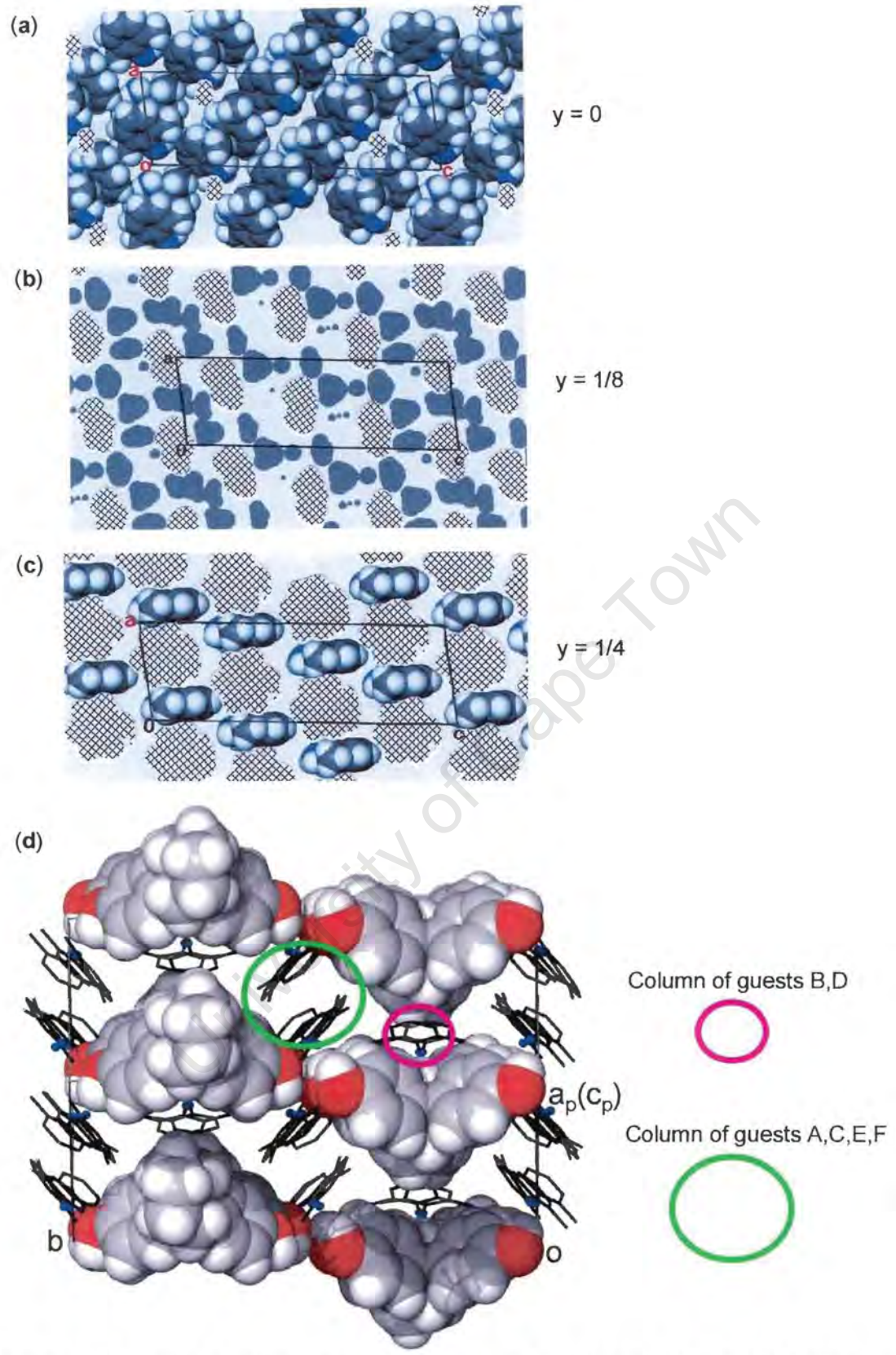

Figure 4.12 (a) (b) and (c) illustrate cross sections cut at y = 0, 1/8 and1/4 respectively for **DHPC•3(26X)**. The diagonal crossed area represents space occupied by the host, while the guests are shown with van der Waals radii in (a) and (c), as grey area in (b). (d) shows space-filling diagram viewed along [$\bar{1}$01], showing the interconnected columns. The host molecules are shown with van der Waals radii. The guests are in stick representation with H atoms omitted and N atoms highlighted.

DHPC•n(23X)

Guest: 2,3-xylidine (**23X**)

DHPC•0.5(23X) ($C_{18}H_{20}O_2$•$0.5C_8H_{11}N$)
Space group: C2/c
a = 18.170(1) Å $\alpha = 90^o$
b = 12.274(1) Å $\beta = 95.30(3)^o$
c = 16.204(1) Å $\gamma = 90^o$
Volume = 3598.5(1) $Å^3$
Z = 8

DHPC•2(23X) ($C_{18}H_{20}O_2$•$2C_8H_{11}N$)
Space group: P $\bar{1}$
a = 6.3593(3) Å $\alpha = 93.429(3)^o$
b = 10.8368(5) Å $\beta = 91.100(3)^o$
c = 21.7366(11) Å $\gamma = 106.912(3)^o$
Volume = 1429.6(1) $Å^3$
Z = 2

Refinement

The structure of **DHPC•0.5(23X)** was refined in space group C2/c. There are eight host molecules and four guest molecules per unit cell (Z = 8), therefore symmetry requires the guest molecule to be located on a special position, on a diad at Wyckoff position *e* [(0,y,¼) and (0, $\bar{y}$,¾)]. The host molecule was located in general position. The guest molecule was disordered over two positions about the diad, with each having s.o.f. of 0.5 (**Figure 4.13**). All of the non-hydrogen atoms were refined anisotropically. The hydroxyl hydrogen atoms of the host molecule were disordered and were located over two sites in the difference electron density maps for each, with <H-O-H = 112° and 130°. This is resulted from directional hydrogen bonding forces towards the disordered guest molecules. They were assigned with s.o.f. of 0.5 each and refined with simple bond length constraints at a value of d(O-H) = 0.98Å and individual isotropic temperature factors. The amino hydrogen atoms on the guest were located in the difference electron density maps and were refined with simple bond lengths constrains and isotropical temperature factors of 1.2 x U_{eq} of their parent atom. The rest of hydrogen atoms were placed with geometric constraints and refined isotropically. The structure refined successfully to $R_1 = 0.0349$.

N(1G) – C(1G)	1.443(5)Å
C(1G) – C(2G)	1.383(7)Å
C(2G) – C(3G)	1.390(5)Å
C(3G) – C(4G)	1.35(2)Å
C(4G) – C(5G)	1.40(3)Å
C(5G) – C(6G)	1.394(9)Å
C(6G) – C(1G)	1.393(5)Å
C(7G) – C(2G)	1.501(6)Å
C(8G) – C(3G)	1.504(8)Å

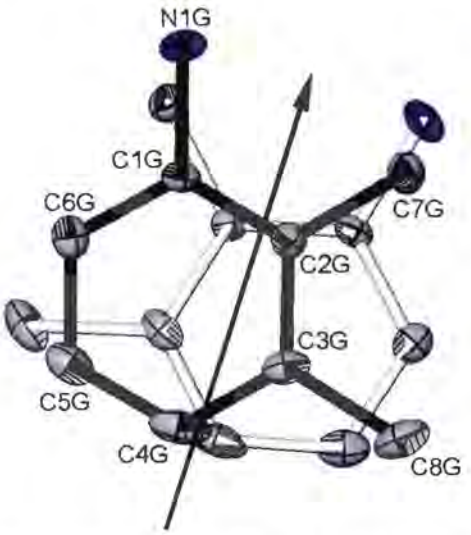

Figure 4.13 Disorder modelled in 2,3-xylidine molecule in **DHPC•0.5(23X)** and the resultant bond lengths. The arrow represents the two-fold rotation axis parallel to [010].

DHPC•2(23X) crystallises in P $\bar{1}$ with Z = 2. The asymmetric unit contains one host molecule and two guest molecules, all located on general positions. All of the non-hydrogen atoms were refined anisotropically. The hydroxyl hydrogen atoms and amino hydrogen atoms were located in the difference intensity maps and refined with simple bond length constraints and individual isotropic temperature factors. The rest of hydrogen atoms were placed geometrically. One of the methyl groups of the guest molecules was disordered and was refined with two positions for each hydrogen atom, offset from each other by 60°. The structure refined successfully to $R_1 = 0.0448$.

Structure analysis

DHPC•0.5(23X)

Four unique hydrogen bonds, of (host)O-H···O(host) and (host)O-H···N(guest) interactions are observed within the structure (**Table 4.7**). Each hydroxyl group of the host forms bifurcated hydrogen bonds to an adjacent host molecule in a head-to-tail fashion and to a guest molecule, which is disordered about a diad, thus forming a closed polygon, as shown in **Figure 4.14**. This result in the formation of two-dimensional hydrogen bonding network perpendicular to [001], centred at c = 1/4 and 3/4, which are related by two-fold rotation symmetry (**Figure 4.15c1**). In the structure the guest molecules are situated in cavities centred at y ≈ 0.28 and y ≈ 0.72. Each cavity adapts the shape to accommodate the 2,3-xylidine guest molecule, which is

disordered about the diad. The topology of the cavities is shown in **Figure 4.15**, where the crystal packing diagrams viewed along [100], [010] and [001], as well as the corresponding representative cross section planes are shown. The cavity has approximate volume of 8 x 9 x 6 $Å^3$ in three dimensions along a, b and c respectively.

Table 4.7 Details of hydrogen bonding in **DHPC•0.5(23X)**.

Donor(D)-H···Acceptor(A)	**D-H /Å**	**H···A /Å**	**D···A /Å**	**<DHA /°**
O(1)-H(1A)···O(2)[1]	0.96(1)	1.71(1)	2.668(1)	177(3)
O(1)-H(1B)···O(1)[2]	0.95(1)	1.75(1)	2.700(2)	176(5)
O(2)-H(2A)···N(1G)[3]	0.99(2)	1.73(2)	2.689(4)	162(3)
O(2)-H(2B)···O(1)[4]	0.96(2)	1.78(2)	2.668(1)	153(3)

Symmetry code: (1) x+1/2, y-1/2, z (2) -x, y, -z+1/2 (3) x-1/2, -y+1/2, z+1/2
(4) x-1/2, y+1/2, z

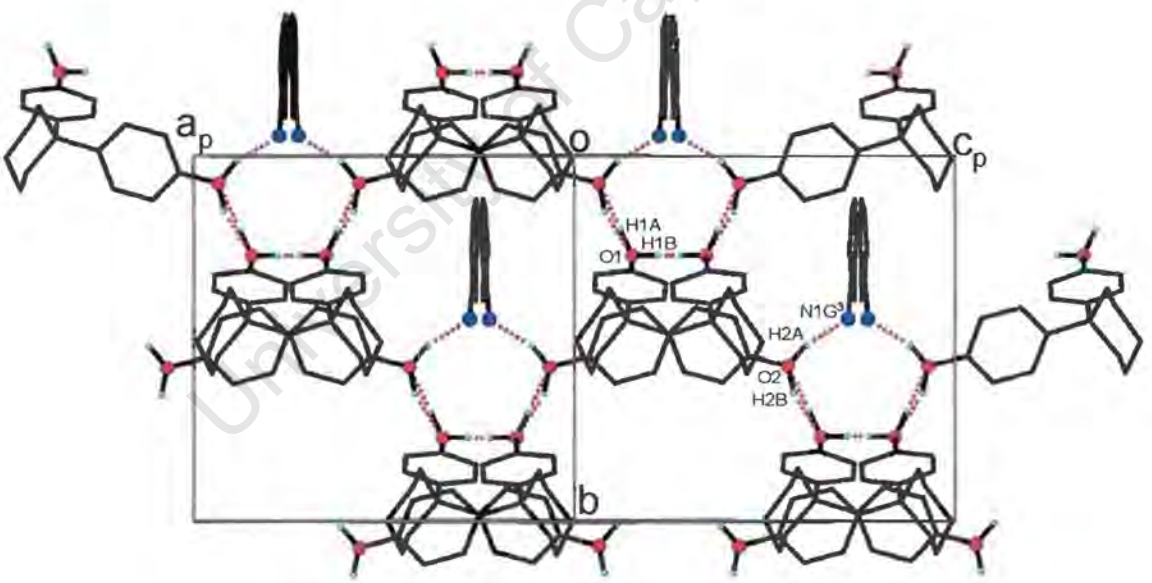

Figure 4.14 Part of the structure of **DHPC•0.5(23X)** viewed along [10 $\bar{1}$] showing the hydrogen bonding scheme. Only the hydroxyl hydrogens are shown.

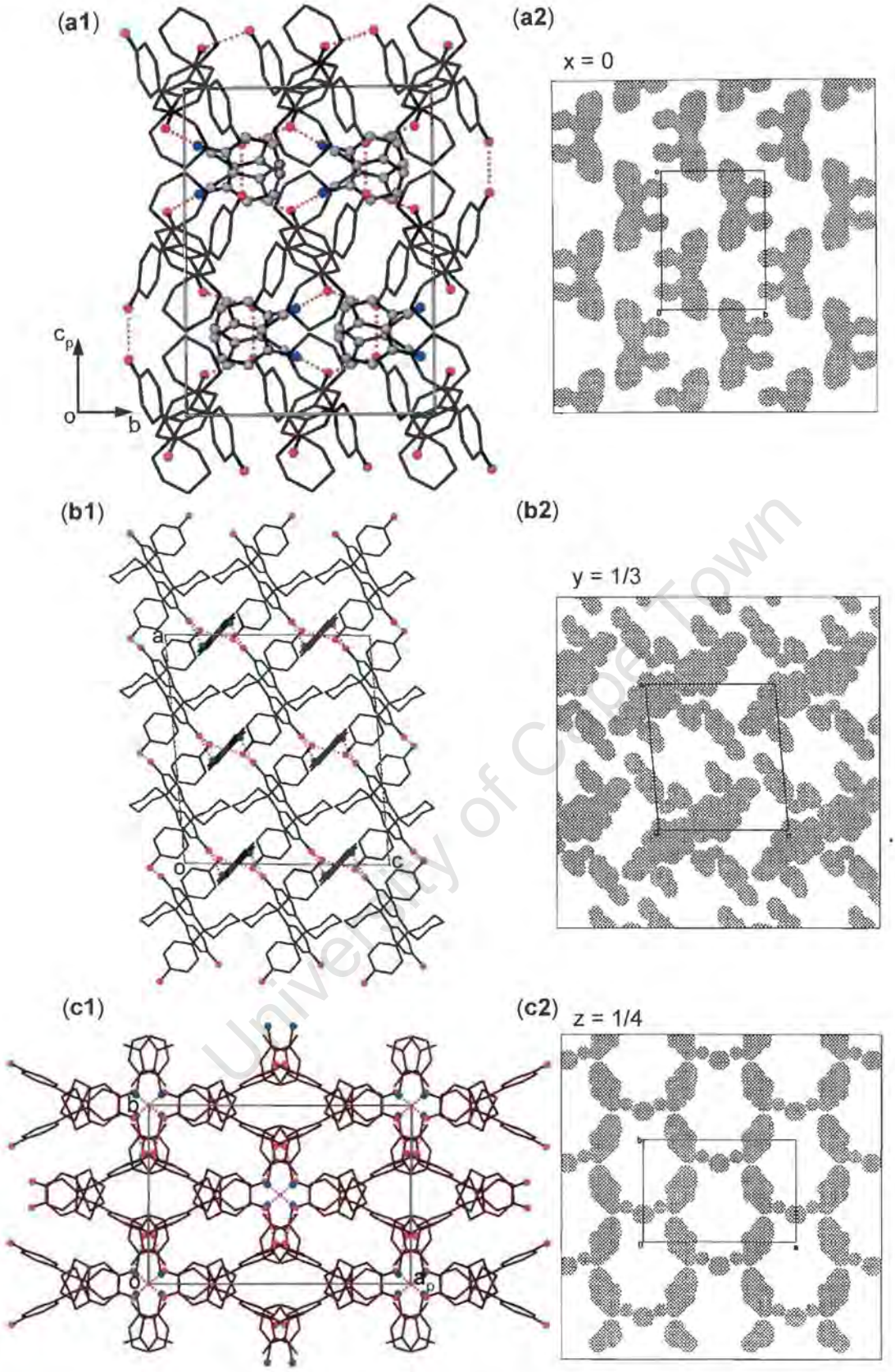

Figure 4.15 (Left) Projections of **DHPC•0.5(23X)**, viewed down (a1) [100], (b1) [010] and (c1) [001] (picture drawing details as in **Figure 4.14**). (Right) cross sections at (a2) x = 0, (b2) y = 1/3 and (c2) z = ¼, showing the topology of cavities in which guest molecules reside. The hatched areas represent the space occupied by the host. The guests are omitted to show the cavities.

DHPC•2(23X)

Again the structure is stabilised by the hydrogen bonds, which generate two-dimensional networks. One column runs along the direction [010] via (host)O-H···O(host) hydrogen bonds, another helix along the direction [100] via (host)O-H···(guest)N-H···(host)O-H hydrogen bonds and in addition the guest molecule is weakly hydrogen bonded to another guest molecule via N-H···N interaction [d(N···N) = 3.789(3)Å]. The hydrogen bonding scheme is shown in **Figure 4.16** and details of the hydrogen bonding interactions are listed in **Table 4.8**. The crystal packing is shown in **Figure 4.17a** and **4.18**, as viewed along [100] and [010] respectively. The [100] projection shows the double ribbons of host molecules running along [010], which form layers perpendicular to [001] (**Figure 4.17b**). It is noted that this structure displays certain similarities to **DHPC•26X** in term of hydrogen bonding pattern, crystal packing projected along two directions ([100], [010]) and inclusion mode, except that c axis is elongated in **DHPC•2(23X)** in order to accommodate one more guest molecule. The gap between layers of host molecules in **DHPC•2(23X)** is measured to be approximately 8Å across c in the narrowest part and 12Å in the widest part, compared to 6 - 9 Å observed in **DHPC•26X**.

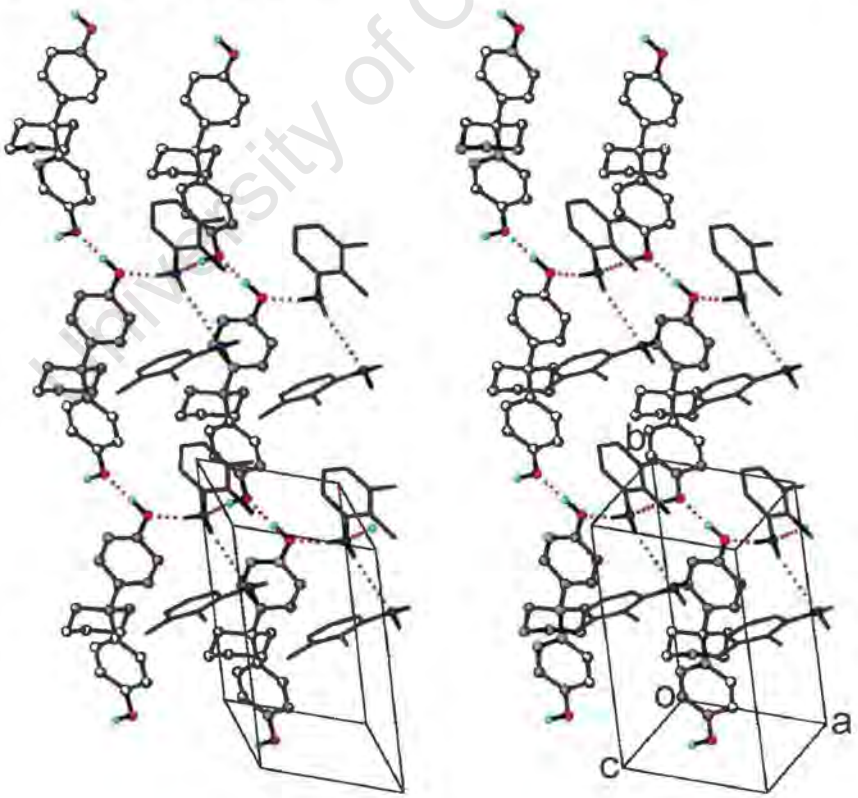

Figure 4.16 A stereoscopic view showing the hydrogen-bonding scheme in the structure of **DHPC•2(23X)**. All of the H atoms except the hydroxyl and amino hydrogens are omitted.

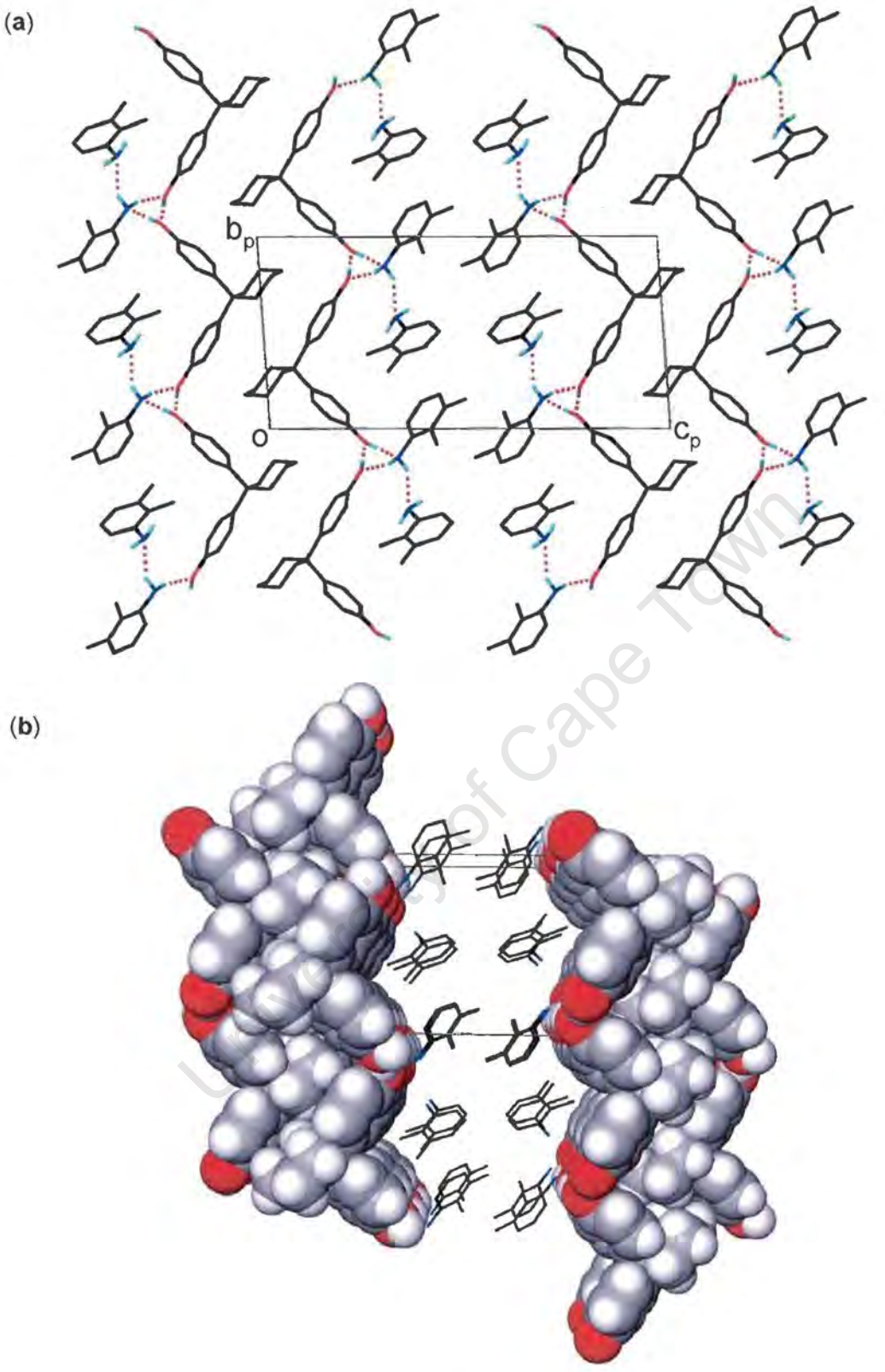

Figure 4.17 Projection viewed along [100] for **DHPC•2(23X)**. The crystal packing is shown in (a). The perspective space-filling diagram are shown in (b), which demonstrates the layers of host (in van der Waals representation) and guest (in stick representation).

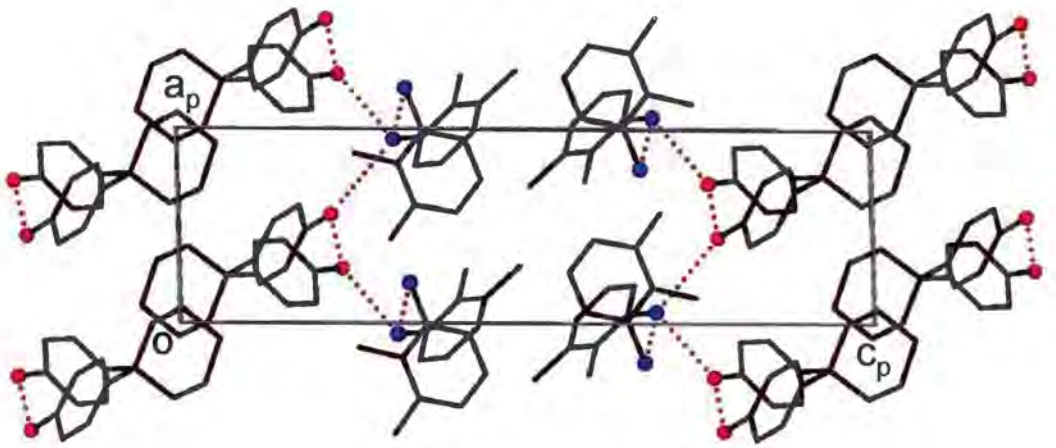

Figure 4.18 Crystal packing in **DHPC•2(23X)** projected down [010]. All of the H atoms are omitted. The hydrogen bonding contacts between O···O, O···N and N···N are indicated as dotted lines.

Table 4.8 Details of hydrogen bonding in **DHPC•2(23X)**.

Donor(D)-H···Acceptor(A)	**D-H /Å**	**H···A /Å**	**D···A /Å**	**<DHA /°**
O(1)-H(1)···O(2)[1]	0.98(1)	1.73(1)	2.707(2)	178(2)
O(2)-H(2)···N(1GA)[2]	0.98(1)	1.76(1)	2.734(2)	172(2)
N(1GA)-H(1A2)···O(1)	0.96(1)	2.10(1)	3.033(2)	163(2)
N(1GA)-H(1A1)···N(1GB)	0.94(1)	2.98(1)	3.789(3)	145(2)

Symmetry code: (1) x, y+1, z (2) x-1, y-1, z

DHPC•n(34X)•nH_2O

Guest: 3,4-xylidine (**34X**) and water(**H_2O**)

DHPC•0.5(34X)•H_2O ($C_{18}H_{20}O_2$•0.5$C_8H_{11}N$•H_2O)
Space group: P $\bar{1}$
a = 10.8979(5) Å α = 106.510(4)°
b = 12.5017(7) Å β = 99.895(3)°
c = 15.1701(7) Å γ = 102.559(2)°
Volume = 1872.93() Å^3
Z = 4

DHPC•34X ($C_{18}H_{20}O_2$•$C_8H_{11}N$)
Space group: C2/c
a = 34.9650(10) Å α = 90°
b = 6.2546(3) Å β = 101.577(1)°
c = 20.2035(8) Å γ = 90°
Volume = 4328.5(3) Å^3
Z = 8

Refinement

DHPC•0.5(34X)•H_2O crystallises in P $\bar{1}$ with Z = 4. The asymmetric unit comprises two host molecules, one 3,4-xylidine guest molecule and two water molecules. They were all located in general positions. All of the non-hydrogen atoms were refined with anisotropic temperature factors. All the hydrogen atoms on the functional groups (-OH and -NH_2) were located in the difference density maps and refined with simple bond length constraints. These hydrogens were assigned individual isotropic temperature factors, except those on the 3,4-xylidine molecules (H1G1, H1G2) and one of the water molecules (H2W1, H2W2) of which values of U_{iso} were fixed at 1.2 times of the U_{iso} of their parent atoms. A maximum residual electron density of 0.38 e/Å^3 was observed. The structure refined successfully to R_1 = 0.0654.

DHPC•34X crystallises in C2/c with Z = 8. The asymmetric unit contains one host molecule and one guest molecule, with both lying on general positions. All of the non-hydrogen atoms were refined anisotropically. The host hydroxyl hydrogen atoms and guest amino hydrogen atoms were found in the difference electron density maps and refined with simple bond length constraints and individual isotropic temperature factors. The rest of the hydrogen atoms were placed with geometric constraints and refined with individual isotropic temperature factors related to their parents atoms. A maximum residual electron density of 0.39 e/Å^3 was observed. This structure refined to R_1 = 0.1043.

Structure analysis

DHPC•0.5(34X)•H_2O

Extensive hydrogen bonds are formed between the host and water molecules in this structure. The water molecules (W1 and W2) act as hydrogen bonding bridges which link the host molecules (X and Y) in the [010] direction, and in addition one water (W2) hydrogen bonds to 3,4-xylidine molecules. The host molecules are also hydrogen bonded to each other along the [100] direction. This result in the formation of two-dimensional hydrogen bonding network, which is clearly illustrated in the projection down [001] (**Figure 4.20a**). The details of the hydrogen bond interactions are listed in **Table 4.9**. This structure is characterised by alternative layers of host molecules and 3,4-xylidine-water guest molecules, perpendicular to [001], as shown in **Figure 4.19b**. The approximate width of the space between the layers of host molecules is in the range 3.5Å to 7Å along c axis. The crystal packing along [010] (**Figure 4.19a**) and [100] (**Figure 4.20b**) indicate, again, similarity between the packing projected along [100] and [010] respectively in the structures of **DHPC•26X** and **DHPC•2(23X)** with respect to the host arrangements. The host molecules pack to form double ribbons running along one of crystallographic axes and in this way result in the formation of layers. The guest molecules are located between the layers.

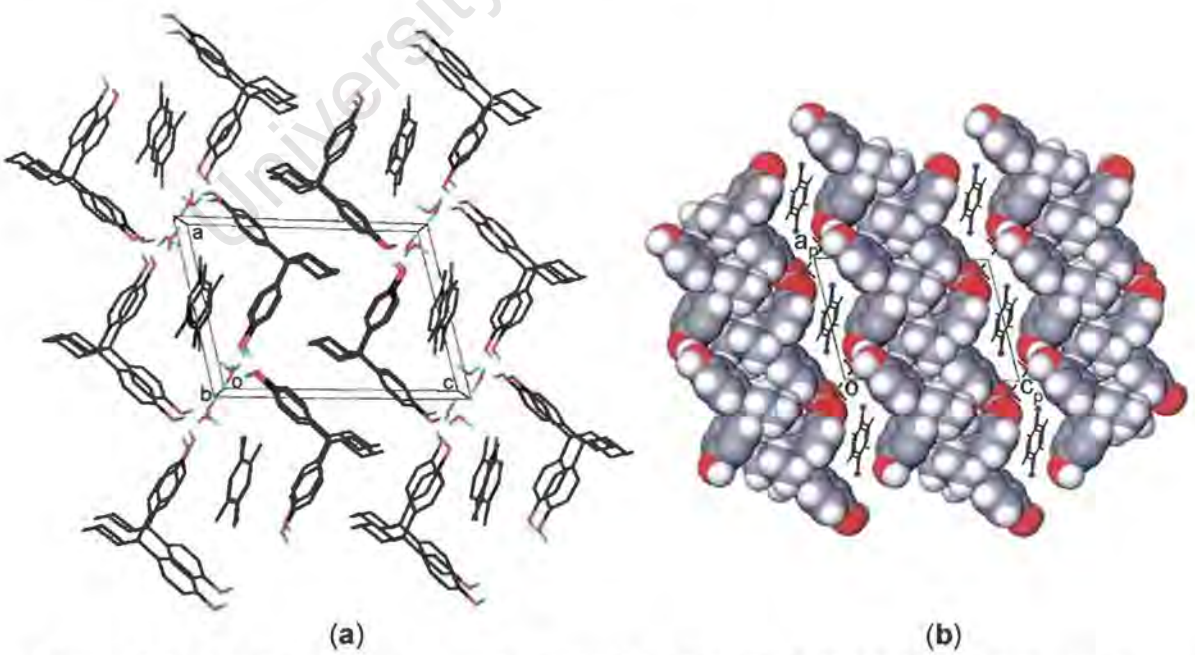

(a) (b)

Figure 4.19 (a) Prospective view along [010] for **DHPC•0.5(34X)•H_2O**. All the H atoms except the hydroxyl and aqueous hydrogens are omitted. The H-bonds are not indicated due to unclarity. (b) Space-filling diagram viewed along [010]. The host molecules are shown with van der Waals radii and the guest as sticks with the N atoms highlighted as circles.

Table 4.9 Details of hydrogen bonding in **DHPC•0.5(34X)•H_2O**.

Donor(D)-H···Acceptor(A)	D-H /Å	H···A /Å	D···A /Å	<DHA /°
O(1X)-H(1X)···O(2X)[1]	0.98(1)	1.74(1)	2.709(3)	168(3)
O(2X)-H(2X)···O(1W)[2]	0.96(1)	1.67(1)	2.628(3)	172(4)
O(1Y)-H(1Y)···O(2W)[2]	0.98(2)	1.70(2)	2.651(3)	165(4)
O(2Y)-H(2Y)···O(1Y)[1]	0.96(1)	1.73(1)	2.688(3)	176(4)
O(1W)-H(1W1)···O(2Y)[3]	0.94(2)	1.82(2)	2.757(3)	173(4)
O(1W)-H(1W2)···O(2W)[4]	0.94(2)	1.80(2)	2.740(3)	175(4)
O(2W)-H(2W1)···O(1X)	0.97(2)	1.83(2)	2.765(3)	161(4)
O(2W)-H(2W2)···N(1G)	0.98(2)	1.95(2)	2.923(4)	170(4)

Symmetry code: (1) x-1, y, z (2) x+1, y, z (3) x, y+1, z (4) -x, -y+1, -z.

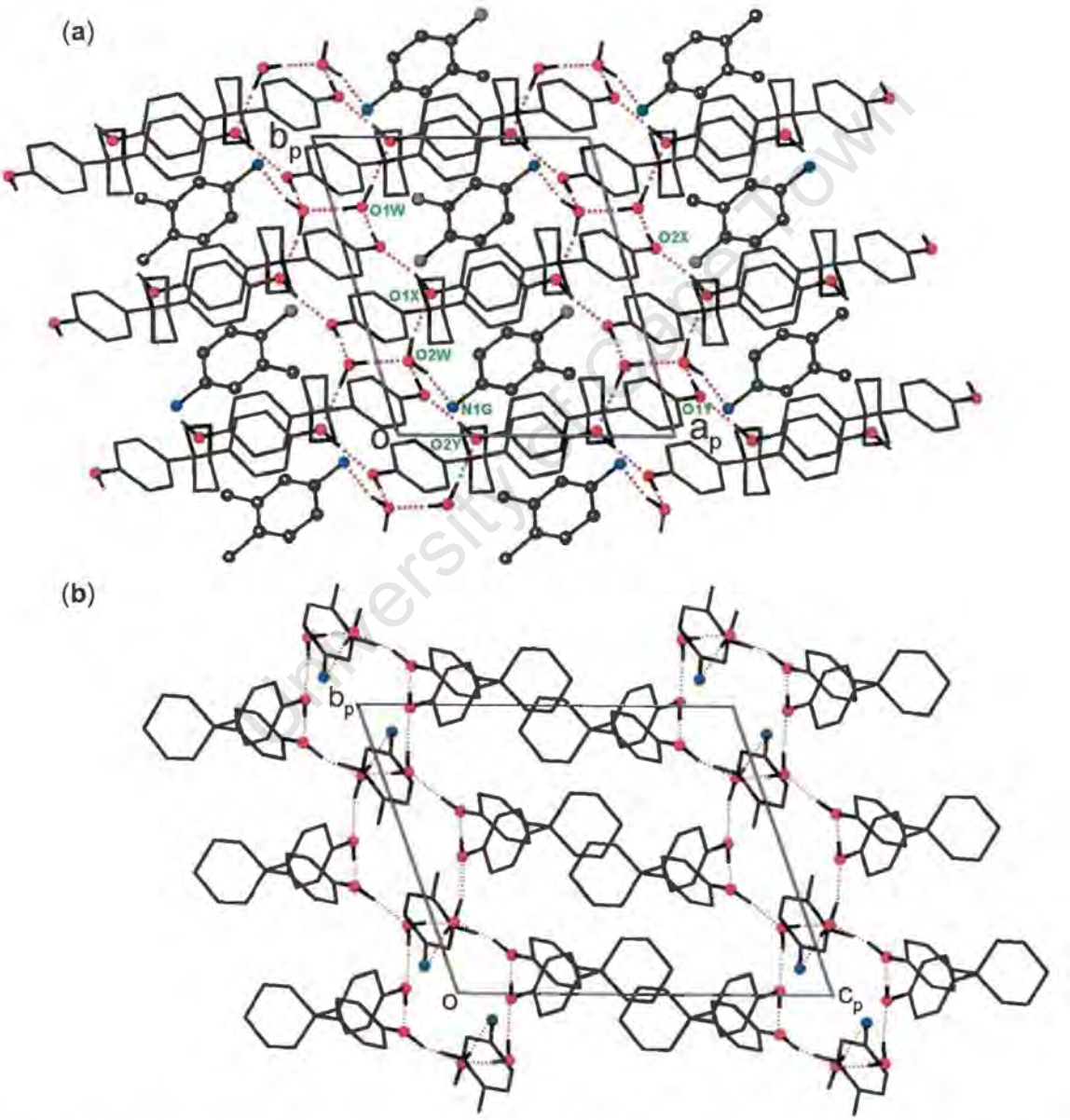

Figure 4.20 Projections viewed along (a) [001] and (b) [100], showing the crystal packing in **DHPC•0.5(34X)•H_2O**. All of the H atoms except those take part in hydrogen bonds are omitted. The O and N atoms are shown as circles. The hydrogen bonds are indicated as dotted lines.

DHPC•34X

The hydrogen bonds link the host and guest molecules in the direction [010] and [001], exhibiting hydrogen bonds motif ···O-H···N-H···O-H···(see **Figure 4.21** and details in **Table 4.10**). The hydrogen bonding pattern is similar to that found in the structure of **DHPC•26X**. Double ribbons of host molecules run along [001] with the guest molecules in between, stabilised by hydrogen bonds (**Figure 4.22a**). Again, the structure has alternate layers of host and guest molecules perpendicular to [100] and the space between the host layers is approximately 4Å to 8Å across a. This is illustrated in two cross sectional diagrams in **Figure 4.22c** and **4.22d**, in which show the narrowest and widest part between the host layers respectively. The projection viewed along [001] is shown in **Figure 4.22b**.

Table 4.10 Details of hydrogen bonding in **DHPC•34X**.

Donor(D)-H···Acceptor(A)	D-H /Å	H···A /Å	D···A /Å	<DHA /°
O(1)-H(1)···O(2)[1]	0.95(2)	1.77(2)	2.706(4)	166(4)
O(2)-H(2)···N(1G)[2]	0.97(2)	1.78(2)	2.744(5)	173(5)
N(1G)-H(1G1)···O(1)	0.98(2)	2.02(2)	2.975(5)	166(3)

Symmetry code: (1) x, -y+2, z-0.5 (2) x, -y+1, z+0.5.

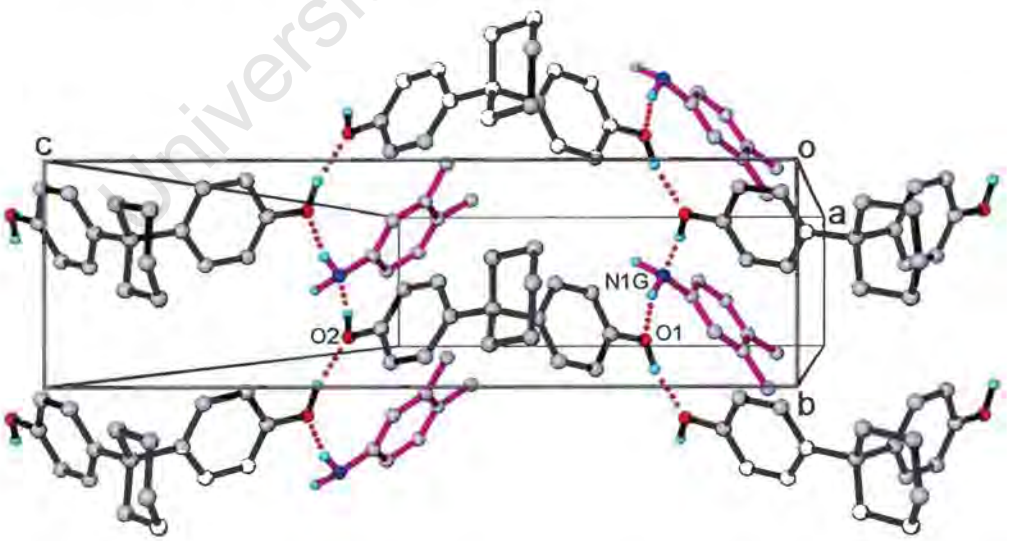

Figure 4.21 Perspective view down the (100) plane, showing the hydrogen bonding scheme for **DHPC•34X**. All of the H atoms except the hydroxyl and amino hydrogens are omitted. The hydrogen bonds are shown as dotted lines.

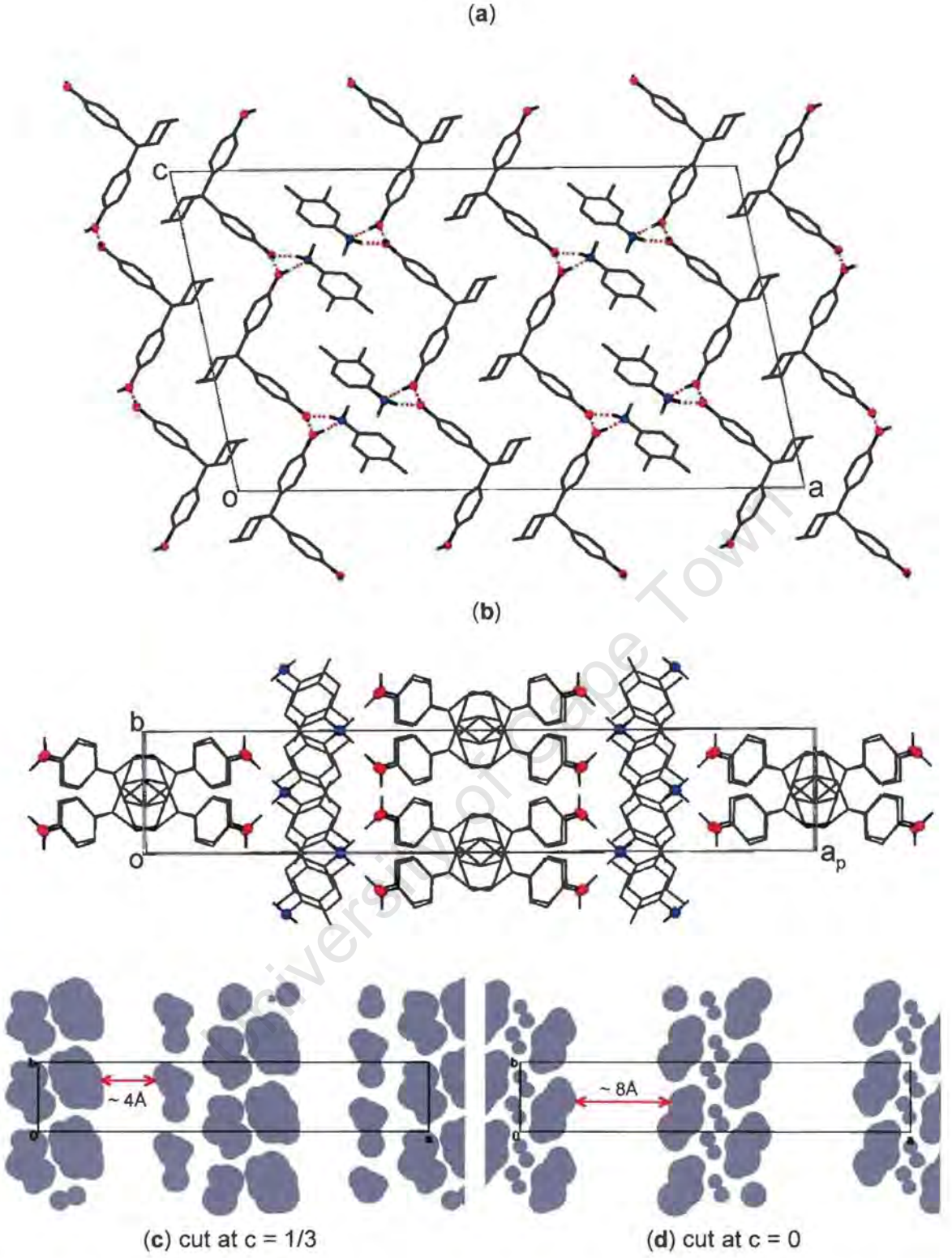

Figure 4.22 (a) and (b) are projections viewed along [010] and [001] respectively, showing the crystal packing in **DHPC•34X**. Only the hydroxyl and amino hydrogen atoms are shown. The hydrogen bonds are indicated in (a), but not in (b) for clarity.
(c) and (d) show the narrowest (~4Å) and widest (~8Å) part between the host layers in which the guest molecules are located. The solid area represents the space occupied by the host. The guest is omitted.

DHPC•35X

Guest: 3,5-xylidine (**35X**)	
$C_{18}H_{20}O_2 \cdot C_8H_{11}N$	
Space group: P $\bar{1}$	
a = 6.327(1) Å	α = 96.48(2)°
b = 10.720(2) Å	β = 100.09(2)°
c = 16.920(4) Å	γ = 99.83(1)°
Volume = 1101.1(4) Å^3	
Z = 2	

Refinement

DHPC•35X crystallises in P $\bar{1}$ with Z = 2. There is one host molecule and one guest molecule in the asymmetric unit and both of them were located in general positions. All of the non-hydrogen atoms were refined anisotropically. The hydroxyl hydrogen atoms on the host and the amino hydrogen atoms on the guest were located in the difference electron density maps and refined with simple bond constraints at a value of d(O-H) = 0.98Å and d(N-H) = 0.97Å. The other hydrogen atoms were calculated and placed with idealised geometric constraints, although most of them could be found in the difference electron density maps. The structure refined successfully to R_1 = 0.0439.

Structure analysis

In the structure, the infinite ···O-H···N-H···O-H··· hydrogen bonds linking the host and guest molecules spiral along [100] (**Figure 4.23a**). In addition O-H···O interactions link host molecules along [010]. Thus a two-dimensional hydrogen bonding network is generated perpendicular to [001]. The hydrogen bonding interactions are listed in **Table 4.11**. This hydrogen bonding pattern is identical to that observed in structure **DHPC•26X**. The crystal packing along both the [100] and [010] directions in **DHPC•35X** are similar to those in **DHPC•26X** with respect to the host molecules. **Figure 4.23b** illustrates the crystal packing projected down [100] for **DHPC•35X**, showing the double ribbons of host molecules running along [010]. However, the crystal packing projected along [001] in the two structures is subtly different, as compared in **Figure 4.24**. The 3,5-xylidine guest molecules, again, are situated between layers of host molecules, perpendicular to [001]. The space between the host layers is approximately 5.5 - 8.5Å in width, compared with 6 - 9Å in **DHPC•26X**.

Lattice energy calculations

The lattice energies were calculated using the program MPA (Williams, 1999) for selected inclusion compounds. It is known that comparative values of the lattice energies are only strictly valid between host-guest systems of the same host with guests which are isomers and where the host:guest ratios are identical. Therefore three structures, **DHPC•26X**, **DHPC•35X** and **DHPC•34X**, in which the host:guest ratios are the same, were selected. The calculations were carried out by summation of the host···host, host···guest and guest···guest non-hydrogen bonding lattice energies and the hydrogen bonding potentials, and yielded the following values for the total lattice potential energies:

DHPC•26X	-74.8 kJ mol^{-1};
DHPC•35X	-173.8 kJ mol^{-1};
DHPC•34X	-181.9 kJ mol^{-1}.

This is a gratifying result, showing that 2,6-xylidine will always be disfavoured with respect to 3,5-xylidine and 3,4-xylidine. The latter two have similar lattice energies and give rise to concentration dependant selectivity as shown in **Figure 4.25c**, while **Figure 4.25d** shows that the 2,6-xylidine is never preferred.

Kinetics of desolvation

Kinetics of desolvation of a number of the inclusion compounds discussed in this chapter were investigated using different methods. For **DHPC•35X**, a series of isothermal TG runs at selected temperatures between 65°C and 115°C have been carried out. The curves of the extent of reaction (α) *versus* time (t) were deceleratory (**Figure 4.26a**) and were best fitted to the contracting area kinetic model R2 (Brown, 1988), over an α-range of 0.05 - 0.95. The Arrhenius plot of ln k *versus* 1/T is shown in **Figure 4.26b** and yields value of 108(5) kJ/mol and 32(2) min^{-1} for the activation energy and the logarithm of the pre-exponential factor A respectively.

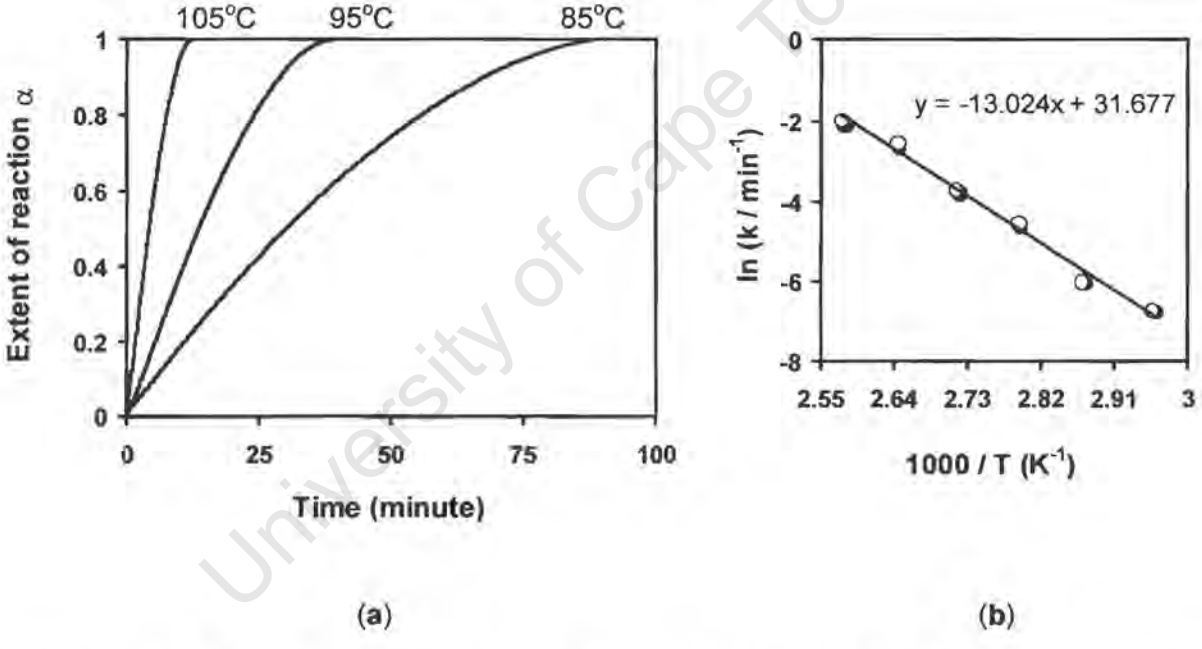

Figure 4.26 (a) Examples of α *versu* time curves at 105°C, 95°C and 85°C respectively for the desolvations of **DHPC•35X**.
(b) Arrhenius plot of ln k *versus* 1/T.

DHPC•2(23X) decomposed in multiple steps and therefore the isothermal temperature method of analysis is not suitable. A series of thermal desolvation at different heating rates were carried out and the data obtained were analysed by a non-isothermal method described by Flynn and Wall (1966). The rate of desolvation is given by

$$d\alpha/dT = (A/\beta)g(\alpha)\exp(-E_a/RT)$$

where β is the constant heating rate. This equation was differentiated with respect to α with the assumption that constant A, $g(\alpha)$ and E_a are independent of temperature and that A and E_a are independent of $g(\alpha)$, and the following equation was derived:

$$d(\log \beta) / d(1/T) \approx (0.457/R)E_a$$

Thus, from weight loss *versus* temperature curves at several heating rates, β, the corresponding temperatures at a constant weight loss (or α) may be read off. A plot of *log* β *versus* $1/T$ yields a straight line with slope = $(R/0.457)E_a$. The procedure is repeated at several values of α, to give a more precise average value of E_a.

In the desolvation of **DHPC•2(23X)**, the TG runs were performed at heating rates of 1, 2.5, 5, 10 and 20°C per minute. The weight losses *versus* temperature data, shown in **Figure 4.27a**, were reduced and analysed for various percentages of decomposition ranging from 5% to 45%. The logarithm of the heating rate (β) *versus* $1/T$ for various percentage decomposition were plotted and are shown in **Figure 4.27b**, which yielded activation energies calculated from these slopes vary from 64(6) to 75(6) kJ mol^{-1}, averaging in 70 kJ mol^{-1}. The results obtained from this non-isothermal method are less satisfactory, since the slopes display a poor consistency which resulted in the activation energies lying in a relatively big range. This behaviour is an indication that the reaction of desolvation of **DHPC•2(23X)** proceeds as non-single, multiple steps.

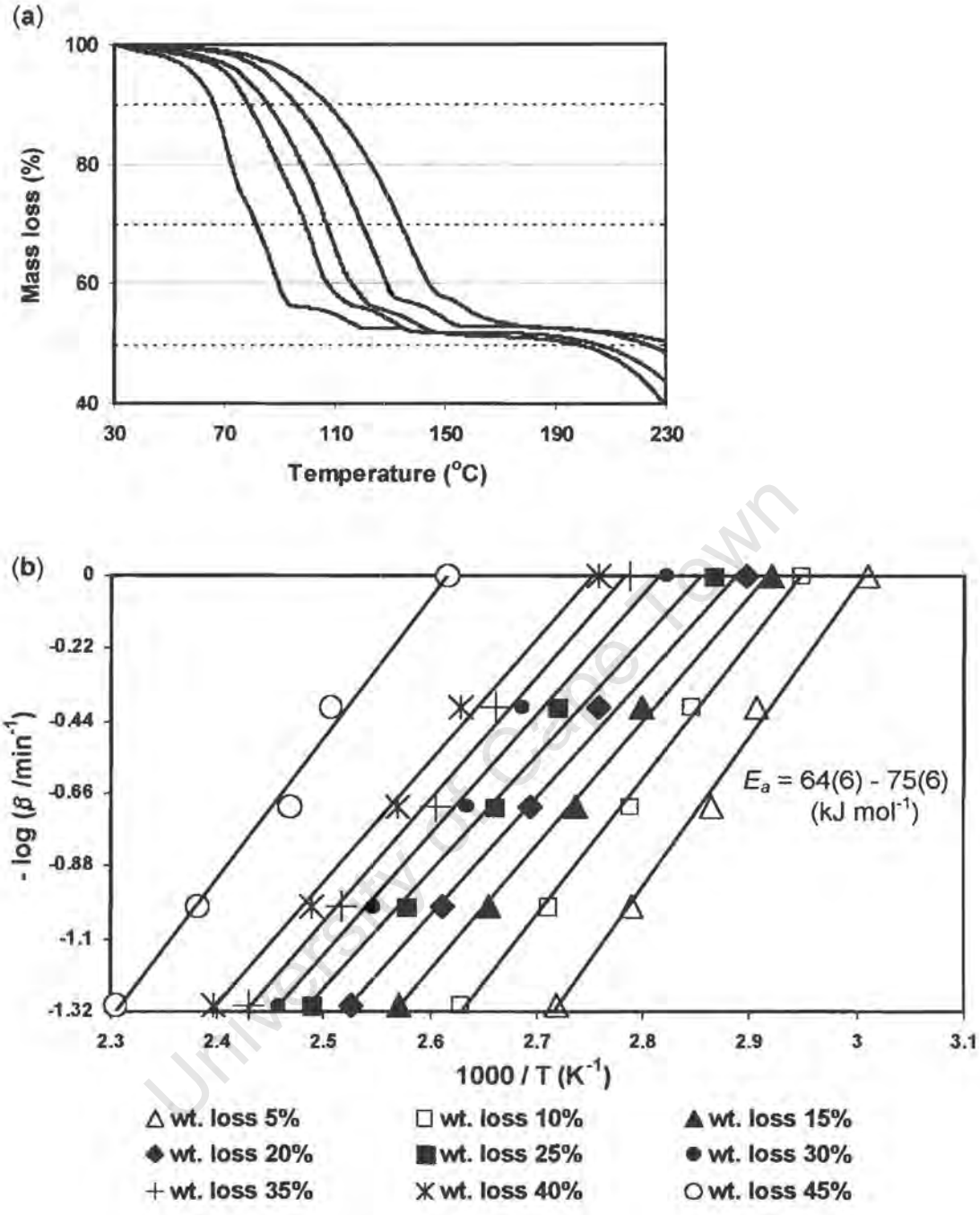

Figure 4.27 (a) Thermal TG runs performed on **DHPC•2(23X)** at heating rates of 1, 2.5, 5, 10 and 20°C min^{-1}, as shown on the picture from left to right. (b) -log β *versus* $1/T$ curves for various percentage mass losses.

The desolvation reaction of **DHPC•0.5(23X)** is of particular interest, since its crystal structure is the only one in which the guest molecules are entrapped in closed cages. Numerous attempts to reproduce the crystals at 80°C failed, because at such high crystallisation temperature the guest solvent readily evaporated and resulted in the formation of dull brown dehydrated powder. In order to obtain Arrhenius parameters for the desolvation of **DHPC•0.5(23X)**, the programmed temperature TG run was analysed according to a method described by Borchardt and Daniels (1957). The mass loss *versus* temperature curve was converted to an α *versus* time curve, shown in **Figure 4.28a**. Since $\alpha = mass_t / mass_{total}$, where $mass_t$ is the mass loss at a given time t. $mass_{total}$ is the total mass loss and $t = T/\beta$, where t is time in minutes, T is temperature in °C and β is the heating rate in °C min^{-1}. An Arrhenius plot can be acquired, if the kinetic model is known, since $g(\alpha) = 1/k^*d\alpha/dt$. A variety of kinetic models were tested for linearity, and the second order reaction mechanism (F2) gave the best fit of the data (**Figure 4.28b**). It yielded an activation energy of 177(2) kJ mol^{-1} for the desolvation reaction, over an α-range of 0.10 - 0.90. This value appears significantly higher than the activation energies calculated for the desolvation of **DHPC•35X** and **DHPC•2(23X)**, suggesting that there is much larger energy barrier to desorption of guest from the host frame work of **DHPC•0.5(23X)** than that of the latter two compounds.

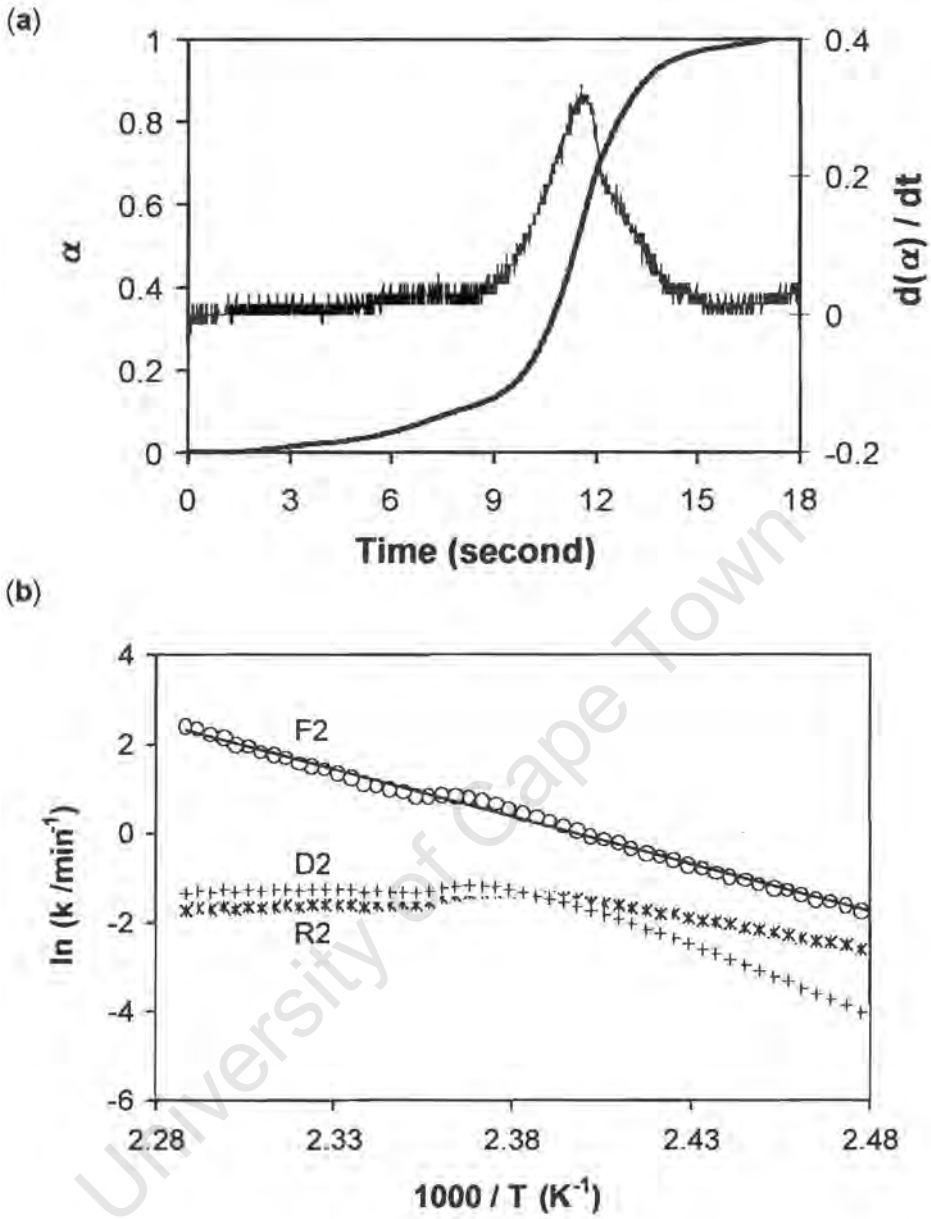

Figure 4.28 (a) α *versus* time curve for the desolvation of **DHPC•0.5(23X)**. (b) Arrhenius plots tested for different kinetic models.

Discussion

Inclusion complexes of various stoichiometries between the host **DHPC** and a number of isomers of xylidine were crystallised at different temperatures. The host:guest ratio increases with increasing crystallisation temperature, but in the case of 3,4-xylidine this pattern is broken by the incorporation of a water of crystallisation.

All of the structures, except **DHPC•3(26X)** and **DHPC•0.5(23X)**, are good examples of layer type clathrates. Their crystal packing are characterised by alternative layers of host and guest molecules perpendicular to one of the crystallographic axes. It is shown clearly that layers of host and guest are the preferred crystal packing for the host **DHPC** enclathrating the xylidine guests. However, the low-temperature structure with 2,6-xylidine, **DHPC•3(26X)** with a low host:guest ratio of 1:3, the guest molecules are situated in interconnected channels. More interestingly, in the high-temperature structure with 2,3-xylidine, **DHPC•0.5(23X)** with a high host:guest ratio of 1:0.5, the guest is entrapped in a closed cage. The later phenomenon well reflects the remarks made by Ibragimov (1999): *"A pseudopolymorphic versatile host compound responds to an increase of the crystallisation temperature by entrapping of the guest component into a "more closed" space in order to withstand the higher thermal mobility of the molecules being enclathrated."*

Another interesting phenomenon observed with regard to crystallisation temperature is that disorder of guest molecule occurred in the structures obtained at relatively high temperature, *i.e.* **DHPC•26X**, **DHPC•1.5(26X)** and **DHPC•0.5(23X)**, which crystallised at 80°C, 60°C and 80°C respectively. In the latter two structures, however, the guest molecules were located at crystallographically special positions, and a lack of symmetry in the guest molecules is therefore compensated for by disordering over two positions. Similar observation has been reported by Makhkamov et. al (1996).

Comparison of parameters obtained from the crystal structures for all the inclusion compounds discussed in this chapter is given in **Table 4.12**, together with the selectivity trends displayed by the host towards each isomer.

Table 4.12 Selected structural parameters for all inclusion compounds discussed.

Inclusion Compound	Calc. density ($g\ cm^{-3}$)	*Packing efficiency (%)	Lattice energy ($kJ\ mol^{-1}$)	Inclusion Mode and space[ε] (Å)	H-bond type And bond length range [†]D···A (Å)
DHPC•26X	1.162	65.9	-74.8	Layer (6 – 9)	**H**···**H** 2.757(3) **H**···**G** 2.768[‡] **G**···**H** 3.135[‡]
DHPC•1.5(26X)	1.191	67.6*	/	Layer (4.5 – 9)	**H**···**H** 2.759(2) **H**···**G** 2.804(3) **G**···**H** 3.191(3) **G**···**G** 3.392(3)
DHPC•2.5(26X)	1.166	64.7*	/	Inter-connected layer[ε]	**H**···**H** 2.752(7) **H**···**G** 2.783(8)-2.84(1) **G**···**H** 3.112(9)-3.692(8) **G**···**G** 3.327(8)
DHPC•3(26X)	1.138	66.6	/	Inter-connected channel[ε]	**H**···**G** 2.783(4)-2.835(4) **G**···**H** 3.025(4)-3.149(4)
DHPC•0.5(23X)	1.214	69.2	/	Cage (6 x 8 x 9)	**H**···**H** 2.668(1)-2.700(2) **H**···**G** 2.689(4)
DHPC•2(23X)	1.186	68.8	/	Layer (8 – 12)	**H**···**H** 2.707(2) **H**···**G** 2.734(2) **G**···**H** 3.033(2) **G**···**G** 3.789(3)
DHPC•0.5(34X)•H_2O	1.230	69.1	/	Layer (3.5 – 7)	**H**···**H** 2.688(3)-2.709(3) **H**···**W** 2.628(3)-2.651(3) **W**···**H** 2.757(3)-2.765(3) **W**···**G** 2.923(4) **W**···**W** 2.740(3)
DHPC•34X	1.195	68.1	-181.9	Layer (4 – 8)	**H**···**H** 2.706(4) **H**···**G** 2.744(5) **G**···**H** 2.975(5)
DHPC•35X	1.175	66.6	-173.8	Layer (5.5 – 8.5)	**H**···**H** 2.701(3) **H**···**G** 2.697(3) **G**···**H** 3.013(4)

Selectivity trends: **34X** ≥ **35X** >> **26X** or **35X** ≥ **23X** >> **26X**

* Packing efficiency, *i.e.* the percent filled space, was obtained using program PLATON (Spek, 1990), or using program X-Seed (Barbour, 1999a) by calculating the molecular volume. The values for structures **DHPC•1.5(26X)** and **DHPC•2.5(26X)** are not precise, since some of the hydrogen atoms on the disordered or distorted guest molecules were not taken into account.

ε The space is the size of the void generated by the host molecules, in which the guest molecules are located. For example, In case of layer inclusion structure, the size of space is the perpendicular distance between two layers of host. For structures of **DHPC•2.5(26X)** and **DHPC•3(26X)**, descriptions regarding the void topology refer to page 87 and 89.

† **D** - Donor **A** - Acceptor
H - O atom on the host **DHPC** **G** - N atom on the xylidine guest molecule
W - O atoms on the water molecule

‡ These values are the average of two distances of O···N and N···O respectively, since the guest is disordered over two sites.

The ability of acting as both hydrogen bond acceptor and donor by both the hydroxyl group of the host **DHPC** and the amino group of the guest xylidines give rise to these versatile inclusion compounds with various host:guest ratios. Intermolecular hydrogen bonds are formed between molecules of host and host, host and guest, and guest and guest with the hydrogen bonding types of (host)O-H···O(host), (host)O-H···N(guest), (guest)N-H···O(host) and (guest)N-H···N(guest). Among them, the relatively strong hydrogen bond, (host)O-H···O(host) with O···O distance varying from 2.668(1)Å to 2.759(2)Å, is present in all structures except **DHPC•3(26X)**. The weakest hydrogen bond is (xylidine)N-H···N(xylidine), which is only present in the structures of **DHPC•1.5(26X)** and **DHPC•2(23X)**, with N···N distance in the range of 3.392(3)Å - 3.789(3)Å. The hydrogen bond interactions between host and xylidine guest are present in all structures except **DHPC•0.5(34X)•H_2O**, in which the water molecules act as hydrogen bonding bridges between the host and xylidine molecules.

Versatile hydrogen bonding patterns are observed in these structures, some of which are schematically shown in **Figure 4.29**. The most frequently occurred hydrogen bonding motif is type **1**, found in the structures of **DHPC•26X**, **DHPC•34X** and **DHPC•35X**, in which two-dimensional hydrogen bonds network formed with chains of (host)O-H···O(host) and ···(host)O-H···N(guest)-H···O(host)··· running along two of the crystallographic axes. The hydrogen bonding pattern in **DHPC•2(23X)** is similar to type **1**, with one addition in that each guest molecule is hydrogen bonded to another guest, conforming to the host:guest ratio of 1:2. A similar pattern is observed in **DHPC•0.5(34X)•H_2O**, with water molecules substituted for the xylidine molecules. The five structures mentioned above are characterised by similar crystal packing pattern with respect to host molecules. In all cases, the host molecules pack back to back to form double ribbons by convenient steric fit of the cyclohexyl ring systems of adjacent single host ribbon, which is linked via O-H···O hydrogen bond. These double ribbons of host molecules form a layer with the hydrophilic side facing the guest molecules.

In the type **3** hydrogen bonding motif, the hosts are hydrogen bonded to each other about a centre of inversion and thus form a dimer, and in addition are hydrogen bonded to the guest. This type is found in the structures of **DHPC•1.5(26X)** and **DHPC•2.5(26X)**, and the latter also has type **4** hydrogen bond motif. Different hydrogen bonding pattern for structures **DHPC•3(26X)** (type **2**) and **DHPC•0.5(23X)** (bifurcated hydrogen bonds, refer to **Figure 4.14**) are also observed. It is clear that the stoichiometry is related to the arrangement of hydrogen bonds. However in the case of **DHPC•3(26X)** structure, two xylidine guest molecules do not take part in hydrogen

bonds and this makes the prediction of hydrogen bonding arrangement from stoichiometry impossible. These hydrogen bonding patterns can serve as templates for predicting crystal packing.

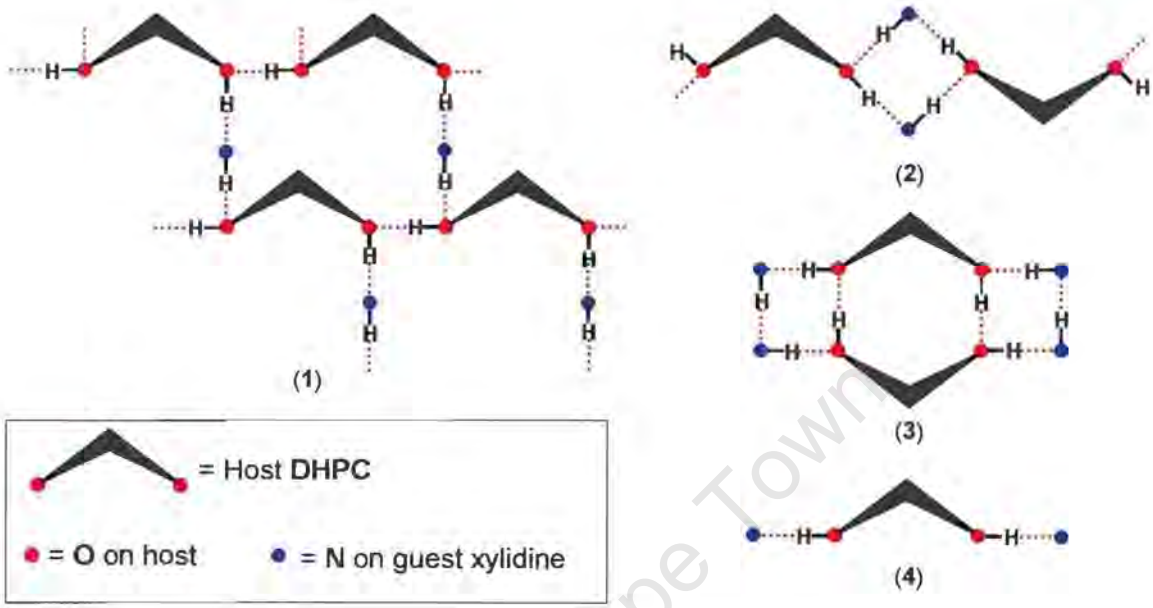

Figure 4.29 Schematically representation of various types of hydrogen bonding motifs observed in the host-guest inclusion structures in this chapter.

The structural parameters given in **Table 4.12** display the compatibilities between the host **DHPC** and guest xylidine isomers, and this gives an explanation for the selectivity of inclusion by the host. Firstly take the hydrogen bonds as example, the (host)O-H···N(xylidine) hydrogen bonding interactions in the host-guest systems between the host and 2,6-isomer, **DHPC•n(26X)**, have O···N distances in the range of 2.768-2.84(1)Å. This is relatively longer than those observed in other host-guest systems between the host and 2,3-, 3,4- and 3,5-xylidines, which lie in the range of 2.689(4)-2.744(5)Å. The (host)O-H···O(host) interactions with O···O distances from 2.752(7)-2.759(2)Å in **DHPC•n(26X)**, are weaker compared to the others in which the O···O distances are in the range of 2.668(1)-2.709(3)Å. This is also true for the (guest)N-H···O(host) hydrogen bonding interactions. Secondly if we consider the 1:1 inclusion complexes **DHPC•26X**, **DHPC•35X** and **DHPC•34X** for comparison: the inter-layer space, which accommodates guest molecules, was measured to be 6 - 9Å, 5.5 - 8.5Å and 4 - 8Å respectively, with that of **DHPC•26X** being the widest; The crystal packing efficiencies are 65.9%, 66.6% and 68.1% respectively, indicating the packing of **DHPC•26X** is the most inefficient; The lattice energies were calculated to be -74.8, -

181.9 and -173.8 in kJ mol^{-1} respectively, with **DHPC•26X** being the least stable structure. Clearly, 2,6-xylidine forms the least optimum host-guest system with the host.

Moreover, thermal analyses for these three 1:1 inclusion compounds show that desolvation of **DHPC•26X** began at much lower onset temperature than the other two compounds (92.4°C versus 130.2°C and 124.2°C). These values are indicative of relative thermal stability and show that **DHPC•26X** is most unstable upon heating.

These results are in good agreement with the competition experiments, which showed that the 2,6-xylidine is the least favoured isomer and the other three isomers, 2,3-xylidine, 3,5-xylidine and 3,4-xylidine, display concentration-dependant preferential selectivity by the host.

It is noted that the inclusion selectivities between isomers of lutidines (Caira *et al.* 1998), xylenols (Caira *et al.* 2000) by the same host **DHPC** follow similar trend as in the case between xylidine isomers. In all the cases, 2,6-substituted isomers are the least favoured isomers. One of the explanations is that the steric hindrance of the methyl substituents at 2 and 6 positions, which is close to the functional group of the guest, impedes the formation of hydrogen bonds which stabilise the host-guest system. This indicates that molecular recognition is governed partly by some stereo-electronic or symmetry property of the guest molecule.

The kinetics of desolvation reactions for inclusion compounds **DHPC•2(23X)** and **DHPC•35X** yield activation energies in the range of 70 - 108 kJ mol^{-1}, and these relatively low values are justified by the open layers structures which do not hinder the movement of guest molecules from the lattice. For the desolvation of **DHPC•0.5(23X)**, a remarkably high activation energy of 177(2) kJ mol^{-1} was obtained. The closed cage structure would imply that the guest can only escape by severely disrupting the host framework. This is also reflected in its thermal stability upon heating – the guest desorption onset temperature is the highest compared to the rest of inclusion compounds.

The calculated powder XRD patterns from single crystal data for all inclusion compounds discussed in this chapter are shown in **Figure 4.30**, as a proof that the structures observed are different.

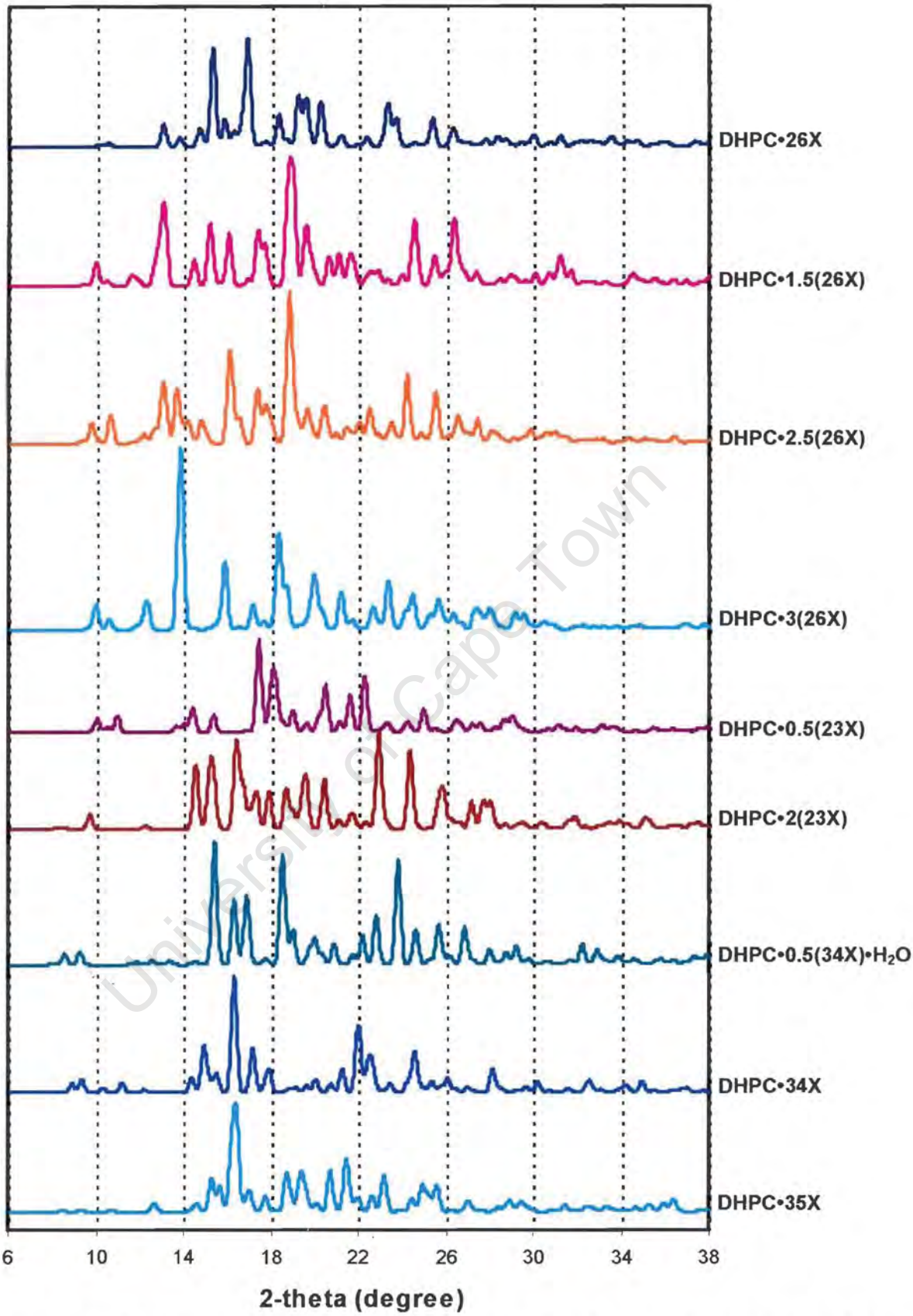

Figure 4.30 Calculated XRD patterns from single crystal structure data, for all of the inclusion compounds of **DHPC** with xylidines, discussed in this chapter.

Table 4.13 Crystal data, data collection and final refinement parameters.

Inclusion compound	**DHPC•26X**	**DHPC•1.5(26X)**	**DHPC•2.5(26X)**
Molecular formula	$C_{18}H_{20}O_2 \bullet C_8H_{11}N$	$C_{18}H_{20}O_2 \bullet 1.5C_8H_{11}N$	$C_{18}H_{20}O_2 \bullet 2.5C_8H_{11}N$
Guest	2,6-xylidine	2,6-xylidine	2,6-xylidine
Formula weight ($gmol^{-1}$)	389.52	450.11	571.29
Crystal Data			
Crystal system	Triclinic	Triclinic	Triclinic
Space group	P $\bar{1}$	P $\bar{1}$	P $\bar{1}$
a (Å)	6.234(1)	7.8594(3)	7.885(1)
b (Å)	10.934(2)	10.015(1)	10.026(1)
c (Å)	16.974(2)	17.169(1)	43.761(3)
α (°)	84.98(1)	78.909(2)	94.661(1)
β (°)	81.29(2)	85.161(1)	91.539(2)
γ (°)	77.10(2)	71.238(1)	109.020(1)
Volume ($Å^3$)	1113.1(3)	1255.3(2)	3254.6(6)
Z	2	2	4
Calculated density D_c (gcm^{-3})	1.162	1.191	1.166
μ (mm^{-1})	0.072	0.074	0.071
F(000)	420	486	1236
Data collection			
Temperature (K)	293 (2)	173 (2)	173 (2)
Range scanned, θ (°)	1.91 - 24.92	2.74 – 25.64	2.16 - 24.44
Range of indices, *h*, *k*, *l*	0,7/±12/-19,20	-6,9/-12,11/±20	±8/±11/-43,50
No. of measured reflections	8203	9284	15321
No. of unique reflections	3918	4613	7844
No. of reflections observed with $I > 2\sigma(I)$	2447	2767	3869
R_{int}	0.018	0.017	0.018
Structure refinement			
Data / restraints / parameters	3885 / 20 / 347	4593 / 6 / 344	7844 / 3 / 609
R indices R_1 / wR_2 [$I > 2\sigma(I)$]	0.0557 / 0.1367	0.0562 / 0.1288	0.1885 / 0.5312
R_1 / wR_2 (all data)	0.1072 / 0.1847	0.1130 / 0.1507	0.2239 / 0.5647
Goodness of fit on F^2, S	1.086	1.042	2.500
Weighting scheme [where $P = (F_o^2+2F_c^2)/3$]	$w = 1/[\sigma^2(F_o^2)+(0.0671P)^2+0.7269P]$	$w = 1/[\sigma^2(F_o^2)+(0.0734P)^2+0.0396P]$	$w = 1/[\sigma^2(F_o^2)+(0.2000P)^2+0.0000P]$
Max. / Mean shift (esd)	0.010 / 0.000	0.000 / 0.000	0.021 / 0.002
Extinction coefficient	0.026(4)	0.015(3)	0.002(7)
Max./Min. height in difference electron density map ($eÅ^{-3}$)	0.779 / -0.168	0.418 / -0.183	2.012 / -1.035

Table 4.13 (cont.) Crystal data, data collection and final refinement parameters.

Inclusion compound	**DHPC•3(26X)**	**DHPC•0.5(23X)**	**DHPC•2(23X)**
Molecular formula	$C_{18}H_{20}O_2$•$3C_8H_{11}N$	$C_{18}H_{20}O_2$•$0.5C_8H_{11}N$	$C_{18}H_{20}O_2$•$2C_8H_{11}N$
Guest	2,6-xylidine	2,3-xylidine	2,3-xylidine
Formula weight ($gmol^{-1}$)	631.87	328.93	510.70
Crystal Data			
Crystal system	Monoclinic	Monoclinic	Triclinic
Space group	$P2_1/n$	C2/c	$P\bar{1}$
a (Å)	9.807(1)	18.170(1)	6.3593(3)
B (Å)	25.464(2)	12.274(1)	10.8368(5)
C (Å)	29.842(3)	16.204(1)	21.7366(11)
α (°)	90	90	93.429(3)
β (°)	98.28(1)	95.30(3)	91.100(3)
γ (°)	90	90	106.912(3)
Volume ($Å^3$)	7375(1)	3598.5(4)	1429.6(1)
Z	8	8	2
Calculated density D_c (gcm^{-3})	1.138	1.214	1.186
μ (mm^{-1})	0.069	0.076	0.073
F(000)	2736	1416	552
Data collection			
Temperature (K)	173 (2)	173 (2)	173 (2)
Range scanned, θ (°)	2.11 - 25.68	3.22 - 25.34	3.33 – 26.26
Range of indices, *h*, *k*, *l*	0,11/0,30/-36,35	-21,20/-14,13/-19,17	±7/±13/-26,22
No. of measured reflections	54484	9988	9863
No. of unique reflections	13722	3285	4517
No. of reflections observed with $I > 2\sigma(I)$	8261	2637	3307
R_{int}	0.070	0.021	0.017
Structure refinement			
Data / restraints / parameters	13716 / 24 / 923	3283 / 13 / 288	4517 / 10 / 371
R indices R_1 / wR_2 [$I > 2\sigma(I)$]	0.0973 / 0.2327	0.0349 / 0.0826	0.0448 / 0.1069
R_1 / wR_2 (all data)	0.1585 / 0.2681	0.0508 / 0.0905	0.0694 / 0.1200
Goodness of fit on F^2, *S*	1.104	1.053	1.027
Weighting scheme [where $P = (F_o^2+2F_c^2)/3$]	$w = 1/[\sigma^2(F_o^2)+(0.1160P)^2+6.6572P]$	$w = 1/[\sigma^2(F_o^2)+(0.0402P)^2+1.4009P]$	$w = 1/[\sigma^2(F_o^2)+(0.0553P)^2+0.3573P]$
Max. / Mean shift (esd)	0.001 / 0.000	0.058 / 0.000	0.000 / 0.000
Extinction coefficient	0.012(1)	0.0027(3)	0.021(2)
Max./Min. height in difference electron density map ($eÅ^{-3}$)	0.916 / -0.517	0.176/-0.154	0.208/-0.176

Table 4.13 (cont.) Crystal data, data collection and final refinement parameters

Inclusion compound	DHPC•0.5(34X)•H_2O	DHPC•34X	DHPC•35X
Molecular formula	$C_{18}H_{20}O_2$•0.5$C_8H_{11}N$ •H_2O	$C_{18}H_{20}O_2$•$C_8H_{11}N$	$C_{18}H_{20}O_2$•$C_8H_{11}N$
Guest	3,4-xylidine and water	3,4-xylidine	3,5-xylidine
Formula weight ($gmol^{-1}$)	346.95	389.52	389.52
Crystal Data			
Crystal system	Triclinic	Monoclinic	Triclinic
Space group	P $\bar{1}$	C2/c	P $\bar{1}$
a (Å)	10.8979(5)	34.965(1)	6.327(1)
b (Å)	12.5017(7)	6.2546(3)	10.720(2)
c (Å)	15.1701(7)	20.2035(8)	16.920(4)
α (°)	106.510(4)	90	96.48(2)
β (°)	99.895(3)	101.577(1)	100.09(2)
γ (°)	102.559(2)	90	99.83(1)
Volume ($Å^3$)	1872.9(2)	4328.5(3)	1101.1(4)
Z	4	8	2
Calculated density D_c (gcm^{-3})	1.230	1.195	1.175
μ (mm^{-1})	0.081	0.074	0.073
F(000)	748	1680	420
Data collection			
Temperature (K)	173 (2)	173 (2)	293 (2)
Range scanned, θ (°)	2.63 - 25.42	2.06 - 28.24	1.95 - 24.97
Range of indices, *h*, *k*, *l*	-13,11/-11,15/-18,15	-43,44/-4,8/±25	0,7/±12/-20,19
No. of measured reflections	15055	12807	7320
No. of unique reflections	6747	4699	3869
No. of reflections observed with $I > 2\sigma(I)$	3622	2949	2075
R_{int}	0.0215	0.043	0.039
Structure refinement			
Data / restraints / parameters	6720 / 22 / 497	4699 / 7 / 278	3869 / 7 / 281
R indices R_1 / wR_2 [$I > 2\sigma(I)$]	0.0654 / 0.1232	0.1043 / 0.2539	0.0439 / 0.0927
R_1 / wR_2 (all data)	0.1311 / 0.1487	0.1468 / 0.2823	0.1351 / 0.1374
Goodness of fit on F^2, *S*	1.027	1.157	1.109
Weighting scheme [where $P = (F_o^2+2F_c^2)/3$]	$w = 1/[\sigma^2(F_o^2)+(0.03221P)^2+2.1868P]$	$w = 1/[\sigma^2(F_o^2)+(0.0000P)^2+16.4095P]$	$w = 1/[\sigma^2(F_o^2)+(0.0323P)^2+0.4445P]$
Max. / Mean shift (esd)	0.000 / 0.000	0.000 / 0.000	0.000 / 0.000
Extinction coefficient	0.027(6)	0.0043(8)	0.038(3)
Max./Min. height in difference Electron density map ($eÅ^{-3}$)	0.818/-0.365	0.393/-0.295	0.202/-0.176

5 SEPARATION OF CLOSE ISOMERS OF PICOLINE, LUTIDINE AND XYLIDINE BY THE HOST BINAP

The inclusion compounds, formed between the host **BINAP** and isomers of picoline, lutidine and xylidine are discussed in this chapter. The results of their thermal characteristics, crystal structures, selectivities of enclathration, lattice energy calculations and kinetics of desolvation are presented.

This chapter is divided into three parts:

Part 1	**BINAP** and Picolines
Part 2	**BINAP** and Lutidines
Part 3	**BINAP** and Xylidines

For all of the structures discussed in this chapter, the crystal data, data collection experimental and final refinement parameters are contained in **Table 5.9** appearing at the end of this chapter. Final fractional atomic co-ordinates, temperature factors, table of bond length and angles, torsion angles and table of observed and calculated structure factors are contained in **Appendices**.

PART 1

BINAP AND PICOLINES

Preparation of the inclusion compounds

Inclusion compounds of the host **BINAP** with three picoline isomers were obtained by dissolving the host in excess amount of liquid guest by warming and allowing the solution to crystallise by slow evaporation. The crystallisation experiments were carried out at both room temperature (~25°C) and 4°C for each guest solvent and the inclusion compounds with constant host:guest ratio of 1:2 were obtained. The crystallisation of **BINAP** with 3-picoline was troublesome and crystals were only obtained after numerous attempts. The mole ratio of host to total guest used was approximately about 1:20 in the crystallisation experiments as well as the competition experiments.

The atomic numbering scheme for the host and guest compounds and the abbreviations for both the guests and the inclusion compounds obtained are shown in **Scheme 5.1**.

Scheme 5.1

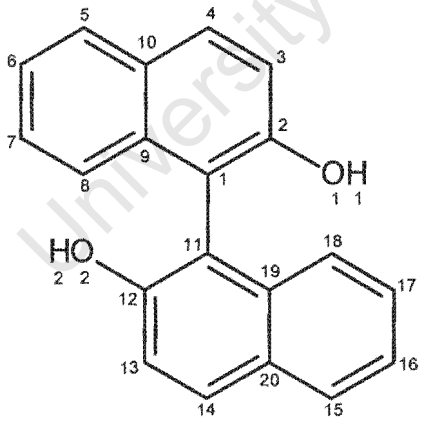

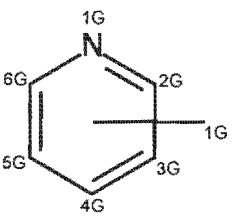

BINAP and 2-picoline (**2PIC**): **BINAP•2(2PIC)**

BINAP and 3-picoline (**3PIC**): **BINAP•2(3PIC)**

BINAP and 4-picoline (**4PIC**): **BINAP•2(4PIC)**

The atomic numbering scheme used for the host **BINAP** is consistent throughout all the structure solutions that contained the same host in this thesis. The hydrogen atoms are numbered according to their parents atoms to which they are bonded. Where necessary, crystallographic independent guest molecules are assigned suffixes "A", "B" etc after the letter "G".

Thermal analysis

The TG and DSC traces of the desolvations of the inclusion compounds, carried out on finely crushed crystallite samples at a constant heating rate of 10°C min^{-1}, are shown in **Figure 5.1**. For all of three inclusion compounds, the TG shows a one step desolvation and corresponds to the first single endothermic peak in the DSC. The last endothermic peak in the DSC, with onset temperature in the range of 216°C-217°C, corresponds to the melting of the apohost. The guest release onset temperatures for **BINAP•2(2PIC)**, **BINAP•2(3PIC)** and **BINAP•2(4PIC)** are at 95.6°C, 59.1°C and 109.7°C respectively. The observed mass losses from TG for each compound, which lie in between 38.5% - 39.3%, are in good agreement with the calculated value (39.41%), and thus justify our acceptance of the host:guest ratio of 1:2 for each compound.

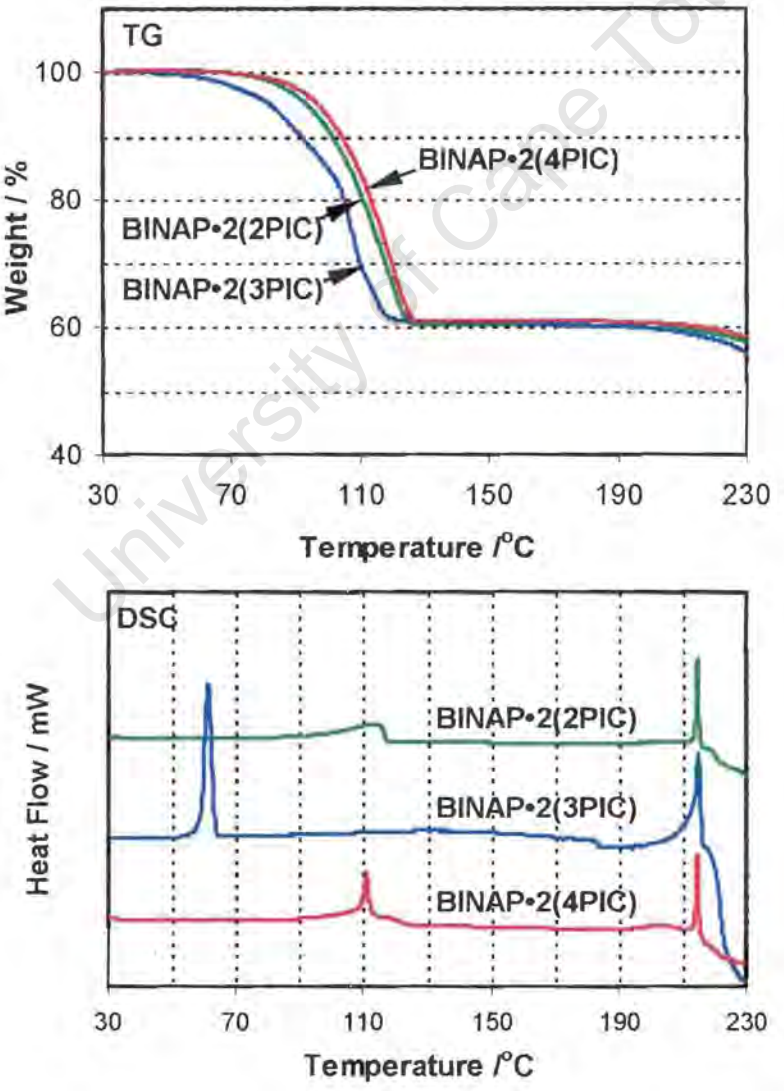

Figure 5.1 TG and DSC curves for inclusion compounds of **BINAP** with three isomers of picoline.

Crystal structures

Preliminary oscillation and Weissenberg photography indicated that **BINAP•2(2PIC)**, as well as **BINAP•2(3PIC)** belongs to the monoclinic crystal system (2/m Laue symmetry), while **BINAP•2(4PIC)** belongs to the orthorhombic crystal system (mmm Laue symmetry).

For **BINAP•2(2PIC)**, the reflection conditions

hkl: $h + k = 2n$
h0l: $l = 2n$; ($h = 2n$)
0kl: ($k = 2n$)

were observed, implying that the space group was either Cc or C2/c. The centrosymmetric space group C2/c was chosen, based on the mean $|E^2-1|$ values obtained from direct methods run for the zonal reflections, *i.e.* 0kl, h0l, hk0, and the reminder of the reflections.

The monoclinic space group $P2_1/c$ was chosen for the crystal structure of **BINAP•2(3PIC)**. This was established from the non-extinct reflection conditions observed from its crystal reflection data as follows:

hkl: none
h0l: $l = 2n$
0k0: $k = 2n$
00l: ($l = 2n$)

For **BINAP•2(4PIC)**, the reflection data exhibit the following non-extinction conditions:

hkl: none
0kl: $k = 2n$
h0l: $l = 2n$
hk0: $h = 2n$
h00: ($h = 2n$)
0k0: ($k = 2n$)
00l: ($l = 2n$)

indicating that the space group is Pbca.

The choice of the space group for each inclusion compound was vindicated by the successful final refinement of the structure.

For all of the three inclusion compounds, direct methods yielded all non-hydrogen atoms in the asymmetric unit. The hydroxyl oxygen atoms on the host molecule and the nitrogen atom on the guest molecule were placed unambiguously, due to their relative higher electron densities. In case of ambiguity, the nitrogen atom was then located within hydrogen bonding distance from the hydroxyl oxygen atom on the host. In the subsequent structure refinements, all of the hydrogen atoms, except the hydroxyl hydrogens of the host, were placed geometrically, though they could be located in the difference electron density maps in most cases, and refined with isotropic temperature factors related to their parent atoms. The aromatic hydrogen atoms of the host and guest were assigned 1.2 times the value of the U_{eq} of their parent atoms. The methyl hydrogen atoms of the guest were assigned isotropic temperature factors 1.5 times the U_{eq} of their parent atoms. The hydroxyl hydrogen atoms of the host were located in difference electron density maps, where possible, and refined with simple bond length constraints and individual isotropic temperature factors.

The crystal structure for each inclusion compound is discussed in terms of refinement and structure analysis. The molecular formula, host:guest ratio, space group, cell parameters and other crystallographic information are summarised at the beginning of the discussion of each structure. This is followed by a brief description of the structure refinement and then by a description of molecular structure and crystal packing. The host conformation data obtained from all the structure solutions in this part of the thesis will be discussed in more detail collectively in **Chapter 7**. The crystal data and final refinement parameters are contained in **Table 5.9**, appearing at the end of this chapter.

BINAP•2(2PIC)

$C_{20}H_{14}O_2 \cdot 2C_6H_7N$	
Guest: 2-picoline	
Space group: C2/c	
a = 18.274(3) Å	$\alpha = 90^\circ$
b = 9.887(2) Å	$\beta = 90.41(3)^\circ$
c = 14.021(2) Å	$\gamma = 90^\circ$
Volume = 2533.2(8) Å^3	
$Z = 4$	

Refinement

BINAP•2(2PIC) crystallises in C2/c. Determination of the unit cell volume suggested four host-guest molecules per unit cell. Since the host:guest ratio is 1:2, the C2/c space group requires the host molecule to be located at a special position with the asymmetric unit consisting of half of a host molecule. The host molecules were therefore situated on a diad at Wyckoff position *e* [(0,y,¼) and (0, $\bar{y}$, ¾)] and the guest molecules in a general position. All the non-hydrogen atoms were refined with anisotropic temperature factors. The hydroxyl hydrogen atom on the host molecule was located in difference electron density maps and refined with a simple bond length constraint at a value of d(O-H) = 0.97Å and independent temperature factor. The rest of the hydrogen atoms were placed in geometrically constrained positions and refined with individual isotropic temperature factors related to their parent atoms. The hydrogen atoms of the methyl group on the guest are disordered and were refined with two positions for each, offset 60° from each other. The structure refined successfully to $R_1 = 0.0415$.

Structure analysis

A stereoscopic view of the molecular structure of **BINAP•2(2PIC)** is shown in **Figure 5.2**. Each host molecule is hydrogen bonded to two symmetry related 2-picoline guests, with O(1)-H(1)···N(1G) having an O···N distance of 2.697(2)Å. Geometric details of the hydrogen bond in this structure, as well as those in the other two structures are given in **Table 5.1**, appearing at the end of this section. The packing of host molecules results in the formation of channels that running parallel to [10 $\bar{1}$] centred at y = 0.25 and 0.75. These channels are interconnected along directions [110] and [1 $\bar{1}$0] at z =0 and 0.5 respectively. The guest molecules are located in the interconnected channels with the N atoms orientated towards the host hydroxyl group, resulting in an intermolecular hydrogen bond which stabilises the structure. The [10 $\bar{1}$] channels, which have an approximately constant cross-sectional area of 5.5 x 5.5Å^2, are

illustrated in **Figure 5.3** as a space filling diagram viewed along [10 $\bar{1}$] and a cross section cut through the host framework at y = 0.25. The crystal packing, as viewed down [010] and [001], is shown in **Figures 5.4**.

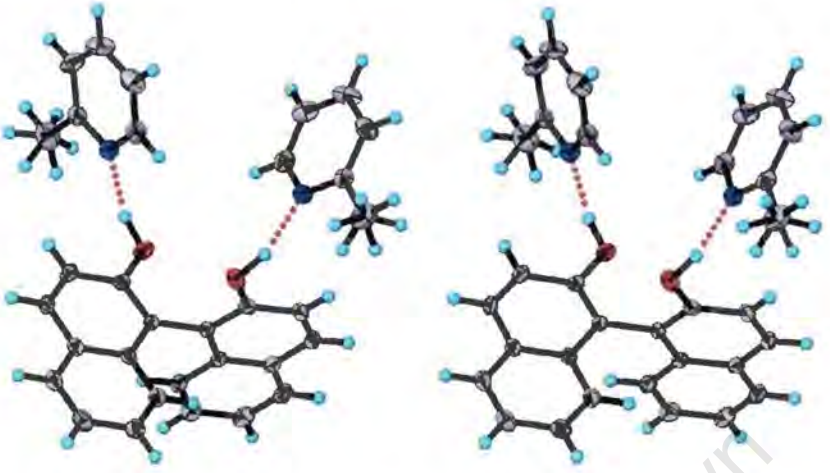

Figure 5.2 Molecular structure of **BINAP•2(2PIC)**. Displacement ellipsoids are drawn at the 45% probability level. Methyl groups on the 2-picoline are disordered.

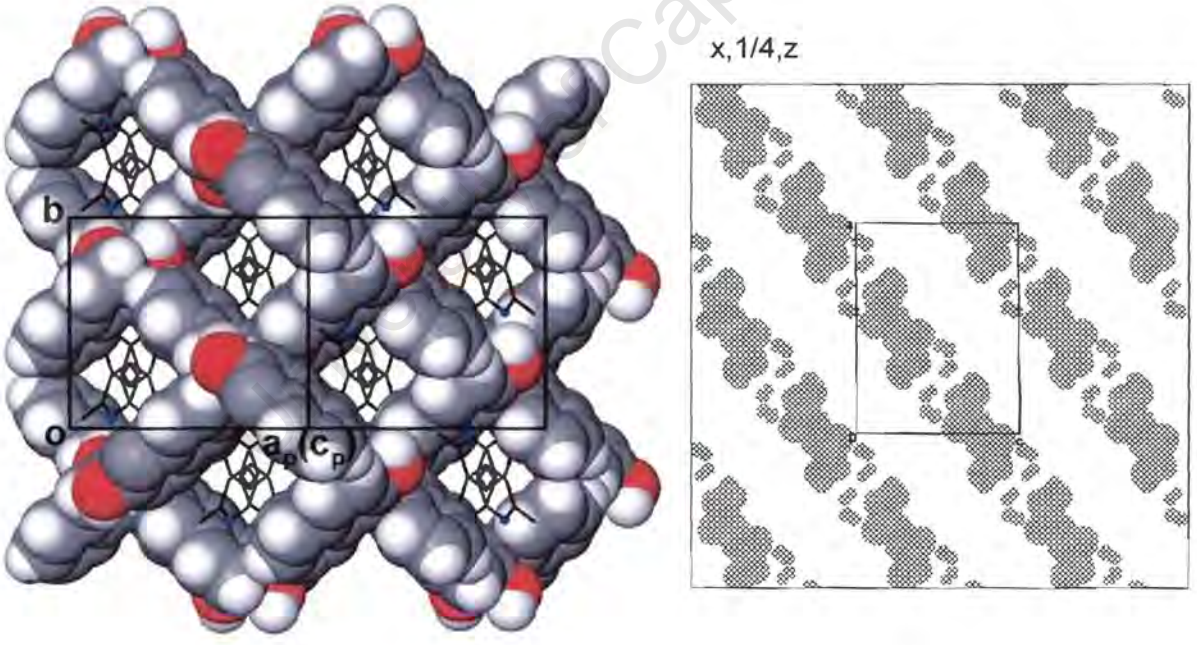

(a) (b)

Figure 5.3 (a) Space-filling diagram for **BINAP•2(2PIC)** viewed along [10 $\bar{1}$], showing the open channels. The host atoms are shown with van der Waals radii and guest molecules shown as sticks with all H atoms omitted and N atoms highlighted.
(b) Cross section cut at y = 0.25 showing the channel running along [10 $\bar{1}$]. The diagonal crossed area represent the space occupied by the host. The guest is omitted.

(a)

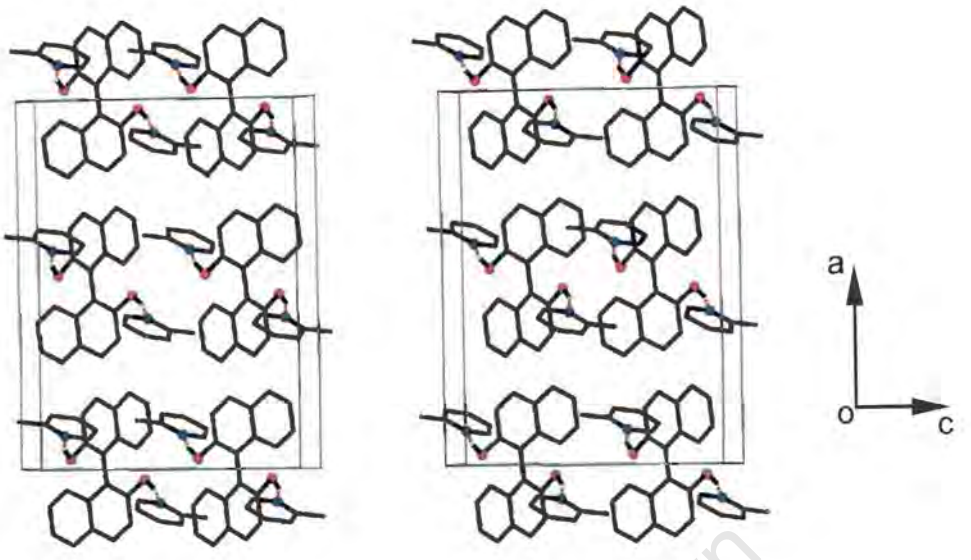

(b)

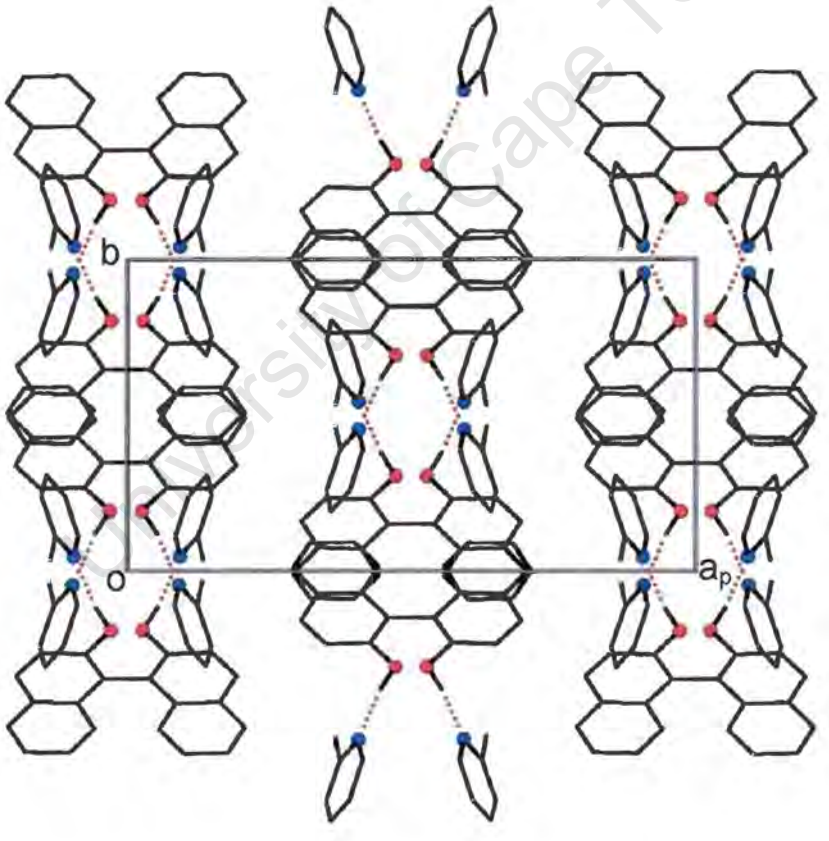

Figure 5.4 Projections of crystal packing in **BINAP•2(2PIC)**, viewed down (a) [010] (stereoscopic view) and (b) [001]. All of the H atoms are omitted except the hydroxyl hydrogen atoms. The H-bonds are shown as dotted lines. The N and O atoms are highlighted as solid circles.

BINAP•2(3PIC)

$C_{20}H_{14}O_2 \cdot 2C_6H_7N$	
Guest: 3-picoline	
Space group: $P2_1/c$	
a = 12.118(1) Å	$\alpha = 90°$
b = 13.261(1) Å	$\beta = 103.448(2)°$
c = 16.581(1) Å	$\gamma = 90°$
Volume = 2591.5(3) Å^3	
Z = 4	

Refinement

BINAP•2(3PIC) crystallised in $P2_1/c$ with Z = 4. Both host and guest molecules are at general positions. The asymmetric unit contains one host molecule and two guest molecules (labelled with suffices "A" and "B" after the letter "G"). Refinements were carried out with the non-hydrogen atoms of both the host and guest treated anisotropically. The hydroxyl hydrogen atoms on the host molecule were independently located in difference electron density maps and refined with simple bond length constraints at values of d(O-H) = 0.97Å and individual temperature factors. The rest of the hydrogen atoms on the host and the guest molecule A were geometrically placed. The methyl hydrogen atoms on guest molecule B were disordered over two positions. The structure refined successfully to R_1 = 0.0410.

Structure analysis

The hydrogen bonding arrangement in this structure is similar to that in the previous structure of **BINAP•2(2PIC)**: each host molecule is hydrogen bonded to two 3-picoline guests, with O(1)-H(1)···N(1GB) and O(2)-H(2)···N(1GA) having O···N distances of 2.708(2)Å and 2.779(2)Å respectively. The geometry details of hydrogen bonds are given in **Table 5.1**. The host molecules pack to generate channels running parallel to [010] which, in addition, are interconnected along [001]. The main channels running along [010] have a cross-sectional area of 5 x 6Å^2 approximately and are shown from the top in **Figure 5.5a**. A column of guest molecules stacked along [010] is shown as a stereo view in **Figure 5.5b**. The crystal packing, viewed down [100], [010] and [001], is shown in **Figure 5.6**.

(a)

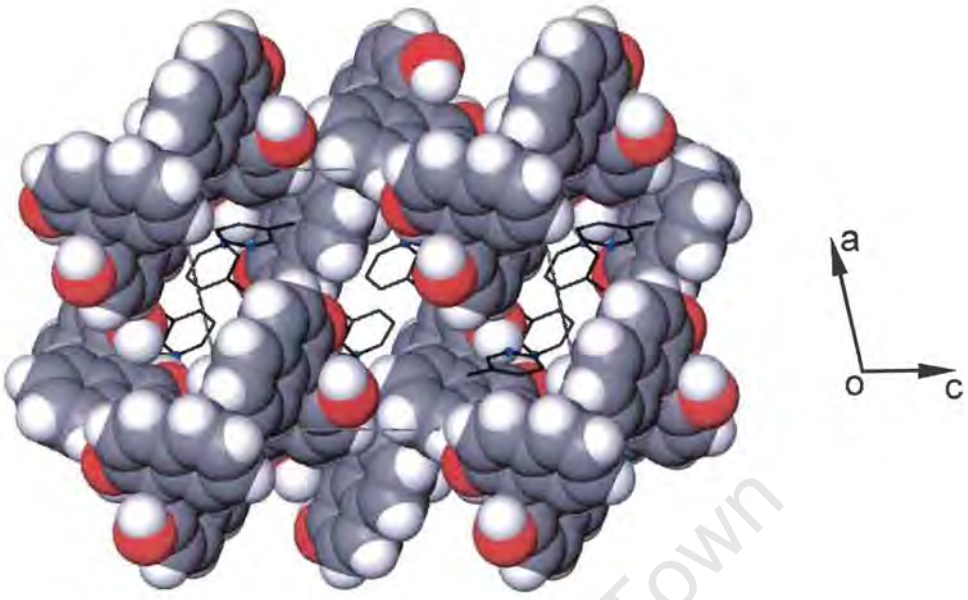

(b)

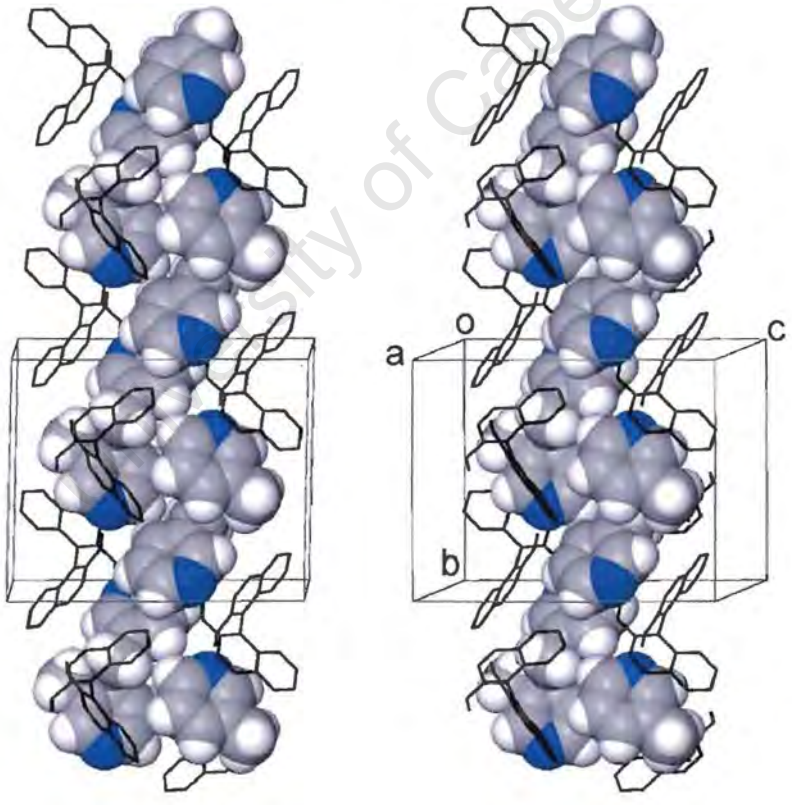

Figure 5.4 (a) Top view of the channel in the space-filling diagram for **BINAP•2(3PIC)**, viewed down [010]. The host atoms are shown with van der Waals radii and guest atoms are shown as sticks with N atoms highlighted. All of the hydrogen atoms on the guest are omitted.
(b) A stereo view showing the column of guest molecules running along [010]. The guest atoms are shown with van der Waals radii and host in stick representation with H atoms omitted (except the hydroxyl H atoms).

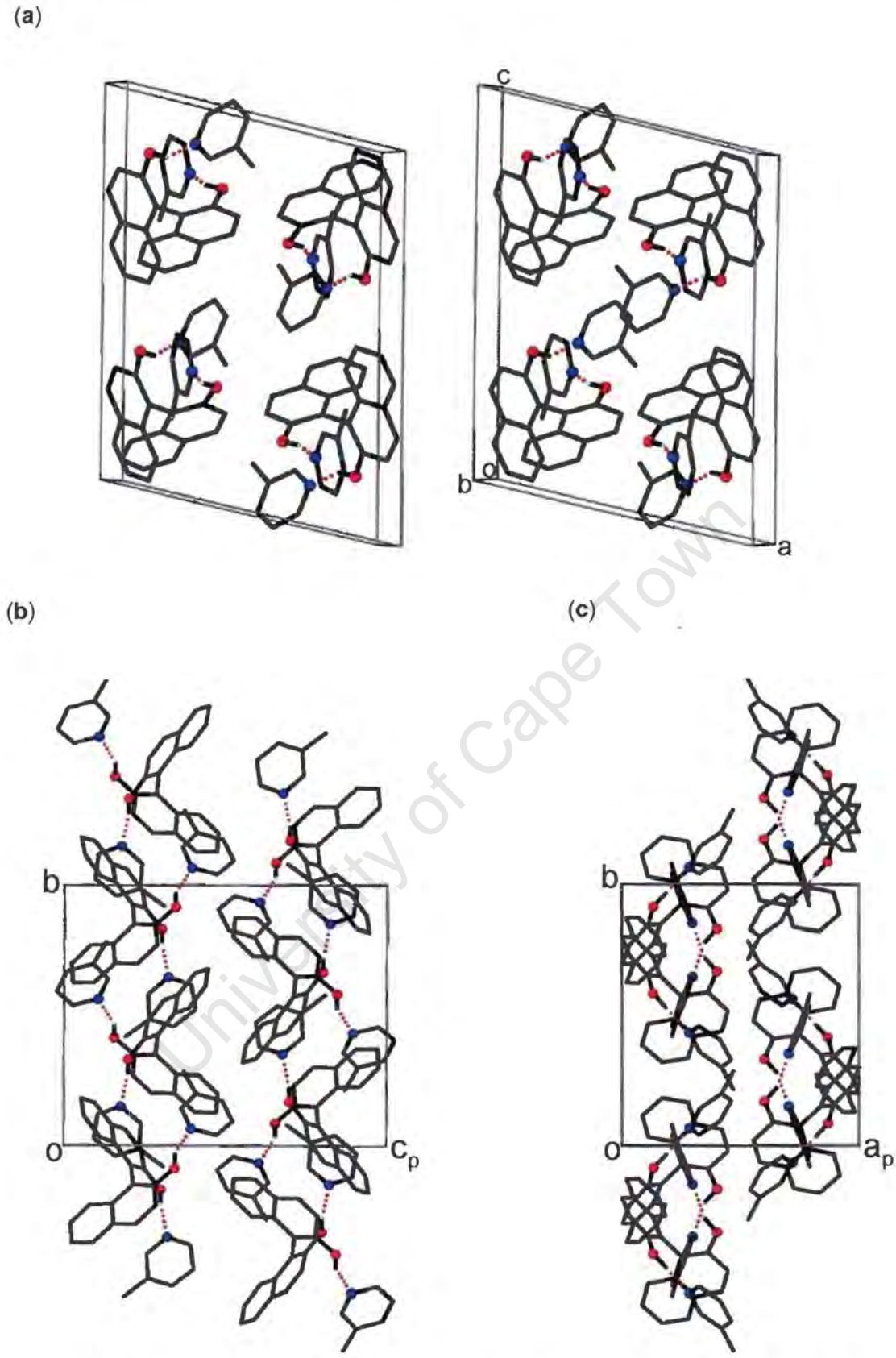

Figure 5.6 Projections down (a) [100] (stereoscopic view), (b) [010] and (c) [001], showing the crystal packing of **BINAP•2(3PIC)**. All of the H atoms are omitted except the hydroxyl hydrogen atoms. The H-bonds are shown as dotted lines. The N and O atoms are highlighted as solid circles.

BINAP•2(4PIC)

$C_{20}H_{14}O_2 \cdot 2C_6H_7N$	
Guest: 4-picoline	
Space group: Pbca	
a = 18.119(3) Å	$\alpha = 90°$
b = 10.812(2) Å	$\beta = 90°$
c = 25.665(5) Å	$\gamma = 90°$
Volume = 5027.8(2) $Å^3$	
Z = 8	

Refinement

BINAP•2(4PIC) crystallises in Pbca with Z = 8. The asymmetric unit contains one host and two guest molecules (A and B), all located in general positions. Refinements were carried out in a very similar manner to that of **BINAP•2(3PIC)**. Again, the methyl hydrogen atoms on guest molecules were disordered and were placed with two positions for each. The structure refined successfully to $R_1 = 0.0430$.

Structure analysis

The **BINAP•2(4PIC)** structure exhibits (host)O-H···N(guest) hydrogen bonds, exhibiting similar arrangement to that of **BINAP•2(3PIC)**, with O···N distances of 2.747(2)Å and 2.746(2)Å respectively (details in **Table 5.1**). The guest molecules are located in channels running parallel to [010] with the nitrogen atoms pointing towards the hydroxyl group of the host. The channel has a cross-sectional area of 7 x 8 $Å^2$. The views of the channels in projection and elevation are illustrated in **Figure 5.7a** and **b** respectively. The crystal packing, viewed along [010] and [001], is shown in **Figure 5.8**.

(a)

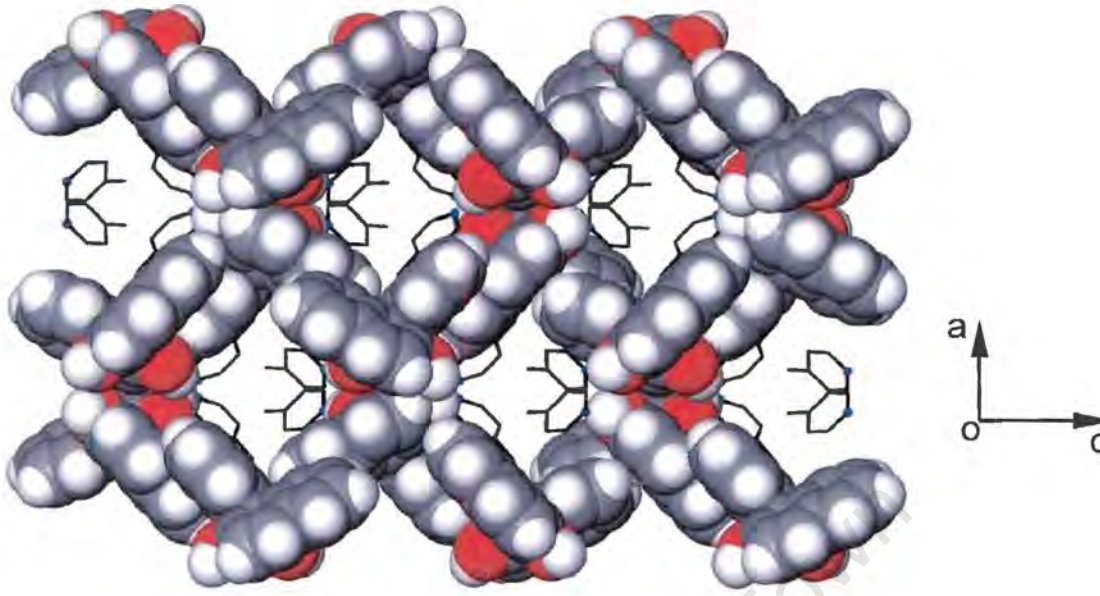

(b)

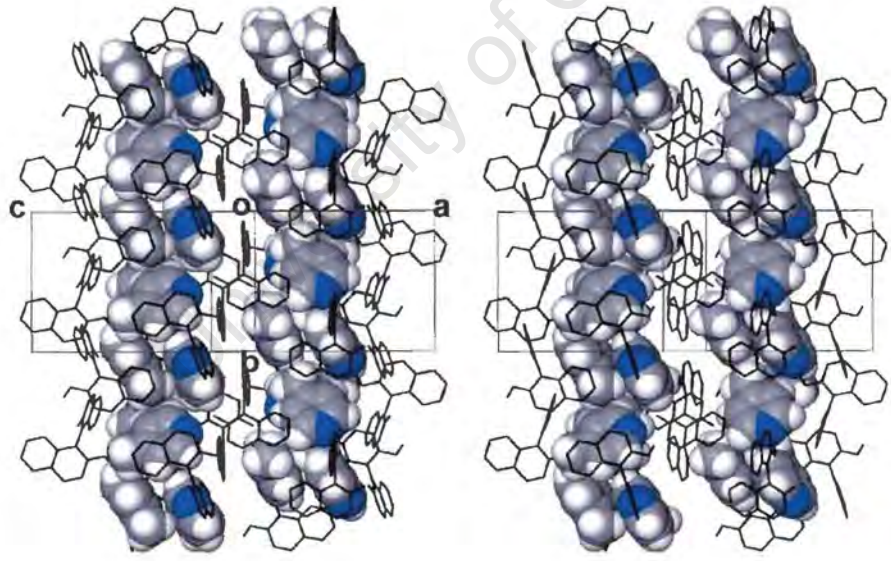

Figure 5.7 (a) A space-filling diagram for **BINAP•2(4PIC)** viewed down [010]. The host atoms are shown with van der Waals radii and guest molecules shown as sticks with N atoms highlighted. All of the hydrogen atoms on the guest are omitted.
(b) A stereoscopic view looked along [10 $\bar{1}$], showing the column of guest molecules running along [010]. The guest atoms are shown with van der Waals radii and host as stick representation with all H atoms except the hydroxyl hydrogens omitted.

(a)

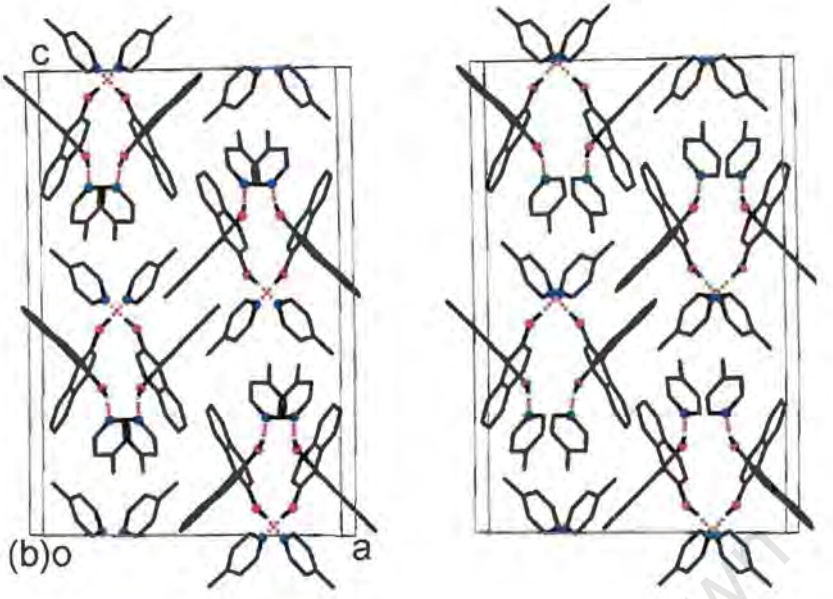

(b)

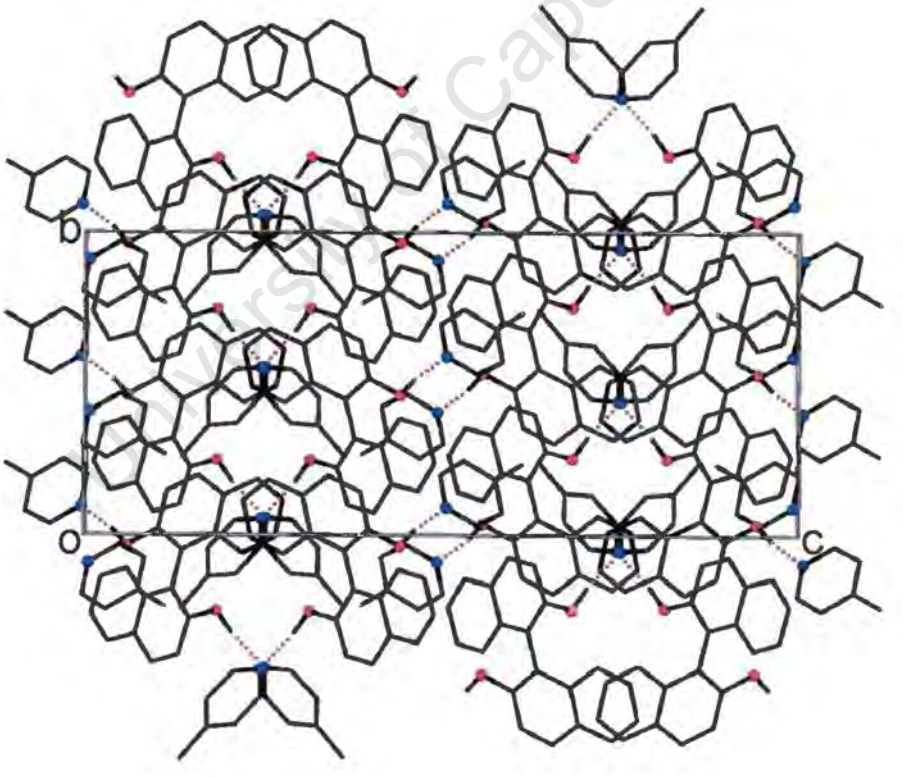

Figure 5.8 Projections down (a) [010] (stereoscopic view) and (b) [100], showing the crystal packing in **BINAP•2(4PIC)**. All of the H atoms are omitted except the hydroxyl hydrogen atoms. The H-bonds are shown as dotted lines. The N and O atoms are highlighted as solid circles.

The following **Table 5.1** summarises the hydrogen bonding details for all of the three structures discussed.

Table 5.2 Hydrogen bonding details for the structures discussed in **Part 1**.

Incl. Comp.	***D-H···A** / Å	**D-H** /Å	**H···A** /Å	**D···A** /Å	**<DHA** /°
BINAP•2(2PIC)	O(1)–H(1)···N(1G)	0.98(3)	1.769(5)	2.697(2)	156(2)
BINAP•2(3PIC)	O(1)–H(1)···N(1GB)[1]	0.97(1)	1.802(8)	2.708(2)	153(2)
	O(2)–H(2)···N(1GA)	0.96(1)	1.869(8)	2.779(2)	158(2)
BINAP•2(4PIC)	O(1)–H(1)···N(1GA)[2]	0.97(1)	1.783(7)	2.747(2)	171(2)
	O(2)–H(2)···N(1GB)	0.98(1)	1.783(8)	2.746(2)	168(2)

***D-H···A**: Donor(**D**)-**H**···Acceptor(**A**)

Symmetry codes: (1) -x+1, -y+1, -z (2) -x+1/2, y+1/2, z

Competition experiments

The competition experiments have been carried out between each pair of picoline isomers and between all three picoline isomers simultaneously. The results are shown in **Figure 5.9**.

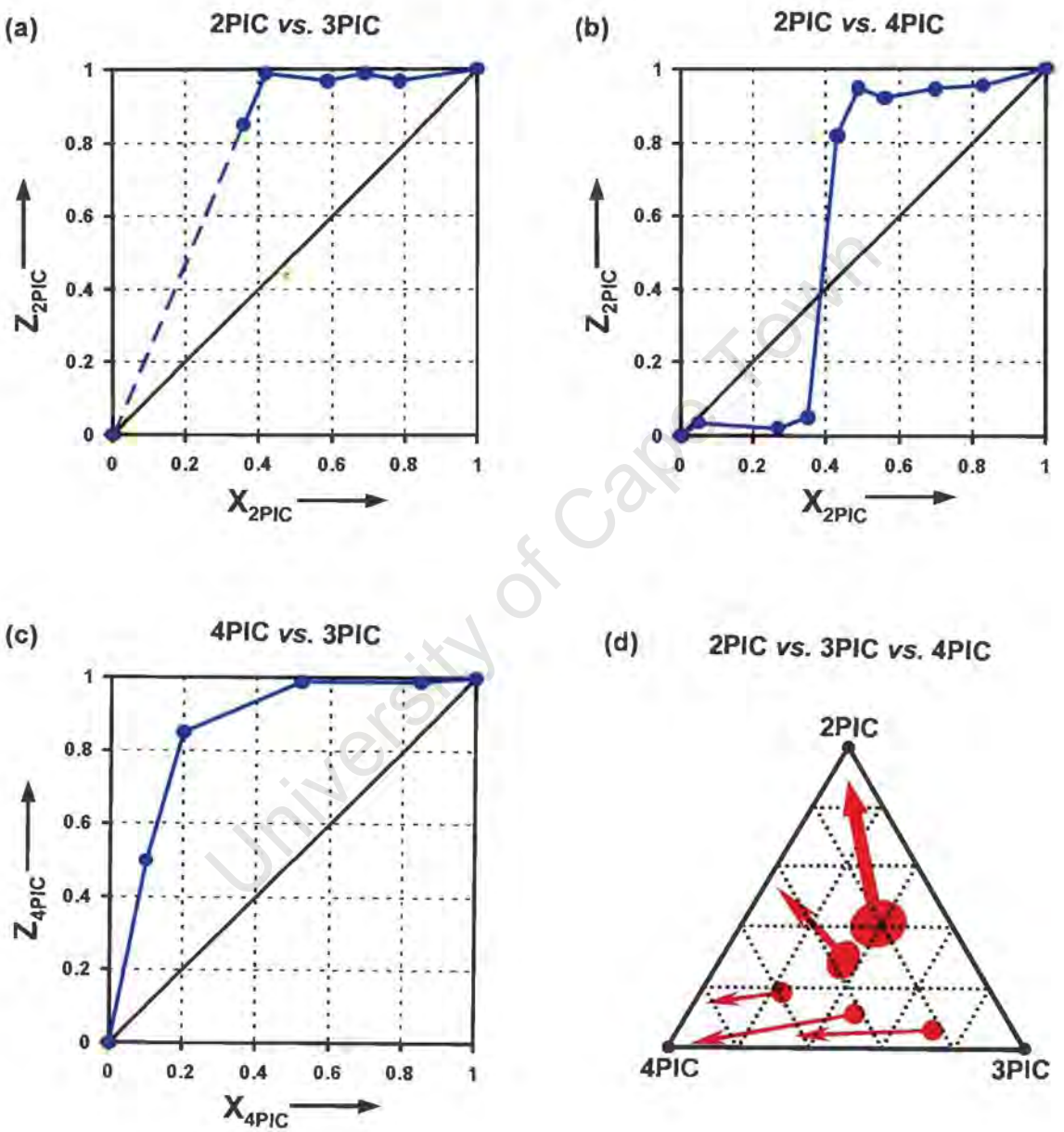

Figure 5.9 Results of the two- and three-component competitions between picoline isomers by the host **BINAP**.

In the 2-picoline *versus* 3-picoline competition experiment (**Figure 5.9a**), it is clearly seen that the former is strongly favoured by the host when its initial mole fraction is above ca. 0.37. Below this concentration ratio no selectivity was determined, since attempts at growing crystals failed. This accords with the difficulty in growing single crystals of inclusion compound of **BINAP** with 3-picoline. Therefore the dashed line shown in **Figure 5.9a** does not represent competition results. The selectivity between 2-picoline and 4-picoline (**Figure 5.9b**) is concentration dependent with parameter $Q_{2PIC:4PIC} = 0.39$. When the initial mole fraction of starting mixture is greater than this value, 2-picoline is favoured with more than 80% included; below this value, 4-picoline is selected. In the 4-picoline *versus* 3-picoline competition experiments (**Figure 5.9c**), the former is selected preferentially to the latter, with more than 80% inclusion at an initial mole fraction of about 20%. The experimental points lie close to a selectivity coefficient of 22.

In the three-component competition experiments (**Figure 5.9d**), for starting mixtures with $X_{2PIC} > 0.4$, the 2-picoline is strongly favoured over the other two isomers. When $0.2 < X_{2PIC} < 0.4$, both 2-picoline and 4-picoline are preferentially selected. The remaining mixtures with $X_{2PIC} < 0.2$ all move towards 4-picoline. Under all cases 3-picoline is disfavoured. The three-component competition results are in general good agreement with those obtained from two-component competitions. The selectivity between the three isomers can be formulated as follow:

4-picoline ≈ 2-picoline > 3-picoline

The separation of picoline isomers has been previously performed using the diol host **DHPC** (Caira *et al.* 1997) and the results show the selectivity tendency is 3-picoline ≈ 4-picoline > 2-picoline. This implies that separation of isomers can be fine-tuned by the choice of host compound with different molecular shape or functionality.

Lattice energy calculations

Lattice energy calculations have been performed on all the three inclusion compounds. The host···host, host···guest and guest···guest interactions plus the hydrogen bonding potential were summed. The following values were obtained for the total lattice potential energies:

BINAP•2(2PIC) -222.4 kJ mol^{-1};
BINAP•2(3PIC) -216.7 kJ mol^{-1};
BINAP•2(4PIC) -225.6 kJ mol^{-1}.

This result shows that the stabilities of the three inclusion compounds are in the order **BINAP•2(4PIC)** > **BINAP•2(2PIC)** > **BINAP•2(3PIC)**. These data explain the least preferred selectivity of 3-picoline by the host. However, the selectivities between 2-picoline and 4-picoline are concentration dependent, and we note that the lattice energies of **BINAP•2(2PIC)** and **BINAP•2(4PIC)** are very close, differing only by 3.2 kJ mol^{-1}. We therefore attribute this concentration dependent selectivity to kinetic effects.

Kinetics of desolvation

The kinetics of desolvation for all of the three inclusion compounds were carried out using the isothermal kinetic method. A series of isothermal TG runs were performed on finely crushed crystallite samples at selected temperatures in the range of 40°C - 90°C. In all cases the resultant curves of the extent of reaction α versus time t were deceleratory and were best fitted to the kinetic model R2, over an α range of 0.05 - 0.95. The contracting area geometrical model R2 describes a phase-boundary-controlled reaction that reacts from the edge inward on a cylindrical particle. In accord with the Arrhenius equation, ln k was plotted against $1/T$. This yielded an activation energy E_a and a pre-exponential factor ln A for each of the three compounds, shown in **Table 5.2**. The Arrthenius plots of ln k versus 1/T are shown in **Figure 5.10**.

Table 5.2 Kinetic parameters for the desolvations of inclusion compounds of **BINAP** with picoline isomers.

Inclusion Compound	Temperature range(°C)	α range	Kinetic model	E_a (kJ mol^{-1})	ln A
BINAP•2(2PIC)	50 - 90	0.05 - 0.95	R2	86(4)	25(2)
BINAP•2(3PIC)	40 - 80	0.05 - 0.95	R2	82(6)	26(2)
BINAP•2(4PIC)	50 - 90	0.05 - 0.95	R2	84(7)	25(2)

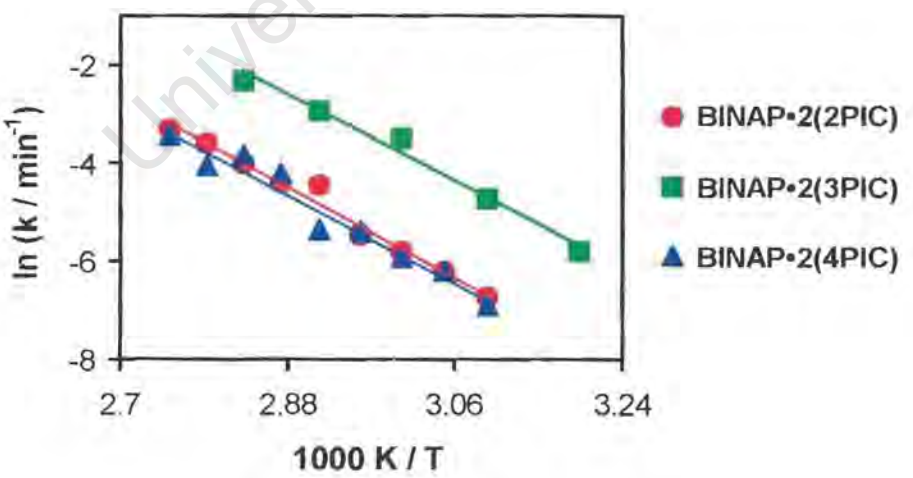

Figure 5.10 Arrhenius plots of ln k *versus* $1/T$ for desolvations of the host-guest compounds **BINAP•2(2PIC)**, **BINAP•2(3PIC)** and **BINAP•2(4PIC)**.

PART 2

BINAP AND LUTIDINES

Preparation of the inclusion compounds

The host **BINAP** was dissolved in excess amount of 2,6-, 2,4- and 3,5-lutidine liquid by warming, and the solutions were allowed to crystallise by slow evaporation at both room temperature (~25°C) and 4°C. Colourless crystals appeared within period of 24 hours to one week. The mole ratio of host to total guest used was approximately about 1:15 in the crystallisation experiments as well as the competition experiments. The crystals of inclusion complex with 3,5-lutidine were finally obtained after numerous attempts, which invariably resulted in a powdery material. The difficulty experienced in obtaining single crystals of this complex also occurred in competition experiments, during which attempts to grow crystals were unsuccessful when the mole fraction of 3,5-lutidine in the initial guest mixtures was more than a certain limit.

The host **BINAP** formed 1:2 inclusion compounds with 2,6 and 2,4-lutidine and 1:1 with 3,5-lutidine. The host:guest ratios were established by TG. The structural skeletons for the lutidine guests, the numbering scheme used in the structure solutions and the abbreviations for both the guests and the inclusion compounds obtained are shown in **Scheme 5.2** as follow:

Scheme 5.2

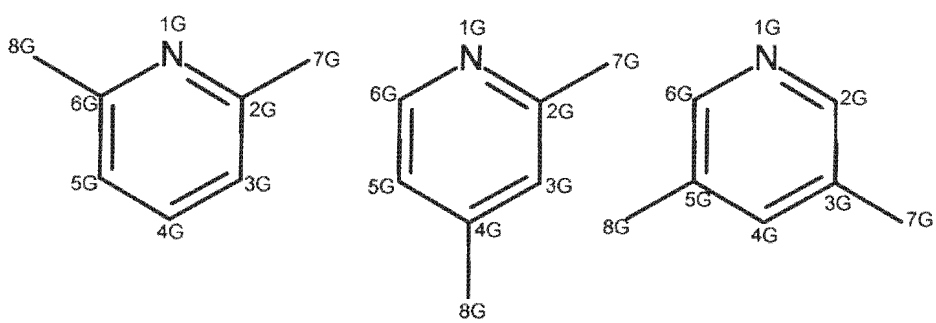

BINAP and 2,6-lutidine (**26LUT**): **BINAP•2(26LUT)**

BINAP and 2,4-lutidine (**24LUT**): **BINAP•2(24LUT)**

BINAP and 3,5-lutidine (**35LUT**): **BINAP•35LUT**

Thermal analysis

The TG and DSC traces for the desolvation of the three inclusion compounds, carried out on finely crushed crystallitic samples at a constant heating rate of 10°C min^{-1}, are shown in **Figure 5.11**. In all cases, the TG shows a single step desolvation and corresponds to the first endothermic peak in the DSC with onset temperatures of 99.8°C, 117.2°C and 137.8°C for **BINAP•2(26LUT)**, **BINAP•2(24LUT)** and **BINAP•35LUT** respectively. The last endothermic peak in the DSC corresponds to the melting of the guest-free host, with onset temperature of between 216°C - 217°C. The observed mass losses from TG for each compound are in good agreement with the calculated value, and thus justify our acceptance of the host:guest ratios assigned for each of the inclusion compounds. The exact values are shown as follow:

BINAP•2(26LUT): observed weight loss 42.9%; calculated weight loss 42.81%.

BINAP•2(24LUT): observed weight loss 42.1%; calculated weight loss 42.81%.

BINAP•35LUT: observed weight loss 28.2%; calculated weight loss 27.23%.

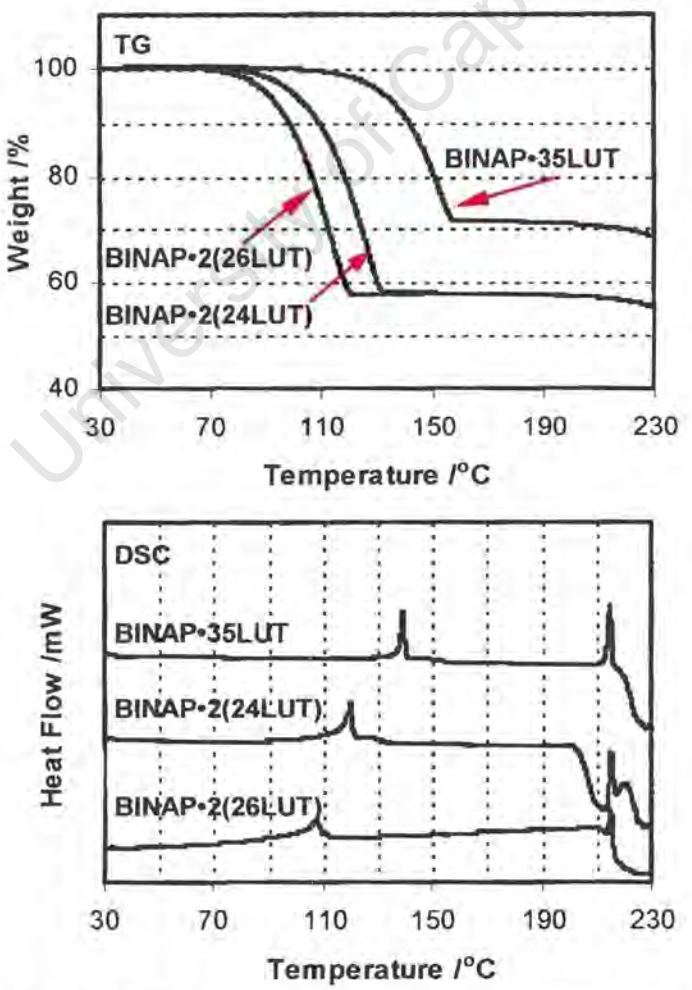

Figure 5.11 TG and DSC curves for the inclusion compounds of **BINAP** with three lutidine isomers.

Crystal structures

Preliminary photography indicated that **BINAP•2(26LUT)** and **BINAP•2(24LUT)** belong to the monoclinic crystal system (2/m Laue symmetry). In both cases, the reflection conditions

hkl: $h + k = 2n$

h0l: $l = 2n$; ($h = 2n$)

0k0: ($k = 2n$)

were observed, implying that the space group was either Cc or C2/c. The centrosymmetric space group C2/c was chosen, based on the mean $|E^2-1|$ values for the zonal reflections, i.e. 0kl, h0l, hk0, and the remainder of the reflections. For **BINAP•35LUT**, the triclinic system was indicated by $\bar{1}$ Laue symmetry of the X-ray diffraction data and the intensity statistics (mean $|E^2-1|$ value for the general *hkl* reflections is 1.072) indicated P $\bar{1}$ as the correct space group rather than P1.

For all of the three inclusion compounds, direct methods yielded all non-hydrogen atoms in the asymmetric unit. The positions of the O and N atoms were placed unambiguously. In case of ambiguity, The N(1G) atom was placed within hydrogen bonding distance from the hydroxyl oxygen atom of the host. For each compound, the molecular formula, host:guest ratio, space group, cell parameters and other crystallographic information are summarised at the beginning of the discussion. This is followed by a brief description of its structure refinement and then by a description of its molecular structure and crystal packing. The host conformation data obtained from all the structure solutions in this part will be discussed in more detail collectively in **Chapter 7**. The crystal data and final refinement parameters are contained in **Table 5.9**, appearing at the end of this chapter.

BINAP•2(26LUT)

$C_{20}H_{14}O_2 \bullet 2C_7H_9N$	
Guest: 2,6-lutidine	
Space group: C2/c	
A = 14.656(7) Å	$\alpha = 90°$
B = 10.703(2) Å	$\beta = 109.84(3)°$
C = 18.365(5) Å	$\gamma = 90°$
Volume = 2710(2) Å^3	
Z = 4	

Refinement

BINAP•2(26LUT) crystallises in the space group C2/c with Z = 4. The host molecule exhibits two-fold symmetry and was placed with central binaphthyl bond on a special position, located on a diad at Wyckoff position *e* [(0,y,¼) and (0, $\bar{y}$, ¾)]. All of the non-hydrogen atoms of host and guest were refined anisotropically. The hydroxyl hydrogen atom was located in the difference electron density maps and refined with bond length constraint at a value of d(O-H) = 0.97Å and independent temperature factor. The rest of the hydrogen atoms were placed with geometric constraints and refined with individual isotropic temperature factors either 1.2 or 1.5 times the U_{eq} of their parent atoms. The structure refined successfully to R_1 = 0.0540.

Structure analysis

This structure is stabilised via an O(1)-H(1)···N(1G) hydrogen bond, formed between each host hydroxyl group and the N atom of guest molecule, having an O···N distance of 2.815(5)Å. The geometric details are given in **Table 5.3** together with those of the other two structures. The hydrogen bonding pattern is illustrated in a projection viewed along [010] in **Figure 5.12**. The guest molecules are located in channel running parallel to [001], with an approximate cross-sectional area of 7 x 6 Å^2, as shown in **Figure 5.13**. These channels are interconnected along [110] and [1 $\bar{1}$0] directions. The crystal packing, projected along [100] and [001], is shown in **Figure 5.14**.

Table 5.3 Hydrogen bonding details for the structures discussed in **Part 2**.

Incl. Comp.	**D-H···A*** / Å	**D-H** /Å	**H···A** /Å	**D···A** /Å	**<DHA** /°
BINAP•2(26LUT)	O(1)–H(1)···N(1G)	0.97(2)	1.87(2)	2.815(5)	164(4)
BINAP•2(24LUT)	O(1)–H(1)···N(1G)	0.97(1)	1.876(8)	2.826(3)	166(2)
BINAP•35LUT	O(1)–H(1)···N(1G)	0.99(1)	1.69(1)	2.658(3)	166(3)
	O(2)–H(2)···O(1)^1	0.96(1)	1.84(1)	2.794(2)	176(3)

*__D-H···A__: Donor(__D__)-H···Acceptor(__A__) Symmetry codes: (1) -x+2, -y+1, -z+1

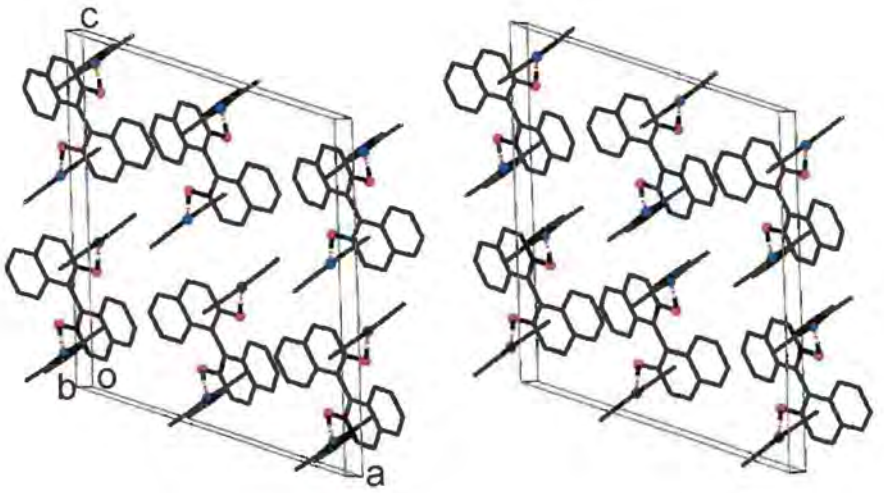

Figure 5.12 Projection down [010], shown as a stereoscopic view for **BINAP•2(26LUT)**. Only the hydroxyl hydrogen atoms of the host are shown. The hydrogen bonds are indicated as dotted lines. The N and O atoms are shown in solid circles.

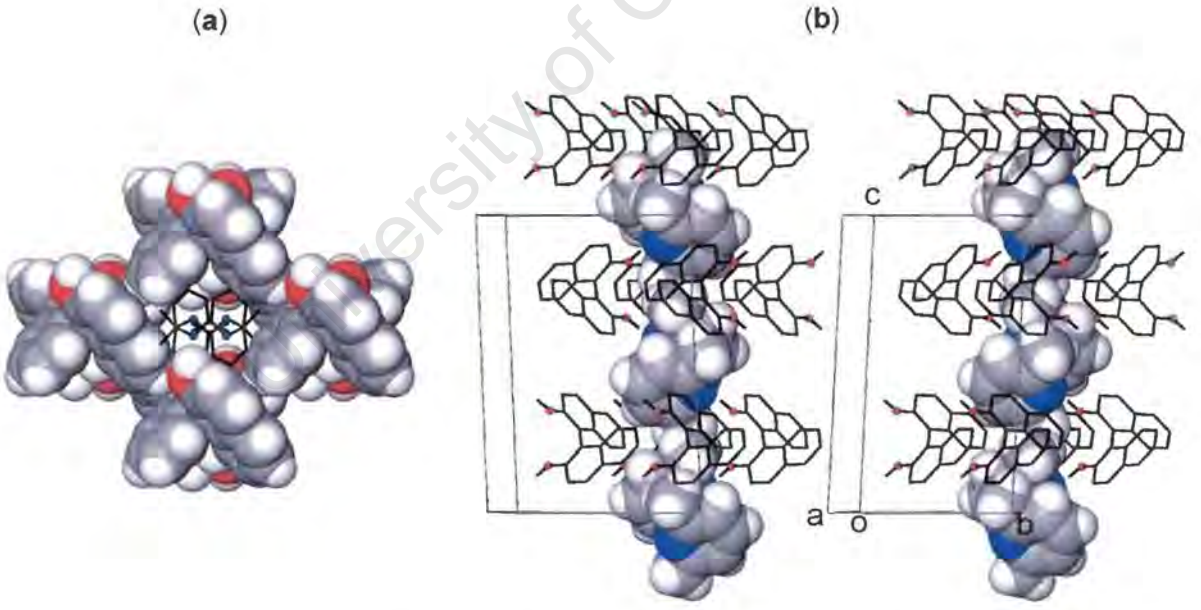

Figure 5.13 (a) Space-filling diagram looking down the channel that running along [001]. The host molecules are depicted with van der Waals radii and the guests are presented in stick model with all H atoms omitted.
(b) Stereoscopic view from side of the column of the guest which running along [001]. The guest molecules are depicted with van der Waals radii and the hosts are presented in stick model with all H atoms except the hydroxyl hydrogens omitted.

(a)

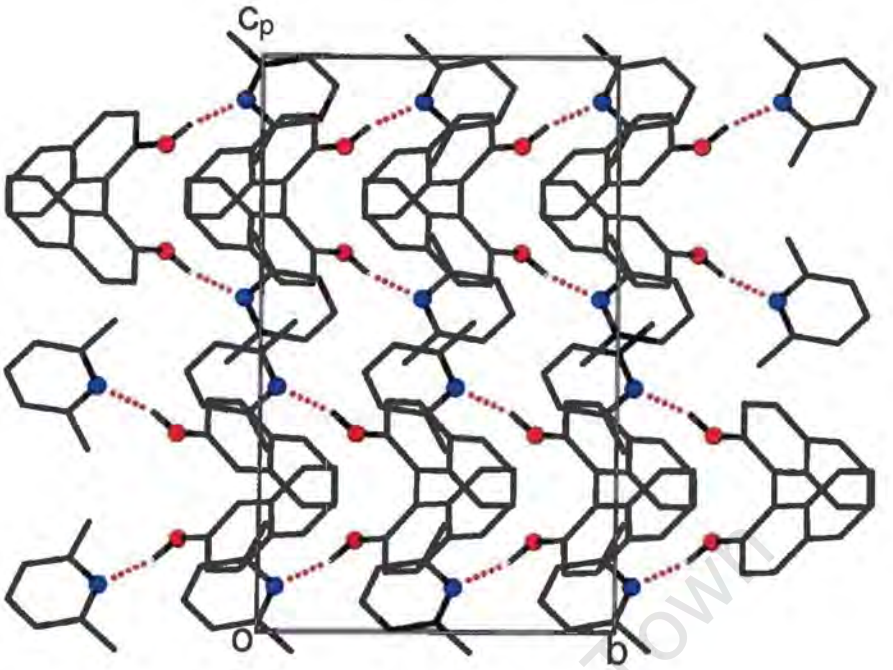

(b)

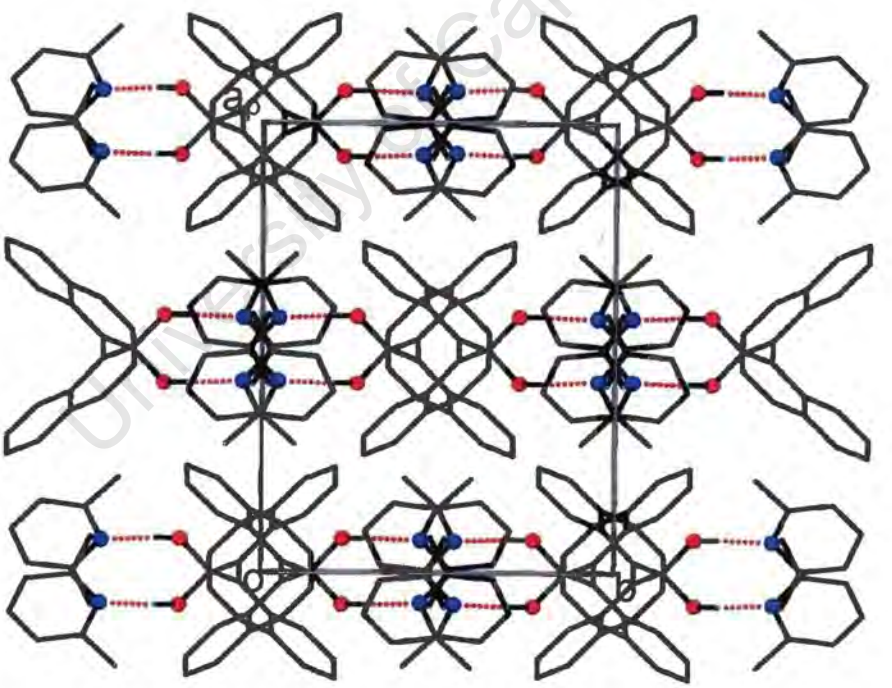

Figure 5.14 Projections viewed down (a) [100] and (b) [001], showing the crystal packing in **BINAP•2(26LUT)**. Details as in **Figure 5.12**.

BINAP•2(24LUT)

$C_{20}H_{14}O_2 \cdot 2C_7H_9N$	
Guest: 2,4-lutidine	
Space group: C2/c	
a = 15.12(2) Å	$\alpha = 90°$
b = 10.76(1) Å	$\beta = 110.9(1)°$
c = 18.19(5) Å	$\gamma = 90°$
Volume = 2764(9) Å^3	
Z = 4	

Refinement

BINAP•2(24LUT) crystallises in C2/c with Z = 4. The host molecule is thus located in a special position. It was placed at Wyckoff position *e* [(0,y,¼) and (0, $\bar{y}$, ¾)], fulfilling the symmetry requirements for the assigned space group. The refinement procedure was similar to that of **BINAP•2(26LUT)**, except the hydrogen atoms of the two methyl groups of the guest were modelled with each hydrogen atom disordered over two positions, each with a site occupancy of 0.50. The structure refined successfully to R_1 = 0.0472.

Structure analysis

The hydrogen bonding scheme of this structure is similar to that of **BINAP•2(26LUT)**, discussed previously. This can be seen in **Figure 5.15**, in which the projection down [010] is shown stereoscopically. Though both inclusion compounds crystallised in the same space group with similar unit cell dimensions, their structures are not isostructural. The *a* axis length and β angle of **BINAP•2(24LUT)** are relatively larger than those of **BINAP•2(26LUT)**, resulting in ~ 54Å^3 bigger cell volume. In this structure, each host is hydrogen bonded to two guest molecules which are related via two-fold symmetry, having host···guest hydrogen bond of O(1)-H(1)···N(1G) with d(O···N) = 2.826(3)Å. The hydrogen bonding details are in **Table 5.3**. The guest molecules, propagated by a two-fold screw axis, are situated mainly in the channels running along [101] at y = 0.25 and 0.75 respectively, with an approximate cross-sectional area of 5 x 8Å^2. These channels, illustrated in **Figure 5.16**, are interconnected along [110] and [1 $\bar{1}$0] directions. The crystal packing, as viewed down [100] and [001], is shown in **Figure 5.17**.

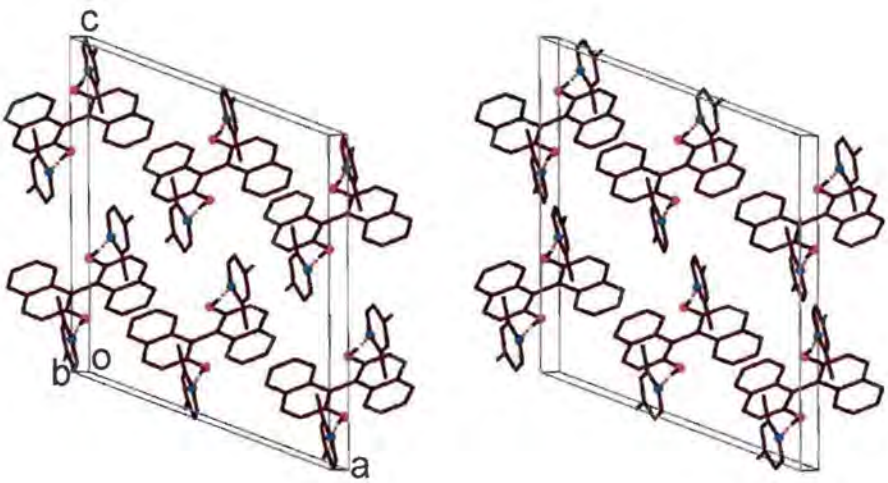

Figure 5.15 Stereo view of **BINAP•2(24LUT)** along [010]. Only the hydroxyl hydrogen atoms are shown. Hydrogen bonds are indicated as dotted lines. The N and O atoms are shown as solid circles.

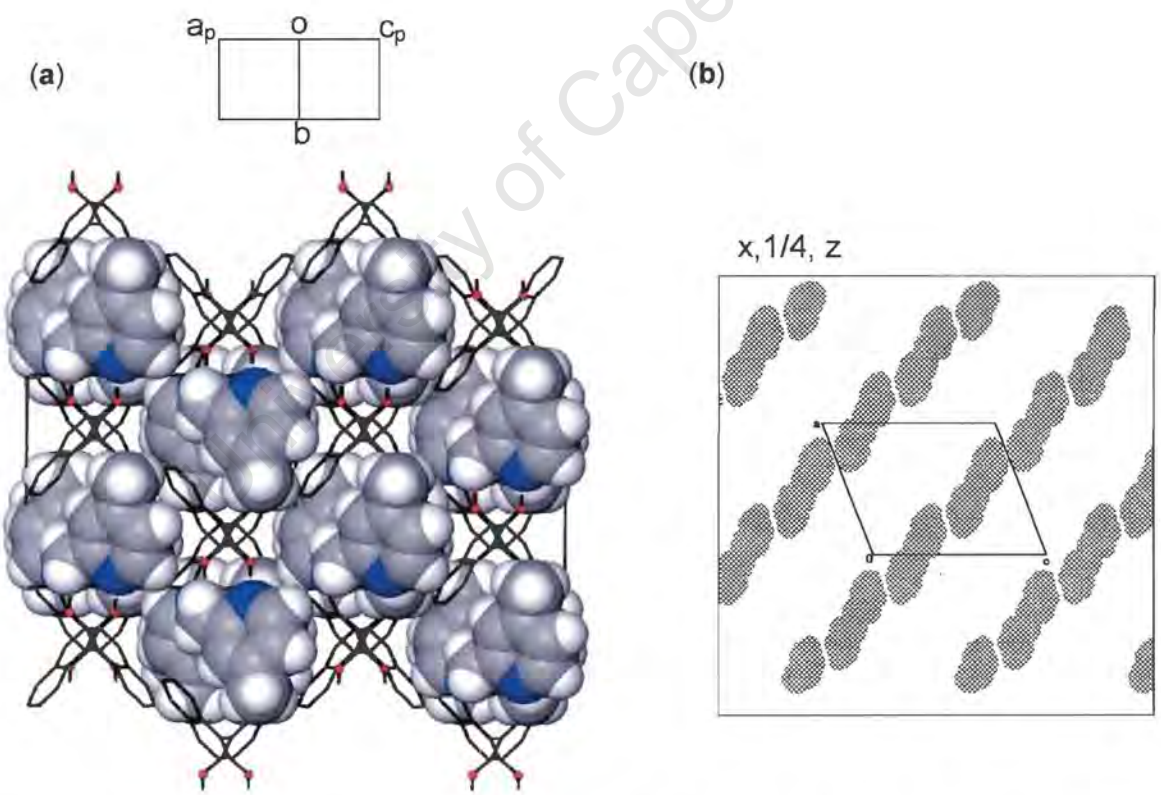

Figure 5.16 (a) Space-filling diagram for **BINAP•2(24LUT)** viewed along [101]. The guest molecules are shown with van der Waals radii and host molecules shown as sticks. Only the hydroxyl hydrogen atoms on the host are shown.
(b) Section plane of the host framework cut at y = 1/4, viewed along [010], with the diagonal crossed area representing the host. The guest is omitted.

(a)

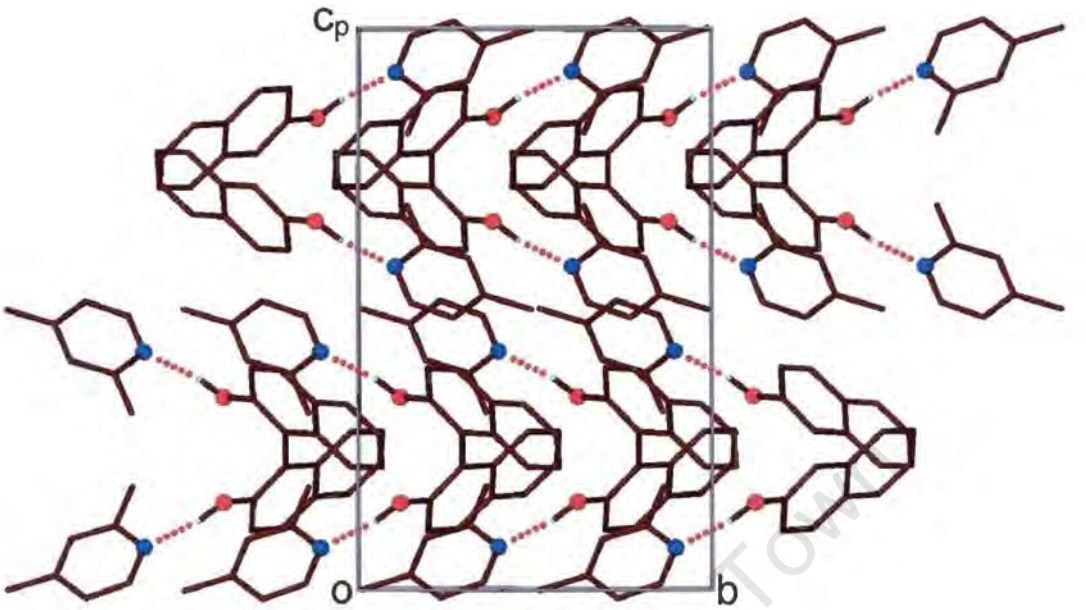

(b)

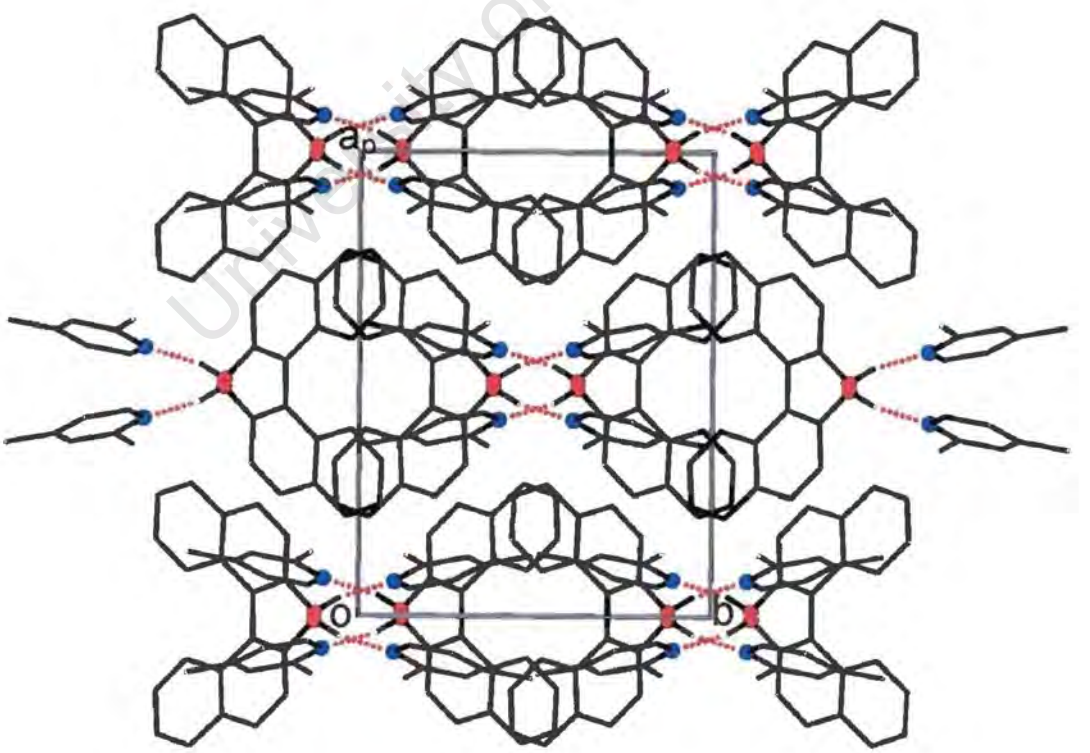

Figure 5.17 Projections viewed down (a) [100] and (b) [001], showing the crystal packing in **BINAP•2(24LUT)**. Details as in **Figure 5.15**.

BINAP•35LUT

$C_{20}H_{14}O_2 \cdot 2C_7H_9N$	
Guest: 3,5-lutidine	
Space group: P $\bar{1}$	
a = 10.341(1) Å	α = 103.651(5)°
b = 10.512(1) Å	β = 113.502(2)°
c = 11.868(1) Å	γ = 102.496(5)°
Volume = 1077.6(2) Å^3	
Z = 2	

Refinement

BINAP•35LUT crystallises in P $\bar{1}$ with Z = 2. Both the host and guest molecule were located in general positions. Refinement was carried out with the non-hydrogen atoms of the host and guest treated anisotropically. The hydrogen atoms on the host were located in the difference electron density maps and refined with simple bond length constraints [d(O···H) = 0.97Å)] and independent isotropic temperature factors. The rest of the hydrogen atoms were placed in geometrically constrained positions and refined with individual temperature factors assigned at either 1.2 or 1.5 times U_{eq} of their parents atoms. The structure refined successfully to R_1 = 0.0515.

Structure analysis

In this structure, each host molecule is hydrogen bonded to a guest molecule and another adjacent host molecule through a centre of inversion, resulting in the formation of a dimer, displaying the hydrogen bonds (host)O-H···N(guest) and (host)O-H···O(host) with O···N and O···O distances of 2.658(3)Å and 2.794(2)Å respectively (geometric details in **Table 5.3**). The molecular structure as well as the H-bonding scheme is shown in **Figure 5.18**. The host molecules pack to generate a unique channel running parallel to [010], centred at (0.5, y, 0.5). This channel accommodates two guest molecules related via a centre of symmetry and has a wave-like nature, with an approximate diameter of 5Å at the narrowest region and 7.5Å at the widest. This is depicted in **Figure 5.19**. The crystal packing diagrams, projected along all three axes, are shown in **Figure 5.20**.

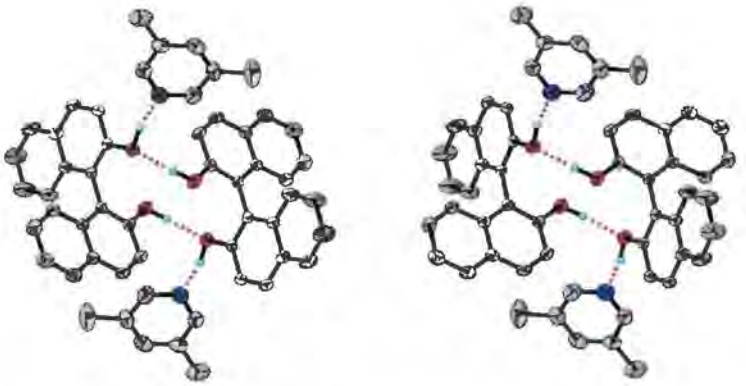

Figure 5.18 Stereoscopic view of the molecular structure of **BINAP•35LUT**. Displacement ellipsoids are drawn at the 45% probability level. All H atoms except the hydroxyl hydrogens are omitted for clarity.

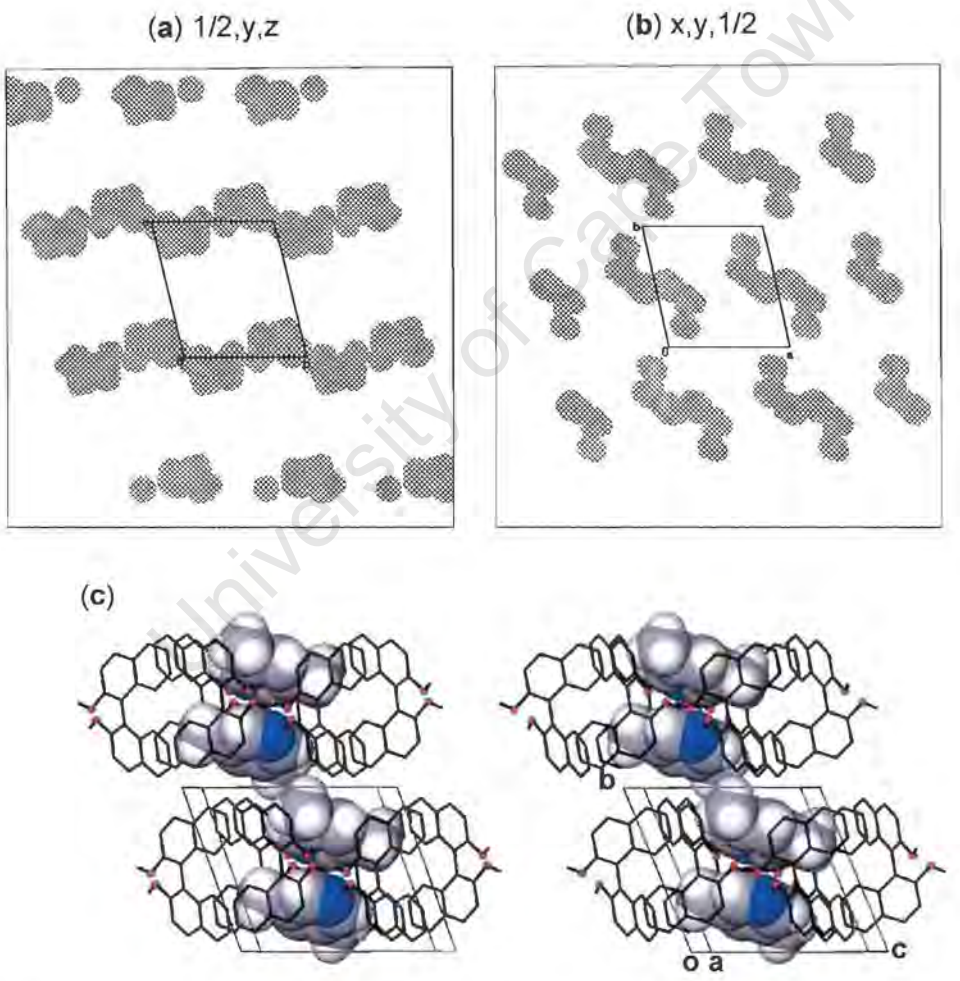

Figure 5.19 (a) and (b) Section planes cut at x = 1/2 and z = 1/2 respectively, with the diagonal crossed area representing the host, showing the channels parallel to [010]. The guest molecules are all omitted.
(a) Stereoscopic view of **BINAP•35LUT** along [010], showing the column of guest molecules running along [010]. The guest molecules are shown with van der Waals radii and the hosts are presented in stick model with all H atoms except the hydroxyl hydrogens omitted.

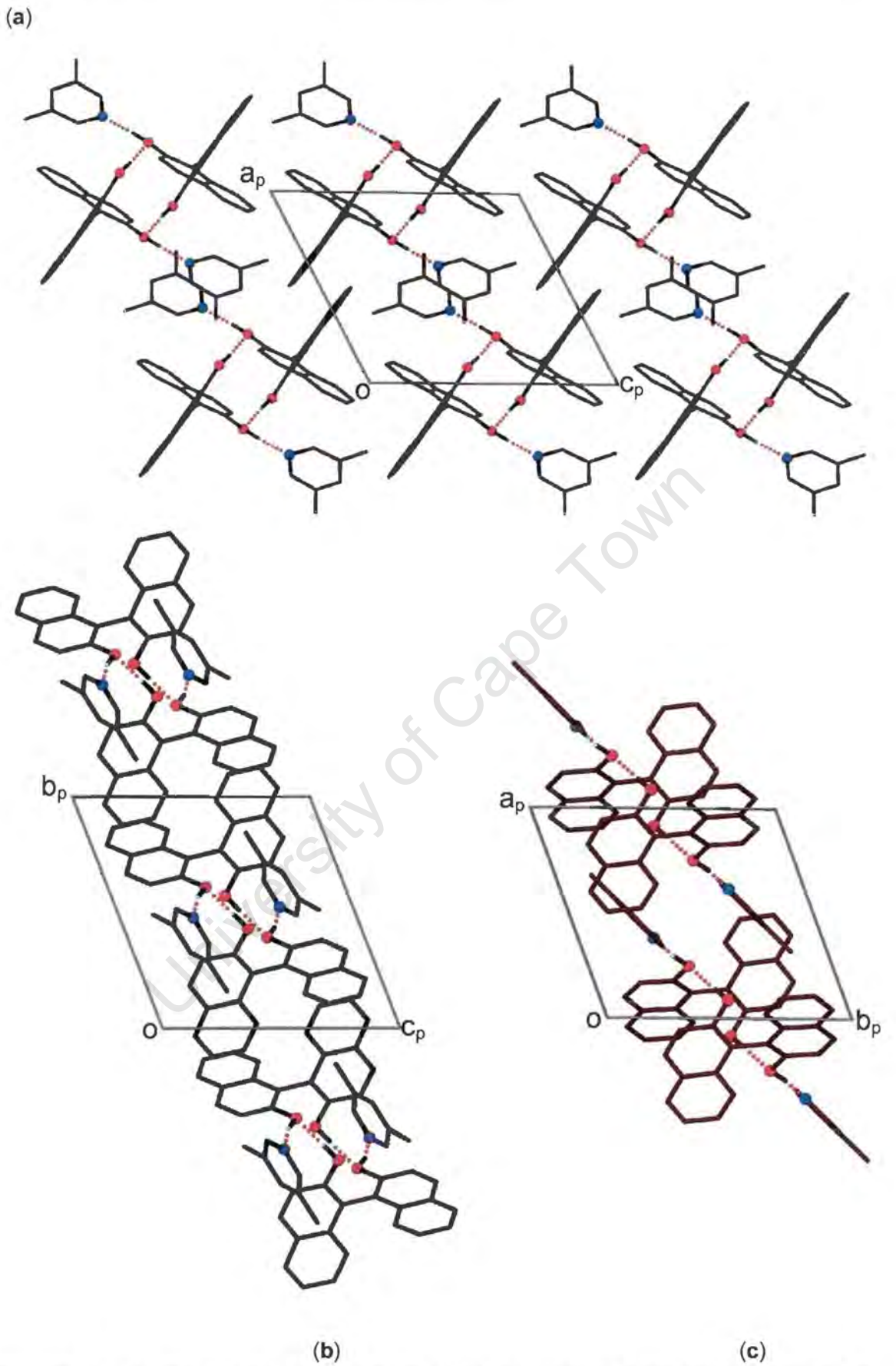

Figure 5.20 Projections viewed down (a) [010], (b) [100] and (c) [001], showing the crystal packing in **BINAP•35LUT**. Details as in **Figure 5.19**.

Competition experiments

The results of the competition experiments carried out at room temperature are shown in **Figure 5.21**.

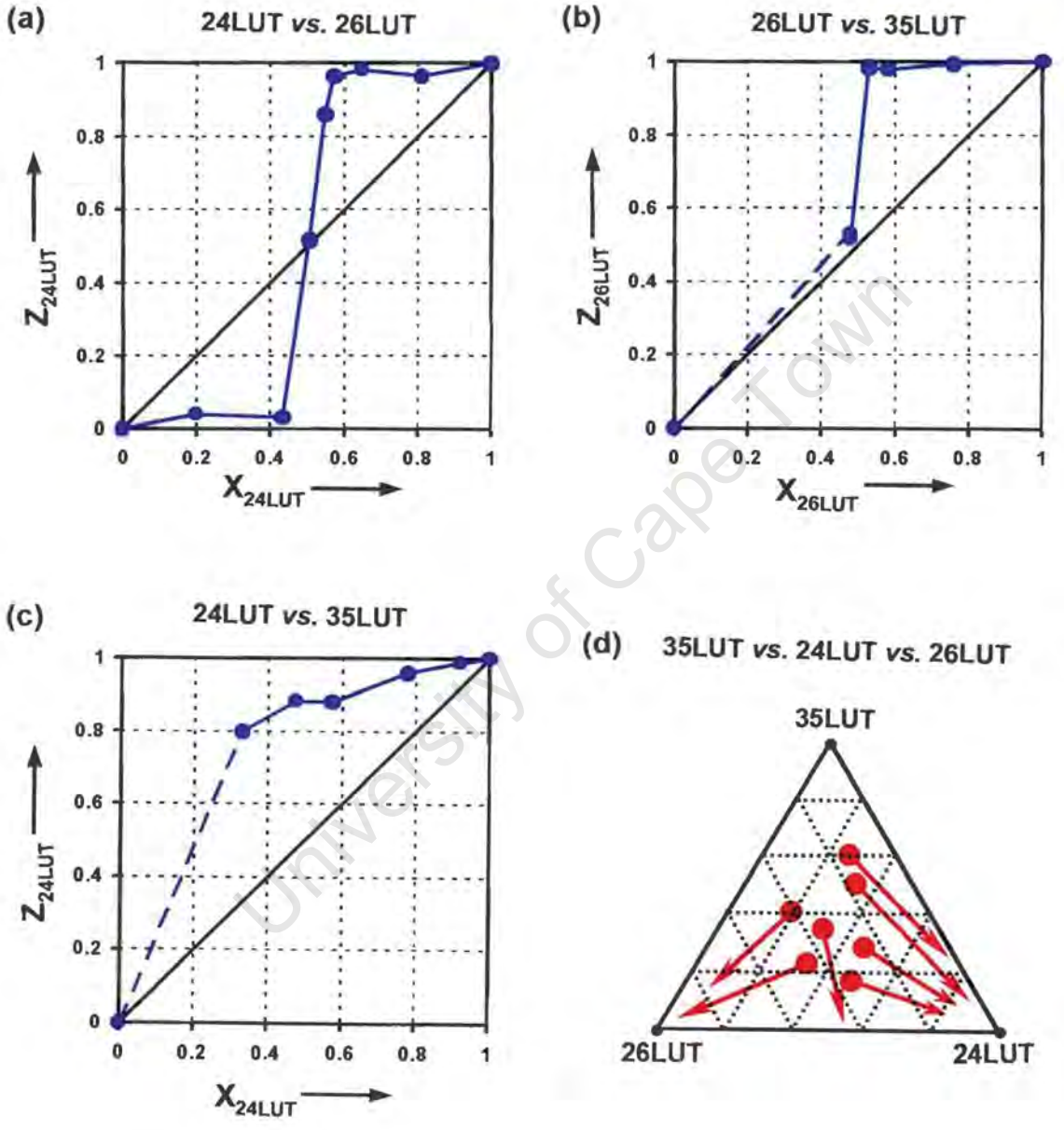

Figure 5.21 Results of the competitions between three isomers of lutidine by host **BINAP**.

The 2,4-lutidine *versus* 2,6-lutidine competition experiments (**Figure 5.21a**) shows concentration-dependent selectivity with parameter $Q_{24LUT:35LUT} = 0.5$, indicating one of them is strongly favoured when its mole fraction X is greater than 0.5. In the competitions between 2,6-lutidine and 3,5-lutidine (**Figure 5.21b**), 2,6-lutidine is preferentially included over 3,5-lutidine when its starting mole fraction $X_{26LUT} > 0.5$. The dashed lines in this figure, as well as in **Figure 5.21c**, do not represent experimental results, due to failure in obtaining crystals in these concentration regions. **Figure 5.21c** shows that the 2,4-lutidine is strongly preferred to 3,5-lutidine when its starting mole fraction is greater than about 0.33, at which point its mole fraction in the ensuing inclusion crystals, $Z_{24LUT} \approx 0.8$.

For the competitions conducted with all three lutidine isomers simultaneously, **Figure 5.21d** shows that for starting mixtures with $X_{26LUT} > X_{24LUT}$, there is a migration towards 2,6-lutidine, with the remaining mixtures moving towards 2,4-lutidine. 3,5-lutidine is disfavoured in all cases. The observations from three-component competitions complement those observed from the two-component competitions. The host compound shows preferential enclathration tendency towards the three lutidine isomers in the following order:

2,4-lutidine ≈ 2,6-lutidine > 3,5-lutidine.

The lutidine isomers separation has been carried out previously using other diol host compounds, **DHPC** (Caira et al. 1998), 1,4-bis(9-hydroxy-9-fluorenyl)benzene (**WEB9**) (Caira *et al.* 1999) and 1,1,6,6-tetraphenylhexa-2,4-diyne-1,6-diol (**TOD7**) (Caira *et al.* 1999). In these three cases, the hosts invariably favoured 3,5-lutidine, contrary to the results obtained in this study. However, the 2,4-lutidine was the least favoured isomer with the host **TOD7**, while 2,6-lutidine was the least favoured isomer in the competition experiments involving **DHPC** and **WEB9**. It is noted that in all the previous separation studies with these three different hosts, the inclusion complexes formed between the host and each isomer have constant host:guest ratio.

Lattice energy calculations

For the three inclusion compounds discussed in this part, summations of the non-hydrogen bonding lattice energies and the hydrogen bonding energies were carried out, and the following values for the total lattice potential energies were obtained:

BINAP•2(26LUT) -262.5 kJ mol^{-1};
BINAP•2(24LUT) -263.2 kJ mol^{-1};
BINAP•35LUT -191.0 kJ mol^{-1}.

It is interesting to note that the hydrogen-bonding interaction is, in fact, stronger for **BINAP•35LUT**, where the (host)O···N(guest) distance of 2.658Å is considerably shorter than that occurring in the other two compounds (2.815Å and 2.826Å). However this is not the only factor contributing to the lattice energy, which incorporates all other non-bonded interaction. It is also noted that the host:guest ratio is different in the compounds **BINAP•2(26LUT)** and **BINAP•2(24LUT)** *verses* **BINAP•35LUT**. This is also an important factor impinging on the values of the lattice energy. Therefore it is not correct to compare the lattice energy of **BINAP•35LUT** with those of other two compounds. However, the lattice energies of **BINAP•2(24LUT)** and **BINAP•2(26LUT)** have practically equal value, which suggesting the two host-guest systems are almost equally stable. This explains the concentration-dependent selectivity between 2,4-lutidine and 2,6-lutidine. We note that in the case of separation of 3- and 4-picoline by the host **DHPC** (Caira *et al.* 1997), where the lattice energy values were nearly equal, there was no selectivity of either isomer (the experimental results line overlaps the diagonal line in the results diagram). We may attribute this phenomenon to kinetic effects.

Kinetics of desolvation

The kinetics of desolvation of all of the three inclusion compounds were studied by carrying out a series of isothermal TG runs at selected temperatures lying between 60°C - 130°C. For the desolvation of **BINAP•2(26LUT)** and **BINAP•2(24LUT)**, the resultant curves of the extent of reaction α versus time t were deceleratory and were best fitted to the kinetic model R2 over an α range of 0.05 - 0.95. For the desolvation of **BINAP•35LUT**, slightly sigmoid α-time curves were obtained and were best fitted to the Avrami-Erofe'ev model A3 over an α range of 0.05 - 0.95. The A3 kinetic law is derived to account for reactions which begin with random and rapid evolution of nuclei which grow in three dimensions. The Arrhenius plots, ln k versus 1/T, were plotted for the desolvation reactions of each of the inclusion compounds as shown in **Figure 5.22**. This yielded an activation energy E_a and a pre-exponential factor ln A for each compound, shown in **Table 5.4**.

Table 5.4 Kinetic parameters for the desolvations of inclusion compounds of **BINAP** with lutidine isomers.

Inclusion Compound	Temperature range(°C)	α range	Kinetic model	E_a (kJ mol^{-1})	ln A
BINAP•2(26LUT)	70 -110	0.05 - 0.95	R2	80(4)	24(1)
BINAP•2(24LUT)	60 -100	0.05 - 0.95	R2	92(3)	27(2)
BINAP•35LUT	80 - 130	0.05 - 0.95	A3	101(7)	28(2)

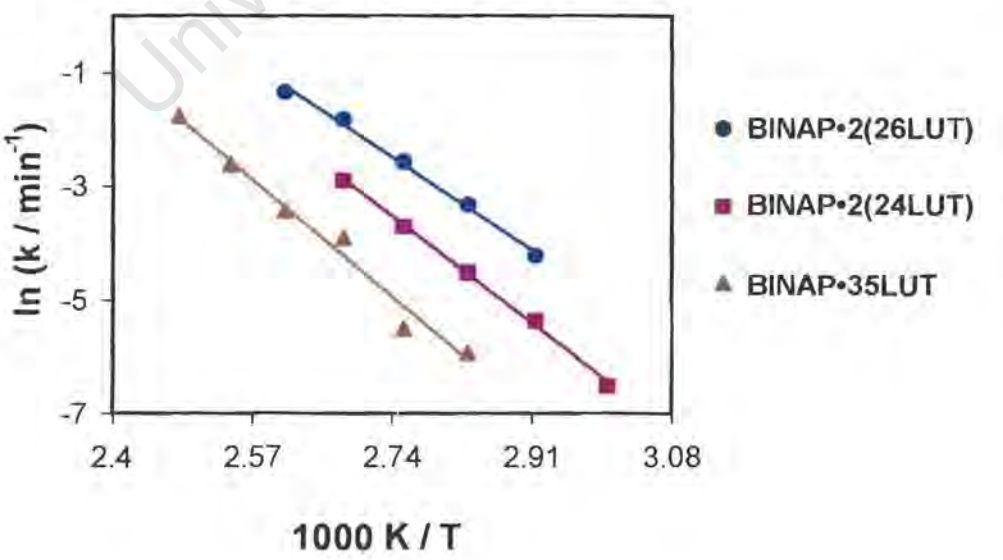

Figure 5.22 Arrhenius plots of ln k *versus* 1/T for desolvations of the inclusion compounds of **BINAP** with lutidine isomers.

PART 3

BINAP AND XYLIDINES

Preparation of the inclusion compounds

The host **BINAP** was dissolved in excess amount of 3,5-, 2,6 and 2,3-xylidine liquids by warming. The solutions were allowed to crystallise at both room temperature (~25°C) and 4°C by slow evaporation. Colourless crystals appeared within 12 hours to several days. The mole ratio of host to total guest used is approximately about 1:15 in the crystallisation experiments as well as the competition experiments. Inclusion compounds with host:guest ratios of 1:1, 1:2 and 1:3 were obtained with 3,5, 2,6 and 2,3-xylidine respectively. The host and 3,4-xylidine, which is solid at ambient temperature, were dissolved in the co-solvent ethanol but the ensuing crystals are the guest-free α-phase host only, which was confirmed by the TG and DSC analysis.

The chemical structures of the xylidine guests, their numbering scheme used in the structure solutions and the abbreviations for both the guests and the inclusion compounds obtained are shown in **Scheme 5.3**: The numbering scheme for the guests is same as that used in **Chapter 4** (**DHPC** and Xylidines).

Scheme 5.3

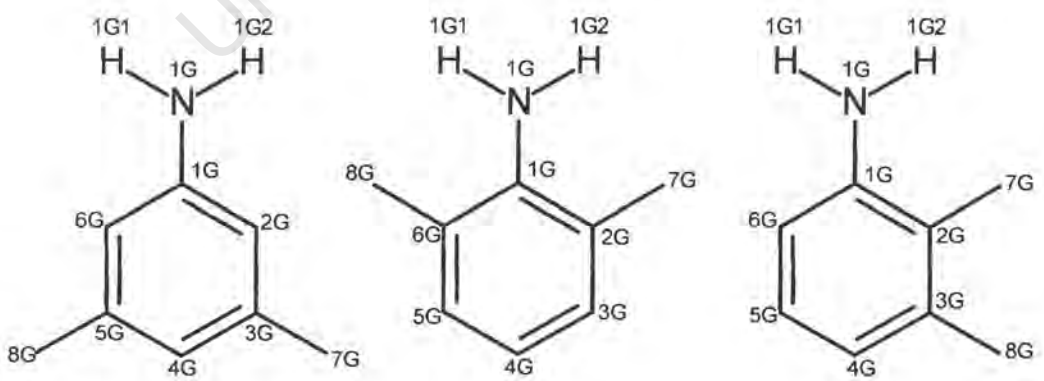

BINAP and 3,5-xylidine (**35X**): **BINPA•35X**
BINAP and 2,6-xylidine (**26X**): **BINPA•2(26X)**
BINAP and 2,3-xylidine (**23X**): **BINPA•3(23X)**

Thermal analysis

The TG and DSC traces for the desolvation of the inclusion compounds, carried out on finely crushed crystalline samples at a constant heating rate of 10°C min^{-1}, are shown in **Figure 5.23**. In all of the three inclusion compounds the TG shows a single step for desolvation and corresponds to the first sharp endothermic peak in the DSC. The last endothermic peak in the DSC, with onset temperature in the range of 215.1°C-216.8°C, corresponds to the melting of the apohost. The guest release endotherm for **BINAP•35X**, **BINAP•2(26X)** and **BINAP•3(23X)** occurred at 131.4°C, 110.9°C and 64.1°C respectively. The observed mass losses from TG for each compound are in good agreement with the calculated values required by stiochiometry:

BINAP•35X: observed weight loss 29.2%; calculated weight loss 29.74%.

BINAP•2(26X): observed weight loss 44.5%; calculated weight loss 45.84%.

BINAP•3(23X): observed weight loss 56.2%; calculated weight loss 55.94%.

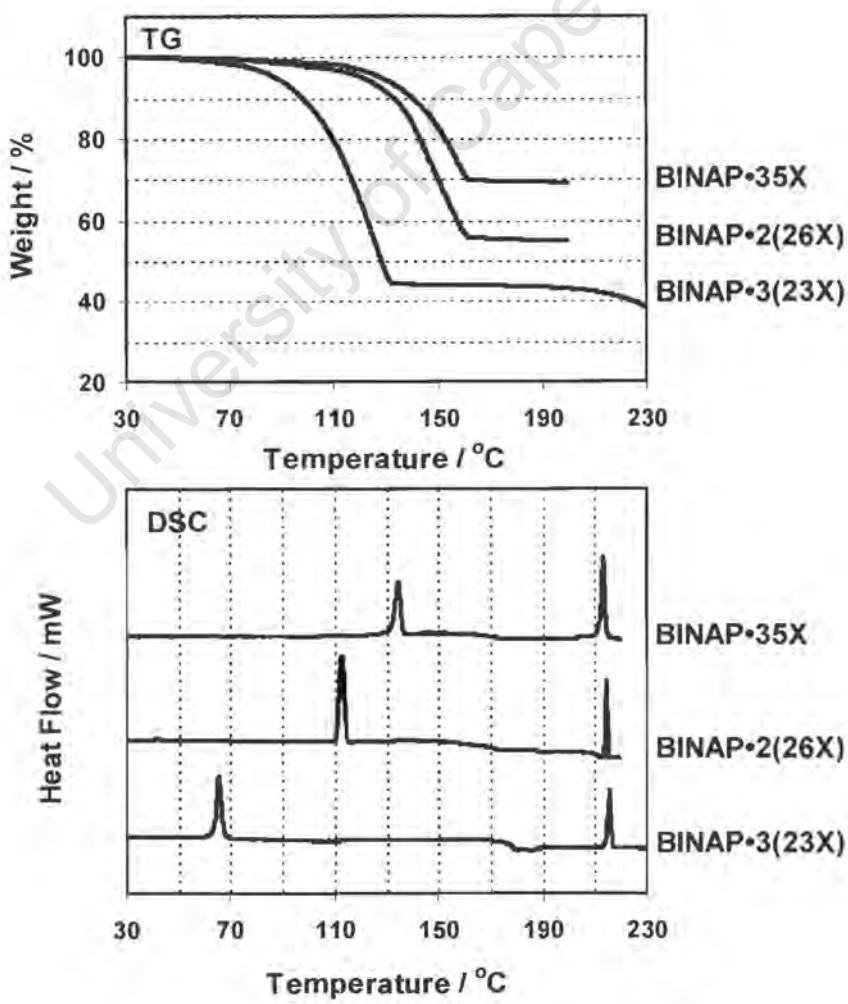

Figure 5.23 TG and DSC curves for inclusion compounds of **BINAP** with the three isomers of xylidine.

Crystal structures

Preliminary photography indicated that the inclusion compound **BINAP•35X** belongs to the triclinic crystal system. The space group P $\bar{1}$ was chosen based on the mean $|E^2-1|$ values obtained from direct methods (mean $|E^2-1|$ for the general *hkl* reflections = 1.111). The structure of **BINAP•2(26X)** was established by preliminary photography as belonging to the monoclinic crystal system (2/m Laue symmetry), and **BINAP•3(23X)** belonging to the orthorhombic crystal system (mmm Laue symmetry). The centrosymmetric space groups C2/c and Pbca were chosen for **BINAP•2(26X)** and **BINAP•3(23X)** respectively based on their non-extinction reflection conditions exhibited by their crystal reflection data and mean $|E^2-1|$ values. The choice of the centrosymmetric space group in each case was always vindicated by the successful final refinement of the structure.

For all of the three inclusion compounds, direct methods yielded all non-hydrogen atoms in the asymmetric unit. The hydroxyl oxygen atoms on the host molecule and the nitrogen atom on the guest molecule were placed unambiguously, due to their relative high electron densities. For each inclusion compound, the molecular formula, host:guest ratio, space group, cell parameters and other crystallographic information are summarised at the beginning of the discussion. This is followed by a brief description of its structure refinement and then by a description of its molecular structure and crystal packing. The host conformation data obtained from all the structure solutions in this part will be discussed in more detail collectively in **chapter 7**. The crystal data and final refinement parameters are contained in **Table 5.9**, appearing at the end of this chapter.

BINAP•35X

$C_{20}H_{14}O_2 \cdot C_8H_{11}N$	
Guest: 3,5-xylidine	
Space group: P $\bar{1}$	
a = 8.907(2) Å	α = 98.68(2)°
b = 8.956(3) Å	β = 98.45(1)°
c = 13.887(2) Å	γ = 94.26(2)°
Volume = 1077.9(5) Å^3	
Z = 2	

Refinement

BINAP•35X crystallises in P $\bar{1}$ with Z =2. The asymmetric unit is compromised of one host and one guest molecule, all located in general positions. All of the non-hydrogen atoms were refined anisotropically. The hydroxyl hydrogen atoms on the host molecule and amino hydrogen atoms on the guest molecule were located and refined with simple bond length constraints at values of d(O-H) = 0.97Å and d(N-H) = 0.97Å. The rest of hydrogen atoms on the host molecule and guest molecule were placed geometrically. The structure refined successfully to R_1 = 0.0401.

Structure analysis

The crystal packing of this structure, viewed along [100] and [010], is shown in **Figures 5.24**. Each host molecule is hydrogen bonded to one guest via an O-H···N hydrogen bond with a O···N distance of 2.837(2)Å. The geometric details of the hydrogen bond are given in **Table 5.5**, together with those of the other two structures. The guest molecules, related via a centre of symmetry, are located in channels running along [100] with cross sectional area of 6 x 5Å^2 at the narrowest part and 7 x 10Å^2 at the widest. The channel is depicted in **Figure 5.25**.

Table 5.5 Hydrogen bonding details for the structures discussed in **Part 3**.

Incl. Comp.	**D-H···A*** / Å	**D-H** /Å	**H···A** /Å	**D···A** /Å	**<DHA** /°
BINAP•35X	O(1)–H(1)···N(1G)	0.96(1)	1.91(1)	2.837(2)	163(2)
BINAP•2(26X)	O(1)–H(1)···N(1G)	0.96(1)	1.86(1)	2.814(3)	171(3)
BINAP•3(23X)	O(1)–H(1)···N(1GA)[1]	0.97(2)	1.82(2)	2.767(5)	164(4)
	O(2)–H(2)···N(1GB)[2]	0.96(2)	1.80(2)	2.735(5)	163(4)
	N(1GA)–H(1A1)···O(2)	0.97(2)	2.12(2)	3.041(5)	158(4)
	N(1GB)–H(1B1)···O(1)	0.96(2)	2.09(2)	2.984(5)	155(4)

***D-H···A**: Donor(**D**)-**H**···Acceptor(**A**)
Symmetry codes: (1) -x+1/2, y-1/2, z (2) -x+1/2, y+1/2, z

(a)

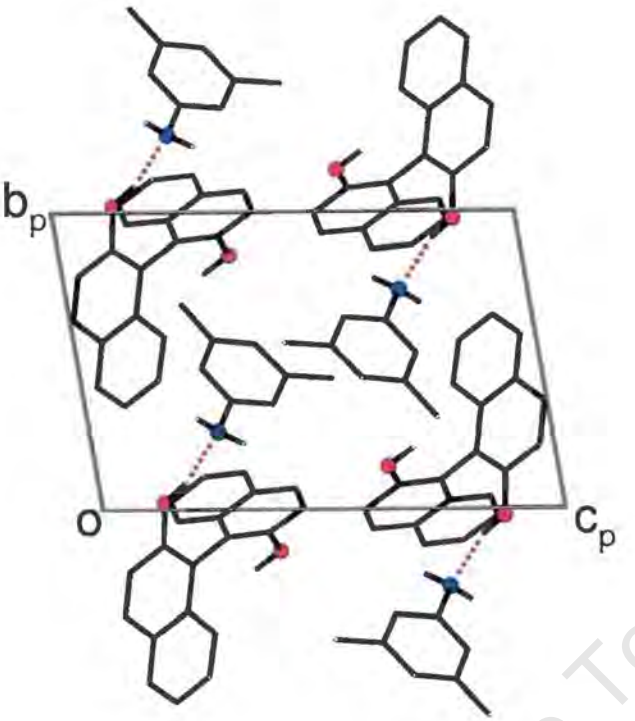

(b)

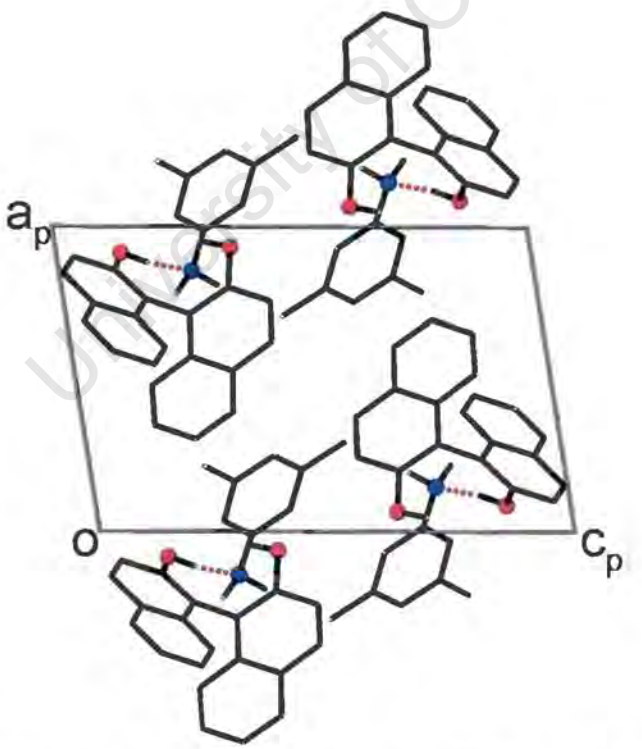

Figure 5.24 Crystal packing viewed along (a) [100] and (b) [010]. All the H atoms except the hydroxyl and amino hydrogens are omitted. The N and O atoms are shown in solid circles.

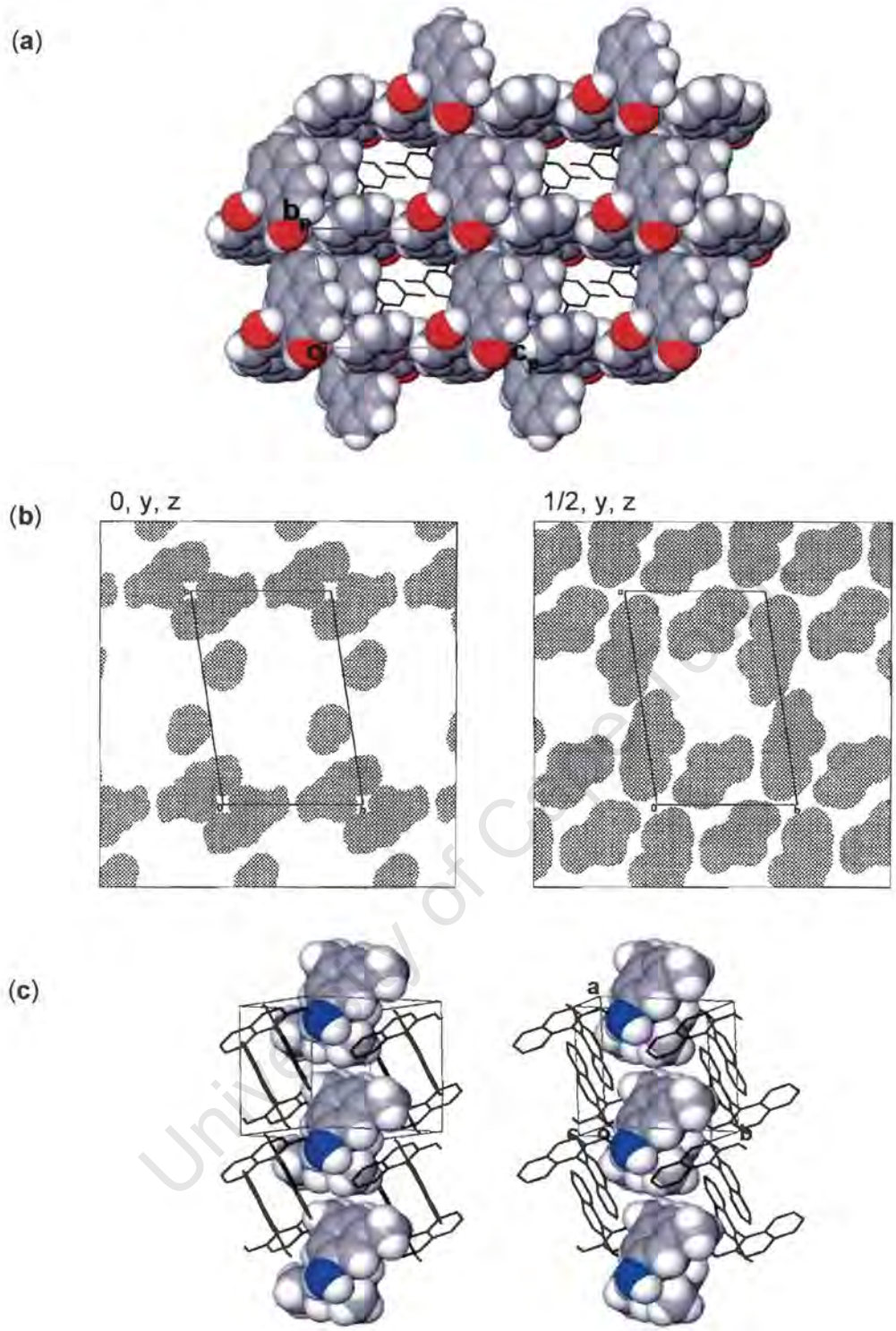

Figure 5.25 (a) A space-filling projection viewed along [100], looking down through the open channels where the guest molecules are situated. The host atoms are shown with van der Waals radii and guest in stick model with all H atoms omitted.
(b) Sections cut at x = 0 and x = 1/2, viewed along [100], showing the channels, centred at y = 1/2 and z = 1/2, at the widest and narrowest part respectively. The diagonal crossed area represents the host. The guest is omitted.
(c) Stereoscopic view of a column of guest molecules running along [100]. The guest atoms are shown with van der Waals radii and host in stick model with all H atoms except the hydroxyl hydrogens omitted.

BINAP•2(26X)

$C_{20}H_{14}O_2 \cdot 2C_8H_{11}N$	
Guest: 2,6-xylidine	
Space group: C2/c	
a = 26.066(2) Å	$\alpha = 90^o$
b = 10.068(2) Å	$\beta = 109.11(5)^o$
c = 11.868(2) Å	$\gamma = 90^o$
Volume = 2943.0(8) Å^3	
Z = 4	

Refinement

BINAP•2(26X) crystallises in C2/c with Z = 4. The host molecules were located in special positions, on a diad at Wyckoff position *e*. Thus the asymmetric unit contains one half of a host molecule and one guest molecule. Refinement was carried out with the non-hydrogen atoms of both the host and guest treated anisotropically. The two methyl carbon atoms on the guest molecule show relative high thermal motions and their U_{eq} of 0.094Å^2 and 0.122Å^2 were obtained respectively in the final refinement. The hydroxyl hydrogen atom H1 on the host molecule was located in difference electron density map and refined with simple bond length constraint [d(O-H) = 0.97Å] and an individual temperature factor. The amino hydrogen atoms on the guest molecule could not be located and thus are omitted from the final structure model. The rest of hydrogen atoms were all geometrically constrained and refined with isotropic temperature factors related to their parent atoms. The residual electron densities of 0.60 e/Å^3 and 0.54 e/Å^3 were observed close to the atom N(1G), but could not be modelled reasonably. The structure refined successfully to R_1 = 0.0662.

Structure analysis

The molecular structure of **BINAP•2(26X)** is shown in **Figure 5.26**. Each hydroxyl group of the host molecule is hydrogen bonded to a guest molecule via (host)O-H···N(guest) with O···N distance of 2.814(3)Å (see **Table 5.5**). The structure is characterised by columns of guest molecules cross running along the [110] and [1 $\bar{1}$0] directions at z = 1/4 and 3/4 respectively. This is shown in **Figure 5.27**. The crystal packing, viewed down [010] and [001], is shown in **Figure 5.28**.

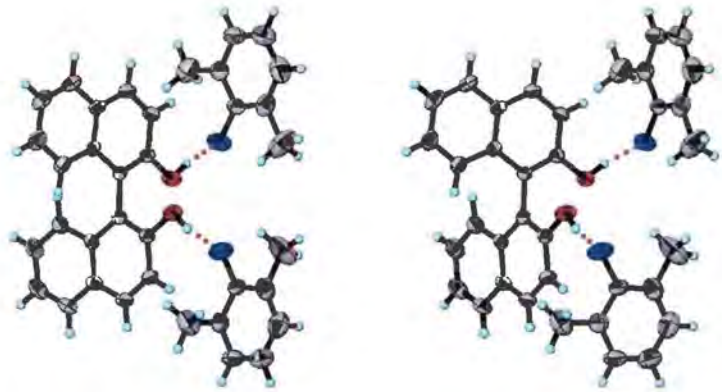

Figure 5.26 Stereoscopic view of the molecular structure of **BINAP•2(26X)**. Displacement ellipsoids are drawn at the 45% probability level.

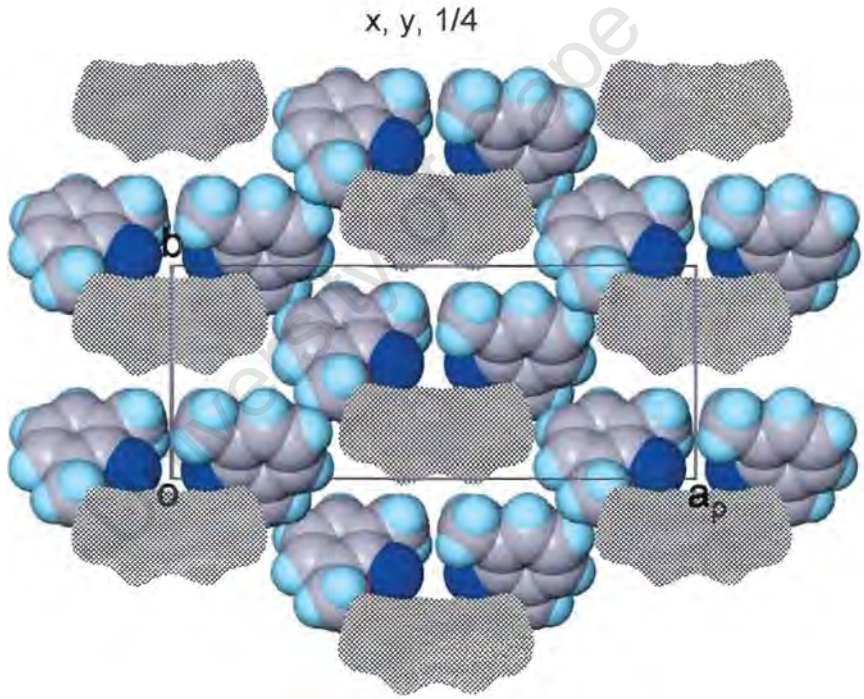

Figure 5.27 **BINAP•2(26X)**: projected cross section of the host molecules (semi-transparent grey areas) on (004), showing the guest molecules in channels cross running along [110] and [1 $\bar{1}$0] directions. The guests are shown as van der Waals representation.

(a)

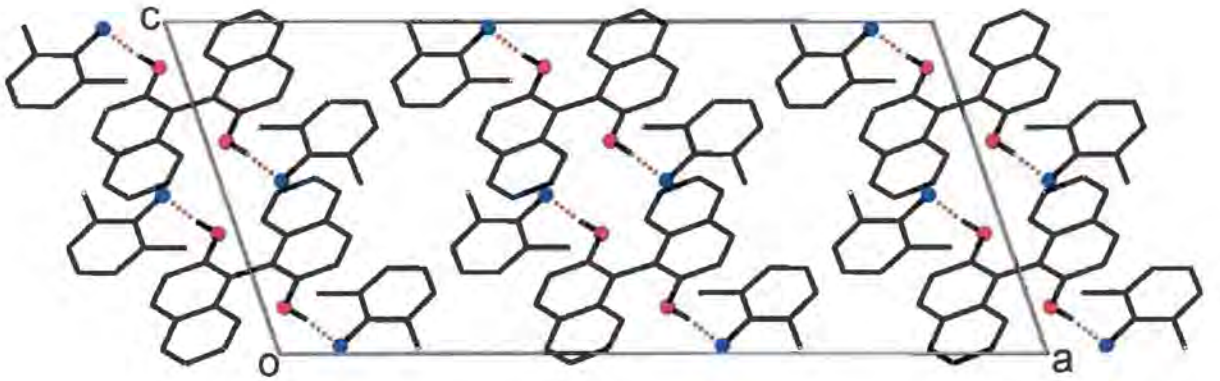

(b)

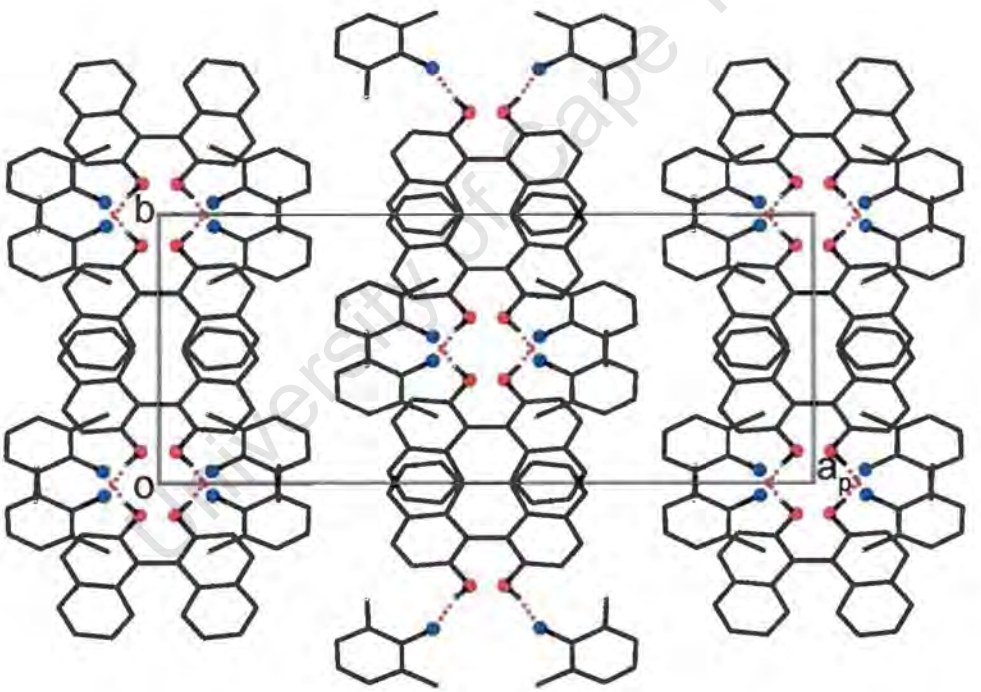

Figure 5.28 Projections viewed down (a) [010] and (b) [001], showing the crystal packing in **BINAP•2(26X)**. All of the H atoms except the hydroxyl hydrogens are omitted. The hydrogen bonds are indicated as dotted lines. The N and O atoms are shown in solid circles.

BINAP•3(23X)

$C_{20}H_{14}O_2•3C_8H_{11}N$	
Guest: 2,3-xylidine	
Space group: Pbca	
a = 22.634(1) Å	$\alpha = 90^o$
b = 10.464(1) Å	$\beta = 90^o$
c = 30.689(1) Å	$\gamma = 90^o$
Volume = 7268.4(8) $Å^3$	
Z = 8	

Refinement

BINAP•3(23X) crystallises in Pbca with Z = 8. There is one host and three guest molecules (A, B and C) in the asymmetric unit, all located in general positions. All of the non-hydrogen atoms were refined anisotropically. A number of carbon atoms of the guest molecule B and C exhibited relative high thermal motion and they were responsible for the unsatisfactory geometries of the benzene rings. The rings were thus geometrically constrained to fit a regular hexagon. The hydroxyl hydrogen atoms of the host and the amino hydrogens of the guest were all located in difference electron density maps. The hydroxyl hydrogens H(1) and H(2), and the amino hydrogens of guest molecule A [H(1A1) and H(1A2)] were refined with simple bond length constraints with their own isotropic temperature factors. The amino hydrogens of the guest molecule B [H(1B1) and H(1B2)] and C [H(1C1) and H(1C2)], were assigned 1.2 x U_{eq} of their parent atoms N(1GB) and N(1GC), owing to their high thermal motions, and were refined with simple bond lengths constraints. The rest of the hydrogen atoms were all placed with geometric constraints and refined with isotropic temperature factors related to their parent atoms. The final R index for this structure is $R_1 = 0.0926$.

Structure analysis

The **BINAP•3(23X)** structure exhibits extensive hydrogen bonding. The host hydroxyl and the guest amino groups act as both proton donors and proton acceptors, displaying the hydrogen bonds (host)O-H···N(guest) and (guest)N-H···O(host). There are three crystallographic independent guest molecules, A, B and C, in the structure and one of them, guest molecule C, does not participate in hydrogen bonding, while the other two act as double bridges that link adjacent host molecules chains along [010] (**Figure 5.29**). The crystal packing diagrams for **BINAP•3(23X)**, viewed down [100] and [010], are shown in **Figure 5.30** and **5.31a** respectively. The structure is characterised by channels of guest molecules cross running along [010] and [001]. The channels that run parallel to [010] contain mostly molecules of guest C (**Figure 5.31b**). The

molecules of guest A and B are located in channels waving along [001] and intersecting with the [010] channels (**Figure 5.31c**).

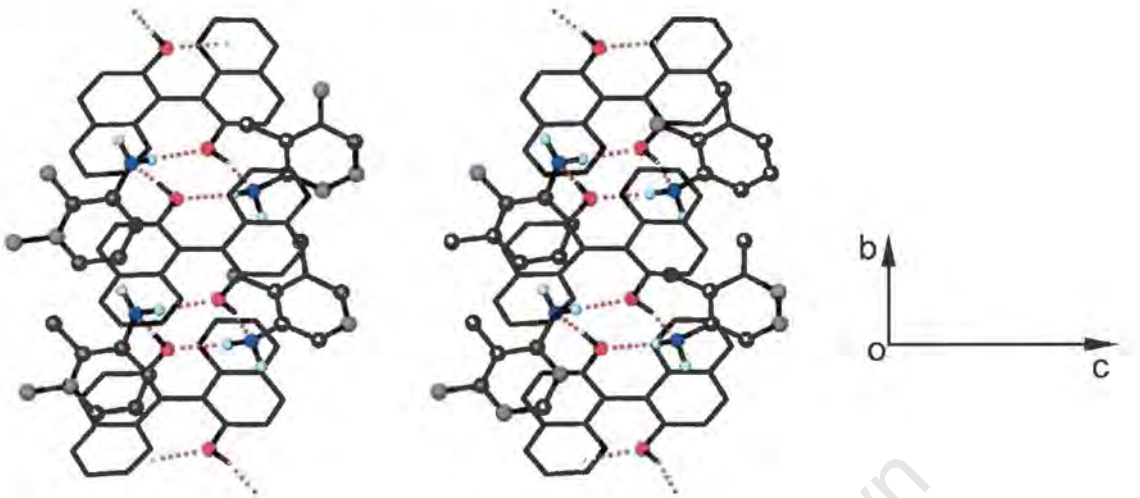

Figure 5.29 Stereoscopic view of part of the structure of **BINAP•3(23X)** along [100], showing one-dimensional hydrogen bonding aggregation running along [010]. The guest atoms and O atoms are in ball representation. All of the H atoms except the hydroxyl and amino hydrogens are omitted. Guest C is omitted. The hydrogen bonds are indicated as dotted lines.

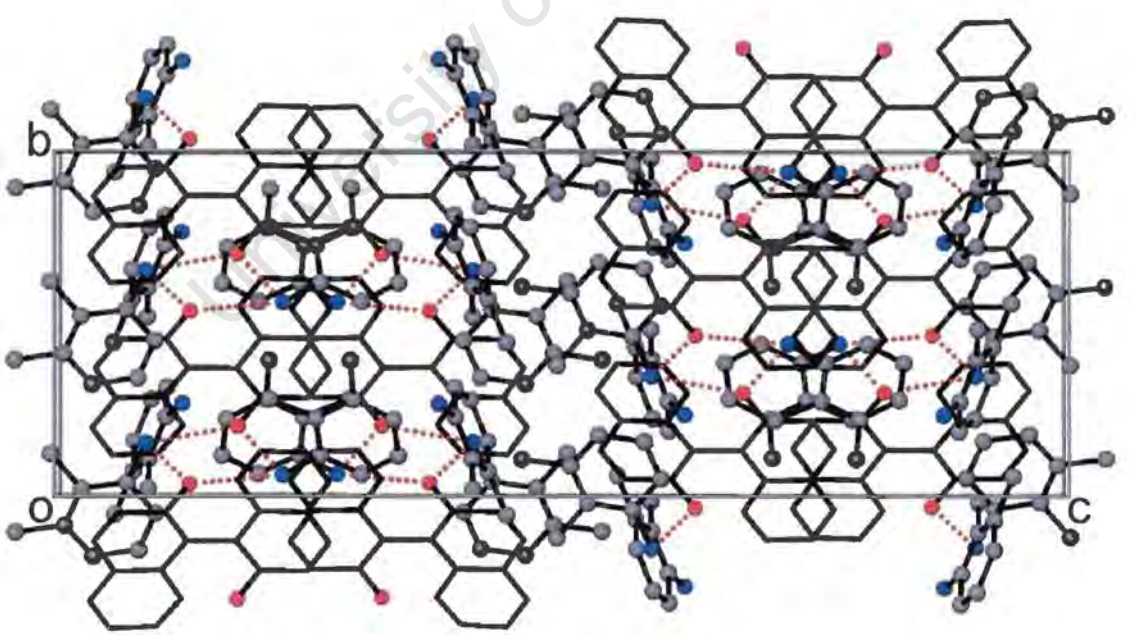

Figure 5.30 Projection viewed along [001], showing the crystal packing in **BINAP•3(23X)**. All of the H atoms are omitted for clarity. The hydrogen bonds are indicated as dotted lines. The guest atoms and O atoms are shown in ball representation.

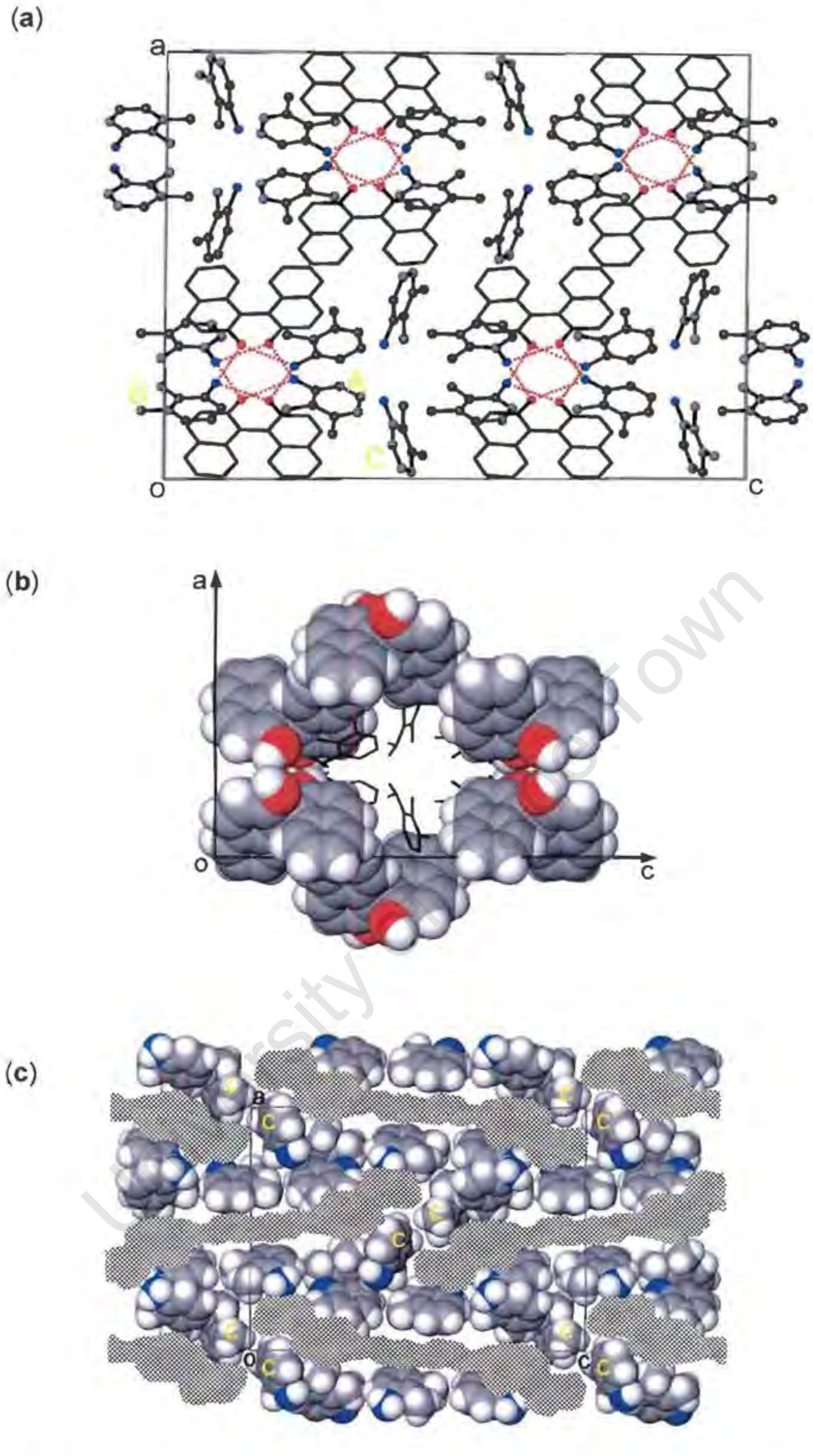

Figure 5.31 (a) Crystal packing of **BINAP•3(23X)**, projected down [010]. The crystallographic independent guests are marked. Detail as in **Figure 5.30**. (b) Space filling diagram projected along [010], viewing from the top of the open [010] channels. The host are shown with van der Waals radii. The H atoms of guest, except the amino hydrogens, are omitted.
(c) Cross section of the host molecules (semi-transparent grey areas) at y = 0, showing the intersecting channels. The guests are shown in van der Waals representation. Only molecules of guest C are marked.

Competition experiments

The results of the competition experiments, carried out as the procedures described in **Chapter 2**, are shown in **Figure 5.32**.

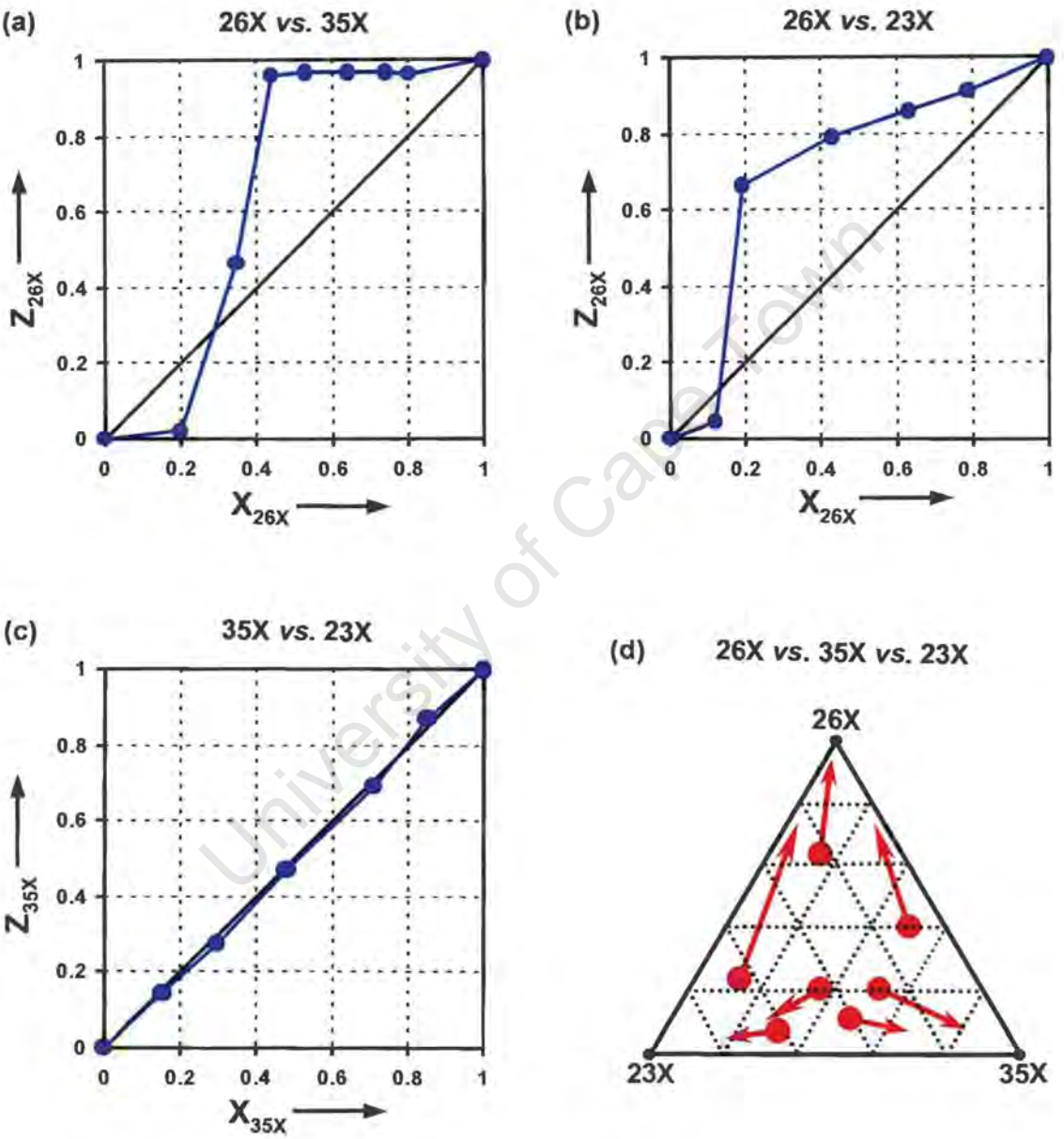

Figure 5.32 Results of the two and three component competition experiments between the three isomers of xylidine by the host **BINAP**.

The competition results between 2,6-xylidine and 3,5-xylidine (**Figure 5.32a**) depend on their concentrations with the selectivity parameter $Q_{26X:35X} \approx 0.29$. It shows that 2,6-xylidine is preferentially enclathrated over 3,5-xylidine when its mole fraction of the starting mixture X_{26X} is greater than about 0.29; below that, the 3,5-xylidine is favoured.

The selectivity between 2,6-xylidine and 2,3-xylidine (**Figure 5.32b**) shows a smaller degree of concentration-dependence, with $Q_{26X:23X} \approx 0.13$. The 2,6-xylidine is favoured when $X_{26X} > 0.13$, otherwise the 2,3-xylidine is favoured. In the 3,5-xylidine *versus* 2,3-xylidine competitions (**Figure 5.32c**), there is no selectivity.

In the competition experiments with all of the three xylidine isomers (**Figure 5.32d**), the 2,6-xylidine is strongly favoured for the starting three-component mixtures of which its mole fraction $X_{26X} > 0.2$, otherwise 2,3-xylidine and 3,5-xylidine are nearly equally selected. The three-component competition results are in good agreement with the results observed from the two-component competitions.

Summarising all these competitions results, the selectivity of enclathration by the host **BINAP** follows the following trend:

2,6-xylidine > 3,5-xylidine ≈ 2,3-xylidine

Kinetics of desolvation

Data for the kinetics of desolvation of all of the three inclusion compounds were obtained by iso-thermal TG experiments carried out on finely crushed microcrystalline samples. The typical α *versus* time curve at certain temperature for each inclusion compound is shown in **Figure 5.33a**. The plots of ln *k versus* 1/*T* are shown in **Figure 5.33b**.

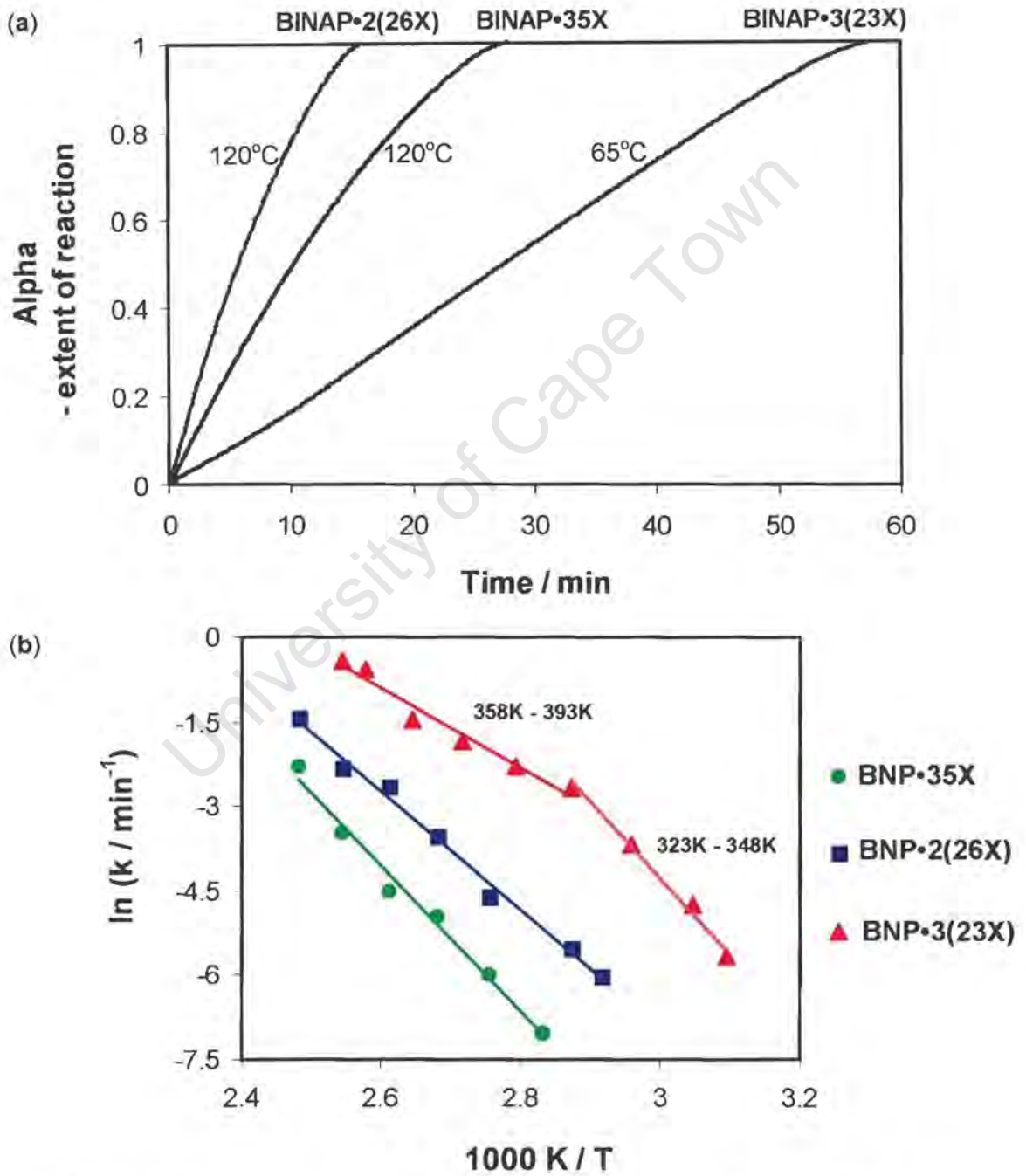

Figure 5.33 (a) Typical α-time curves for the desolvations of **BINAP•35X**, **BINAP•2(26X)** and **BINAP•3(23X)** at 120°C, 120°C and 65°C respectively. (b) Arrhenius plots of ln *k versus* 1/*T* for the desolvation reactions.

For the desolvation of **BINAP•35X** and **BINAP•2(26X)**, their α-time curves were deceleratory and were best described by the contracting area (R2) kinetic equation. The semilogarithmic plots of ln *k* versus 1/*T* are linear over the investigated temperature range for both of the inclusion compounds, as shown in **Figure 5.33b**. Arrhenius parameters were obtained over an α range of 0.05 -0.95 with coefficients between 0.993 to 0.999. The Activation energies for the desolvation reactions of **BINAP•35X** and **BINAP•2(26X)** were calculated to be 106(8) kJ mol^{-1} and 88(4) $kJmol^{-1}$ respectively and they are summarised in **Table 5.6**, together with other relevant Arrhenius parameters.

Table 5.6 Kinetic parameters for the desolvations of the inclusion compounds of **BINAP** with xylidine isomers.

Inclusion Compound	Temperature range	α range	Kinetic model	E_a (kJ mol^{-1})	ln A
BINAP•35X	80 - 130	0.05 - 0.95	R2	106(8)	29(3)
BINAP•2(26X)	70 - 130	0.05 - 0.95	R2	88(4)	24(1)
BINAP•3(23X)	50 - 75 (323K - 348K)*	0.07 - 0.93	A2	108(8)	35(3)
	85 - 120 (358K - 393K)	0.07 - 0.93	A2	59(5)	18(2)

* K is quoted here for easy reference.

For the desolvation of **BINAP•3(23X)**, the *α-time* curves, which were slightly sigmoidal in shape (**Figure 5.33a**), fitted the Avrami-Erofe'ev (A2) equation. The Arrhenius semilogarithmic plot, however, is not linear over the complete temperature range of 50°C to 120°C, but yields two distinct lines of differing slopes which cross at 1/*T* at 2.91 x 10^{-3} K^{-1} (T ≈ 344K or 70°C), corresponding to two activation energies of 108(8) and 59(5) kJ mol^{-1}. This was initially puzzling, as the fit of the *α-time* curves to the A2 rate equation was good over the entire temperature range. Therefore we investigated the crystals by Hot Stage Microscopy, of which pictures are shown in **Photo 5.1**. This revealed that the crystals, which were initially transparent, developed cracks and became opaque in the temperature range 25°C to 72°C, at which point liquid guest appeared and partly dissolved the crystals. By 85°C most of the liquid had disappeared, leaving opaque crystals which melted at 215°C. We therefore surmise that from 72°C to 120°C the *α-time* curves represent a combination of desolvation and liquid evaporation, yielding the lower activation energy. It is interesting to note that the

desolvation reaction with melting obeys the same solid state mechanism (A2 model) as the desolvation reaction without melting.

While a number of inclusion compounds, other than **BINAP•3(23X)**, might undergo partial or complete melting concomitant with guest release under heating, the temperature range for desolavtion should be carefully chosen to ensure that the desolvation reaction monitored was the loss of guest from the microcrystalline inclusion complex rather than from the melt containing the mixture of host and guest.

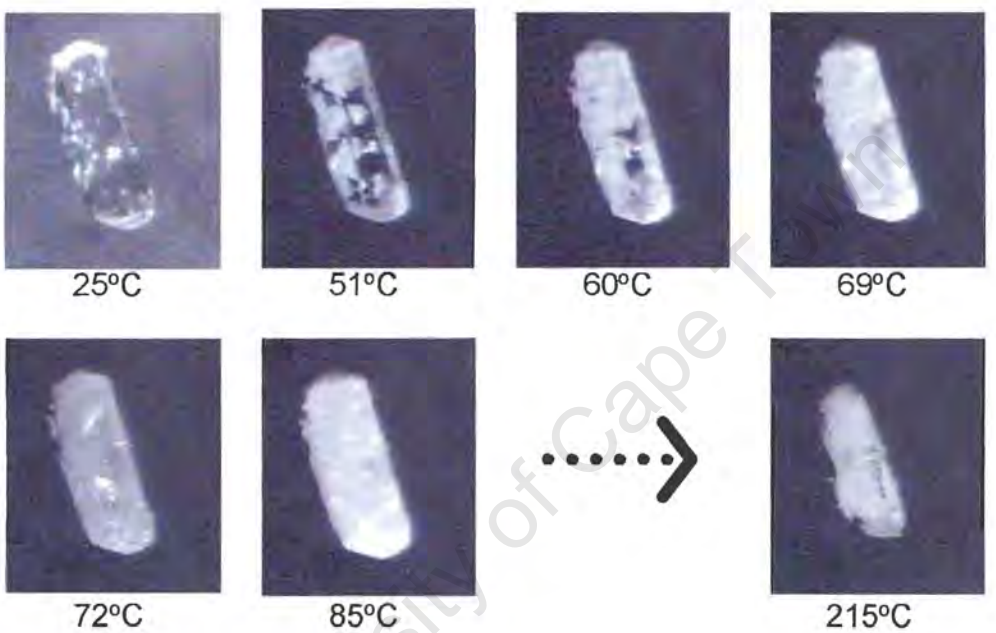

Photo 5.1 HSM photographs for crystal of **BINAP•3(23X)** under heating at a rate of 10°C min^{-1}. The size of the crystal is about 0.25 x 0.1 x 0.05 in mm.

IR spectra studies

IR spectra were recorded for the apohost compound **BINAP** as well as the three xylidine inclusion compounds investigated in the 3000 - 3600cm^{-1} region, where the hydroxyl group O-H stretching absorption occurs (Brown *et al.* 1998). The crystal structure of **BINAP**, which is discussed in **Chapter 6**, shows that only one of the two hydroxyl groups is hydrogen bonded. Its IR spectra displayed two sharp peaks, at 3483.7cm^{-1} which is attributed to the 'free' O-H (ν_f) and at 3398.7cm^{-1} due to the hydrogen bonded hydroxyl [d(O-H···O) = 2.839(2)Å]. For all inclusion complexes, the recorded IR bonds occur at lower frequencies, and the frequency change, the shift from 'free' O-H band, $\Delta = \nu_f - \nu_{OH}$ are recorded in **Table 5.7**, together with selected parameters of hydrogen bonding observed in their crystal structures. The case of **BINAP•35X** merits special mention, in that only one host hydroxyl is hydrogen bonded with (host)O-H···N(guest) having d(O···N) = 2.837(2)Å and Δ = 165.1cm^{-1}, but the other O-H has a close contact with a methyl group from the 3,5-xylidine with (host)O-H···CH_3(guest) having d(H···C) = 2.763(2)Å, resulting in a vibrational shift of 95.4cm^{-1}.

Table 5.7 IR spectra results: the hydroxyl group O-H stretching absorption frequencies.

Compound name	Peak wavenumber ν_{OH} (cm^{-1})	$\Delta = \nu_f - \nu_{OH}$	Type of hydrogen Bond	Hydrogen bonding distance (Å)
BINAP	3483.7(ν_f)	/	'Free' O-H bond	/
	3398.7	85	O-H···O	d(O···O) = 2.839(2)
BINAP•35X	3388.3	95.4	O-H···CH_3	d(H···C) = 2.763(2)
	3318.6	165.1	O–H···N	d(O···N) = 2.837(2)
BINAP•2(26X)	3311.2	172.5	O–H···N	d(O···N) = 2.814(3)
BINAP•3(23X)	3370.8	112.9	O–H···N	d(O···N) = 2.767(5)
	3281.3	202.4	O–H···N	d(O···N) = 2.735(5)

The IR spectra clearly support the presence of the hydrogen bonds: the ν_{OH} bands are shifted from 3483.7cm^{-1} ('free' OH group of the host) to lower frequencies upon inclusion complexation. Similar observations have been reported by Toda and his co-workers (Toyota *et al.* 2001). The IR technique has provided most of the evidence for hydrogen bonding for over half a century. Badger and Bauer (1937) have suggested that there was a linear relationship between the (donor)D-H bond shift and the hydrogen bond energy. **Table 5.7** shows that, there is a general trend showing that the shorter the O···N distance, the greater is the shift, but the correlation is poor.

Discussion

In the work presented in this chapter, separations of the close isomers of picoline, lutidine and xylidine were attempted using the same host compound **BINAP**. The inclusion compounds formed between the host and the pure isomer were analysed by TG and DSC, and their crystal structures were elucidated. In order to interpret the enclathration selectivity by the host towards each close isomer group, the structural features and thermal behaviours of the inclusion complexes are reviewed together, followed by discussion. The relevant thermal data and structural parameters are summarised in **Table 5.8**, together with the selectivity trends for each close isomer group.

Table 5. 8 Relevant thermal data, structural parameters and selectivity trend for three related isomer groups discussed in this chapter.

Inclusion compound	T_{on} - T_b (°C)	E_a of desolvation (kJ mol^{-1})	Inclusion mode	Packing efficiency (%)	Lattice energy (kJ mol^{-1})	H-bond type and bond length range D···A (Å)
BINAP•2(2PIC)	-32.9	86(4)	Interconnected channels	68.1	-222.4	**H**···**G** 2.697(2)
BINAP•2(3PIC)	-84.4	82(6)	Interconnected channel	66.4	-216.7	**H**···**G** 2.708(2) -2.779(2)
BINAP•2(4PIC)	-35.3	84(7)	Channel	68.7	-225.6	**H**···**G** 2.747(2) 2.746(2)
Selectivity trend: **4PIC ≈ 2PIC > 3PIC**						
BINAP•2(26LUT)	-44.2	80(4)	Interconnected channel	67.9	-262.5	**H**···**G** 2.815(5)
BINAP•2(24LUT)	-41.8	92(3)	Interconnected channel	67.7	-263.2	**H**···**G** 2.826(3)
BINAP•35LUT	-34.2	101(7)	Channel	65.6	-191.0	**H**···**H** 2.658(3) **H**···**G** 2.794(2)
Selectivity trend: **24LUT ≈ 26LUT > 35LUT**						
BINAP•35X	-89.6	106(8)	Channel	68.5	-	**H**···**G** 2.837(2)
BINAP•2(26X)	-103.1	88(4)	Interconnected channel	65.2	-	**H**···**G** 2.814(3)
BINAP•3(23X)	-158.9	108(8)	Interconnected channel	67.7	-	**H**···**G** 2.735(5) 2.767(5) **G**···**H** 2.984(5) 3.041(5)
Selectivity trend: **26X > 35X ≈ 23X**						

* **D**···**A** Donor···Acceptor.
H Host O atom of **BINAP**.
G Guest N atom.

BINAP forms 1:2 inclusion compound with each of the three picoline isomers. The inclusion compounds, **BINAP•2(2PIC)**, **BINAP•2(3PIC)** and **BINAP•2(4PIC)**, crystallise in the respective space groups C2/c, $P2_1/c$ and Pbca. The host molecules are on diads in the structure of **BINAP•2(2PIC)**, and are in general positions in other two structures. Each structure is stabilised by (host)O-H···N(guest) hydrogen bonds, which hold two guest molecules to one host molecule via the two hydroxyl groups. The hydrogen bonding distances for these three compounds are in a small range [2.697(2) - 2.779(2)Å], with that of **BINAP•2(2PIC)** being the shortest. The 2-picoline and 3-picoline guest molecules are located in interconnected channels, whereas 4-picoline guest is in unique channels.

The desolvation of these three inclusion compounds proceeded in one single step and followed the deceleratory contracting area kinetic model (R2). The activation energies obtained for the desolvation of the three compounds are similar [82(6) - 86(4)kJ mol^{-1}], with that of **BINAP•2(3PIC)** being the lowest.

For all three inclusion compounds, the guest desorps before its boiling point. The T_{on} - T_b values are given in **Table 5.8**. The difference between the guest release onset temperature T_{on} and its boiling point T_b is an indicator of the relative thermal stability of the inclusion compound, as suggested by Caira and Nassimbeni (1996). When $T_{on} > T_b$, for a group of similar inclusion compounds a large positive $T_{on} - T_b$ value implies the ability of the system to hold the guest more tightly and thus rendering the complex more stable. When $T_{on} < T_b$, an unstable compound yields a larger negative value of $T_{on} - T_b$. The $T_{on} - T_b$ value for **BINAP•2(3PIC)** is significant lower, suggesting its thermal stability is much lower than those of the other two inclusion compounds, of which $T_{on} - T_b$ values are similar.

In addition, the comparisons of the lattice energy and crystal packing efficiency show that **BINAP•2(3PIC)** is the least stable complex. These results are in good agreement with the selectivity trend, which shows that the 3-picoline is the least favoured isomer and the selectivity between 2-picoline and 4-picoline is dependent on concentration with the selectivity parameter $Q_{2PIC:4PIC} = 0.39$.

BINAP forms 1:2 host-guest compounds with 2,6 and 2,4-lutidine, while it forms a 1:1 complex with 3,5-lutidine. Both **BINAP•2(26LUT)** and **BINAP•2(24LUT)** crystallise in the same space group C2/c with Z = 4. In both structures, each host molecule, located on a diad, is hydrogen bonded to two guest molecules which are related via two fold symmetry, displaying (host)O-H···N(guest) hydrogen bonds with similar O···N distances

[2.815(5) - 2.826(3)Å]. The inclusion mode in each case is characterised by interconnected channels in which the guest molecules are located. The lattice energies for both structures are practically equal (-262.5 - -263.2 kJ mol^{-1}) and their crystal packing efficiencies are very close.

BINAP•35LUT crystallises in the space group P $\bar{1}$ with Z = 2. In this structure, each host molecule is hydrogen bonded to an adjacent host, forming a dimer about the centre of inversion, and in addition hydrogen bonded to a guest molecule. The 3,5-lutidine molecules are located in channels that running along [010]. On the basis of hydrogen bonding distances, the (host)O-H···N(guest) interaction with 3,5-lutidine is stronger [d(O···N) = 2.794(2)Å], compared with 2,6- and 2,4-derivetives, probably because of the increase of acidity of the hydroxyl group of the host due to the formation of (host)O-H···O(host) bond. But, the overall lattice potential energy of **BINAP•35LUT** is significantly higher, as a consequence of a fewer number of atom-pair interactions, arising from the different host:guest ratios of 1:1 *versus* 1:2. In fact, the different host:guest stoichiometry makes a comparison of the lattice energies invalid.

The desolvation of all three inclusion compounds are in a single step and their T_{on} - T_b (where $T_{on} < T_b$) values are in small range (34.2 - 44.2°C), with that of **BINAP•35LUT** being the highest. The desolvation reaction of **BINAP•2(26LUT)** and of **BINAP•2(24LUT)** followed a common kinetic mechanism - the contracting area geometric model (R2) and activation energies within a small range were obtained [80(4) - 92(3)kJ mol^{-1}]. The desolvation of **BINAP•35LUT** obeyed the Avrami-Efofe'ev A3 equation and yielded the relative higher activation energy [101(7)kJ mol^{-1}].

The results of competition experiments show that the 3,5-lutidine is less favoured by the host, whereas the selectivity between the other two isomers is concentration dependent with parameter $Q_{24LUT:35LUT}$ = 0.5, implying one of them is strongly favoured when its component is greater than 0.5 in mole ratio. The selectivity trend for 2,6-lutidine and 2,4-lutinde accords with the results obtained by analysing the crystal structure and thermal stability of their inclusion complexes with the host. However, as for 3,5-lutidine, its inclusion compound with the host, **BINAP•35LUT**, shows relatively high thermal and kinetic stabilities, which do not correspond to its selectivity trend. This disagreement is possible due to the difference in stoichiometry, yielding a diiferent structure made comparison invalid.

BINAP forms 1:1, 1:2 and 1:3 inclusion compounds with 3,5-, 2,6- and 2,3-xylidines respectively, all crystallised in different crystal systems with varying host-guest

interactions. For **BINAP•35X**, which crystallises in P $\bar{1}$, each host molecule is hydrogen bonded to one guest molecule via (host)O-H···N(guest) interaction with d(O···N) = 2.837(2)Å. The 3,5-xylidine molecules are located in channels running parallel to the direction [100]. For **BINAP•2(26X)**, which crystallises in C2/c with Z = 4, the host, located on a diad, is hydrogen bonded to two symmetry related guest molecules with (host)O-H···N(guest) interaction having O···N distance of 2.814(3)Å. The 2,6-xylidine molecules are located in channels that cross running along [110] and [1 $\bar{1}$0]. For **BINAP•3(23X)** which crystallises in Pbca with Z = 8, both (host)O-H···N(guest) and (guest)N-H···O(host) hydrogen bonds are present. In this structure, three crystallographically independent guest molecules are observed and two of them (guests A and B) act as double bridges linking host molecules chaining along [010], while the remaining one guest molecule (C) is not hydrogen bonded. All the guest molecules are located in interconnected channels. The host···guest hydrogen bond interactions in this structure are relatively strong with O···N distances of 2.735(5)Å and 2.767(5)Å. The IR spectra clearly indicated the existence and strength of hydrogen bonds in all of the three structures.

For these three inclusion compounds, single step desolvation is observed for each of them with guest desorption onset temperature $T_{on} < T_b$. The $T_{on} - T_b$ values vary widely, from –89.6°C through –103.1°C to –158.9°C, implying the thermal stability trend is as follows: **BINAP•35X** > **BINAP•2(26X)** > **BINAP•3(23X)**. The desolvation of **BINAP•35X** and of **BINAP•2(26X)** follow the deceleratory model R2 and the respective activation energies of 106(8) kJ mol^{-1} and 88(4) kJ mol^{-1} were obtained. The desolvation of **BINAP•3(23X)** follows the sigmoidal A2 mechanism and yielded an activation energy of 108(8) kJ mol^{-1}.

The competition experiments between 2,6- and 3,5-xylidine or between 2,6- and 2,3-xylidine show concentration dependent with selectivity parameters $Q_{26X:35X}$ = 0.29 and $Q_{26X:23X}$ = 0.13 respectively. The host did not discriminate between 3,5- and 2,3-xylidine, exhibiting null selectivity with the selectivity parameter $K_{35X:23X}$ = 1. It seems that none of the parameters given in **Table 5.7** gives an accurate indication of the host selectivity. Although there are many parameters that could be used to interpret the enclathration preference of the host towards different guests, the lattice potential energy appears the best. This may be because lattice energy calculations take account of all intermolecular interactions and measures all the strengths and directionality of intermolecular interactions which are responsible for the stability of a given host-guest compound. However, no calculations of lattice energy for these three inclusion

compounds were carried out, as comparison is invalid due to their differing stoichiometries.

Enclathration selectivity utilises the essential principle of molecular recognition. In general the degree of electronic and steric complementarity between host and guest dictate the magnitude of molecular recognition that occurs for a given supramolecular system. However, stoichiometry may also influence recognition behaviour (Lindoy & Atkinson, 2000). The prediction of the selectivity trend is still at its infancy, but one can try to understand it by studying the physicochemical properties of host-guest systems.

From all the crystal structures discussed in this chapter, we know that the guest molecules are located either in interconnected channels or in unique channels. There seems to be no severe physical barrier to guest loss, except for hydrogen bonding which stabilises the structures. Activation energies in the range from 82(6)kJ mol^{-1} to 108(8)kJ mol^{-1} were obtained for the desolvations of all the inclusion compounds discussed in this chapter. The results fall in the typical activation energy range of 60-150 kJ mol^{-1}, which has been observed for the channel type inclusion compounds (Nash, 1998).

Table 5.9 Crystal data, data collection and final refinement parameters.

Inclusion compound	**BINAP•2(2PIC)**	**BINAP•2(3PIC)**	**BINAP•2(4PIC)**
Molecular formula	$C_{20}H_{14}O_2 \bullet 2C_6H_7N$	$C_{20}H_{14}O_2 \bullet 2C_6H_7N$	$C_{20}H_{14}O_2 \bullet 2C_6H_7N$
Guest	2-Picoline	3-Picoline	4-Picoline
Formula weight ($gmol^{-1}$)	472.56	472.56	472.56
Crystal Data			
Crystal system	Monoclinic	Monoclinic	Orthorhombic
Space group	C2/c	$P2_1/c$	Pbca
a (Å)	18.274(3)	12.118(1)	18.119(3)
b (Å)	9.887(2)	13.261(1)	10.812(2)
c (Å)	14.021(2)	16.581(1)	25.665(5)
α (°)	90	90	90
β (°)	90.41(3)	103.448(2)	90
γ (°)	90	90	90
Volume ($Å^3$)	2533.2(8)	2591.5(3)	5027.8(2)
Z	4	4	8
Calculated density D_c (gcm^{-3})	1.239	1.211	1.249
μ (mm^{-1})	0.077	0.076	0.078
F(000)	1000	1000	1000
Data collection			
Temperature (K)	173 (2)	173 (2)	173 (2)
Range scanned, θ (°)	2.23 - 26.41	2.71 - 26.36	2.25 - 25.40
Range of indices, *h*, *k*, *l*	-22,21/-12,0/±17	-14,15/±16/-16,19	-20,19/-9,11/-26,28
No. of measured reflections	4593	13104	17012
No. of unique reflections	2461	4286	4135
No. of reflections observed with $I > 2\sigma(I)$	1727	3380	2669
R_{int}	0.0238	0.0342	0.0531
Structure refinement			
Data / restraints / parameters	2461 / 2 / 165	4826 / 4 / 335	4135 / 4 / 334
R indices R_1 / wR_2 [$I > 2\sigma(I)$]	0.0415 / 0.0989	0.0410 / 0.0925	0.0430 / 0.0958
R_1 / wR_2 (all data)	0.0693 / 0.1105	0.0860 / 0.1056	0.0860 / 0.1126
Goodness of fit on F^2, S	1.035	1.021	1.027
Weighting scheme [where $P = (F_o^2+2F_c^2)/3$]	$w = 1/[\sigma^2(F_o^2)+(0.0531P)^2+0.6403P]$	$w = 1/[\sigma^2(F_o^2)+(0.0463P)^2+0.4283P]$	$w = 1/[\sigma^2(F_o^2)+(0.0564P)^2+0.3890P]$
Max. / Mean shift (esd)	0.048 / 0.000	0.000 / 0.000	0.001 / 0.000
Extinction coefficient	0.0035(6)	0.0100(9)	0.0027(4)
Max./Min. height in difference electron density map ($eÅ^{-3}$)	0.170 / -0.173	0.175 / -0.152	0.172 / -0.167

Table 5.9 (cont.) Crystal data, data collection and final refinement parameters.

Inclusion compound	**BINAP•2(26LUT)**	**BINAP•2(24LUT)**	**BINAP•35LUT**
Molecular formula	$C_{20}H_{14}O_2 \bullet 2C_7H_9N$	$C_{20}H_{14}O_2 \bullet 2C_7H_9N$	$C_{20}H_{14}O_2 \bullet C_7H_9N$
Guest	2,6-Lutidine	2,4-Lutidine	3,5-Lutidine
Formula weight ($gmol^{-1}$)	500.62	500.62	393.46
Crystal Data			
Crystal system	Monoclinic	Monoclinic	Triclinic
Space group	C2/c	C2/c	$P\bar{1}$
a (Å)	14.656(7)	15.12(2)	10.341(1)
b (Å)	10.703(2)	10.76(1)	10.511(1)
c (Å)	18.365(5)	18.19(5)	11.868(1)
α (°)	90	90	103.651(5)
β (°)	109.84(3)	110.9(1)	113.502(2)
γ (°)	90	90	102.496(5)
Volume ($Å^3$)	2710(2)	2764(9)	1077.6(2)
Z	4	4	2
Calculated density D_c (gcm^{-3})	1.227	1.203	1.213
μ (mm^{-1})	0.076	0.075	0.076
F(000)	1064	1064	416
Data collection			
Temperature (K)	293 (2)	173 (2)	293 (2)
Range scanned, θ (°)	2.36 - 24.95	2.88 - 27.27	2.01 – 26.31
Range of indices, *h*, *k*, *l*	0,17/±12/-21,20	-11,17/-9,13/-19,16	±12/±9/-14,10
No. of measured reflections	11871	13552	4660
No. of unique reflections	2376	2665	3479
No. of reflections observed with $I > 2\sigma(I)$	937	1719	2186
R_{int}	0.072	0.031	0.021
Structure refinement			
Data / restraints / parameters	2376 / 2 / 178	2665 / 2 / 177	3479 / 4 / 282
R indices R_1 / wR_2 [$I > 2\sigma(I)$]	0.0540 / 0.1097	0.0472 / 0.1072	0.0515 / 0.1039
R_1 / wR_2 (all data)	0.2208 / 0.1771	0.0892 / 0.1220	0.0972 /
Goodness of fit on F^2, *S*	1.083	1.037	1.024
Weighting scheme	$w = 1/[\sigma^2(F_o^2)+$	$w = 1/[\sigma^2(F_o^2)+$	$w = 1/[\sigma^2(F_o^2)+$
[where $P = (F_o^2+2F_c^2)/3$]	$(0.0359P)^2+4.2223P]$	$(0.0568P)^2+0.4666P]$	$(0.0401P)^2+0.3473P]$
Max. / Mean shift (esd)	0.000 / 0.000	0.000 / 0.000	0.001 / 0.000
Extinction coefficient	0.0032(5)	0.0035(6)	0.018(2)
Max./Min. height in difference electron density map ($eÅ^{-3}$)	0.255 / -0.222	0.200 / -0.161	0.171 / -0.155

Table 5.9 (cont.) Crystal data, data collection and final refinement parameters

Inclusion compound	**BINAP•35X**	**BINAP•2(26X)**	**BINAP•3(23X)**
Molecular formula	$C_{20}H_{14}O_2 \bullet C_8H_{11}N$	$C_{20}H_{14}O_2 \bullet 2C_8H_{11}N$	$C_{20}H_{14}O_2 \bullet 3C_8H_{11}N$
Guest	3,5-Xylidine	2,6-Xylidine	2,3-Xylidine
Formula weight ($gmol^{-1}$)	407.49	528.67	649.85
Crystal Data			
Crystal system	Triclinic	Monoclinic	Orthorhombic
Space group	$P\bar{1}$	C2/c	Pbca
a (Å)	8.907(2)	26.066(2)	22.634(1)
b (Å)	8.956(3)	10.068(2)	10.464(1)
c (Å)	13.887(2)	11.868(2)	30.689(1)
α (°)	98.68(2)	90	90
β (°)	98.45(1)	109.11(5)	90
γ (°)	94.26(2)	90	90
Volume ($Å^3$)	1077.9(5)	2943.0(8)	7268.4(8)
Z	2	4	8
Calculated density D_c (gcm^{-3})	1.255	1.193	1.188
μ (mm^{-1})	0.078	0.073	0.073
F(000)	432	1128	2784
Data collection			
Temperature (K)	253 (2)	293 (2)	173 (2)
Range scanned, θ (°)	2.31 - 24.97	1.65 - 24.97	1.60 - 24.66
Range of indices, *h*, *k*, *l*	±10/±10/0,16	-30,11/±11/-13,14	-19,26/-9,11/-33,36
No. of measured reflections	12101	8926	24311
No. of unique reflections	3787	2574	5926
No. of reflections observed with $I > 2\sigma(I)$	2615	1791	3329
R_{int}	0.0243	0.0259	0.0721
Structure refinement			
Data / restraints / parameters	3785 / 5 / 299	2574 / 2 / 188	5922 / 18 / 447
R indices R_1 / wR_2 [$I > 2\sigma(I)$]	0.0401 / 0.1096	0.0662 / 0.1960	0.0926 / 0.2539
R_1 / wR_2 (all data)	0.0740 / 0.1237	0.1006 / 0.2198	0.1879 / 0.3103
Goodness of fit on F^2, *S*	1.034	1.068	1.044
Weighting scheme [where $P = (F_o^2+2F_c^2)/3$]	$w = 1/[\sigma^2(F_o^2)+(0.0611P)^2+0.1463P]$	$w = 1/[\sigma^2(F_o^2)+(0.1232P)^2+2.1800P]$	$w = 1/[\sigma^2(F_o^2)+(0.1501P)^2+7.4380P]$
Max. / Mean shift (esd)	0.000 / 0.000	0.000 / 0.000	0.023 / 0.000
Extinction coefficient	0.020(3)	0.001(1)	0.0012(5)
Max./Min. height in difference electron density map ($eÅ^{-3}$)	0.180 / -0.166	0.602 / -0.256	0.968 / -0.411

6 INCLUSION COMPOUNDS OF BINAP WITH VOLATILE GUESTS

In this chapter, the inclusion compounds, formed between the host **BINAP** and 1,4-dioxane(**DOX**), dimethyl sulfoxide (**DMSO**), morpholine(**MOP**), tetrahydrofuran (**THF**) and acetone (**ACT**), are studied. The crystal structure of the host alone (**BINAP**) is elucidated. For ease of reference, the atomic numbering scheme of the host is again shown in **Scheme 6.1**, together with the numbering schemes of guests.

For all of the structures discussed in this chapter, the crystal data, data collection, experimental and final refinement parameters are contained in **Table 6.5** appearing at the end of this chapter. Final fractional atomic co-ordinates, temperature factors, table of bond length and angles, torsion angles and table of observed and calculated structure factors are contained in **Appendices**.

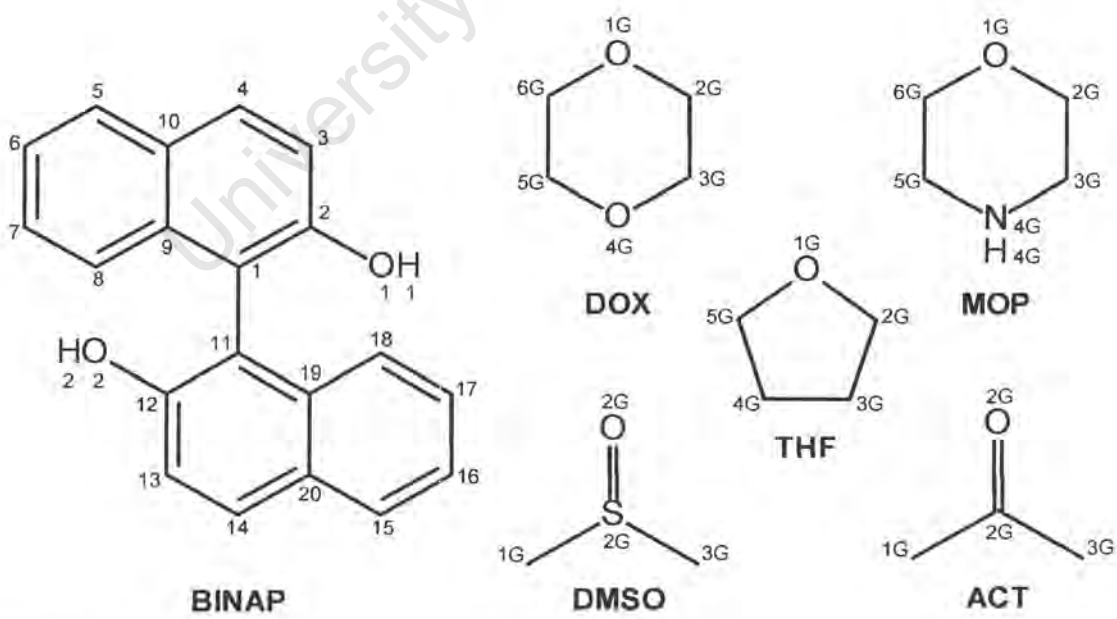

Scheme 6.1

Preparation of the inclusion compounds

In preparation of each inclusion compound, the host **BINAP** was dissolved in excess amount of guest solvent by gentle warming and the solution was maintained at a certain temperature to allow crystals to form by slow evaporation. The host with each guest solvent has been crystallised at three different temperatures: 4°C and 60°C, which were controlled to about ±1°C, and at room temperature (~25°C). Single crystals, which appeared within periods between 24 hours and 7 days, were first subjected to TG analysis to determine the host:guest ratio. The host formed inclusion compounds with different host:guest ratios with 1,4-dioxane (1:1.5 and 1:3.5) and with dimethyl sulfoxide (1:1 and 1:2), at different crystallisation temperatures. An inclusion compound of constant stoichiometry was obtained at different temperatures in the cases of morpholine, acetone and tetrahydrofuran as guests. The inclusion compounds and the crystallisation temperatures at which single crystals were obtained are listed as follows:

BINAP and 1,4-dioxane (**DOX**):	**BINAP•1.5DOX**	(60°C)
	BINAP•3.5DOX	(4°C / 25°C)
BINAP and dimethyl sulfoxide (**DMSO**):	**BINAP•DMSO**	(60°C)
	BINAP•2DMSO	(4°C / 25°C)
BINAP and morpholine (**MOP**):	**BINAP•1.5MOP(I)**	(60°C)
BINAP and morpholine (**MOP**):	**BINAP•1.5MOP(II)**	(4°C)
BINAP and tetrahydrofuran (**THF**):	**BINAP•1.5THF**	(4°C / 25°C / 60°C)
BINAP and acetone (**ACT**):	**BINAP•ACT**	(4°C / 25°C / 60°C)

Two polymorphic forms of the inclusion compound **BINAP•1.5MOP** were obtained. The crystals of form **I** were obtained at 60°C, while the crystals of form **II** were obtained at 4°C. It was very difficult to crystallise an inclusion complex with morpholine, especially at elevated temperature. Attempts to reproduce crystals of both the forms **I** and **II** at respective temperatures failed - the solution always yielded an oily, brown residue. Therefore powder samples were prepared by evaporation of a continuously stirred solution of **BINAP** and morpholine at room temperature (~25°C). The powder was subjected to XRD analysis and kinetics study using isothermal TG.

The guest-free host **BINAP** was crystallised from the solvent propionaldehyde after trying many other solvents.

Thermal analysis

For each inclusion compound, the TG and DSC analyses were generally carried out on powder samples at a constant heating rate of 10°C min^{-1} over a temperature range of 30°C to 230°C. The samples were prepared by crushing single crystals. The results are shown in combined TG/DSC diagrams for each inclusion compound, followed by a brief description. The relevant thermal data are summarised in **Table 6.1**.

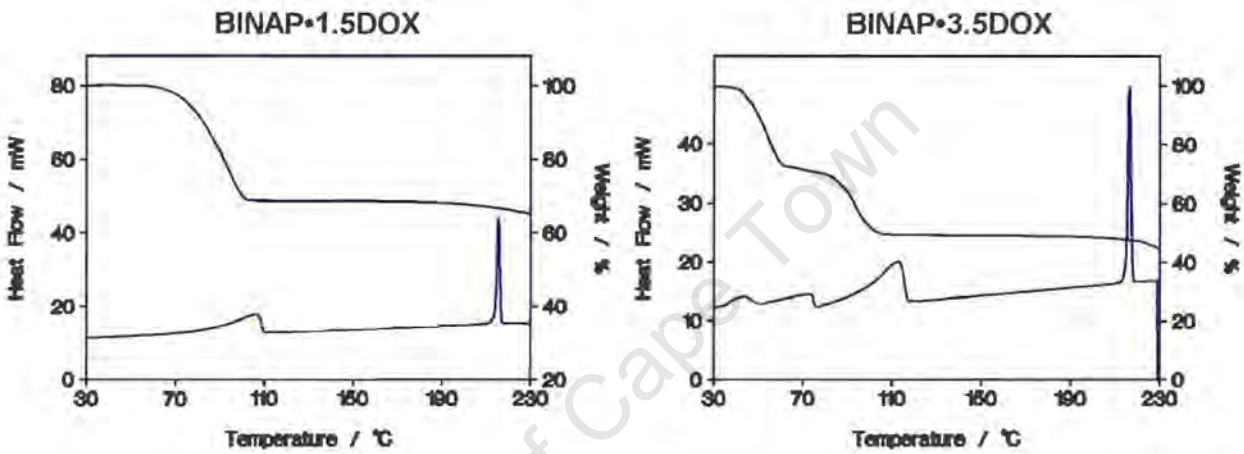

The TG/DSC traces for **BINAP•1.5DOX** show a single mass loss for desolvation, corresponding to a concomitant endotherm peaking at 106.0°C with onset temperature of 83.6°C, followed by the melting endotherm at 215.8°C. The mass loss step of 31.2% corresponds to the loss of one and half moles of 1,4-dioxane (calc. 31.58%), confirming a host:guest ratio of 1:1.5.

The TG trace for the desorption of **BINAP•3.5DOX** indicates two distinct mass loss steps. The first step, occurring between 40°C and 75°C, corresponds to the loss of two molecules of guest dioxane (calc. 29.63%, obs. 28.6%). This is followed by the second step, which corresponds to the loss of the remaining 1.5 dioxanes (calc. 22.22%, obs. 22.3%). The DSC curve is more complex, yielding the first two endotherms for the first step and a larger endotherm for the second step. These have peaks at 42.8°C, 73.2°C and 112.1°C. The final sharp endotherm at 216.2°C corresponds to the melting of the apohost.

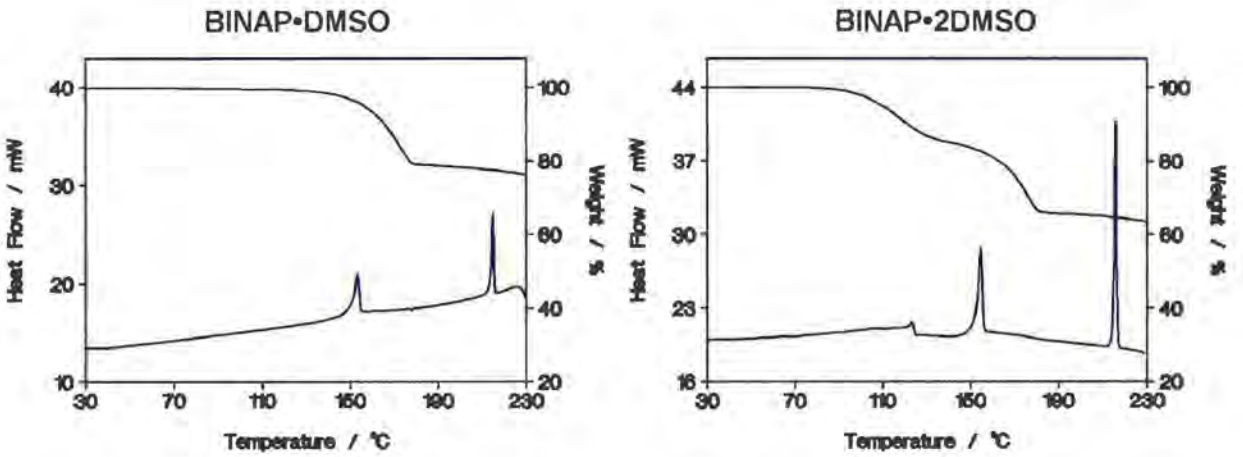

The TG/DSC traces for **BINAP•DMSO** show a single mass loss step of 20.9%, confirming the host:guest ratio of 1:1 (calc. 21.44%), corresponding to a single sharp endotherm with an onset temperature of 153.2°C, followed by the melt at 215.7°C.

The TG run for **BINAP•2DMSO** yielded two mass loss steps, showing similar features to the case of **BINAP•3.5DOX**. The two steps correspond to the loss of one mole of **DMSO** (calc. 17.65%, obs. 15.9%), followed by the loss of the remaining guest (calc. 17.66%, obs. 18.9%). The DSC run yielded two endotherms, with onset temperatures of 120.6°C and 153.8°C, corresponding to the two mass loss steps observed in the TG. The last endotherm at 216.1°C corresponds to the melt of the host.

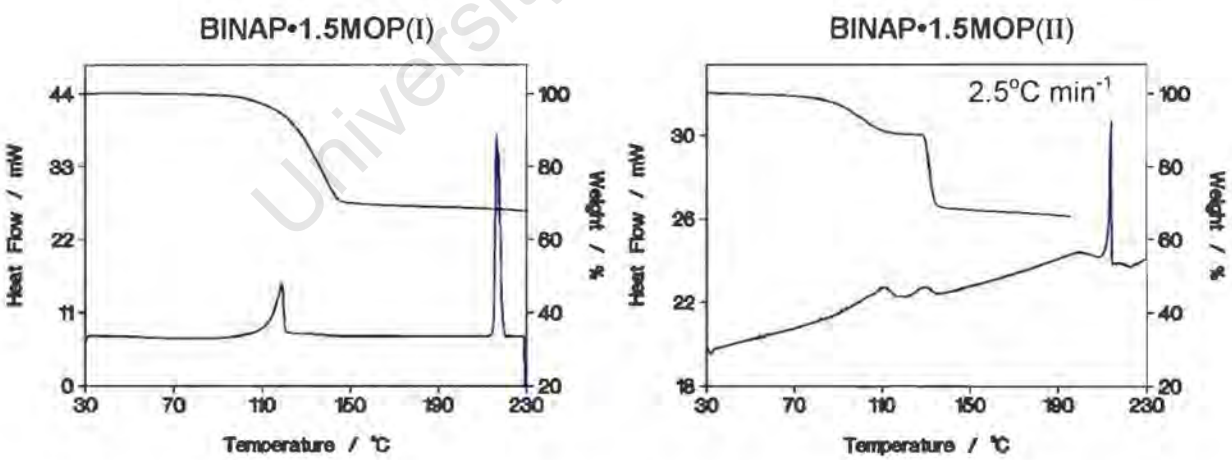

The TG/DSC traces for the form I of **BINAP•1.5MOP** show a single endothermic mass loss step of 30.5% (calc. 31.34%) with an onset temperature of 108.3°C. The desorption is followed by the melt of the host at 216.4°C. The desolvation of the form II proceeds in two diffuse steps at the standard heating rate of 10°C min^{-1}. When the heating rate was decreased to 2.5°C min^{-1}, the TG result yielded two well defined mass loss steps and the DSC trace at the same heating rate yielded two diffuse peaks

associated with the guest loss processes and one sharp endotherm due to the melt of the host. Only the TG and DSC traces at the lower heating rate are shown here. The two mass loss steps correspond to the first loss of 1/2 guest molecule (calc. 10.45%, obs. 10.8%), followed by the loss of the remaining one guest molecule (calc. 20.89%, obs. 20.6%). The two diffuse endotherms peak at 111.7°C and 130.6°C.

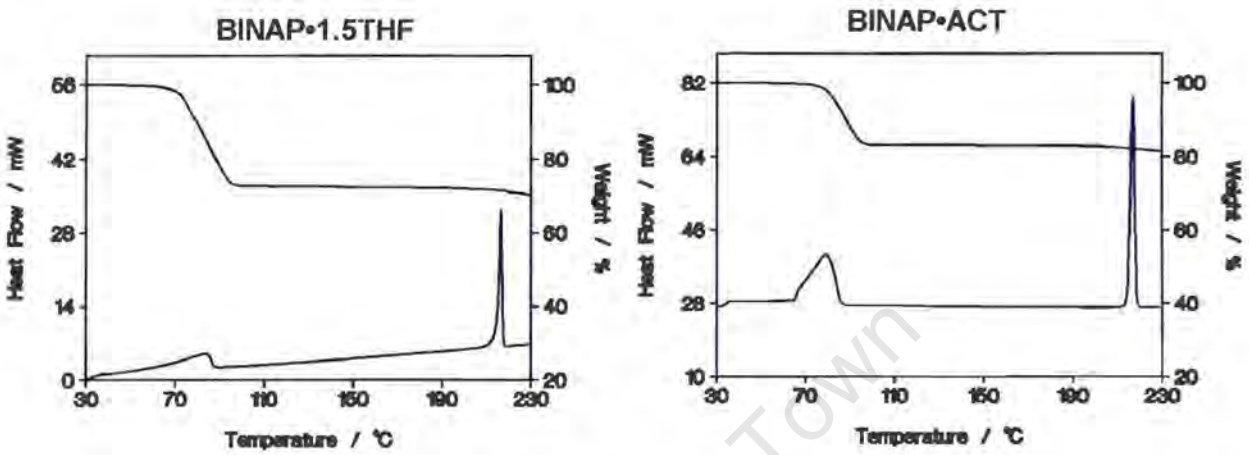

The desolvation of **BINAP•1.5THF** and of **BINAP•ACT** behaved in a similar pattern, with the TG exhibiting a single mass loss and with the DSC yielding the corresponding one endotherm to the guest release, followed by the host melt. The thermal data are shown in **Table 6.1**, together with those of all other inclusion compounds.

Table 6.1 Relevant thermal TG/DSC data for all the inclusion compounds.

Inclusion Compounds	Observed weight loss from TG (%)	Calculated weight loss (%)	Guest release T_{on} (°C)	$T_{on} - T_b$ (°C)	Host melt (°C)
BINAP•1.5DOX	20.9	21.44	83.6	-17.5	215.8
BINAP•3.5DOX	1st step 15.9	17.65	42.8, 73.2*	-	216.2
	2nd step 18.9	17.66	112.1*	-	
BINAP•DMSO	20.9	21.44	153.2	-35.8	215.7
BINAP•2DMSO	1st step 15.9	17.65	120.6	-	216.1
	2nd step 18.9	17.66	153.8	-	
BINAP•1.5MOP(I)	30.5	31.34	108.3	-20.6	216.4
BINAP•1.5MOP(II)	1st step 10.8	10.45	111.7*	-	215.7
	2nd step 20.6	20.89	130.6*	-	
BINAP•1.5THF	27.3	27.42	74.1	8.1	215.3
BINAP•ACT	16.6	16.86	65.6	9.1	216.0

* Peak temperatures, not onset temperatures.

Crystal structures

BINAP•3.5DOX belongs to the triclinic crystal system ($\bar{1}$ Laue symmetry) and was assigned the space group P $\bar{1}$, rather than P1, based on the reflection intensity statistics (mean $|E^2-1|$ value for the general *hkl* reflections = 1.036).

The crystal structures of **BINAP•1.5DOX**, **BINAP•DMSO**, **BINAP•2DMSO**, **BINAP•1.5MOP**(I), **BINAP•1.5MOP**(II) and **BINAP•ACT** belong to monoclinic crystal system (2/m Laue symmetry). Based on the non-extinction reflection conditions observed from their crystal reflection data, the structures of **BINAP•1.5DOX**, **BINAP•2DMSO,** as well as the both forms of **BINAP•1.5MOP** were assigned the space group $P2_1/c$, while the others were assigned the space group $P2_1/n$. The two space group are equivalent to each other, but refer to a different cell choice which results in the *c*-glide plane in $P2_1/c$ being converted into an *n*-glide plane in $P2_1/n$. The space group of **BINAP•1.5MOP**(II) was later transformed from $P2_1/c$ into $P2_1/n$, so that its unit cell dimensions correspond with those of the form I for comparison purpose.

Both **BINAP•1.5THF** and **BINAP** structures belong to the orthorhombic crystal system (mmm Laue symmetry). The reflection data of **BINAP•1.5THF** exhibit the following non-extinction conditions:

hkl: $h + k = 2n$, $h + l = 2n$, $k + l = 2n$
0kl: ($k + l = 2n$, $k = 2n$, $l = 2n$)
h0l: ($h + l = 2n$, $h = 2n$, $l = 2n$)
hk0: ($h = 2n$, $k = 2n$)

suggesting the non-centrosymmetric space group Fdd2. This is confirmed by the mean $|E^2-1|$ value of 0.803 for general *hkl* reflections. Whereas the reflection data of **BINAP** exhibit

hkl: $h + k + l = 2n$
0kl: $k = 2n$, $l = 2n$
h0l: $h = 2n$, $l = 2n$
hk0: ($h + k = 2n$)

conditions, implying that the space group was either Ibam or Iba2. Inspection of the intensity statistics (mean $|E^2-1|$ values for 0kl, 0.678; h0l, 0.781; hk0, 1.052, and 0.804 for the general *hkl* reflections) revealed that the space group was non-centric, hence Iba2 was assumed to be the correct choice. The choice of the space group for each compound is vindicated by the successful final refinement of the structure.

All the structures were solved by direct methods, which yielded the non-hydrogen atoms in the asymmetric unit. In most cases, the O atoms on the host and guest molecules were placed at the locations of the highest peaks. In the case of structures of **BINAP** and morpholine, the electron densities at the possible positions of the O and N atoms were almost equal. In such case the O atoms were placed within hydrogen bonding distance with respect to the hydroxyl O atoms of the host molecules.

The crystal structure for each inclusion compound is discussed in terms of refinement and structure analysis. The molecular formula, host:guest ratio, space group, cell parameters and other crystallographic information are summarised at the beginning of the discussion of each structure. This is followed by a brief description of the structure refinement and then by a description of molecular structure and crystal packing. The host conformation data obtained from all the structure solutions in this part will be discussed in more detail collectively in **Chapter 7**. The crystal data and final refinement parameters are contained in **Table 6.5**, appearing at the end of this chapter.

For the apohost **BINAP**, its crystal structure in the space group Iba2 has been elucidated previously and appeared in several reports (Gridunova *et al.* 1982; Mori *et al.* 1993; Toda *et al.* 1997; Nieger, 1999). The latter solved the structure at low-temperature with R factor of 4.34%. It was again solved and refined at low temperature in this study, and the results are present in this chapter, because the structure was refined to a slightly lower R factor and the result is relevant to the studies of the inclusion compounds containing this host.

BINAP•1.5DIOX

$C_{20}H_{14}O_2 \bullet 1.5C_4H_8O_2$	
Guest: 1,4-Dioxane	
Space group: $P2_1/c$	
a = 8.938(1) Å	$\alpha = 90^\circ$
b = 28.013(2) Å	$\beta = 110.213(5)^\circ$
c = 9.137(1) Å	$\gamma = 90^\circ$
Volume = 2146.8(4) Å^3	
Z = 4	

Refinement

BINAP•1.5DIOX crystallises in $P2_1/c$. Determination of the unit cell volume suggested four host-guest assemblies per unit cell. Since the host:guest ratio is 1:1.5, the space group requires one dioxane guest molecule to be located on special position about a centre of inversion, at Wyckoff position *d* [(½,0,½) or (½,½,0)]. Therefore the asymmetric unit contains one host molecule and one and half guest molecules. All the non-hydrogen atoms were refined with anisotropic temperature factors. The hydroxyl hydrogen atoms on the host molecule, which were located in difference electron density maps, were refined with simple bond length constraints according to a function of O-H versus O···O distances (Schuster *et al.* 1976). The rest of hydrogen atoms were placed in geometrically constrained positions and refined with isotropic temperature factors 1.2 x U_{eq} of their parent atoms. The guest molecule B, located in general position, exhibits relatively high thermal motions, especially the O4GA atom (U_{eq} = 0.168Å^2). A residual electron density of 0.80eÅ^{-3} was observed close to O(4GA), but could not be sensibly modelled. The structure refined successfully to R_1 = 0.0764.

Structure analysis

The host-guest arrangement, consisting of two host molecules and three guest molecules is shown in **Figure 6.1**. Each host molecule is hydrogen bonded to a single dioxane (A), via O(2)–H(2)···O(1GA) with d(O···O) = 2.676(3)Å, and a second dioxane (B), located on a centre of inversion, links two host molecules, via two hydrogen bonds O(1)–H(1)···O(1GB), related by the centre of symmetry, with d(O···O) = 2.760(3)Å. The hydrogen bonding details for this structure and other structures discussed in this chapter, are given in **Table 6.2**, appearing at the end of the 'Crystal Structures' section. The guest molecules lie in channels running in the [011] and [01 $\bar{1}$] directions, with both centred at a = 1/2. The guest channels are depicted in **Figure 6.2**. The crystal packing, viewed down [100] and [001], is shown in **Figure 6.3**.

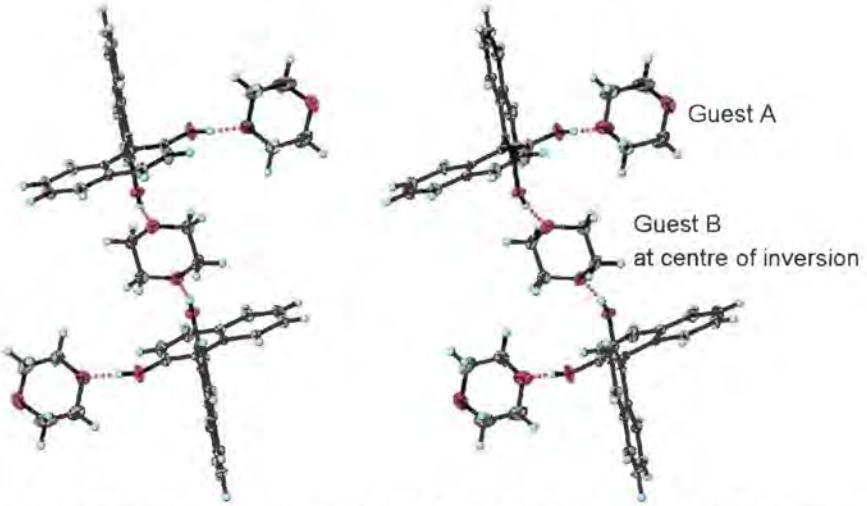

Figure 6.1 Molecular structure of **BINAP•1.5DOX**. Displacement ellipsoids are drawn at the 40% probability level.

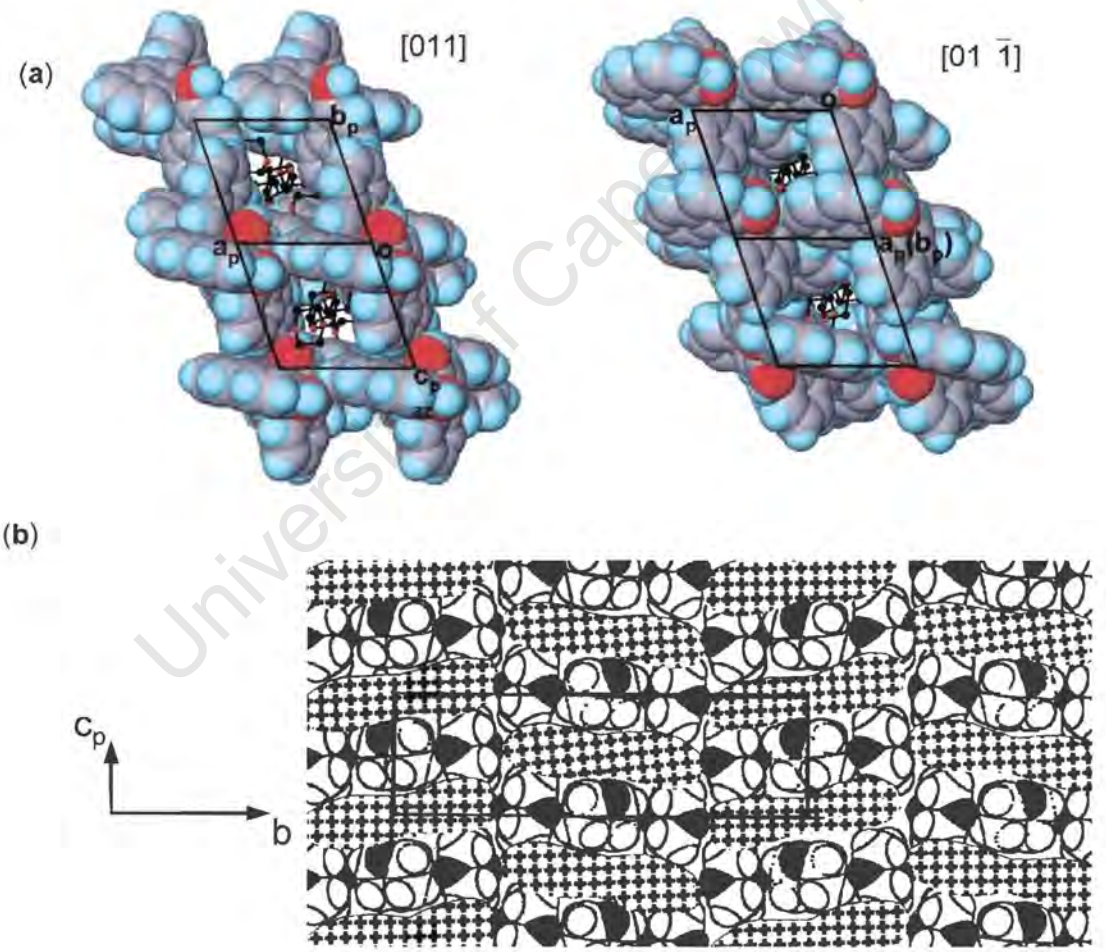

Figure 6.2 (a) Space-filling diagram for **BINAP•1.5DOX**, viewed from the top of the open channels. The host atoms are shown with van der Waals radii and guest molecules shown as balls and sticks with all H atoms omitted.
(b) Cross section cut at a = 0.5 showing the two cross running channels along [011] and [01 $\bar{1}$]. The diagonally crossed areas represent the space occupied by the host. The guests are shown in van der Waals radii with oxygen atoms shaded.

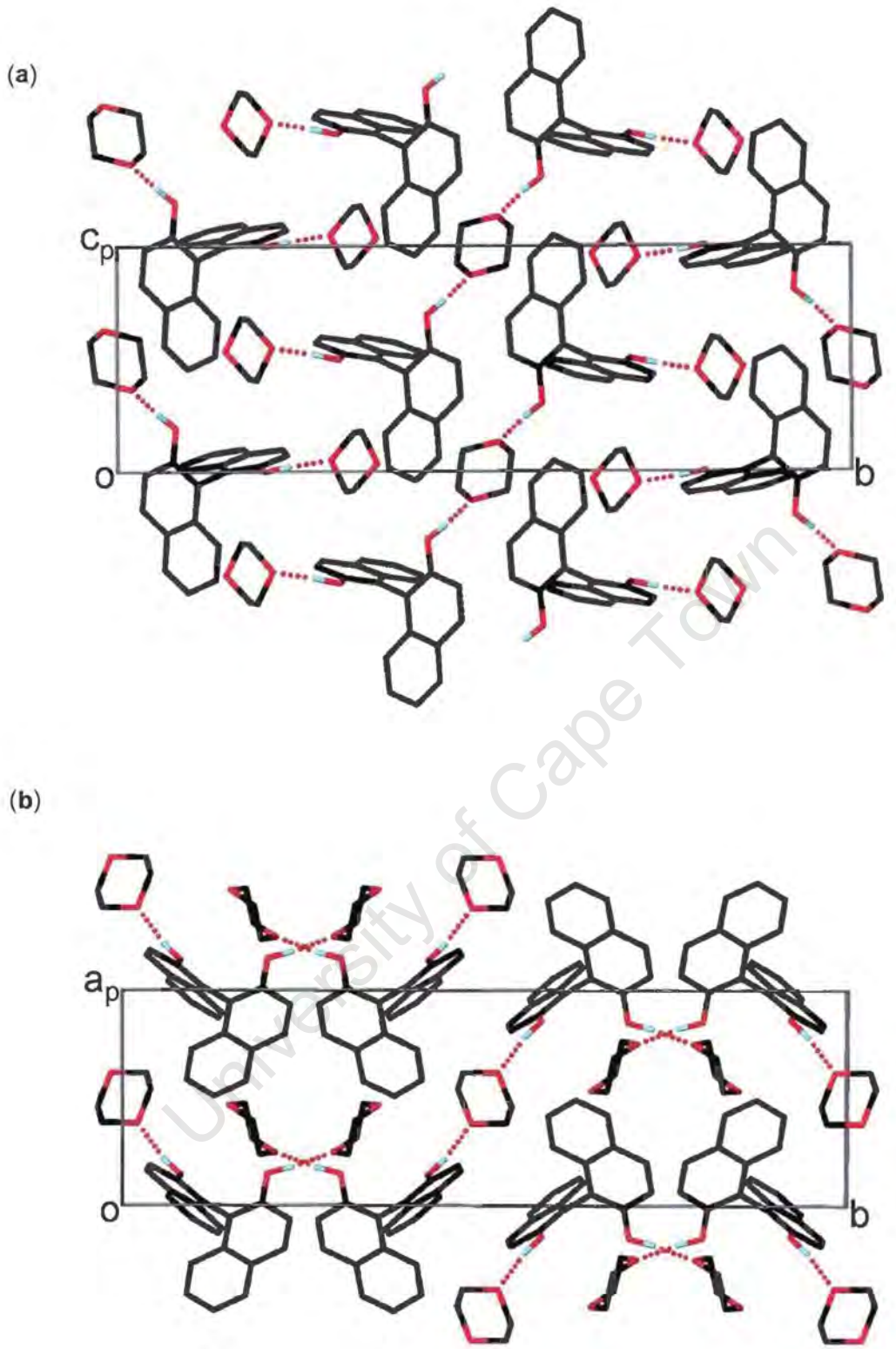

Figure 6.3 Projections of crystal packing in **BINAP•1.5DOX**, viewed down (a) [100], (b) [001] respectively. All of the H atoms are omitted except the hydroxyl hydrogen atoms of the host. The H-bonds are shown as dotted lines.

BINAP•3.5(DIOX)

$C_{20}H_{14}O_2 \cdot 3.5C_4H_8O_2$	
Guest: 1,4-Dioxane	
Space group: P $\bar{1}$	
a = 10.322(1) Å	α = 111.651(3)°
b = 12.023(1) Å	β = 91.955(3)°
c = 13.432(1) Å	γ = 90.716(3)°
Volume = 1547.9(2) Å^3	
Z = 2	

Refinement

BINAP•3.5DOX crystallises in P $\bar{1}$ with Z = 2. One host molecule and three dioxane guest molecules (A, B and C) were located in general positions in the asymmetric unit, while one guest dioxane (D) lies at a centre of inversion, at Wyckoff position *f* (½,0,½), thus yielding a host:guest ratio of 1:3.5, which was confirmed by the TG analysis. Refinement was carried out with all the non-hydrogen atoms of both the host and guest molecules treated anisotropically. The hydroxyl hydrogen atoms on the host were located in difference density maps and refined with bond length constraints according to the hydrogen bonding O···O distance and their own temperature factors. The rest of the hydrogen atoms on the host and guest molecules were geometrically constrained and refined with isotropic temperature factors 1.2 x U_{eq} of their parent atoms. The structure refined successfully to R_1 = 0.0464.

Structure analysis

The host-guest arrangement, consisting of one host molecule and four crystallographically independent guest molecules is shown in **Figure 6.4**. Only two of the dioxane guests, A and B, are hydrogen bonded to the two hydroxyl groups of the host molecule [O(1)-H(1)···O(1GB) and O(2)-H(2)···O(1GA) with the O···O distances of 2.685(2)Å and 2.679(2)Å respectively] (details see **Table 6.2**). The crystal packing, viewed down [100] and [010], is shown in **Figure 6.5**. In the structure, the host molecules pack in such a way that form a number of channels running along [100], [010], [001], [011] and [111] directions respectively. These channels, in which the guest molecules reside, are interconnected with each other. Two channels which running parallel to [011] and [111] are illustrated in **Figure 6.6**, as examples.

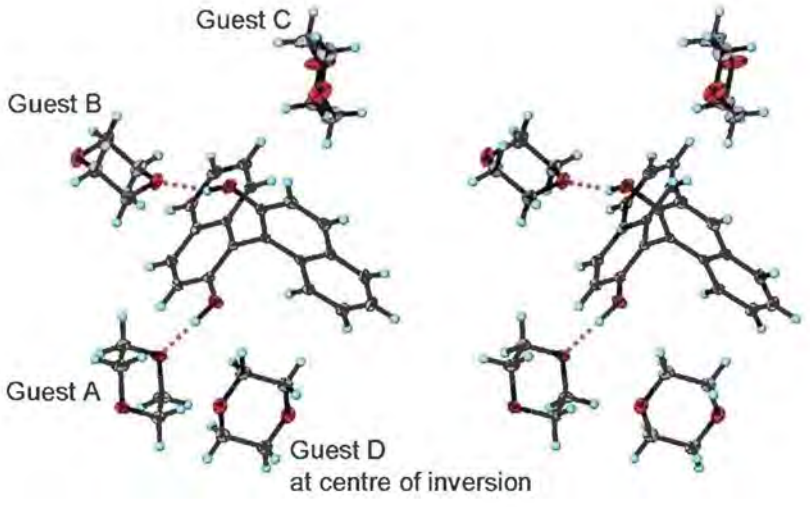

Figure 6.4 Molecular structure of **BINAP•3.5DOX**. Displacement ellipsoids are drawn at the 45% probability level.

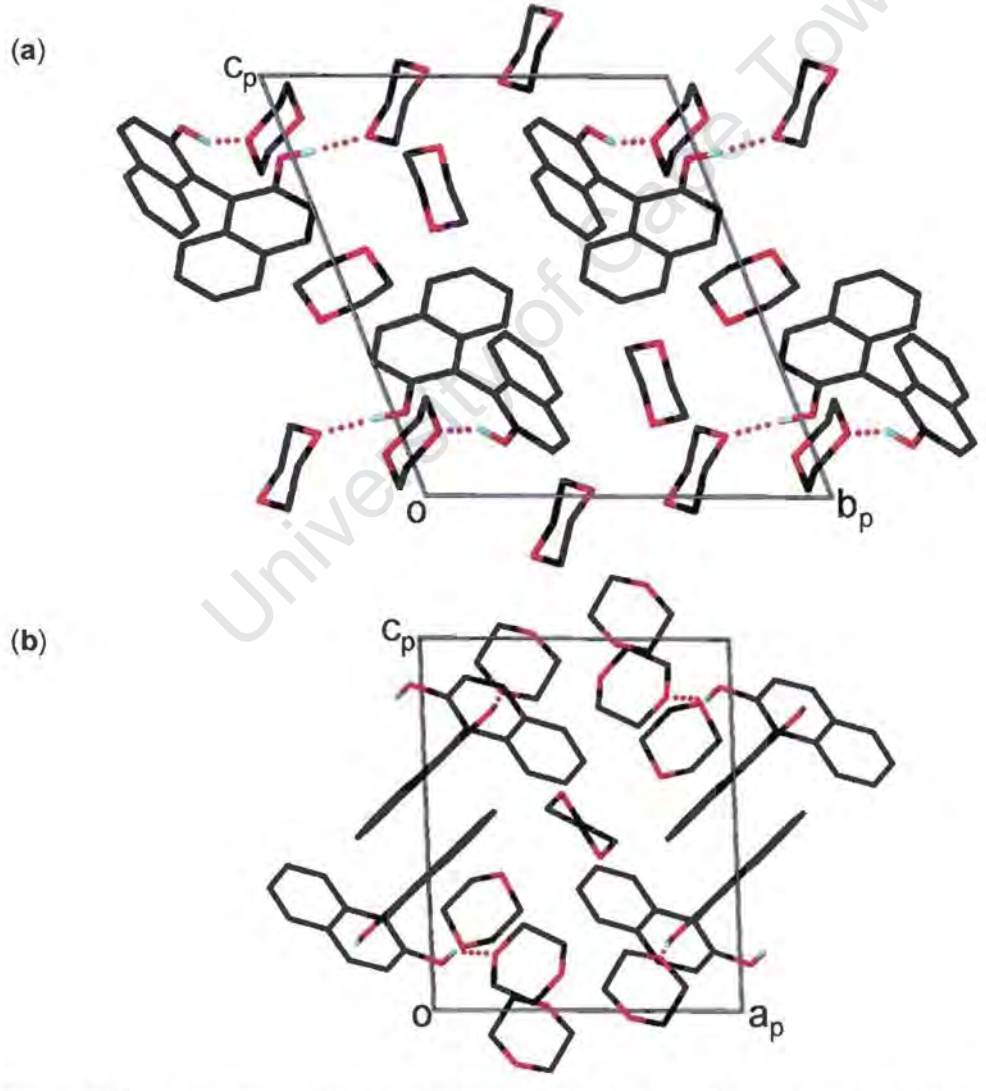

Figure 6.5 Projections along (a) [100], (b) [010], showing the crystal packing in **BINAP•3.5DOX**. All of the H atoms are omitted except the hydroxyl hydrogen atoms of the host. The H-bonds are shown as dotted lines.

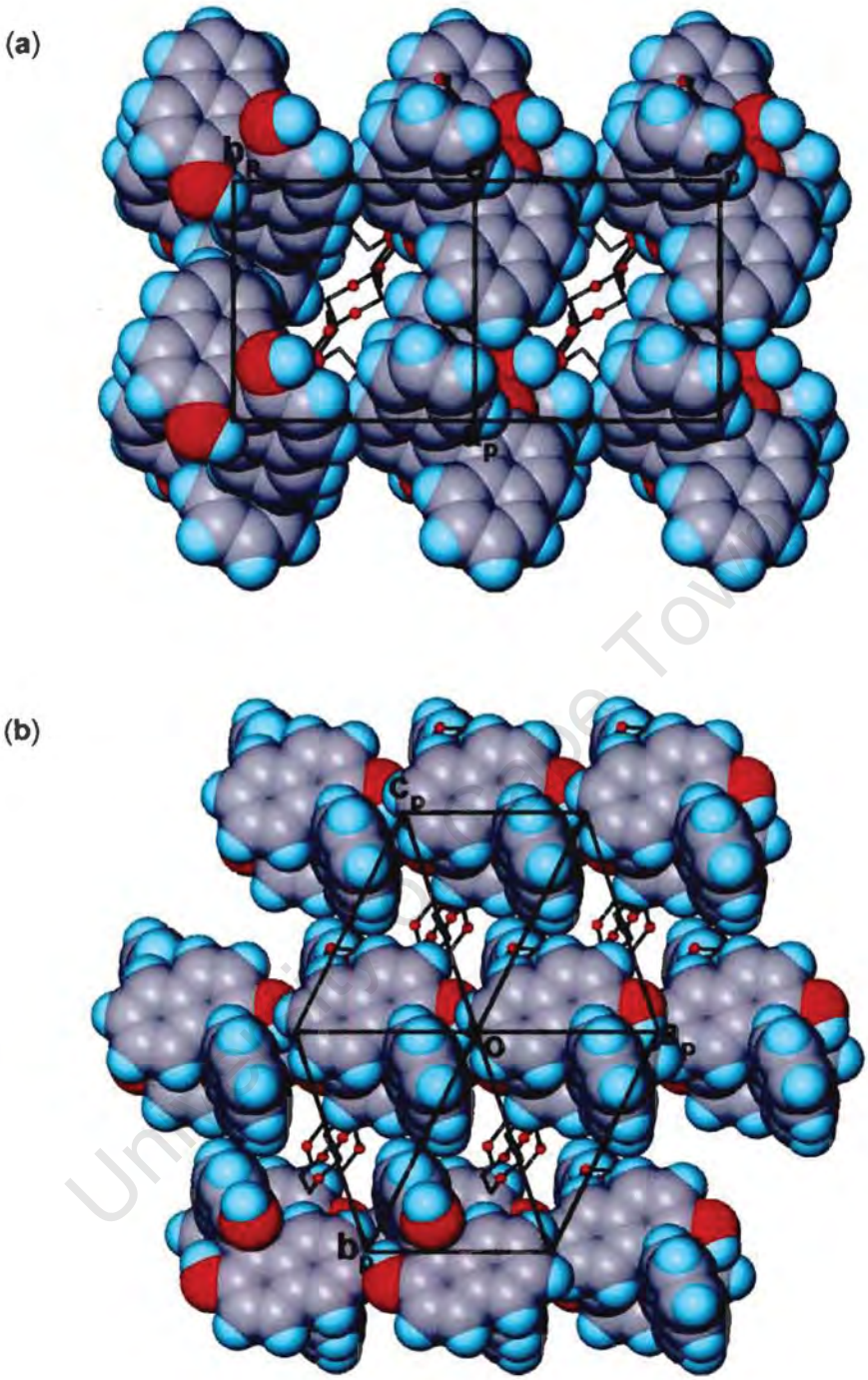

Figure 6.6 Space-filling diagrams for **BINAP•3.5DOX**, viewed down (a) [011] and (b) [111], showing the open channels. The host atoms are shown with van der Waals radii and guest molecules shown as sticks with O atoms highlighted. All of the hydrogen atoms on the guest are omitted.

BINAP•DMSO

$C_{20}H_{14}O_2 \bullet C_2H_6OS$	
Guest: Dimethyl sulfoxide	
Space group: $P2_1/n$	
a = 20.792(3) Å	$\alpha = 90^\circ$
b = 8.883(1) Å	$\beta = 105.115(5)^\circ$
c = 20.800(3) Å	$\gamma = 90^\circ$
Volume = 3708.8(9) $Å^3$	
Z = 8	

Refinement

BINAP•DMSO crystallises in $P2_1/n$ with Z = 8. The asymmetric unit consists of two host molecules (X and Y) and two DMSO guest molecules (A and B), all located in general positions as required by the space group symmetry. All non-hydrogen atoms were refined anisotropically. The hydroxyl hydrogen atoms were located in the difference electron density maps and refined with bond length constraints and individual temperature factors. The rest of the hydrogen atoms were placed with geometric constraints and the isotropic temperature factors were constrained at 120% and 150% that of the parent atoms for the aromatic and the methyl hydrogens respectively. A residual electron density of 0.98e$Å^{-3}$ was observed in the region of the host and could not be modelled sensibly. The structure refined finally to $R_1 = 0.1197$.

Structure analysis

In the structure, the DMSO molecules act as hydrogen bonding bridges between pairs of host molecules giving rise to continuous ribbons of host-guest pair running parallel to [101], as shown in **Figure 6.7a**. Host···guest hydrogen bonding interaction O-H···O=S are present with O···O distances in the range of 2.662(8) - 2.727(7)Å (details see **Table 6.2**). The DMSO guests lie in centrosymmetric lacunae which accommodate pairs of guests. This is represented as a section plane cut at b = 1/2 in **Figure 6.8a**. These cavities are interconnected along [010]. This is evident in **Figure 6.8b** in which a space-filling projection along [010] is shown. The crystal packing, viewed down [010], is illustrated in **Figure 6.7b**.

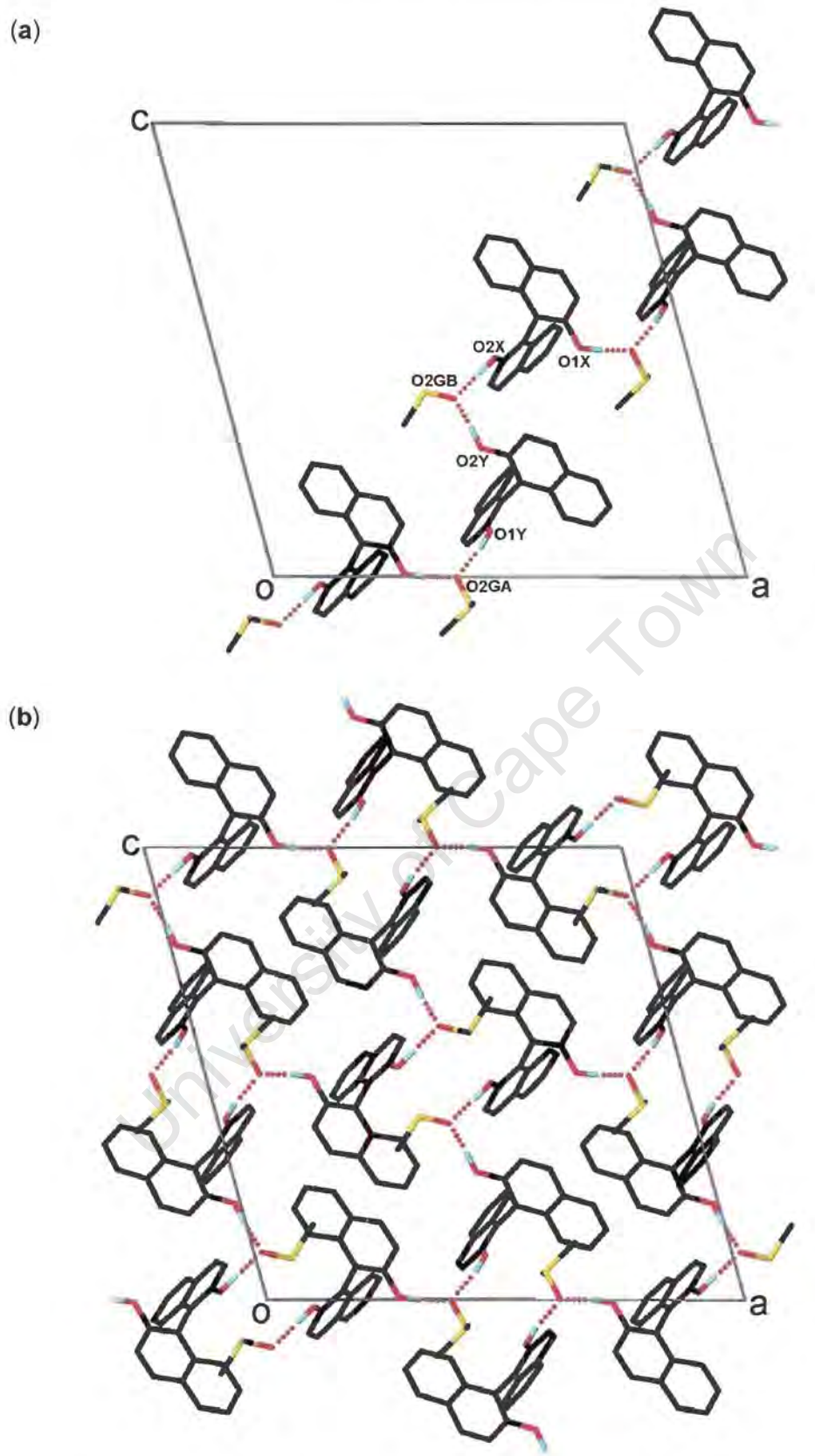

Figure 6.7 (a) Projection along [010] showing the hydrogen bonding scheme. The hydrogen bonds link the host and guest molecules running along [101]. (b) Projection along [010] showing the crystal packing. All of the H atoms except the hydroxyl hydrogens are omitted.

(a)

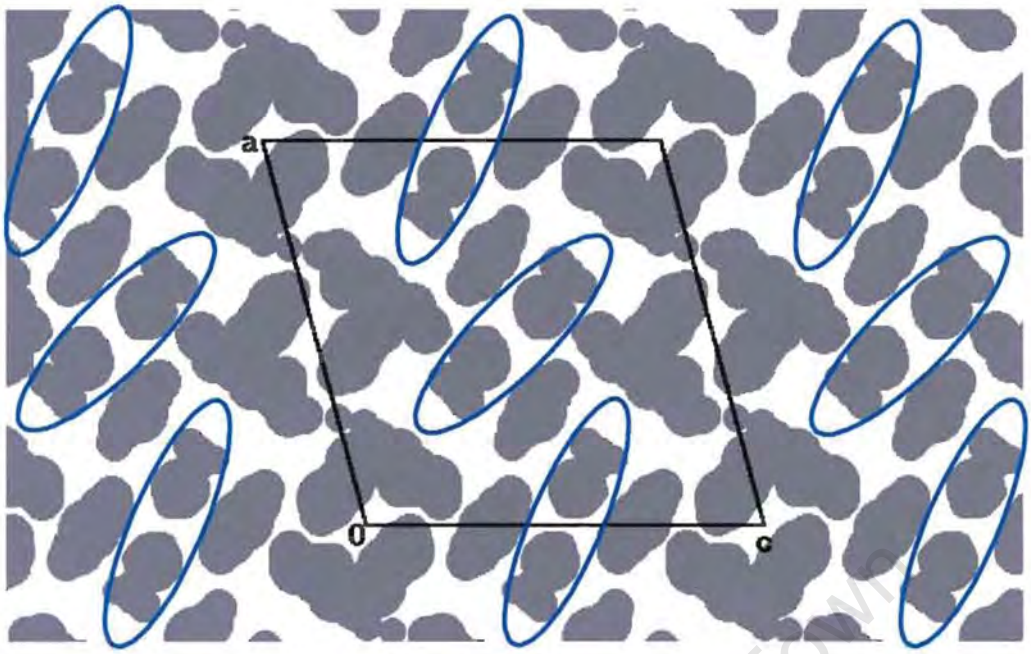

(b)

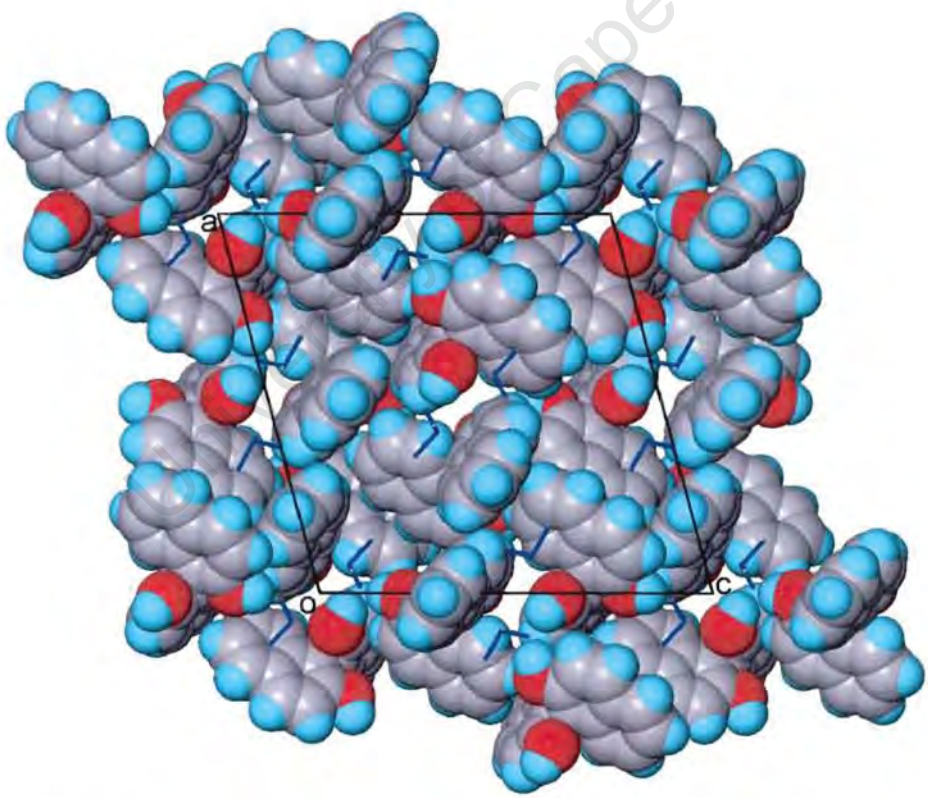

Figure 6.8 (a) A cut through the unit cell of **BINAP•DMSO** at b = 0.5. Pairs of DMSO molecules which are related by centre of symmetry are circled in oval-shaped blue lines. The rest of the grey areas are the space occupied by the host. It shows the guests are in cavities.
(b) A projection viewed along [010] showing the cavities are interconnected along [010]. The hosts are in van der Waals representation and the guests are in blue stick representation.

BINAP•2DMSO

$C_{20}H_{14}O_2 \cdot 2C_2H_6OS$	
Guest: Dimethyl sulfoxide	
Space group: $P2_1/c$	
a = 8.453(1) Å	$\alpha = 90^\circ$
b = 8.931(1) Å	$\beta = 92.928(5)^\circ$
c = 29.573(3) Å	$\gamma = 90^\circ$
Volume = 2229.7(4) $Å^3$	
Z = 4	

Refinement

BINAP•2DMSO crystallised in $P2_1/c$ with Z = 4. There are one host and two **DMSO** guest molecules (A and B) in the asymmetric unit, all located in general positions. The host non-hydrogen atoms were refined with anisotropic temperature factors. Both DMSO guests are disordered with S atoms occupying two positions. Their site occupancies refined with starting value of 0.73 and 0.27 for S(2GA) and S(2A) of guest A, 0.62 and 0.38 for S(2GB) and S(2B) of guest B respectively. These values have been derived from relative peak heights in the electron density map and refined to 0.74 and 0.26 for guest A, 0.61 and 0.39 for guest B. The two possible arrangements of the guest molecule A are shown in **Figure 6.9** as an example. This is a common form of disorder for DMSO molecule in inclusion compounds (Barbour *et al.* 1994). The guest atoms were modelled anisotropically and the hydrogen atoms were placed with the usual geometric constraints. The host hydroxyl hydrogen atoms were located in the difference electron density maps and refined with bond length constraints and individual isotropical temperature factors. The host aromatic hydrogen atoms were placed geometrically and refined with 1.5 x U_{eq} of their parent atoms. The structure refined successfully to R_1 = 0.0459. The S=O bond lengths in the disordered DMSO molecules range from 1.438(2)Å to 1.664(3)Å with the average of 1.528Å, the C-S bond lengths range from 1.544(2)Å to 1.848(3)Å with the average of 1.701Å and the S···S distances are 1.202(3)Å and 1.344(4)Å in guest A and B respectively. These values are considered acceptable when compare with the literature values of 1.44(1)Å and 1.78(2)Å for S=O and S-C bond lengths respectively (Allen *et al.* 1992).

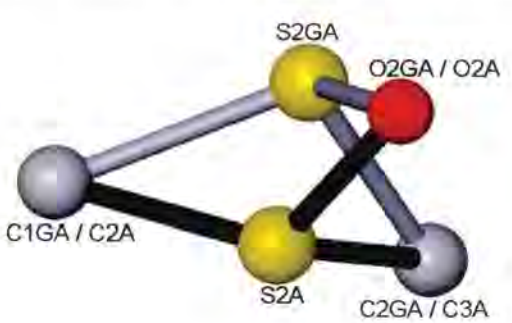

Figure 6.9 Two possible arrangements of guest molecule A. The sulphur atom is disordered over two positions. Similar disorder model and numbering scheme are employed for guest B.

Structure analysis

In the structure, each hydroxyl moiety of the host donates the proton to a DMSO guest molecule, forming hydrogen bonds O-H···O=S with O···O distance of 2.666(2)Å and 2.641(3)Å (see **Table 6.2**). The two unique guest molecules, A and B, are situated mainly in separated channels running along [010] and [100] respectively. Careful inspection of the sections revealed that a channel parallel to [001] interconnects these two columns of guest molecules. This is illustrated in **Figure 6.10**, which shows how the channels traverse the unit cell. The molecular structure and crystal packing are shown in **Figure 6.11**.

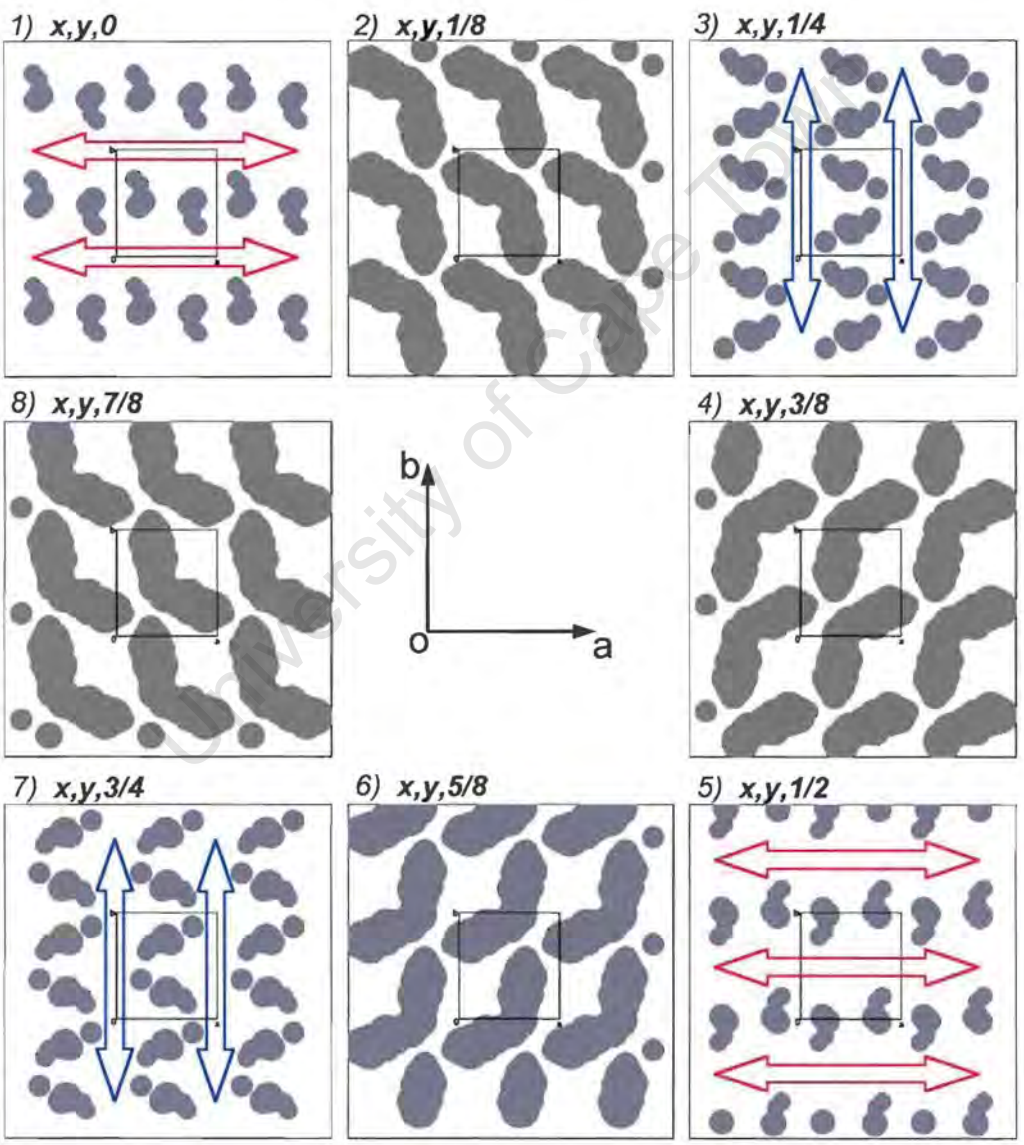

Figure 6.10 Sections at intervals of 0.125c through **BINAP•2DMSO**, viewed along [001]. The host is represented as solid area and the guest is omitted. The blue and red arrows represent the propagation of columns of guest A and B along [010] and [100] respectively.

(a)

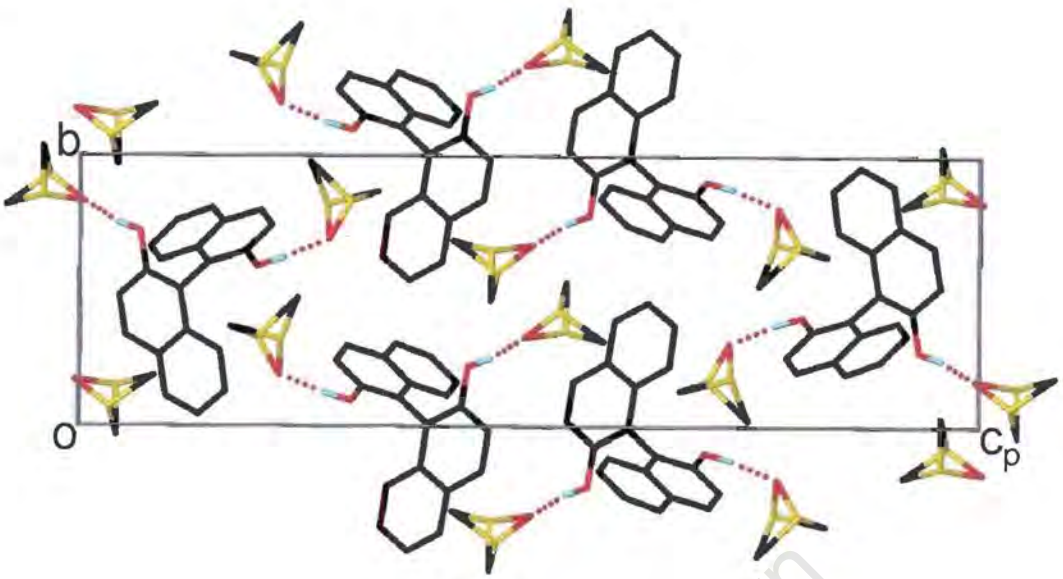

(b)

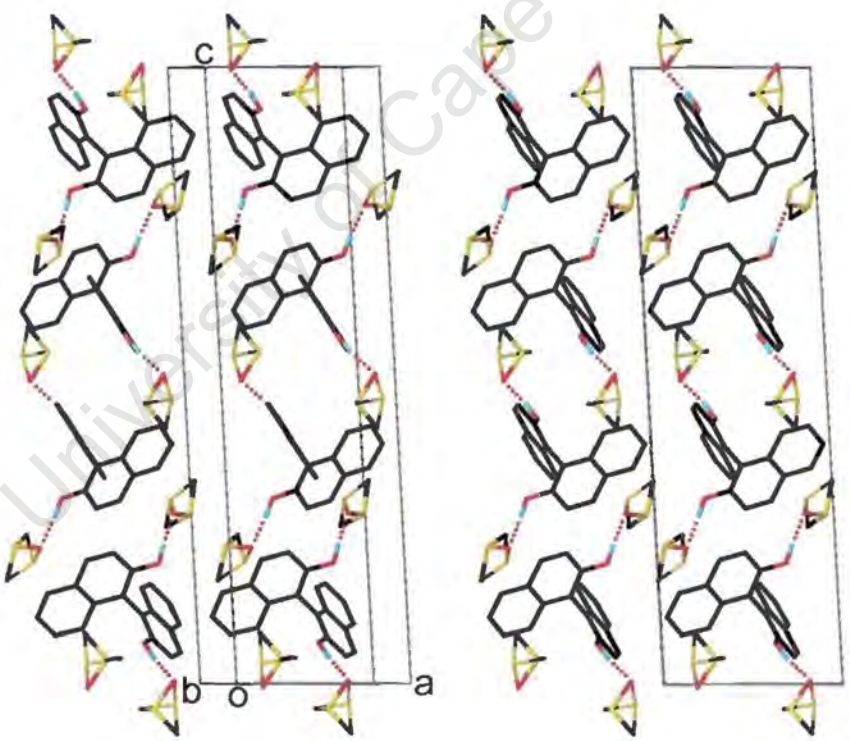

Figure 6.11 Projections of crystal packing in **BINAP•2DMSO**, viewed along (a) [100] and (b) [010] respectively. All of the H atoms except the hydroxyl hydrogens are omitted. The H-bonds are shown as dotted lines.

BINAP•1.5MOP

$C_{20}H_{14}O_2 \cdot 1.5C_4H_9ON$
Guest: Morpholine

I
Space group: $P2_1/c$

a = 9.139(2) Å	$\alpha = 90^\circ$
b = 27.672(6) Å	$\beta = 112.98(3)^\circ$
c = 9.204(2) Å	$\gamma = 90^\circ$

Volume = 2143.0(8) Å^3
Z = 4

II
Space group: $P2_1/n$

a = 18.2465(2) Å	$\alpha = 90^\circ$
b = 27.6212(7) Å	$\beta = 113.851(1)^\circ$
c = 9.2313(5) Å	$\gamma = 90^\circ$

Volume = 4255.2(3) Å^3
Z = 8

Refinement

BINAP•1.5MOP(I) crystallises in $P2_1/c$ with Z = 4. The space group requires one morpholine guest molecule, A, to be located in general position, while another one, B, to be located at a special position, on a centre of inversion, at Wyckoff position *c* [(0,0,½) and (0,½,0)]. The guest A is disordered over two sites with no shared atoms. The two possible arrangements, shown in **Figure 6.12**, have refined site occupancy factors of 0.537 and 0.463 respectively. The guest B, which located on a centre of inversion, was refined with common positions for the O and N atoms [O(1GB) and N(4GB)] with site occupancies of 0.5. All of the non-hydrogen atoms of both the host and guest molecules were treated anisotropically in the final model, even though the O(1) atom and a number of carbon atoms on the host and guest molecules showed high thermal motions. The hydroxyl hydrogen atoms on the host molecule were located in the difference electron density maps and refined with simple bond length constraints and individual temperature factors. The hydrogen atom of the -NH group on the guest could not be located and was omitted from the final model. The rest of the hydrogen atoms on the host and guest molecules were geometrically constrained and assigned isotropic temperature factors relating to their parent atoms. The structure refined to R_1 = 0.0917.

O(1GA)-C(2GA) 1.42(2)Å	O(1A)-C(2A) 1.48(3)Å
C(2GA)-C(3GA) 1.46(2)Å	C(2A)-C(3A) 1.54(3)Å
C(3GA)-N(4GA) 1.35(2)Å	C(3A)-N(4A) 1.53(2)Å
N(4GA)-C(5GA) 1.41(2)Å	N(4A)-C(5A) 1.31(2)Å
C(5GA)-C(6GA) 1.45(2)Å	C(5A)-C(6A) 1.42(2)Å
C(6GA)-O(1GA) 1.52(2)Å	C(6A)-O(1A) 1.45(2)Å

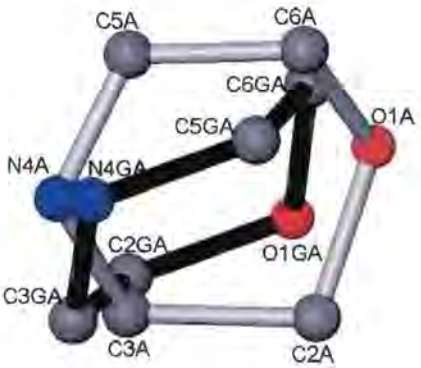

Figure 6.12 Disorder modelled in morpholine molecule A in **BINAP•1.5MOP**(I). The two arrangements have s.o.f. of 0.516 and 0.484 respectively. The resultant bond lengths are listed above.

BINAP•1.5MOP(II) crystallises in $P2_1/n$ with Z = 8. There are four crystallographically independent guest molecules (A, B C and D) and two host molecules (X and Y) in the asymmetric unit. The hosts and guest A and B are located in general positions, while guests C and D are located at a special position, on a centre of inversion, at Wyckoff positions *d* and *a* respectively. All of the non-hydrogen atoms of both the host and guest molecules were treated anisotropically. The hydrogen atoms of the OH groups on the hosts were located in the difference electron density maps and refined with simple bond length constraints and individual temperature factors. The hydrogens of the NH groups on the guests could not be located and were omitted from the final refinement model. The rest of the hydrogen atoms on the host and guest molecules were geometrically constrained and assigned isotropic temperature factors related to their parent atoms. The structure refined to $R_1 = 0.0668$.

Structure analysis

The host-guest arrangement of **BINAP•1.5MOP**(I), consisting of two host and three guest molecules, is shown in **Figure 6.13**. The guest B, located at the centre of inversion, links two host molecules, each of which is hydrogen bonded to another guest A via O-H···N interaction (metrics in **Table 6.2**). This structure is isostructural to that of **BINAP•1.5DOX**. Both of the two structures were refined in the same space group and have similar cell dimensions. Their crystal packing is similar; differ only in so far as the guest conformations are concerned. The topologies of the two structures are similar, and they give rise to comparable powder diffraction patterns, which are discussed in the next section.

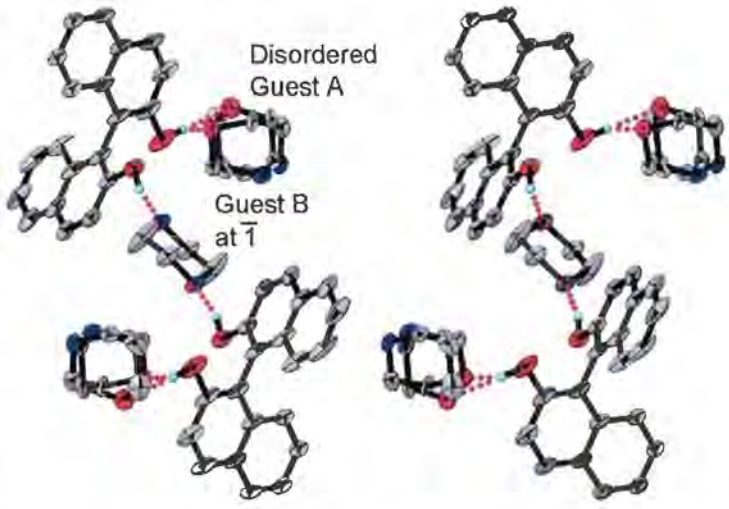

Figure 6.13 Molecular structure of **BINAP•1.5MOP**(I). Displacement ellipsoids are drawn at the 35% probability level. All H atoms except the hydroxyl hydrogens are omitted for clarity.

BINAP•1.5MOP(II) contains two crystallographically independent host molecules in the asymmetric unit. Each host molecule is hydrogen bonded to a single morpholine and to another morpholine located on $\bar{1}$, forming similar hydrogen bonding motif to that in the form I. This is shown in **Figure 6.14**. The crystal packing in both the form I and II is remarkably similar. The projections down [001] and [010] for the two polymorphs are shown together in **Figure 6.15** for comparison. Analogous polymorphism occurs to sulfathiazole (N'-2-thiazolylsulfanilamide), of which two polymorphs show significantly similar molecular packing (Anwar *et al.* 1989).

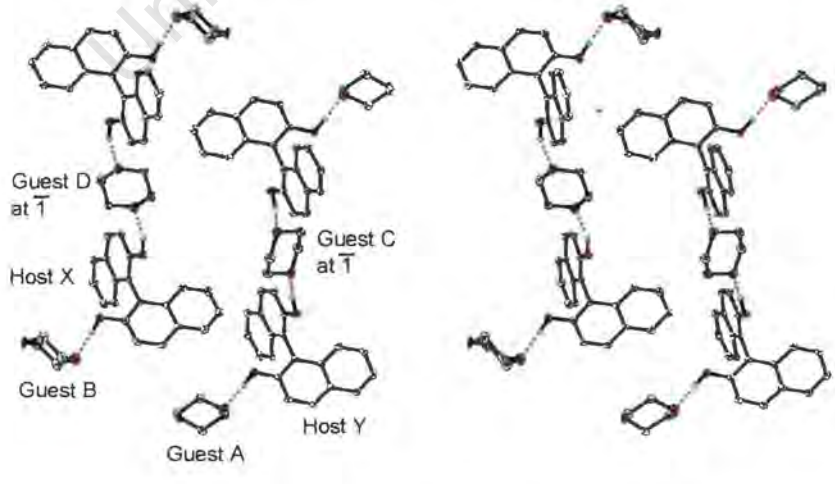

Figure 6.14 Molecular structure of **BINAP•1.5MOP**(II). Displacement ellipsoids are drawn at the 35% probability level. Only the H atoms of OH group are shown.

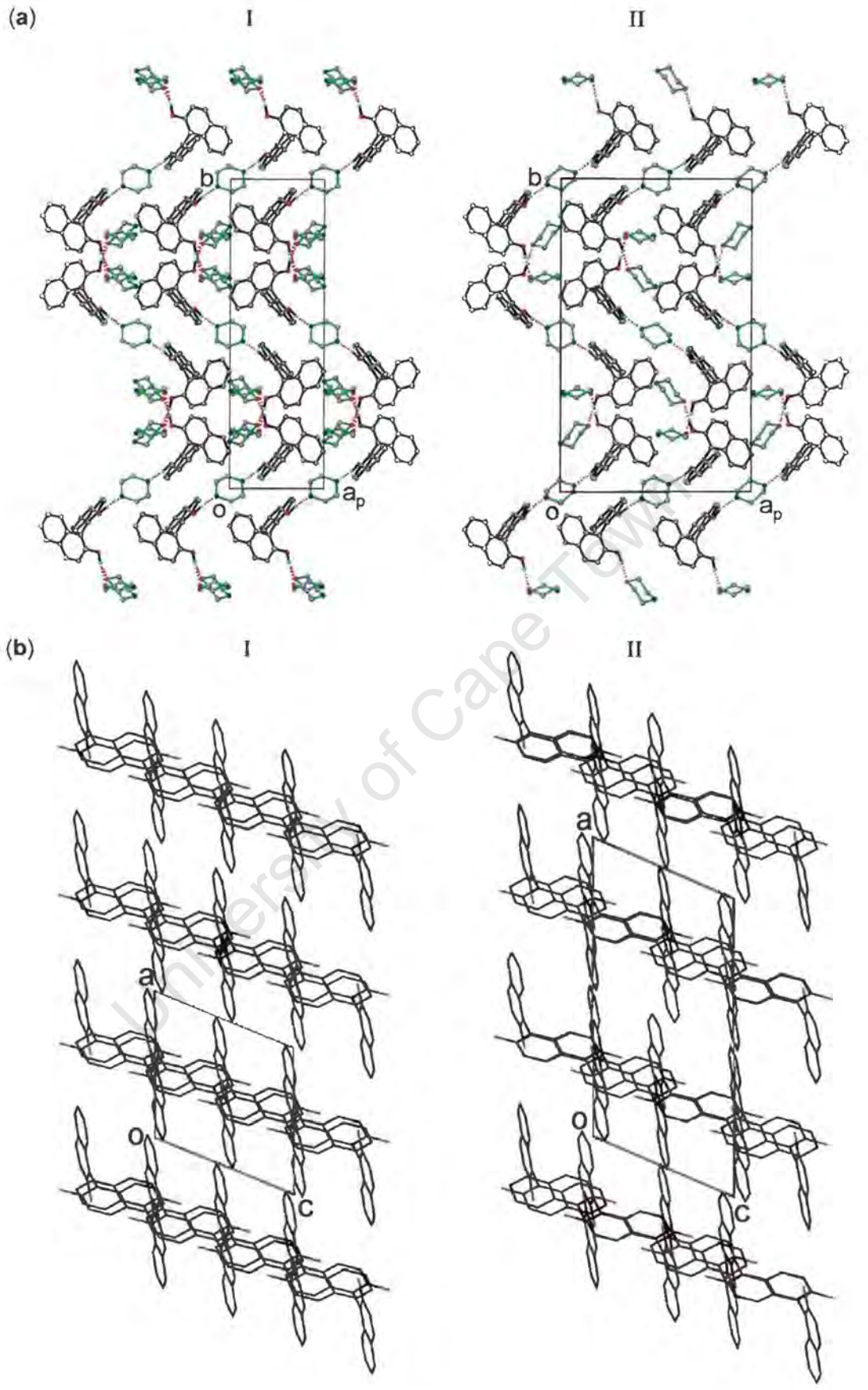

Figure 6.15 Molecular packing in structures of form I and II of **BINAP•1.5MOP**, viewed along (a) [001] and (b) [010]. The guests are omitted in (b) for clarity.

BINAP•1.5THF

$C_{20}H_{14}O_2$•1.5C_4H_8O	
Guest: Tetrahydrofuran	
Space group: Fdd2	
a = 14.651(2) Å	$\alpha = 90^o$
b = 55.471(6) Å	$\beta = 90^o$
c = 10.259(1) Å	$\gamma = 90^o$
Volume = 8338(2) $Å^3$	
Z = 16	

Refinement

BINAP•1.5THF crystallises in Fdd2 with Z = 16. The host and one THF molecule (A) were located in general positions, and another THF molecule (B) was located on a diad at Wyckoff position *a* [(0,0,z) and (¼,¼, z+¼)]. The non-hydrogen atoms of host were refined anisotropically, while those of the guest were refined isotropically due to their relatively high thermal motions with all $U_{iso} > 0.09Å^2$. The host hydroxyl hydrogen atoms were located and the rest of the hydrogen atoms were geometrically constrained. A maximum residual peak of 0.82 $eÅ^{-3}$ was observed close to the O atom of guest B. The structure refined to $R_1 = 0.0993$.

Structure analysis

In this structure, the **BINAP** is hydrogen bonded to the THF (guest A) in the general position, while another THF (guest B) located at the diad acts as an acceptor to two symmetry related hosts, as shown in **Figure 6.16**. The O···O distances are 2.61(1)Å and 3.05(2)Å for guests A and B respectively (details in **Table 6.2**). All guest molecules are located in cavities interconnected along [101], [10 $\bar{1}$] and [1 $\bar{1}$0] directions. The typical examples of these are shown in **Figure 6.17b** and **6.17c**, while **6.17a** shows the crystal packing viewed along [100].

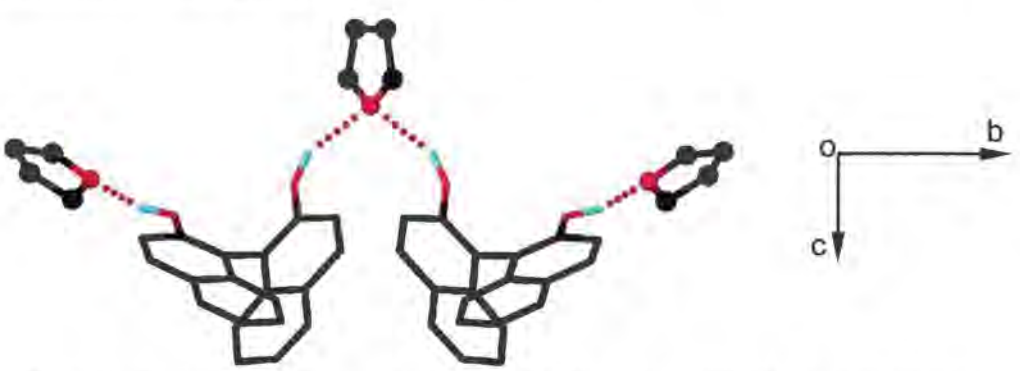

Figure 6.16 Hydrogen bonding scheme for **BINAP•1.5THF**. Only host hydroxyl H atoms are shown.

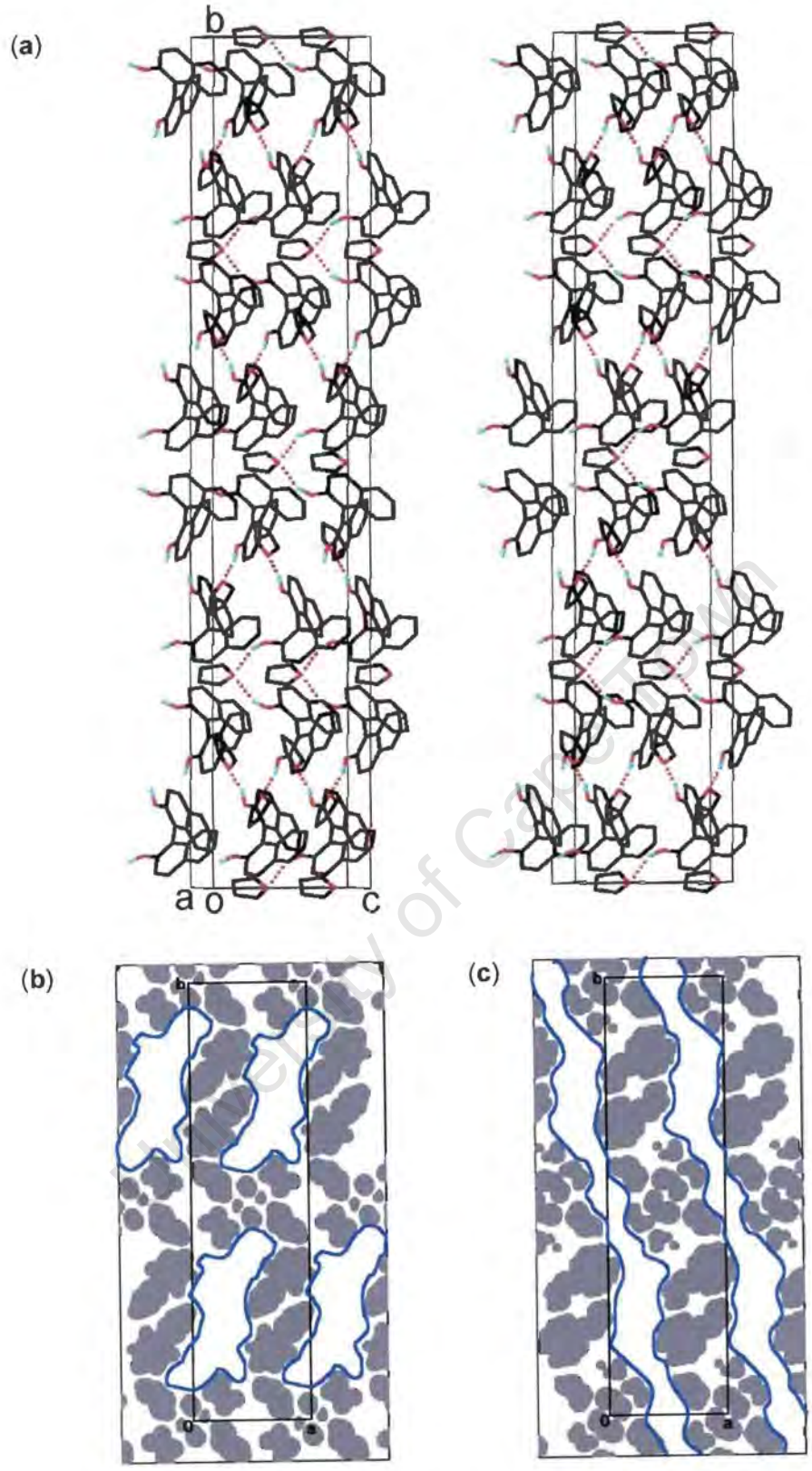

Figure 6.17 (a) Stereo view of crystal packing along [100] for **BINAP•1.5THF**. Only the host hydroxyl H atoms are shown.
(b) Section cut at c = 1/16 showing the cavities where the guests are located. The grey area represents the space occupied by the host. All guests are omitted for clarity.
(c) Section cut at c = 1/8 showing the cavities are interconnected along [110].

BINAP•ACT

$C_{20}H_{14}O_2 \bullet C_3H_6O$	
Guest: Acetone	
Space group: $P2_1/n$	
a = 8.083(1) Å	$\alpha = 90^\circ$
b = 21.290(1) Å	$\beta = 107.36(1)^\circ$
c = 11.094(1) Å	$\gamma = 90^\circ$
Volume = 1822.2(3) $Å^3$	
Z = 8	

Refinement

BINAP•ACT crystallises in $P2_1/n$ with Z = 8. Both the host and guest molecules were located in general positions. All the non-hydrogen atoms were refined anisotropically. The host hydroxyl hydrogen atoms were located. The rest of the hydrogen atoms on the host and the guest molecules were geometrically constrained and assigned isotropic temperature factors relating to their parent atoms. The structure refined successfully to $R_1 = 0.0471$.

Structure analysis

The molecular structure of **BINAP•ACT** is shown in **Figure 6.18**. The oxygen atom on acetone guest molecule is the acceptor of two hydrogen bonds from adjacent host molecules, giving rise to a closed tetramer, about a centre of symmetry, comprising two hosts and two guests. The (host)O-H···O(guest) hydrogen bonds, O(1)-H(1)···O(2G) and O(2)-H(2)···O(2G), have O···O distances of 2.849(2)Å and 2.807(2)Å respectively (details in **Table 6.2**)

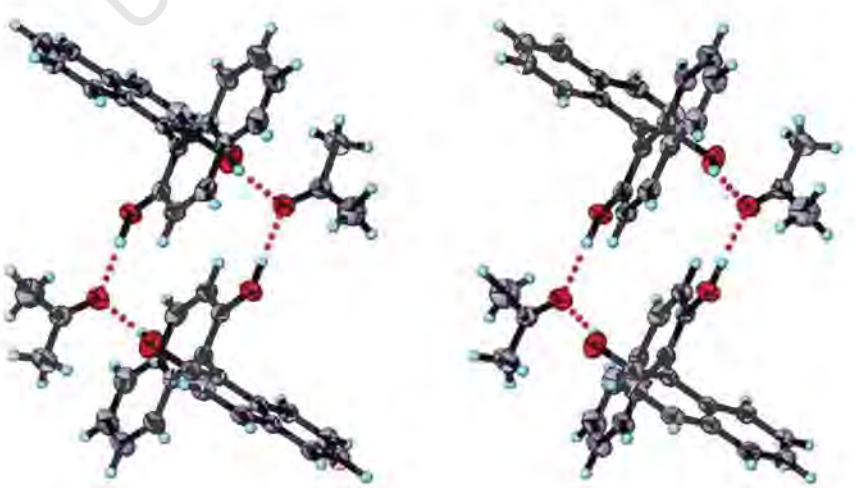

Figure 6.18 Stereo view of the molecular structure of **BINAP•ACT**. Displacement ellipsoids are drawn at the 40% probability level.

The acetone guest molecules are located in open channels, running parallel to the [101] direction, with the oxygen atoms pointing towards the hydroxyl group of the host. The channels can be seen from the projection down [101], shown as stick presentation as well as space-filling presentation in **Figure 6.19a** and **b** respectively. The crystal packing, viewed down [100] and [001], is illustrated in **Figure 6.20**.

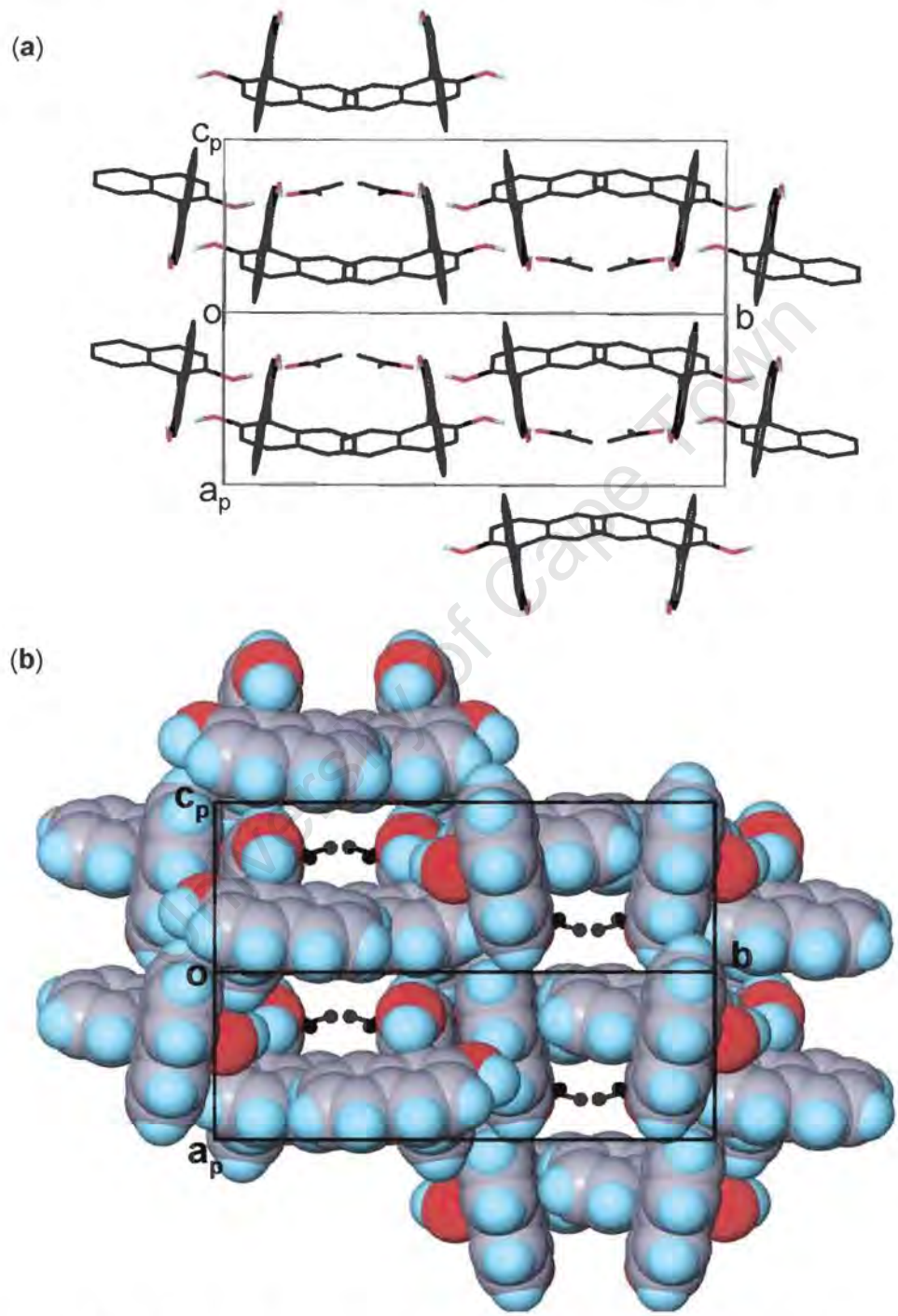

Figure 6.19 Projection down [101] for **BINAP•ACT**, showing the open channels. In (a), only the hydroxyl hydrogens are shown. H-bonds are not indicated for clarity. In (b), The host atoms are shown with van der Waals radii and guest as balls and sticks representation. All hydrogen atoms on the guest are omitted.

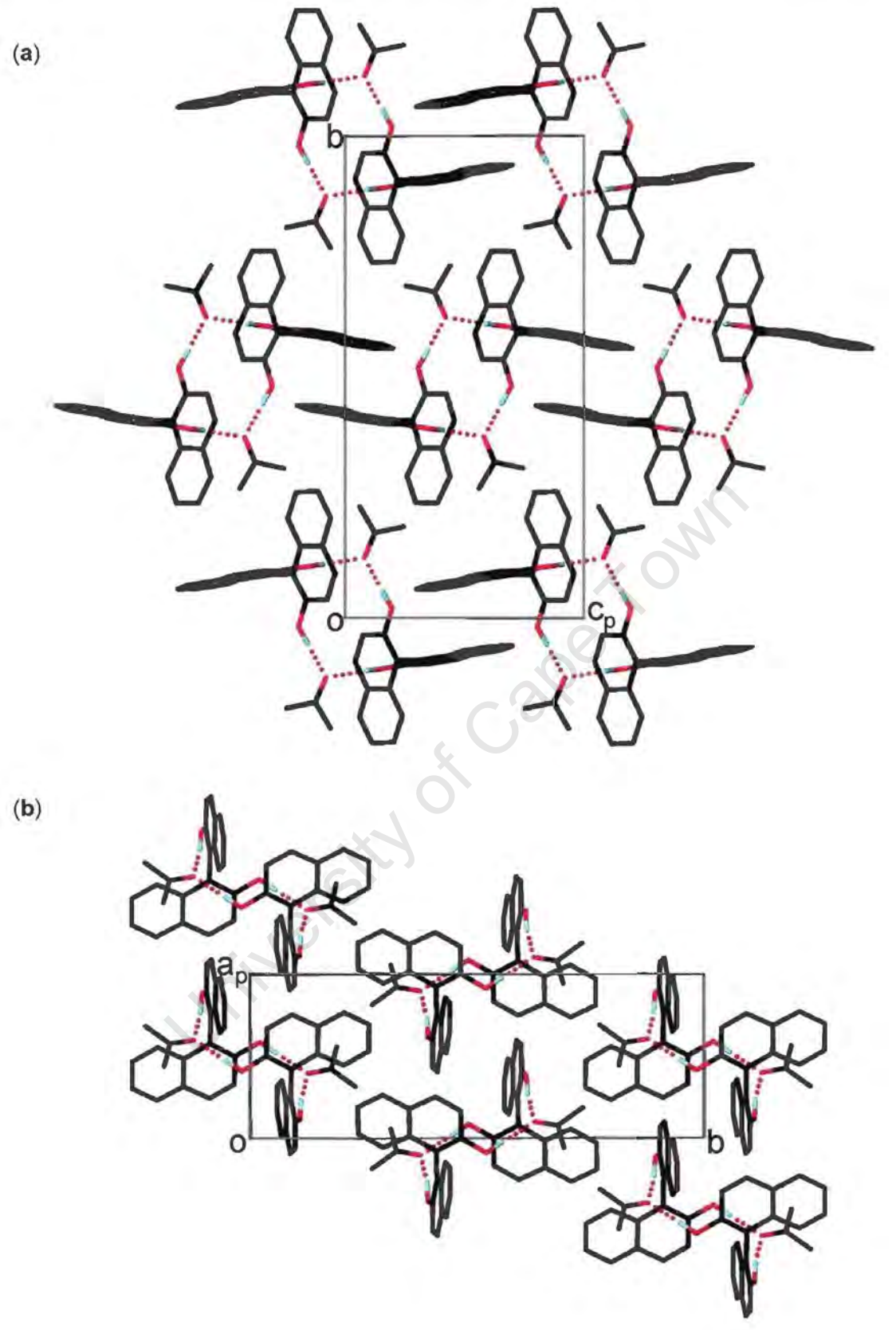

Figure 6.20 Projections down (a) [100] and (b) [001], showing the crystal packing in **BINAP•ACT**. Only the hydroxyl hydrogen atoms are shown. The H-bonds are indicated as dotted lines.

BINAP

$C_{20}H_{14}O_2$	
Space group: Iba2	
a = 15.637(3) Å	$\alpha = 90^o$
b = 21.523(4) Å	$\beta = 90^o$
c = 8.595(2) Å	$\gamma = 90^o$
Volume = 2893(1) $Å^3$	
Z = 8	

Refinement

The guest-free host compound, **BINAP**, crystallises in Iba2. The **BINAP** molecules were located in general positions to fulfil the space group requirements (Z = 8). All the non-hydrogen atoms were refined anisotropically. The hydrogen atoms were all located in the difference electron density maps and were refined with individual isotropic temperature factors without any bond length constraints. The structure refined successfully to $R_1 = 0.0347$.

Structure analysis

The **BINAP** structure is mainly stabilised by the intermolecular hydrogen bonds O(1)-H(1)···O(2) with d(O···O) = 2.839(2)Å (details in **Table 6.2**). However, close contact of C(13)-H(13)···O(1) with d(C···O) = 3.276(2)Å, d(O···H) = 2.855(2)Å and <CHO = 108(1)°, which is considered as weak hydrogen bond, is also observed. Both of the strong and weak hydrogen bonds link molecules, which are related by the two-fold symmetry, to form infinite chains zigzagging along [001]. The O-H···O hydrogen bonding scheme is shown in **Figure 6.21b**. The crystal packing, viewed down [100] and [001], is shown in **Figure 6.21a** and **c** respectively.

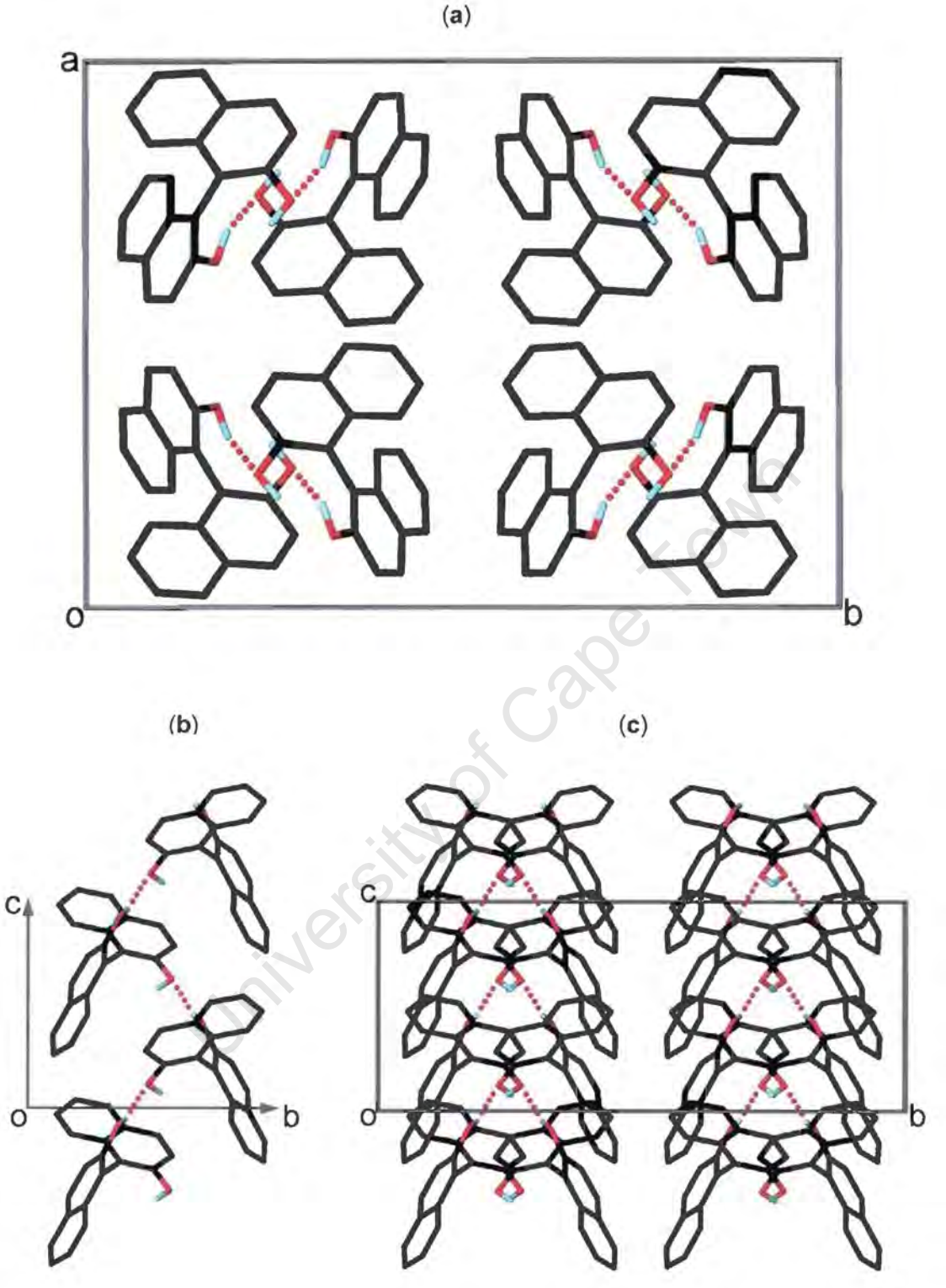

Figure 6.21 (a) Crystal packing viewed down [001] for the structure of **BINAP**.
(b) The O-H···O hydrogen bonds generate chains of molecules running along [001].
(c) Projection viewed along [100]. Only the hydroxyl hydrogen atoms are shown and hydrogen bonds are indicated.

The following **Table 6.2** summarises the hydrogen bonding details for all the structures discussed in this chapter.

Table 6.2 Hydrogen bonding details for all the structures discussed in this chapter.

Incl. Comp.	**D-H···A*** / Å	**D-H** /Å	**H···A** /Å	**D···A** /Å	**<DHA** /°
BINAP•1.5DOX	O(1)–H(1)···O(1GB)[1]	0.96(1)	1.81(1)	2.760(3)	169(3)
	O(2)–H(2)···O(1GA)[2]	0.98(1)	1.70(1)	2.676(3)	171(4)
BINAP•3.5DOX	O(1)–H(1)···O(1GB)[3]	0.97(1)	1.71(1)	2.685(2)	176(3)
	O(2)–H(2)···O(1GA)[4]	0.98(1)	1.82(1)	2.679(2)	146(2)
BINAP•DMSO	O(1X)–H(1X)···O(1GA)[5]	0.98(2)	1.76(2)	2.727(7)	168(7)
	O(2X)–H(2X)···O(2GB)	0.98(2)	1.73(2)	2.698(8)	171(8)
	O(1Y)–H(1Y)···O(2GA)	0.99(2)	1.78(2)	2.720(8)	157(5)
	O(2Y)–H(2Y)···O(2GB)[6]	1.01(2)	1.66(2)	2.662(8)	175(9)
BINAP•2DMSO	O(1)–H(1)···O(2GA)[7]	0.95(1)	1.72(1)	2.666(2)	176(3)
	O(2)–H(2)···O(2GB)[3]	0.97(1)	1.68(1)	2.641(3)	168(3)
BINAP•1.5MOP(I)	O(1)–H(1)···O(1GA)	0.97(1)	1.66(2)	2.58(1)	158(4)
	O(1)–H(1)···O(1A)	0.97(1)	2.11(2)	3.06(1)	170(5)
	O(2)–H(2)···O(1GB)/ N(4GB)	0.97(1)	1.81(2)	2.762(4)	165(5)
BINAP•1.5MOP(II)	O(1X)–H(1X)···O(1GD)/ N(4GD)	0.97(1)	1.88(1)	2.814(3)	161(4)
	O(2X)–H(2X)···O(1GB)	0.97(1)	1.83(1)	2.794(3)	175(3)
	O(1Y)–H(1Y)···O(1GA)	0.97(1)	1.77(1)	2.728(3)	170(3)
	O(2Y)–H(2Y)···O(1GC)/ N(4GC)	0.97(1)	1.84(1)	2.753(3)	156(3)
BINAP•1.5THF	O(1)–H(1)···O(1GA)[8]	0.98(2)	1.66(2)	2.61(1)	161(6)
	O(2)–H(2)···O(1GB)[9]	0.96(2)	2.17(2)	3.05(2)	152(6)
BINAP•ACT	O(1)–H(1)···O(2G)	0.96(1)	1.99(1)	2.849(2)	147(2)
	O(2)–H(2)···O(2G)[10]	0.95(1)	1.86(1)	2.807(2)	179(2)
BINAP	O(1)–H(1)···O(2)[11]	0.96(3)	2.00(3)	2.839(2)	145(3)

***D-H···A**: Donor(**D**)-**H**···Acceptor(**A**)

Symmetry codes: (1) -x, -y, -z (2) x, -y+1/2, z-1/2 (3) -x+1, -y, -z (4) -x+2, -y, -z (5) x, y-1, z (6) x+1/2, -y+1/2, z+1/2 (7) -x+1, y-1/2, -z+1/2 (8) x-1/4, -y+1/4, z-1/4 (9) x+1/2, y, z-1/2 (10) -x+1, -y, -z+2 (11) -x+1/2, -y+1/2, z+1/2

Competition experiments

1,4-dioxane and morpholine are very similar in shape and size. Acetone and tetrahydrofuran are of close melting and boiling points. Competition experiments were carried out between the two pairs to determine which would be preferentially included by the host. The competitions were done at room temperature and in solution. The results are shown in **Figure 6.22**, in which general selectivity curves are drawn instead of the experimental lines that simply join the experimental points.

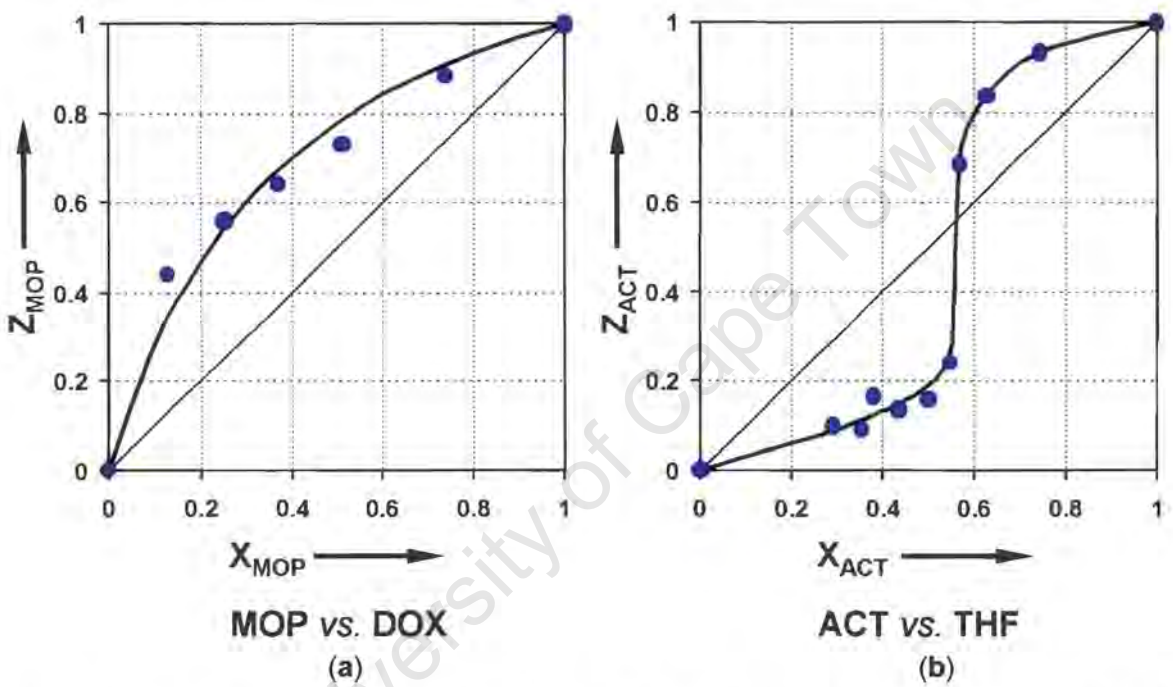

Figure 6.22 Competition experiments results of (a) morpholine versus 1,4-dioxane; (b) acetone versus tetrahydrofuran. The blue dots are experimental points. The black curve in (a) has selectivity coefficient of 3.5.

Figure 6.22a shows that morpholine is slightly favoured over 1,4-dioxane by the host **BINAP** over the whole concentration range. The experimental points lie close to a selectivity coefficient of 3.5.

In contrast, the competitions between acetone and THF (**Figure 6.22b**) show the selectivity to be concentration dependent with $Q_{ACT:THF}$ = 0.56. The acetone is enclathrated when its mole fraction is greater than 0.56, whereas THF is favoured below this limit.

Lattice energy calculations

To interpret the competition results between 1,4-dioxane and morpholine, lattice energy calculations were performed on the inclusion compounds **BINAP•1.5DOX** and both forms of **BINAP•1.5MOP** for comparison. These compounds were chosen based on the fact that they have the same host:guest ratio and close number of atoms per host-guest unit, with the latter two compounds having one more H atom arising from the NH group. The calculations, following the procedure described in **Chapter 2**, yielded non-hydrogen-bond lattice energies -158.6 kJ mol^{-1}, -164.4 kJ mol^{-1} and -165.8 kJ mol^{-1}, and hydrogen bonding energies -30.2 kJ mol^{-1}, -22.7 kJ mol^{-1} and -31.3 kJ mol^{-1}, for the respective crystal structures of **BINAP•1.5DOX**, **BINAP•1.5MOP**(I) and **BINAP•1.5MOP**(II). Thus the overall lattice energies are added up to as follows:

BINAP•1.5DOX	-188.8 kJ mol^{-1}
BINAP•1.5MOP(I)	-187.1 kJ mol^{-1}
BINAP•1.5MOP(II)	-197.1 kJ mol^{-1}

The non-hydrogen-bond lattice energy of **BINAP•1.5DOX** is about 5.8 - 7.2 kJ mol^{-1} less negative than those of both forms of **BINAP•1.5MOP**. This implies that the latter two structures are more stable in terms of the overall packing. However when incorporating the hydrogen bonding potentials, this difference is compensated and the resultant total lattice energies for **BINAP•1.5DOX** and **BINAP•1.5MOP**(I) become close, while the energy value for **BINAP•1.5MOP**(II) is still the most negative. These results show that the morpholine is capable of forming a relatively stable host-guest system in form II. Even though the crystal structures formed during the competition experiments were unknown, this may explain the preferred selectivity of morpholine over dioxane by the host.

X-ray powder diffraction

The phase changes that occur upon desolvation of both **BINAP•3.5DOX** and **BINAP•2DMSO** compounds were monitored by x-ray powder diffraction.

Figure 6.23 compares the XRD patterns of known compounds for the desolvation of the inclusion compound **BINAP•2DMSO**. Trace 1 is the XRD trace calculated from the single crystal structure of **BINAP•2DMSO** (the β-phase). Trace 2 was obtained after the first desolvation step and matches with the XRD pattern calculated from the crystal structure of **BINAP•DMSO** (trace 2a, γ-phase). Trace 3 is that achieved after complete desolvation and corresponds to the apohost **BINAP**, the so-called non-porous α-phase (trace 3a). This indicates that the inclusion compound **BINAP•2DMSO**, the β-phase, which loses one mole of DMSO molecules upon the first step desolvation, yielded an intermediate inclusion compound **BINAP•DMSO** (the γ-phase). The γ-phase **BINAP•DMSO**, which loses the remaining one mole of DMSO molecules upon the second step desolvation, converted back to the non-porous α-phase of the apohost.

Similar results were obtained for the desolvation of **BINAP•3.5DOX**. Upon partial guest loss (2 out of 3.5) in the first step, the structure of **BINAP•3.5DOX** (the β-phase) is rearranged to form the stable intermediate γ-phase **BINAP•1.5DOX**. The γ-phase converts back to the non-porous α-phase of the apohost upon the second step of desolvation by losing the remaining 1.5 dioxanes. The XRD traces are shown in **Figure 6.24**, in which the calculated and experimental γ-phase is represented by trace 1 and 1a.

Therefore the desolvation reactions of the inclusion compounds **BINAP•3.5DOX** and **BINAP•2DMSO** can be formulated as following:

BINAP•3.5DOX (β,*s*) → 2**DOX** (*g*)↑ + **BINAP•1.5DOX** (γ,*s*) → 1.5**DOX** (*g*)↑ + **BINAP** (α,s)

BINAP•2DMSO (β,*s*) → **DMSO** (*g*)↑ + **BINAP•DMSO** (γ,*s*) → **DMSO** (*g*)↑ + **BINAP** (α,*s*)

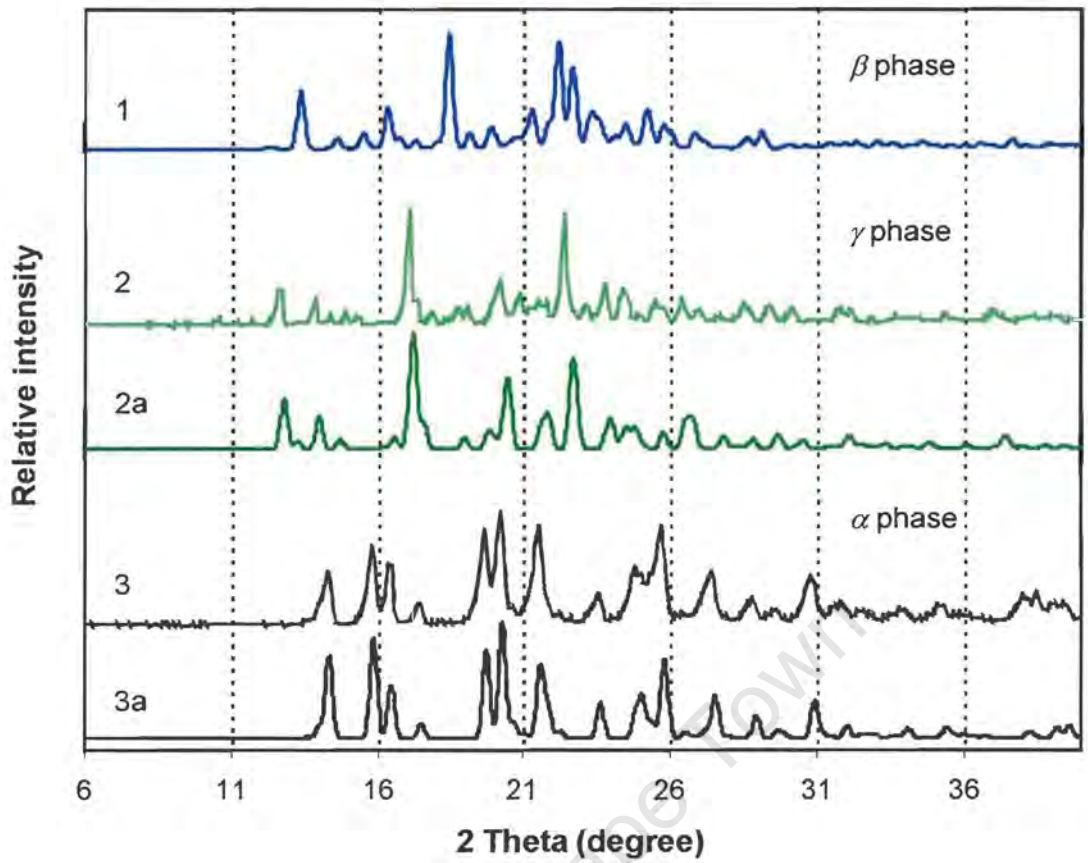

Figure 6.23 (1) Calculated XRD trace from single crystal of **BINAP•2DMSO**.
(2) Experimental XRD trace after first step desolvation of **BINAP•2DMSO**.
(2a) Calculated XRD trace from single crystal of **BINAP•DMSO**.
(3) Experimental XRD trace after second step desolvation of **BINAP•2DMSO**.
(3a) Experimental XRD trace for the guest-free host **BINAP**.

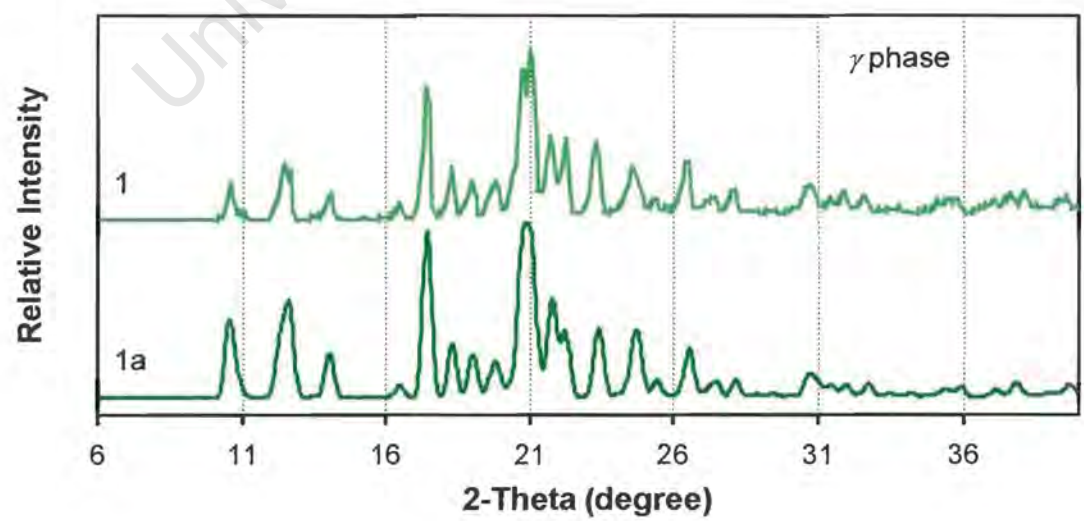

Figure 6.24 (1) Experimental XRD trace after first step desolvation of **BINAP•3.5DOX**.
(1a) Calculated XRD trace from single crystal of **BINAP•1.5DOX**.

The calculated XRD patterns for the two polymorphic inclusion compounds of **BINAP** with morpholine, as well as the inclusion compound **BINAP•1.5DOX** are shown in **Figure 6.25**. These patterns are also compared with the experimental XRD trace **a**, obtained from a powder sample prepared by evaporation of a continuously stirred solution of **BINAP** and morpholine at room temperature (~25°C). The XRD pattern calculated from the inclusion compound **BINAP•1.5MOP**(I) correlates generally well with that calculated from the crystal structure of **BINAP•1.5DOX**, since both the two structures are isostructural. The calculated XRD patterns for the two polymorphs, form I and form II of **BINAP•1.5MOP** that crystallised at 60°C and 4°C respectively, are almost non-distinguishable and this can be attributed to the close structural relationship between the two forms. The experimental XRD trace **a** resembles each of the three calculated XRD traces, therefore whether the crystal phase of the corresponding powder inclusion compound is the form **I** or the form **II** is non-determinable by the XRD diffraction. We note however that both forms could be distinguished by DSC (see section 'Thermal analysis').

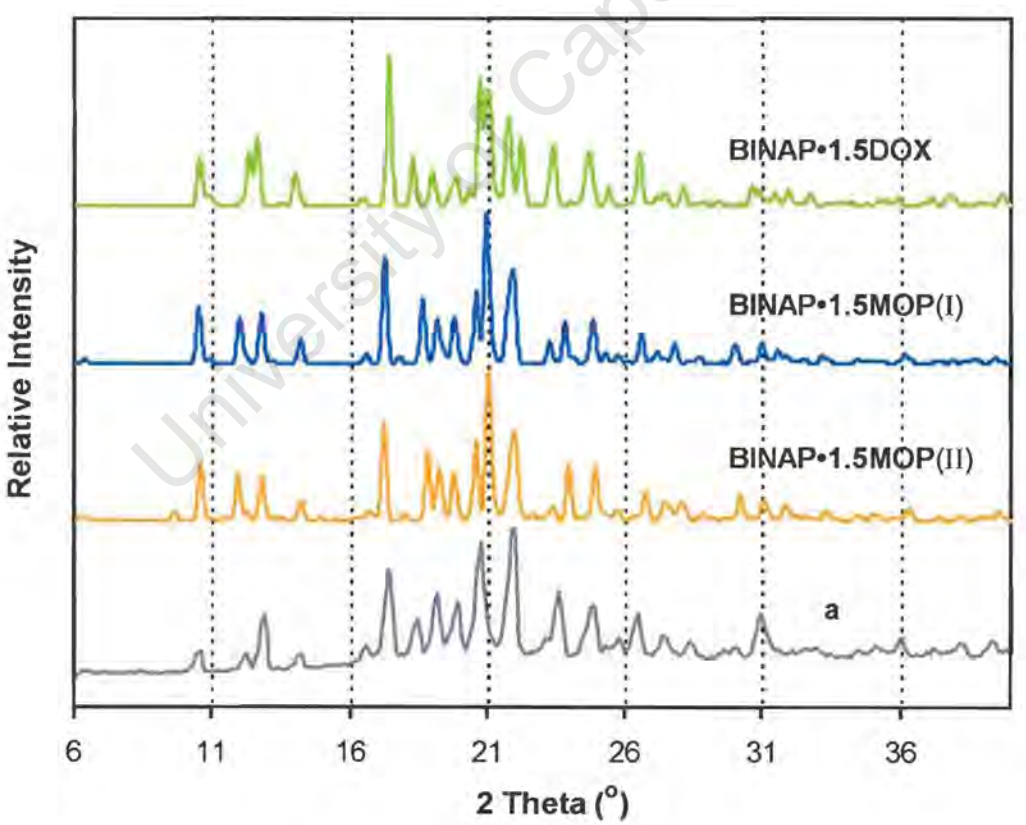

Figure 6.25 Experimental XRD trace **a** obtained from the powder sample of **BINAP•1.5MOP** and calculated XRD patterns from crystal structures of **BINAP•1.5DOX**, **BINAP•1.5MOP**(I) and **BINAP•1.5MOP**(II).

Hot Stage Microscopy

The HSM investigations for selected inclusion compounds were followed up to investigate physical change during either single step or multi-step desolvation. The HSM photographs for the inclusion compounds **BINAP•1.5DOX**, **BINAP•3.5DOX** and **BINAP•2DMSO** are shown in **Photo 6.1**, **6.2** and **6.3** respectively. The HSM studies were carried out at constant heating rate of 10°C min^{-1}. In the case of the crystal of **BINAP•3.5DOX** being immersed in silicon oil, bubbling commenced at about 106°C. This could not be regarded as the onset temperature of guest release, since bubbles formed as consequences of sufficient amount of guest escaping form the crystal and accumulating in the silicon oil. It is also noted that this crystal was so unstable that part of it turned opaque due to formation of product phase shortly after removal from the mother liquor. For the inclusion compounds of **BINAP•3.5DOX** and **BINAP•2DMSO**, of which the TG analytical results indicated two well defined guest loss steps, it can be clearly seen that their crystals shattered at about 106°C and 140°C respectively. This shows that the multi-step guest desorptions are accompanied by change in particle size of the samples. In contrast, the crystals of the inclusion compound **BINAP•1.5DOX**, which underwent single step decomposition in the programmed TG run, retained their original shape after guest loss.

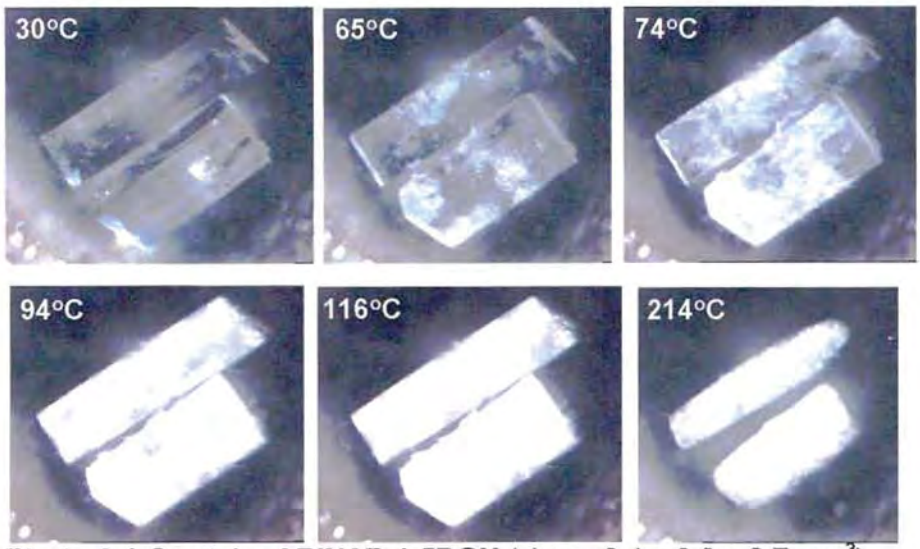

Photo 6.1 Crystals of **BINAP•1.5DOX** (size: ~0.1 x 0.3 x 0.7 mm^3).

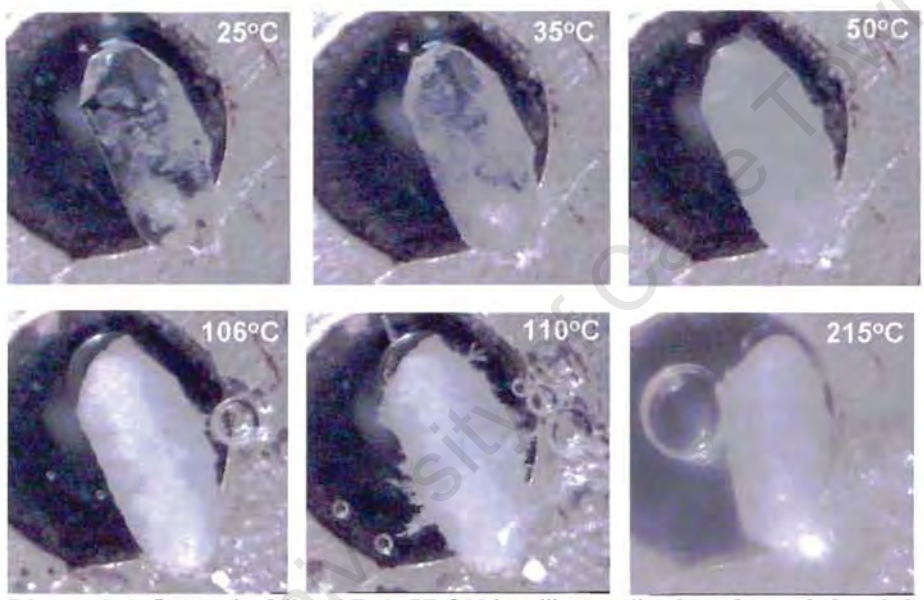

Photo 6.2 Crystal of **BINAP•3.5DOX** in silicon oil (size: 0.5 x 0.8 x 1.6 mm^3).

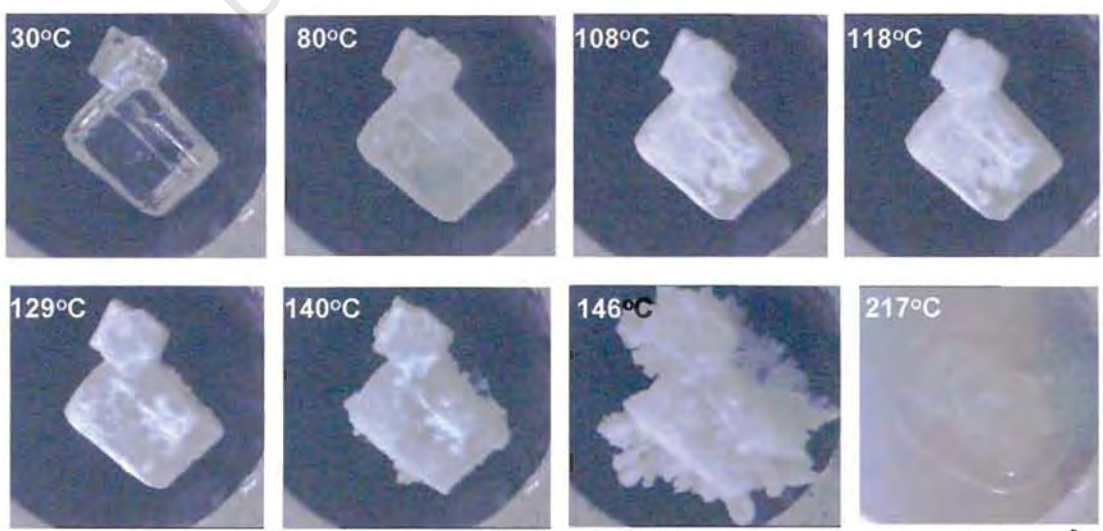

Photo 6.3 Crystals of **BINAP•2DMSO** (size of the biggest one: 0.5 x 0.6 x 0.9 mm^3).

Kinetics of desolvation

In the programmed temperature TG experiments, discussed previously, two distinct desolvation steps were observed for both the inclusion compounds of **BINAP•3.5DOX** and **BINAP•2DMSO**. The two steps were readily isolated in the isothermal TG experiments. A typical example of the two-step mass loss *versus* time curve obtained from isothermal TG run is shown in **Figure 6.26**. In order to procure kinetic parameters, each step was analysed separately over an appropriate pre-selected temperature range. The data, for each step, were reduced to curves of fractional reaction (α) versus time and fitted to various kinetic model.

For the inclusion compounds of **BINAP•1.5DOX**, **BINAP•DMSO** and **BINAP•ACT**, of which programmed temperature TG curves show single step mass losses, the kinetics of desolvation were studied by isothermal TG method over appropriate temperature ranges.

Because the crystalline samples of the form I and form II of **BINAP•1.5MOP** compounds could not be reproduced at respective crystallisation temperatures of 60°C and 4°C, the isothermal kinetic studies were attempted to carry out using the powder samples obtained at 25°C. The isothermal TG runs at different temperatures invariably yielded overlapping non-single mass loss curves. Therefore the kinetic parameters of desolvation for **BINAP•1.5MOP** could not be measured sensibly.

The semilogarithmic plots of *ln k* versus *1/T* for each desorption reaction are shown in **Figure 6.27** and the Arrhenius parameters are given in **Table 6.3**.

For the inclusion compounds containing dioxane and DMSO as guests, the desolvation fitted the contracting area mechanism R2. For **BINAP•ACT**, the α-time curves were slightly sigmoidal and the data were best fitted over an α range of 0.05 - 0.95 by the second Avrami-Erofe'ev equation A2:

$$[-\ln(1-\alpha)]^{1/2} = kt$$

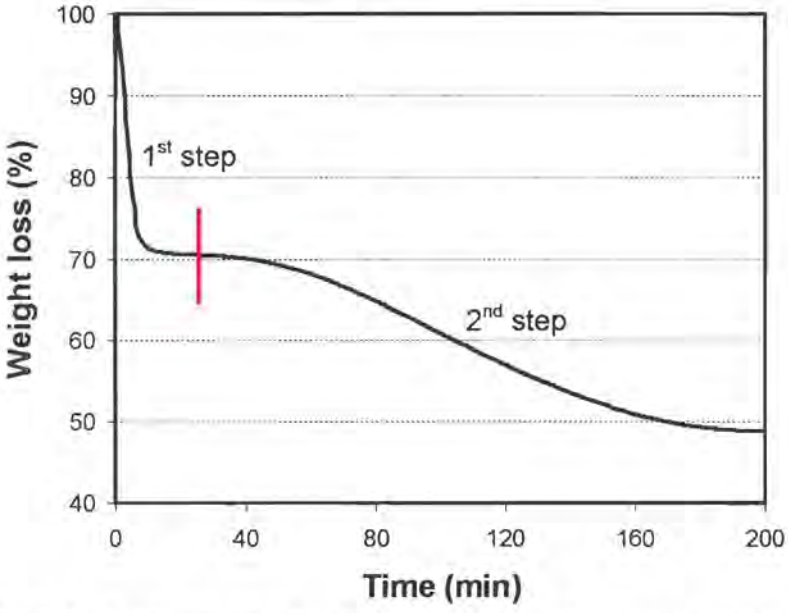

Figure 6.26 An typical example of two-step mass loss *versus* time curve, taken from the desolvation of **BINAP•3.5DOX** at 40°C.

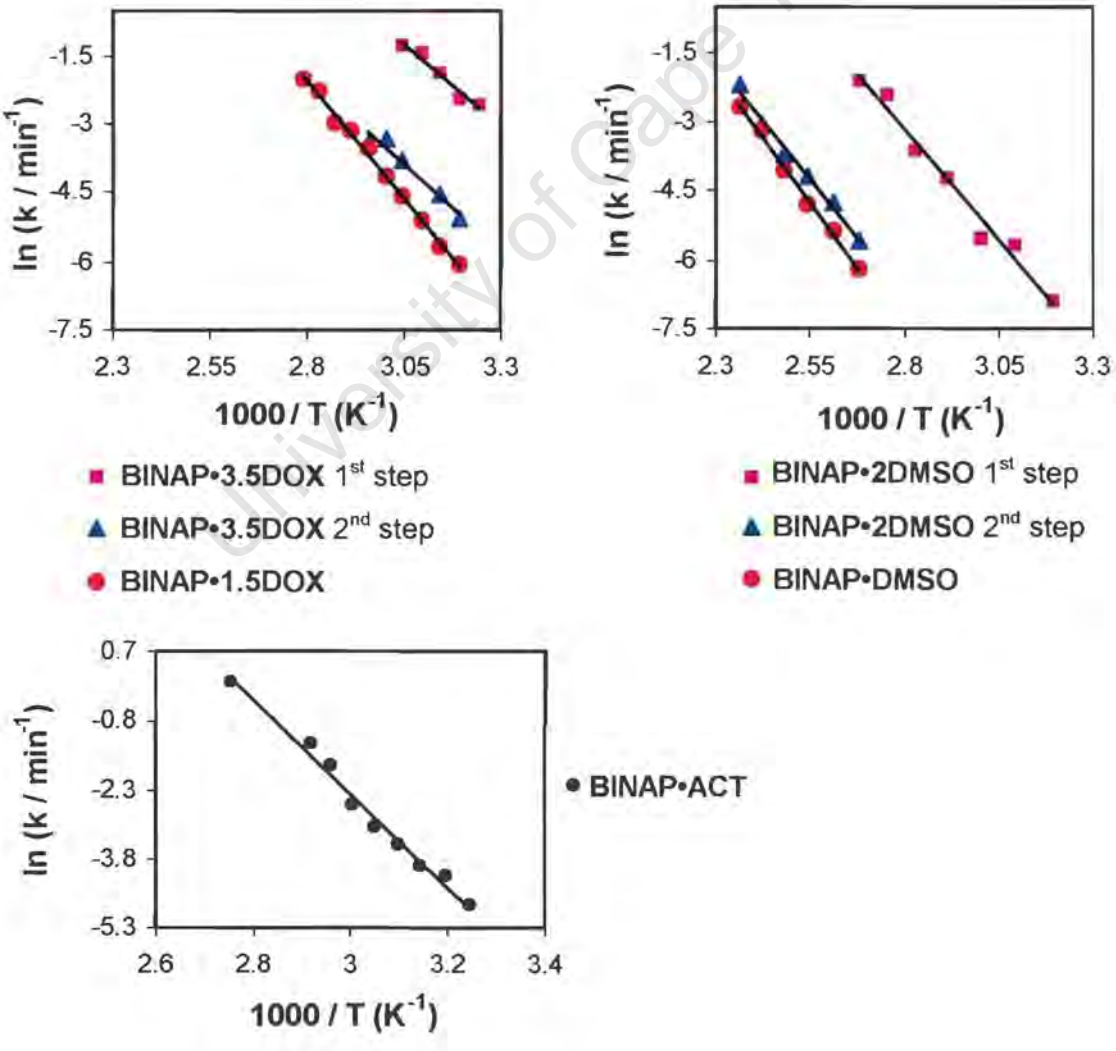

Figure 6.27 Arrhenius plots of ln *k versus* 1/*T*.

Table 6.3 Kinetic parameters for the desolvations of inclusion compounds discussed in this chapter.

Inclusion Compound	Temp. range(°C)	α range	Kinetic model	E_a (kJ mol^{-1})	ln A
BINAP•3.5DOX —1st step	35 - 55	0.05 - 0.90	R2	61(6)	21(2)
—2nd step	40 - 65	0.10 - 0.90	R2	63(8)	19(3)
BINAP•1.5DOX	40 - 85	0.05 - 0.95	R2	86(2)	27(1)
BINAP•2DMSO —1st step	40 - 100	0.05 - 0.95	R2	79(5)	23(2)
—2nd step	100 - 150	0.10 - 0.90	R2	85(5)	22(1)
BINAP•DMSO	100 - 150	0.05 - 0.95	R2	94(3)	24(1)
BINAP•ACT	35 - 90	0.05 - 0.95	A2	85(4)	28(1)

As discussed earlier, the decomposition of **BINAP•3.5DOX** occurs in two distinct steps:

$$\text{BINAP}\cdot 3.5\text{DOX} \xrightarrow{-2\text{DOX}} \text{BINAP}\cdot 1.5DOX \xrightarrow{-1.5DOX} \text{BINAP}$$

The first step corresponds to the loss of two dioxane guest molecules. The compound obtained after the first desorption step is identical to the inclusion compound **BINAP•1.5DOX** obtained from the crystallisation carried out at 60°C. This was shown by matching the x-ray powder pattern of the compound obtained after the loss of 2 dioxanes with that calculated from the single crystal structure of **BINAP•1.5DOX**. The activation energies of 61(6) kJ mol^{-1} and 63(8) kJ mol^{-1} were obtained for the first and second desolvation steps respectively. It is interesting to note that the activation energy obtained from the second step desorption of **BINAP•3.5DOX** has a lower value than that obtained from the freshly grown **BINAP•1.5DOX** (86±2 kJ mol^{-1}), even though the compounds are identical. This is attributed to a particle size effect, because it has been noted that the crystallites obtained after the first desorption step are generally much smaller than those of the starting materials. The effect of crystallite size on decomposition kinetics is difficult to quantify (Brown, 1997; Galway & Brown, 1998), but it has been noted that at a given temperature the rate of reaction increases with decreasing particle size. **Figure 6.26** shows that the semilogarithmic plots for **BINAP•3.5DOX** (2nd step) and **BINAP•1.5DOX** are very close even though they yield somewhat different activation energies

An analogous situation occurs in the desolvation of BINAP•2DMSO which proceeded in two steps. The compound formed after the loss of one DMSO guest is identical to BINAP•DMSO synthesised from solution and the kinetic parameters follow a similar pattern to those of the dioxane inclusion compounds.

Discussion

The host **BINAP** forms inclusion complexes of differing host:guest ratio with 1,4-dioxane and dimethyl sulfoxide at different crystallisation temperatures. The inclusion compounds including the larger number of guest molecules crystallised at relative lower temperatures, *i.e.* **BINAP•3.5DOX** and **BINAP•2DMSO** (4°C/25°C), whereas the inclusion compounds including fewer guest molecules crystallised at higher temperatures, *i.e.* **BINAP•1.5DOX** and **BINAP•DMSO** (60°C).

In the high-temperature structure **BINAP•1.5DOX**, each host molecule is hydrogen bonded to a single dioxane (A), and a second dioxane (B), located on a centre of inversion, links two host molecules. The dioxane A exhibits relatively high thermal motion. In the low-temperature structure **BINAP•3.5DOX**, the host is hydrogen bonded to dioxanes A and B, while dioxanes C and D (the latter located at $\bar{1}$), are only stabilised by van der Waals interactions. The dioxane guest molecules are located in interconnected channels in both of the structures. The thermal analytical results show that **BINAP•1.5DOX** loses all of the dioxane guest in a single step, while **BINAP•3.5DOX** desolvates in two distinct steps, of which the first step corresponding to the loss of two dioxane molecules. The latter is counterintuitive, because only 2 of the 3.5 guest molecules are hydrogen bonded to the host, and one would only expect an initial loss of the 1.5 dioxane molecules which are not stabilised by hydrogen bonds. Indeed this is what occurred in the desolvation of the inclusion compound 2,2'-bis(hydroxydiphenylmethyl)-1,1'-binaphthyl•3pyridine (Weber *et al.* 1993), in which only one pyridine guest is hydrogen bonded to the host. This compound desorbs in two distinct steps, the first conforming to the loss of two pyridines (T_{on} = 94°C) and the second to the loss of the remaining pyridine (T_{on} = 143°C), and it was surmised that the latter step corresponds to the hydrogen bonded guest.

In the high-temperature inclusion compound **BINAP•DMSO**, each DMSO molecule is the acceptor of two hydrogen bonds from two adjacent host molecules, giving rise to continuous ribbons of host-guest pairs. The DMSO molecules are located in interconnected cavities. In the low-temperature structure **BINAP•2DMSO**, each hydroxyl moiety of the host acts as a hydrogen bond donor to a DMSO guest, and the DMSO molecules are located in interconnecting channels. **BINAP•DMSO** desorbs in a single endothermic step, while **BINAP•2DMSO** desorbs in two distinct steps, each corresponding to the loss of a single DMSO guest.

The desolvation of **BINAP•3.5DOX** and of **BINAP•2DMSO** follow two steps and can be expressed as the following general form:

BINAP•G$_n$(β,*s*) ⟶ **BINAP•G**$_{n-m}$(γ,*s*) + m**G**(*g*) ↑ (1st step)

BINAP•G$_{n-m}$(γ,*s*) ⟶ **BINAP**(α,*s*) + (n-m)**G**(*g*) ↑ (2nd step)

It is important to note that the guest loss processes are accompanied by changes in the structures of inclusion compounds. The phase changes were confirmed by X-ray powder diffraction on the compounds, taken before and after desolvation. The β-phase was transformed to the intermediate γ-phase, which was then transformed to the non-porous α-phase of the host. The meta-stable intermediate γ-phase corresponds to the single crystal structures of **BINAP•1.5DOX** and **BINAP•DMSO**.

It was possible to separate the two distinct steps for the desolvations of both inclusion compounds of **BINAP•3.5DOX** and **BINAP•2DMSO** using the isothermal TG method and the kinetics of each step could be successfully analysed. In both cases, the activation energies for the second step desolvation are notably lower than that obtained from the desolvations of freshly grown **BINAP•1.5DOX** and **BINAP•DMSO**. This is attributed to the particle size effect. All of the desolvation processes follow the R2 kinetic mechanism. It is noted that the activation energy obtained for the desolvation of **BINAP•DMSO** is relatively high [94(3) kJ mol^{-1}], while for the other three inclusion compounds the activation energies are in the range of 61(6) - 86(2) kJ mol^{-1}. From their crystal structures we know that the guest in **BINAP•DMSO** is located in an interconnected cavity. The relatively constricted structure would imply that the guest molecules encounter a greater physical barrier in escaping the host framework, compared to the relatively open channel structures.

The structural characteristics and thermal parameters are summarised in **Table 6.4**, for the above mentioned four inclusion compounds, as well as the inclusion compounds of the host with other volatile guests, which are discussed in this chapter.

Table 6.4 Relevant thermal data and structural parameters for the inclusion compounds of the host with volatile guests.

Inclusion compound	T_{on} - T_b (°C)†	E_a of desolvation (kJ mol^{-1})	Inclusion mode	Packing efficiency (%)	H-bond type and bond length range D···A (Å)‡
BINAP•1.5DOX‡	-17.5	86(2)	Interconnected channel	69.0	**H···G** 2.676(2) -2.760(3)
BINAP•3.5DOX	/	1st step 61(6) 2nd step 63(8)	Interconnected channel	68.9	**H···G** 2.679(2) -2.685(2)
BINAP•DMSO	-35.8	94(3)	Interconnected cage	68.3	**H···G** 2.662(8) -2.727(7)
BINAP•2DMSO	/	1st step 79(5) 2nd step 85(5)	Interconnected channel	68.4	**H···G** 2.641(3) -2.666(2)
BINAP•1.5MOP(I)	-20.6	/	Interconnected channel	68.9	**H···G** 2.762(4) -2.82*
BINAP•1.5MOP(II)	/	/	Interconnected channel	70.0	**H···G** 2.728(3) -2.814(3)
BINAP•1.5THF	8.1	/	Interconnected cage	68.0	**H···G** 2.61(1) -3.05(2)
BINAP•ACT	9.1	85(4)	Channel	67.8	**H···G** 2.807(2) -2.849(2)

† No T_{on} - T_b values were calculated for the multi-step desolvation reactions.

‡ **D···A** Donor···Acceptor.

H···G (host)O-H···O(guest) hydrogen bond with bond lengths of O···O, or (host)O-H···N(guest) hydrogen bond with bond lengths of O···N in the case of morpholine as guest molecule.

* This value is an average of the distances of O···O, due to disorder.

Two polymorphs of the 1:1.5 inclusion compound with morpholine guest were obtained at different temperatures. Form I, which was obtained at 60°C and crystallises in $P2_1/c$ with $Z = 4$, is isostructural to **BINAP•1.5DOX** with respect to the packing and conformation of the host molecules and the positions of the guest molecules of similar shape and size. In **BINAP•1.5MOP**(I), the morpholine located in the general position is, however, disordered. Form II, obtained at 4°C, crystallises in $P2_1/n$ with $Z = 8$. The crystal packing in both the forms is remarkably similar, the conformations of the host molecules are, however, different (this is discussed in **Chapter 7**). This close relationship between the two structures is entirely responsible for the similarity in their experimental and calculated XRD patterns. But the thermal desolvation behaviours for the two forms show a difference. Form I desorbs in a single step, while form II desorbs

in two step with the first step corresponding the loss of half mole of morpholine. No explanation could be given from their structure analyses.

Although morpholine and 1,4-dioxane are similar in molecular shape and size, competition experiments show that the host preferentially entrapped the former guest to a small extent (the selectivity parameter K = 3.5). The lattice energy calculation results indicate that **BINAP•1.5MOP**(II) is the most stable system. This gives a possible explanation for the selective favour toward morpholine.

The host form 1:1 and 1:1.5 inclusion compounds with acetone and tetrahydrofuran respectively, at both high and low crystallisation temperatures. In **BINAP•ACT**, the acetone oxygen is the acceptor of two hydrogen bonds from adjacent host molecules, giving rise to a closed tetramer comprising two hosts and two guests. The acetone molecules are located in channels. In **BINAP•1.5THF**, the host is hydrogen bonded to the THF in general position, while the THF located at the diad acts as an acceptor to two symmetry related hosts. All THF guests are located in interconnected cavities. The thermal behaviours of the two inclusion compounds are similar: both of them desolvate in a single step and at temperatures which are about 8 - 9°C higher than the normal boiling point of the guest solvent. The selectivity between acetone and THF is concentration dependent, having the selective parameter $Q_{ACT:THF}$ = 0.56. In addition an isothermal kinetic study for the desolvation of **BINAP•ACT** has been carried out and it revealed that the desolvation reaction complied with the A2 kinetic law, which accounts for the sigmoidal curve according to two-dimensional growth of the reaction interface (Avrami, 1939; Erofe'ev & Dokl, 1946).

The crystal structure of the unsolvated α-phase of the host compound **BINAP** was obtained by crystallising the host from propionaldehyde. In this structure, which is of space group Iba2 with Z =8, one of the hydroxyl groups is hydrogen bonded to the adjacent host molecule and another one is not hydrogen bonded, giving rise to one-dimensional chain along the *c* axis, via hydrogen bonds O-H···O with O···O distance of 2.839(2)Å. The host molecules of this α-phase structure are packed more densely, with packing efficiency of 69.4, which is the highest compared with those of all other solvated structures discussed in this thesis.

Table 6.5 Crystal data, data collection and final refinement parameters.

Inclusion compound	**BINAP•1.5DOX**	**BINAP•3.5DOX**	**BINAP•1.5THF**
Molecular formula	$C_{20}H_{14}O_2$•1.5$C_4H_8O_2$	$C_{20}H_{14}O_2$•3.5$C_4H_8O_2$	$C_{20}H_{14}O_2$•1.5C_4H_8O
Guest	1,4-Dioxane	1,4-Dioxane	Tetrahydrofuran
Formula weight ($gmol^{-1}$)	418.47	594.68	394.47
Crystal Data			
Crystal system	Monoclinic	Triclinic	Orthorhombic
Space group	$P2_1/c$	$P\bar{1}$	Fdd2
a (Å)	8.938(1)	10.322(1)	14.651(2)
b (Å)	28.013(2)	12.023(1)	55.471(6)
c (Å)	9.137(1)	13.432(1)	10.259(1)
α (°)	90	111.651(3)	90
β (°)	110.213(5)	91.955(3)	90
γ (°)	90	90.716(3)	90
Volume ($Å^3$)	2146.8(4)	1547.9(2)	8338(2)
Z	4	2	16
Calculated density D_c (gcm^{-3})	1.295	1.276	1.257
μ (mm^{-1})	0.089	0.092	0.082
F(000)	888	636	3360
Data collection			
Temperature (K)	173 (2)	173 (2)	173 (2)
Range scanned, θ (°)	2.48 - 27.48	2.72 - 26.13	3.04 – 26.04
Range of indices, *h*, *k*, *l*	±10/±36/±11	0,12/±14/±15	±15/-58,33/-7,12
No. of measured reflections	18862	10436	9863
No. of unique reflections	4394	4474	1537
No. of reflections observed with $I > 2\sigma(I)$	2973	3189	1412
R_{int}	0.068	0.037	0.0205
Structure refinement			
Data / restraints / parameters	4394 / 2 / 289	4474 / 4 / 397	1537 / 5 / 238
R indices R_1 / wR_2 [$I > 2\sigma(I)$]	0.0764 / 0.2007	0.0464 / 0.1140	0.0993 / 0.2664
R_1 / wR_2 (all data)	0.1113 / 0.2254	0.0752 / 0.1306	0.1052 / 0.2748
Goodness of fit on F^2, S	1.062	1.025	1.032
Weighting scheme [where P = $(F_o^2+2F_c^2)/3$]	w = $1/[\sigma^2(F_o^2)+(0.1007P)^2+1.6226\ P]$	w = $1/[\sigma^2(F_o^2)+(0.0643P)^2+0.5059P]$	$w = 1/[\sigma^2(F_o^2)+(0.1868P)^2+74.7998P]$
Max. / Mean shift (esd)	0.000 / 0.000	0.001 / 0.000	0.002 / 0.000
Extinction coefficient	0.015(5)	0.007(1)	0.0028(8)
Flack x parameter			1(5)
Max./Min. height in difference electron density map ($eÅ^{-3}$)	0.800 / -0.516	0.303 / -0.245	0.824 / -0.564

Table 6.5 (cont.) Crystal data, data collection and final refinement parameters.

Inclusion compound	**BINAP•DMSO**	**BINAP•2DMSO**	**BINAP•ACT**
Molecular formula	$C_{20}H_{14}O_2 \bullet C_2H_6OS$	$C_{20}H_{14}O_2 \bullet 2C_2H_6OS$	$C_{20}H_{14}O_2 \bullet C_3H_6O$
Guest	Dimethyl sulfoxide	Dimethyl sulfoxide	Acetone
Formula weight ($gmol^{-1}$)	364.44	442.57	344.39
Crystal Data			
Crystal system	Monoclinic	Monoclinic	Monoclinic
Space group	$P2_1/n$	$P2_1/c$	$P2_1/n$
a (Å)	20.792(3)	8.453(1)	8.083 (1)
b (Å)	8.883(1)	8.931(1)	21.290(1)
c (Å)	20.800(3)	29.573(3)	11.094(1)
α (°)	90	90	90
β (°)	105.115(5)	92.928(5)	107.36(1)
γ (°)	90	90	90
Volume ($Å^3$)	3708.8(9)	2229.7(4)	1822.2(3)
Z	8	4	4
Calculated density D_c (gcm^{-3})	1.305	1.318	1.255
μ (mm^{-1})	0.193	0.267	0.082
F(000)	1536	936	728
Data collection			
Temperature (K)	293 (2)	293 (2)	293 (2)
Range scanned, θ (°)	2.03 - 25.94	2.72 - 25.31	3.82 - 26.46
Range of indices, *h*, *k*, *l*	-13,25/-9,10/-24,25	-10,6/-10,9/-35,33	0,10/±26/±13
No. of measured reflections	14062	5681	5938
No. of unique reflections	6074	3250	3541
No. of reflections observed with $I > 2\sigma(I)$	4126	2652	1973
R_{int}	0.0472	0.036	0.0346
Structure refinement			
Data / restraints / parameters	6074 / 8 / 486	3241 / 4 / 308	3541 / 4 / 247
R indices R_1 / wR_2 [$I > 2\sigma(I)$]	0.1197 / 0.2698	0.0459 / 0.1061	0.0471 / 0.1134
R_1 / wR_2 (all data)	0.1625 / 0.2886	0.0604 / 0.1146	0.0978 / 0.1308
Goodness of fit on F^2, *S*	1.160	1.051	0.980
Weighting scheme [where $P = (F_o^2+2F_c^2)/3$]	$w = 1/[\sigma^2(F_o^2)+(0.0322P)^2+40.2883P]$	$w = 1/[\sigma^2(F_o^2)+(0.0322P)^2+1.5845P]$	$w = 1/[\sigma^2(F_o^2)+(0.0646P)^2+0.0000P]$
Max. / Mean shift (esd)	0.001 / 0.000	0.003 / 0.000	0.001 / 0.000
Extinction coefficient	0.0009(3)	0.005(3)	0.042(6)
Max./Min. height in difference electron density map ($eÅ^{-3}$)	0.976 / -0.486	0.308 / -0.241	0.193 / -0.130

Table 6.5 (cont.) Crystal data, data collection and final refinement parameters.

Compound	**BINAP•1.5MOP(I)**	**BINAP•1.5MOP(II)**	**BINAP**
Molecular formula	$C_{20}H_{14}O_2$•1.5C_4H_9ON	$C_{20}H_{14}O_2$•1.5C_4H_9ON	$C_{20}H_{14}O_2$
Guest	Morpholine	Morpholine	/
Formula weight ($gmol^{-1}$)	417.00	417.00	286.34
Crystal Data			
Crystal system	Monoclinic	Monoclinic	Orthorhombic
Space group	$P2_1/c$	$P2_1/n$	Iba2
a (Å)	9.139(2)	18.2465(2)	15.637(3)
b (Å)	27.672(6)	27.6212(7)	21.523(4)
c (Å)	9.204(2)	9.2313(5)	8.595(2)
α (°)	90	90	90
β (°)	112.98(3)	113.851(1)	90
γ (°)	90	90	90
Volume ($Å^3$)	2143.0(8)	4255.2(3)	2893(1)
Z	4	8	8
Calculated density D_c (gcm^{-3})	1.292	1.302	1.315
μ (mm^{-1})	0.086	0.086	0.084
F(000)	888	1776	1200
Data collection			
Temperature (K)	173 (2)	173 (2)	173 (2)
Range scanned, θ (°)	2.53 - 25.58	2.34 – 27.13	3.12 - 26.40
Range of indices, *h*, *k*, *l*	0,10 / ±32 / -11,9	±23/-35,34/±11	-19,17/±26/-10,9
No. of measured reflections	5845	15856	8483
No. of unique reflections	3758	9210	2804
No. of reflections observed with $I > 2\sigma(I)$	1984	4495	2282
R_{int}	0.0343	0.0480	0.0420
Structure refinement			
Data / restraints / parameters	3758 / 2 / 344	9205 / 4 / 576	2804 / 1 / 256
R indices R_1 / wR_2 [$I > 2\sigma(I)$]	0.0917 / 0.2133	0.0668 / 0.1701	0.0347 / 0.0689
R_1 / wR_2 (all data)	0.1704 / 0.2530	0.1578 / 0.2068	0.0508 / 0.0745
Goodness of fit on F^2, *S*	1.052	1.039	1.065
Weighting scheme [where $P = (F_o^2+2F_c^2)/3$]	$w = 1/[\sigma^2(F_o^2)+(0.0925P)^2+2.1900P]$	$w = 1/[\sigma^2(F_o^2)+(0.0975P)^2+0.1984P]$	$w = 1/[\sigma^2(F_o^2)+(0.0377P)^2+0.000P]$
Max. / Mean shift (esd)	0.000 / 0.000	0.009 / 0.001	0.042 / 0.005
Extinction coefficient	0.011(3)	0.0017(9)	0.0050(5)
Flack x parameter			-1.5(1)
Max./Min. height in difference electron density map ($eÅ^{-3}$)	0.458 / -0.345	0.645 / -0.435	0.129 / -0.140

7 THE HOST CONFORMATIONS

The host conformations of the inclusion compounds, of which structures have been elucidated in this study, are discussed collectively in this chapter. For ease of reference, the numbering schemes for the host compounds are again shown in **Scheme 7.1**.

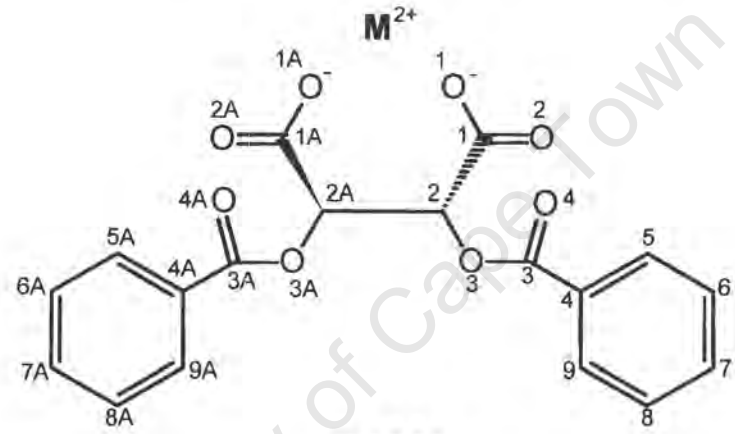

DBTAM

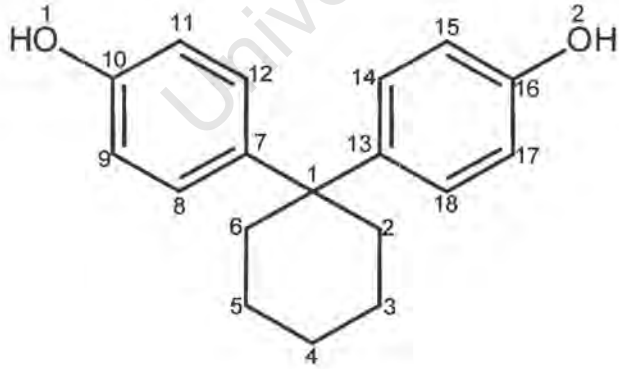

DHPC

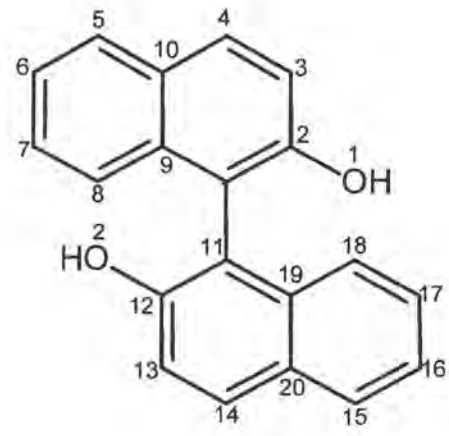

BINAP

Scheme 7.1

Host DBTAM

A search of CSD (version 5.22, 2001) revealed no previous structures involving O,O'-dibenzoyl-tartrate. The molecule is chiral with two chiral centres at C(2) and C(2A). The crystal structures **MGDAME**, **CADAME** and **SRDAME** are that of the R-enantiomer of O,O'-dibenzoyl-tartrate. The latter two structures are isostructural. The differences in host packing between the three structures were discussed in **Chapter 3**. The comparison of the geometry of the O,O'-dibenzoyl tartaric moiety of the tartrate host molecule is described in this chapter. The general conformation of the host molecule, extracted from **CADAME**, is shown in **Figure 7.1**.

Selected bond and torsion angles, which are important in describing the orientation of the host molecule, are given in **Table 7.1**. The dihedral angle, υ, between the planes of the two phenyl rings is also recorded in this table. **Figure 7.2** shows the three molecular structures viewed along the central bond C(2A)-C(2) which joins the two benzoyl moieties.

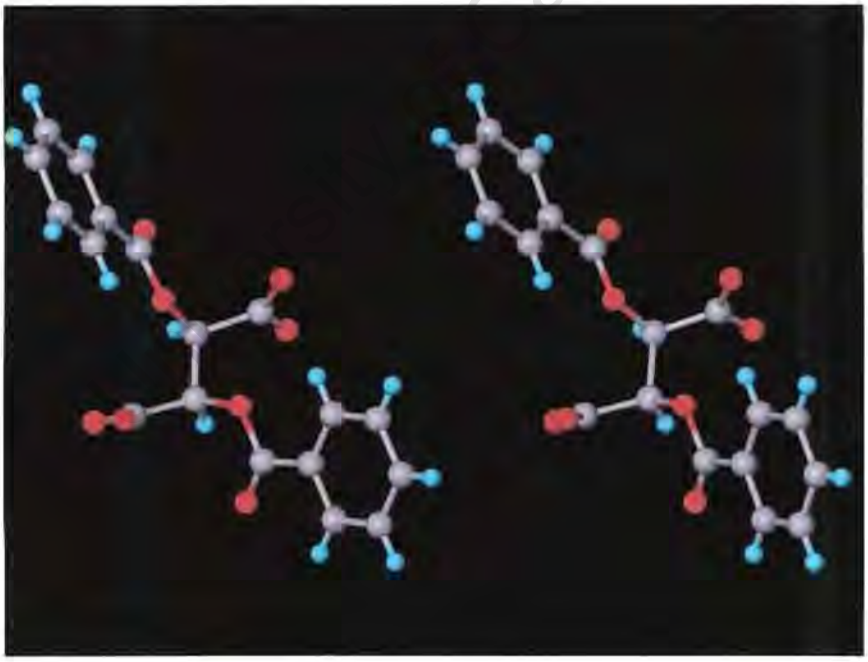

Figure 7.1 Stereoscopic view of the general conformation of the host **DBTAM**, which is extracted from the structure of **CADAME**.

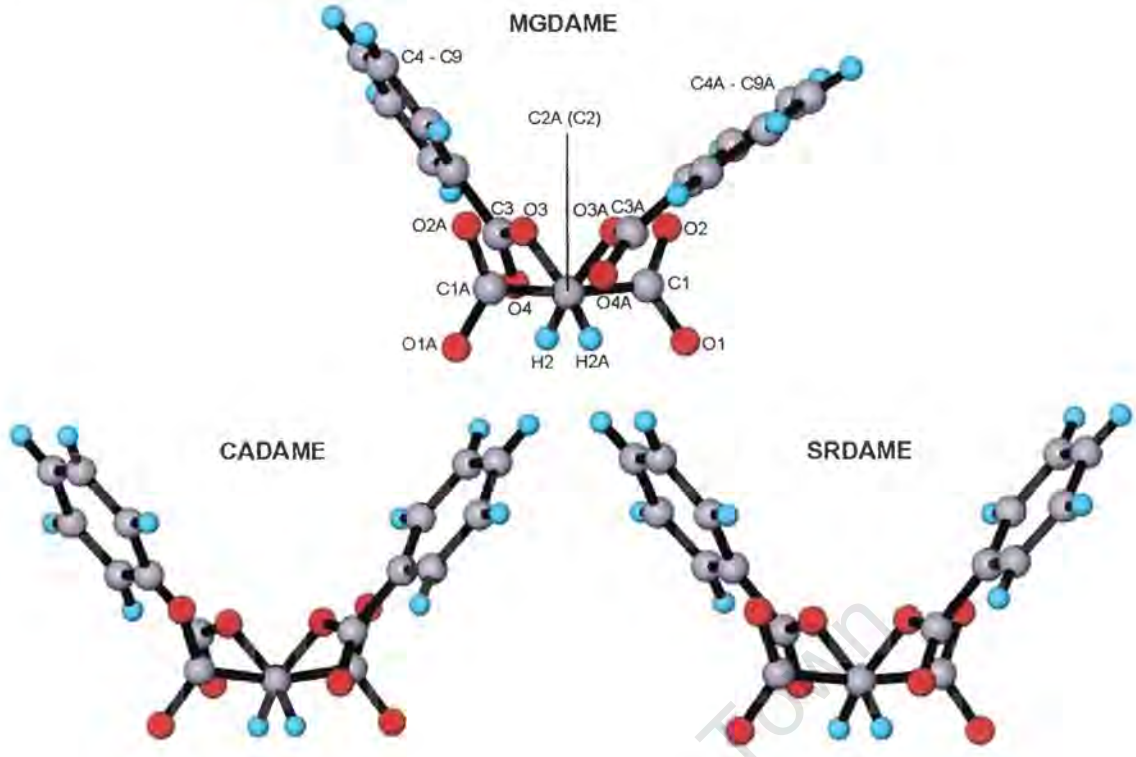

Figure 7.2 View of the host along the central bond C(2A)-C(2) in the three structures.

Table 7.1 Selected bond angels, dihedral angel and torsion angles in the three structures containing O,O'-dibenzoyl-(2R, 3R)-tartrate.

Angle (°)*	**MGDAME**	**CADAME**	**SRDAME**
at ∠C2	107.34 - 112.0	109.1 - 111.6	107.9 – 112.3
∠O(1)-C(1)-O(2) †	127.0 - 127.3	127.2	127.5
∠C(2)-O(3)-C(3) †	114.1 - 116.2	115.8	114.9
∠O(3)-C(3)-C(4) †	112.4 - 113.4	112.2	112.2
$\angle C_{ar}$-C_{ar}-C_{ar}	118.7 - 121.3	119.6 - 120.5	119.7 - 120.4
Dihedral angle υ	89.4	69.2	70.8
τ_1 = O(3)-C(2)-C(2A)-O(3A)	74.3	79.7	77.0
τ_2 = C(1)-C(2)-C(2A)-C(1A)	171.8	164.0	168.8
τ_3 = C(3)-O(3)-C(2)-C(2A) †	161.4 - 168.2	153.7	156.0
τ_4 = O(3)-C(3)-C(4)-C(5) †	11.9 - 12.0	7.0	8.6
τ_5 = O(2)-C(1)-C(2)-C(3) †	9.2 - 22.8	16.6	15.1

* Standard deviations are in the range 0.09 - 1.2° for **MGDAME** and 0.1 - 0.2° for **CADAME** and **SRDAME**.

† The structurally equivalent angles are not shown. For example, τ_1 represents either O(3)-C(2)-C(2A)-O(3A) or O(3A)-C(2A)-C(2)-O(3) in **MGDAME**.

The host molecule adopts a symmetrical conformation in both of the structures **CADAME** and **SRDAME**, since there is a two-fold rotation axis perpendicular to the central bond C(2)-C(2A). The orientation of the host molecule is thus very similar in the two isometric structures, as can be seen from the specific view shown in **Figure 7.2**. The conformation of the host remains remarkably constant in the structure **MGDAME**. The only notable variation is the dihedral angle υ and the torsion angle $\tau 3$, which represents either C(3)-O(3)-C(2)-C(2A) or C(3A)-O(3A)-C(2A)-C(2). This implies that the two phenyl ring systems of the host are relatively flexible and can twist with respect to each other.

In all three structures, the bond lengths are in good agreement with the typical bond lengths of the similar type (Allen *et al.* 1992). The bond length ranges are schematically shown in **Figure 7.3**. The bond lengths of the carboxylate groups are of interest, and range from 1.238(8) to 1.256(3)Å, thus falling between the typical C=O value of 1.21Å and C-OH value of 1.31Å (Allen *et al.* 1987), which is consistent with the delocalisation of the negative charge over the $-CO_2$ moieties.

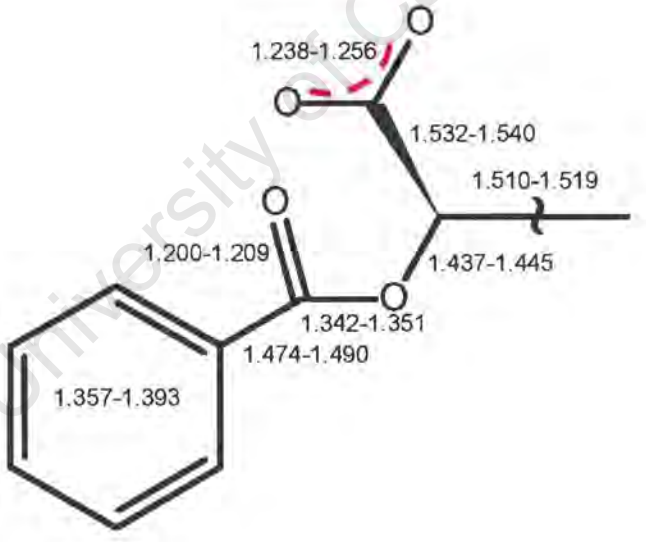

Figure 7.3 Bond length ranges (Å) of the host observed in the three structures. Standard deviations are in the range 0.002 - 0.018Å for **MGDAME** and 0.001 - 0.003Å for **CADAME** and **SRDAME**.

Host DHPC

The conformation of the host **DHPC**, of which nine crystal structures of inclusion compounds with xylidine isomers have been discussed in **Chapter 4 (DHPC and Xylidines)**, is described here. Parameters obtained from the structure **DHPC•2.5(26X)** have been excluded from the analysis due to incomplete solution of the structure with $R_1 = 0.1885$.

The general conformation of **DHPC** is shown in **figure 7.4** and may be best described by the torsion angles τ_1 and τ_2, illustrated in **Figure 7.5**, and by the dihedral angle between the planes of the two phenyl rings. Labelling of the host in each structure, although following the prescribed numbering scheme (**Scheme 7.1**), was initially done arbitrarily and thus various combination of τ_1 and τ_2 for each structure would be obtained, therefore it is not feasible to compare the various angles directly. A systematic search was performed for the combination of τ_1 and τ_2, which yielded the minimum absolute values for τ_1 and τ_2, with $\tau_1 < \tau_2$. The results are listed in **Table 7.2**

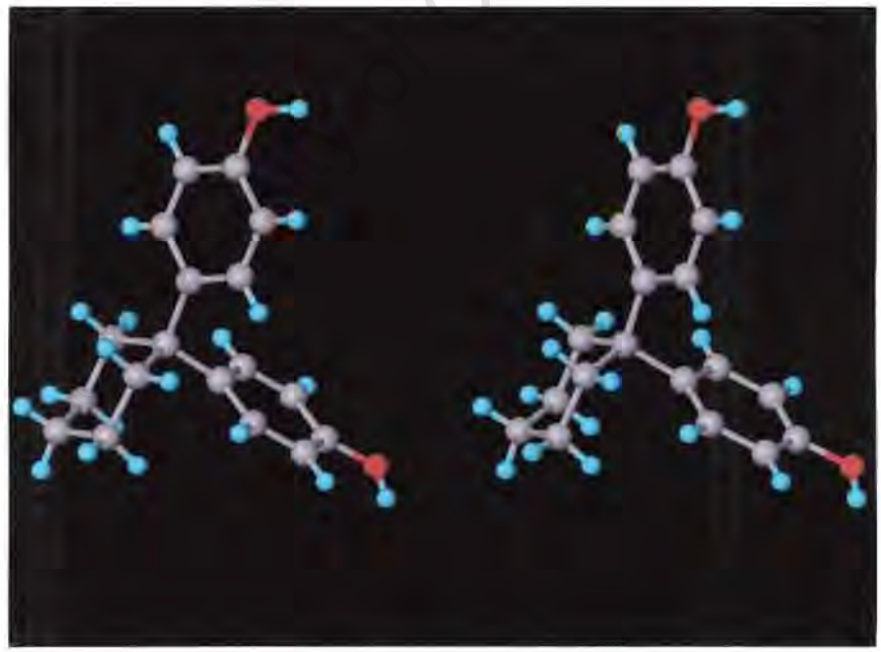

Figure 7.4 Stereoscopic view of the general conformation of the host **DHPC**, which is extracted from the structure of **DHPC•35X**.

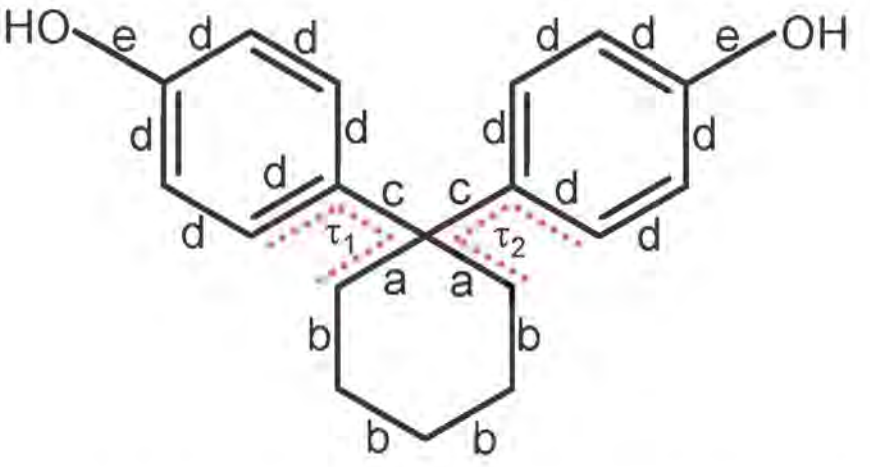

Figure 7.5 Torsion angles τ_1 and τ_2 describing the host conformation and five types of bonds classifying the host **DHPC**.

Table 7.2 Torsion and dihedral angles describing the host conformation of **DHPC**.

Inclusion compounds		τ_1 / °	τ_2 / °	$\Delta\tau = \tau_2 - \tau_1$ / °	Dihedral angle / °
DHPC•26X		0.5(4)	16.9(3)	16.4	84.24(8)
DHPC•1.5(26X)		31.9(3)	56.8(3)	24.9	89.88(7)
DHPC•3(26X)	(X)*	25.2(5)	35.9(5)	10.7	76.52(9)
	(Y)*	15.3(5)	34.6(5)	19.3	79.37(9)
DHPC•0.5(23X)		32.7(2)	55.7(2)	23.0	89.52(5)
DHPC•2(23X)		1.4(2)	18.0(2)	16.6	87.78(5)
DHPC•0.5(34X)•H_2O	(X)*	0.7(4)	16.7(4)	16.0	86.04(7)
	(Y)*	0.8(4)	16.4(4)	15.6	87.16(7)
DHPC•34X		23.0(6)	38.0(5)	15.0	79.6(1)
DHPC•35X		4.3(4)	19.1(3)	14.8	84.35(7)

* X and Y are symbols for the two host molecules in the asymmetric unit.

The τ_1 and τ_2 exhibit considerable variation in values with τ_1 varying from 0.5(4)° to 32.7(2)° and τ_2 varying from 16.4(4)° to 56.8(3)°. This indicates that the host **DHPC** is relatively flexible in respect of the two phenol rings and the cyclohexane ring. The three rings system of **DHPC** can twist with respect to each other in order to accommodate guest molecules that are different in stiochiometry, size and shape. The dihedral

angles, lying in a small range of 79.37(9) - 89.88(7)°, are relatively constant, showing the rigidity of **DHPC**, in which the two aromatic rings tend to be perpendicularly orientated due to the repulsion between the two phenol rings. The smallest dihedral angle of **DHPC**, observed in the Cambridge Structural Database System (CSDS version 5.22, 2001), is 75.16(7)°, which occurred in the structure of **DHPC** and 2,4-lutidine (Caira *et al.* 1998).

The cyclohexane rings are in the chair conformation in all structures presented in **Table 7.2**, and the puckering parameter θ, as defined by Cremer and Pople (1975), is always in the range 175.9 - 179.9°. The aromatic rings are all planar, and the maximum root mean squared (RMS) deviation from the least-squares plane through the ring atoms are in the range 0.0007 - 0.015Å. Based on the work done by Duax and Norton (1975), the RMS deviation of the ring with value not less than 0.03Å indicate significant deviation from planarity. The bond angles of the aromatic ring are in the acceptable range of 115.5(3) - 123.1(3)°.

The bonds of **DHPC** may be classified into five different types, as shown in **Figure 7.5**. Statistical analysis for the bond lengths was performed for structures of higher precision on the basis of R factor was less than 0.07. Thus only six out of eight structures were included and the statistical results are summarised in **Table 7.3**, in which the maximum, minimum, median and mean values for each type of bond are reported. For the structures **DHPC•3(26X)** and **DHPC•34X**, of which R factors are about 0.10, the bond length ranges for each type of bond are reported in **Table 7.4**. The typical bond length ranges for each type of bond (Allen *et al.* 1992), which are extracted from International Tables For Crystallography (volume C), are also listed in **Table 7.4**.

The results in **Table 7.3** and **7.4** show that, all of the bond lengths of **DHPC** are comparable to the typical values of the same type. It is noted that the carbon-carbon bonds within the same cyclohexane ring are different: the type **a** bond lengths are longer than the type **b** bond lengths. This is possibly due to repulsion between the C(2) and C(6) atoms and between the two aromatic rings. This is also notable from the angle C(6)-C(1)-C(2), varying from 105.0(3) - 106.8(2)°, which is smaller than the other angles of the cyclohexyl ring, which varying from 110.1(4) - 115.4(3)°, possibly due to the same reason.

Table 7.3 Bond length statistics of host **DHPC** in the six structures with $R_1 < 0.07$.

	Minimum / Å	Maximum / Å	Median / Å[1]	Mean / Å[2]	N[3]
a = C_{sp3} - C_{sp3}	1.540(3)	1.554(3)	1.545	1.547(4)	14
b = C_{sp3} - C_{sp3}	1.515(4)	1.532(4)	1.524	1.524(5)	28
c = C_{sp3} - C_{ar}	1.531(3)	1.548(4)	1.541	1.540(4)	14
d = $C_{ar} \cong C_{ar}$	1.368(4)	1.402(3)	1.385	1.385(7)	84
e = C_{ar} - **O**	1.371(3)	1.387(2)	1.377	1.378(5)	14

1. The sample median, m, has the property that half of the observations in the sample exceed m and half fall short of it.
2. The unweighted sample mean, calculated as described by Allen *et al.* (1992)
3. n, the number of observations in the sample.

Table 7.4 Bond length ranges for host **DHPC** observed in structures of **DHPC•3(26X)** and **DHPC•34X**.

	DHPC•3(26X) / Å	DHPC•34X1 / Å	Typical range[1]
a = C_{sp3} - C_{sp3}	1.550(5) - 1.562(5)	1.542(6) – 1.549(6)	1.533(10) - 1.544(10)
b = C_{sp3} - C_{sp3}	1.481(5) - 1.530(5)	1.519(6) – 1.539(6)	1.516(14) - 1.532(14)
c = C_{sp3} - C_{ar}	1.522(5) - 1.553(5)	1.546(6) – 1.551(5)	1.517(16) - 1.539(16)
d = $C_{ar} \cong C_{ar}$	1.370(5) - 1.396(4)	1.358(6) – 1.401(5)	1.375(13) - 1.391(13)
e = C_{ar} - **O**	1.369(4) - 1.373(5)	1.379(4) – 1.383(5)	1.353(15) - 1.373(15)

1. Taken from reference Allen *et al.* (1992)

Host BINAP

A total of seventeen crystal structures of inclusion compounds of host **BINAP** and one structure of the apohost were elucidated in this study (**Chapter 5** and **6**). The host conformations of these inclusion compounds are compared with that of guest-free host, and with those containing the same host found in the CSD.

The general conformation of host **BINAP** is shown in **Figure 7.6**. One torsion angle τ_o governs the host conformation and three types of bond (**a**, **b** and **c**) classify the host, as shown in **Figure 7.7**. **Table 7.5** lists the torsion angle τ_o and bond length ranges for the three types of bond for each of the eighteen structure solutions presented in this study.

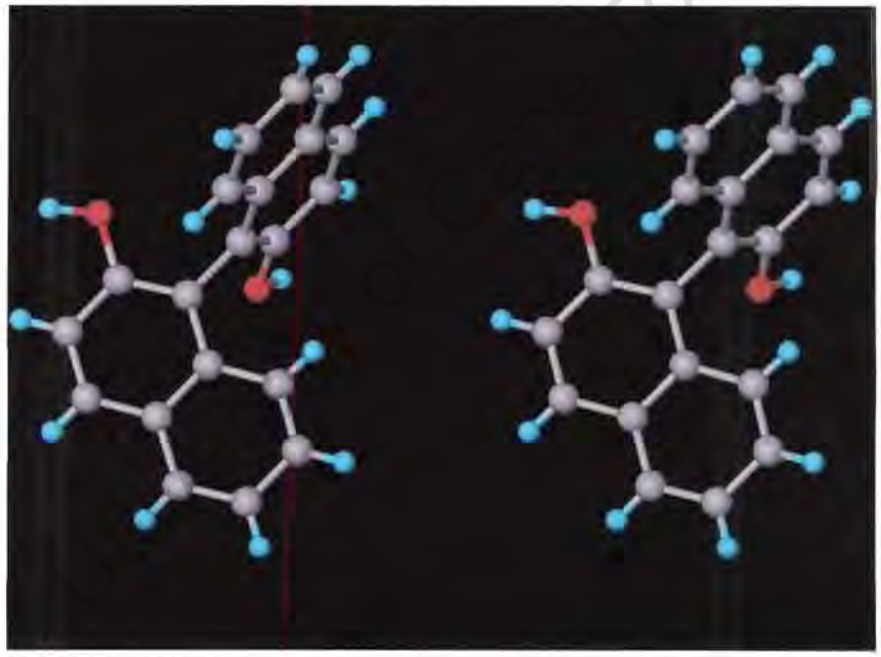

Figure 7.6 Stereoscopic view of the general conformation of the host **BINAP**, which is extracted from the structure of **BINAP•2DMSO**.

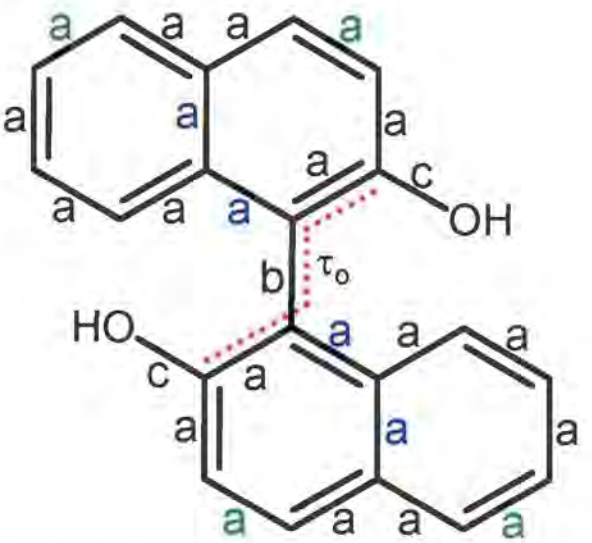

Figure 7.7 Torsion angle τ_o and classification of bonds for the host **BINAP**. τ_o represents any of the angles: C(2)-C(1)-C(11)-C(12) or C(2)-C(1)-C(1)'-C(2)'. C(1)' and C(2)' represent symmetry related atoms in the case of the host molecule possesses a symmetrical conformation (*i.e.* two-fold symmetry).

Table 7.5 shows that the torsion angle τ_o is distributed over a fairly wide range from 73.5(3)° in **BINAP•2(24LUT)** to 104.8(3)° in **BINAP•2DMSO**. This is the characteristic behaviour of the scissor-type host compounds, in that the two naphthalene plane systems of the host molecule can twist with respect to each other about the central bi-naphthol bond, in order to accommodate guest molecules of different size and geometry. A search of the CSD yielded 37 entries containing this host molecule, with this torsion angle τ_o varying from 68.9° to 109.5°, and averaging 90.1°. Among the 37 structures, five are structures of host alone with τ_o range 87.8° - 88.3° for the racemic form and 76.7° - 77.2° for the enantiomeric form. Distribution of τ_o for the inclusion compounds discussed in this study fell in the general pattern of distribution of τ_o for the 32 clathrates structures found in CSD, as shown in **Figure 7.8**. The structures of the inclusion compounds of **BINAP•1.5DOX** and **BINAP•1.5MOP(I)** are isostructural (see **Chapter 6**) and it is noted that their τ_o of host molecule are 99.9(3)° and 102.8(5)° respectively, differing about 2.9°. The τ_o values for **BINAP•1.5MOP(II)** deviate about 2.4° and 4.2° form that of **BINAP•1.5MOP(I)**. The difference in τ_o values in comparing with **BINAP•1.5MOP(I)** and **BINAP•1.5MOP(II)** gives strong evidence for the existence of the two polymorphs, even though their crystal packing appears similar (see **Chapter 6**).

Table 7.5 Torsion angles (τ_0) and bond length ranges observed for **BINAP** molecule.

Inclusion compounds		τ_o / °	a = $C_{ar} \cong C_{ar}$ min. / Å max. / Å	b = C_{ar} - C_{ar} min. / Å max. / Å	c = C_{ar} - O min. / Å max. / Å
BINAP•2(2PIC)		95.3(2)	1.360(2)	1.493(3)	1.364(2)
			1.428(2)		
BINAP•2(3PIC)		83.5(2)	1.356(2)	1.494(2)	1.358(2)
			1.424(2)		1.359(2)
BINAP•2(4PIC)		103.1(2)	1.354(3)	1.498(2)	1.357(2)
			1.427(2)		1.361(2)
BINAP•2(26LUT)		77.5(7)	1.356(6)	1.491(7)	1.365(5)
			1.426(5)		
BINAP•2(24LUT)		73.5(3)	1.370(3)	1.515(4)	1.382(2)
			1.455(3)		
BINAP•35LUT		85.1(3)	1.354(4)	1.490(3)	1.365(3)
			1.425(3)		1.371(3)
BINAP•35X		88.3(2)	1.352(3)	1.498(2)	1.353(2)
			1.428(2)		1.366(2)
BINAP•2(26X)		75.9(4)	1.356(4)	1.493(5)	1.359(3)
			1.428(3)		
BINAP•3(23X)		94.8(5)	1.343(7)	1.486(5)	1.358(5)
			1.433(6)		1.362(5)
BINAP•3.5DOX		101.4(2)	1.354(3)	1.492(3)	1.363(3)
			1.430(3)		1.366(3)
BINAP•1.5DOX		99.9(3)	1.352(4)	1.492(3)	1.359(3)
			1.426(3)		1.360(3)
BINAP•2DMSO		104.8(3)	1.356(4)	1.495(3)	1.360(3)
			1.430(3)		1.363(3)
BINAP•DMSO	X*	95.5(9)	1.32(1)	1.50(1)	1.37(1)
			1.45(1)		1.375(9)
	Y*	100.3(9)	1.34(1)	1.51(1)	1.368(9)
			1.44(1)		1.36(1)
BINAP•1.5MOP(I)		102.8(5)	1.347(6)	1.496(7)	1.365(6)
			1.436(8)		1.369(6)
BINAP•1.5MOP(II)	X*	107.4(3)	1.359(3)	1.494(3)	1.366(3)
			1.432(3)		1.370(3)
	Y*	100.6(3)	1.357(3)	1.500(3)	1.352(3)
			1.432(3)		1.366(3)
BINAP•1.5THF		95(1)	1.32(2)	1.49(1)	1.372(9)
			1.47(1)		1.368(9)
BINAP•ACT		92.1(2)	1.350(3)	1.502(2)	1.365(2)
			1.428(2)		1.366(2)
BINAP		88.5(2)	1.351(3)	1.495(2)	1.363(2)
			1.431(2)		1.378(2)

* X and Y are symbols for the two host molecules in the asymmetric unit.

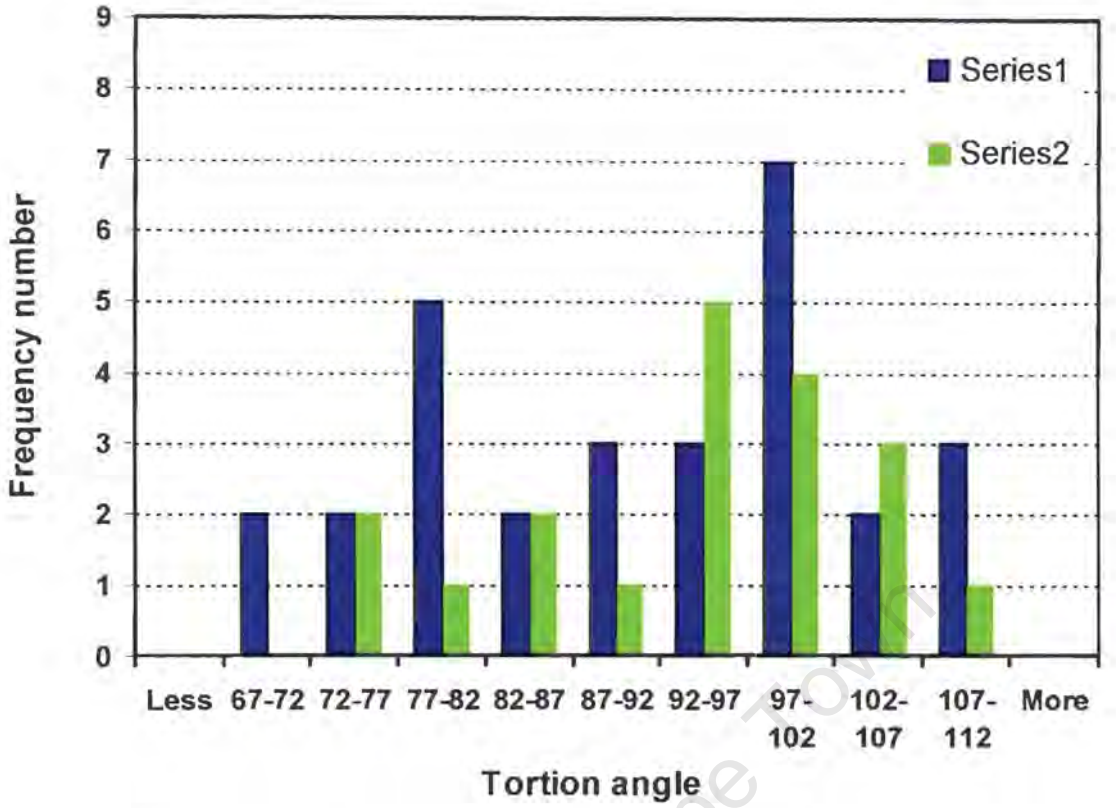

Figure 7.8 Distribution of the torsion angle τ_o of host **BINAP** in
Series 1: thirty-two clathrates structures of the same host found in CSD.
Series 2: Seventeen clathrates structures elucidated in this study.

All bond lengths and angles observed in the structures are comparable with known values for similar structures (Allen *et al.* 1992). The typical bond length ranges, which are extracted from International Tables For Crystallography (volume C), are 1.484(7)-1.493(7)Å and 1.353(15)-1.373(15)Å for **b** and **c** types of bond respectively, and 1.356(7)-1.429(11)Å for overall naphthalene ring system (type **a**). It is noted that, in contrast to benzene, the $\mathbf{C_{ar}}$ - $\mathbf{C_{ar}}$ bonds in the same naphthalene ring are not the same. In particular, the type **a** bonds marked as **a** in green in **Figure 7.7**, which represent either C(3)-C(4) or C(13)-C(14) and C(5)-C(6) or C(15)-C(16), having bond lengths falling in the range of 1.32(2) - 1.382(3)Å, is considerably shorter than the bond **a** in blue, which represent either C(1)-C(9) or C(11)-C(19) and C(9)-C(10) or C(19)-C(20), having bond lengths in the range of 1.41(1) - 1.455(3)Å. This is possibly attributed to the hybrid resonance of the naphthalene structure and the repulsion between the two naphthalene ring systems. The naphthalene rings are all planar, and the maximum root mean squared (RMS) deviation of the ten fitted ring atoms from the least-squares plane are in the range 0.0036 - 0.0287Å.

8 FINAL REMARKS

This study has explored the structure/reactivity/selectivity relationships for a variety of inclusion compounds which contain small volatile organic guests. The host compounds vary from alkaline-earth metal salts (**DBTAM**) to organic diol compounds (**DHPC** and **BINAP**). The crystal structures of all the inclusion compounds obtained have been elucidated. These inclusion compounds form a diverse range of lattice inclusion types depending on the packing arrangement of the host molecules. They vary from tubulate (the guest molecules are located in one-dimensional channels or interconnecting channels) to laminae (the guest is sandwiched between layers of host molecules) and cryptate (the guest is entrapped in an isolated cage). Selected characteristics of the inclusion compound structures elucidated here are summarised in **Table 8.1**, together with the crystallisation temperatures under which the crystalline compounds were formed.

Each of the two organic diol hosts formed inclusion compounds with differing stoichiometries with a number of specific guests, *i.e.* **DHPC** with xylidines, **BINAP** with 1,4-dioxane and DMSO. The number of guest molecules included per host molecule varied from 0.5 to 3.5 depending on the crystallisation temperatures. Under the condition of approximately constant concentration and ambient pressure, decreasing crystallisation temperature decreased the host:guest ratio. The guest molecules of the high temperature structures tended to show high thermal motions and in most cases were disordered. In the cases of the guests being located at special symmetry-required positions, disordering made up for the lack of symmetry in the original guest molecule, *e.g.* **DHPC•1.5(26X)**, **DHPC•0.5(23X)**. It can be said that disordering take place because of the requirement for the entropy to be increased. The inclusion topology changed with the crystallisation temperatures as the stoichiometry changes and the structural modification is considered as an adaptation to the changing crystallisation environment. The guest molecules were encapsulated into more compact cavities to prevent their escaping from the growing crystals at relative high crystallisation temperatures. This is obviously noted for the host-guest compounds of **DHPC** with 2,3-xylidine, and of **BINAP** with DMSO. The guest molecules of the low temperature

structures are located in relatively open space, *e.g.* the structures of **DHPC•2(23X)** and **BINAP•2DMSO**, where the guests are accommodated between host layers and in channels respectively, whereas in the high temperature structures the guest molecules are entrapped in more constrained space, *e.g.* the structures of **DHPC•0.5(23X)** (closed cage) and of **BINAP•DMSO** (interconnected cage). Moreover, changing crystallisation temperature has resulted in the formation of polymorphic inclusion compounds, *i.e.* the host **BINAP** and morpholine. In the high temperature polymorphic form, *i.e.* **BINAP•1.5MOP**(I), the morpholine guest on the general position is disordered over two arrangements.

Thermal stabilities of the inclusion compounds were estimated by measuring onset temperature, T_{on}, of guest release from the host framework. The difference between T_{on} and the boiling point of pure guest compound, T_b, served as an approximate measure of relative thermal stability for a similar group of inclusion compounds. A feature of the inclusion complexes of the earth-metal salts was that the desolvation of guests began at a higher temperature than the boiling points of the pure guests ($T_{on} > T_b$), with the compound **MGDAME** being an exception with regard to the 2-methoxylethanol guest ($T_{on} - T_b = -7.2^{\circ}C$). For the inclusion compounds of organic diol hosts, the desolvation occurred at a lower temperature than the boiling point of the pure guest ($T_{on} < T_b$), except in the case of acetone and THF being guests ($T_{on} - T_b \approx 8^{\circ}C$). It is noted that in the former inclusion compounds of metal salts, the guest molecules form part of the outer coordination sphere of the metal ions. Whereas in the latter purely organic inclusion compounds, the only interactions between host and guest are weak van der Waals interactions, or at most hydrogen-bonded interactions.

The principles of molecular recognition have been applied in this study in the form of competition experiments. Lattice enclathration competition has a primary application of separation of solvents with similar physical properties, which could not otherwise be readily separated using conventional physical methods, *e.g.* distillation. A series of competition experiments carried out for specific mixtures yielded a selectivity trend. Many efforts have been made to interpret the selectivity trend with the physico-chemical properties of the inclusion compounds formed between the host and the pure guest competitor. It is noted that the selectivity trend is in good agreement with the results of the structure analysis, thermal stabilities and lattice energies, obtained from those inclusion compounds with the same host:guest ratio, for example, the selectivity of xylidines by **DHPC**, picolines by **BINAP**, 2,6- and 2,4-lutidine by **BINAP**, as well as

Table 8.1 The inclusion compounds investigated in this study: structural characteristics and crystallisation temperatures.

Inclusion Compound	Guest	H:G	Space group	Inclusion mode	Cryst. temp.(°C)
MGDAME	2-Methoxyethanol /Ethanol/H_2O	1:1:1:1	$P2_1$	Channel	25
CADAME	2-Methoxyethanol /H_2O	1:2:1	$C222_1$	Channel	25
SRDAME	2-Methoxyethanol /H_2O	1:2:1	$C222_1$	Channel	25
DHPC•26X	2,6-Xylidine	1:1	$P\bar{1}$	Layer	80
DHPC•1.5(26X)	2,6-Xylidine	1:1.5	$P\bar{1}$	Layer	60 / 25
DHPC•2.5(26X)	2,6-Xylidine	1:2.5	$P\bar{1}$	Int. Layer	4
DHPC•3(26X)	2,6-Xylidine	1:3	$P2_1/n$	Int. Channel	1
DHPC•0.5(23X)	2,3-Xylidine	1:0.5	C2/c	Closed Cage	80
DHPC•2(23X)	2,3-Xylidine	1:2	$P\bar{1}$	Layer	25
DHPC•0.5(34X)•H_2O	3,4-Xylidine /H_2O	1:0.5:1	$P\bar{1}$	Layer	25
DHPC•34X	3,4-Xylidine	1:1	C2/c	Layer	80
DHPC•35X	3,5-Xylidine	1:1	$P\bar{1}$	Layer	25
BINAP•2(2PIC)	2-Picoline	1:2	C2/c	Int. Channel	25 / 4
BINAP•2(3PIC)	3-Picoline	1:2	$P2_1/c$	Int. Channel	25 / 4
BINAP•2(4PIC)	4-Picoline	1:2	Pbca	Channel	25 / 4
BINAP•2(26LUT)	2,6-Lutidine	1:2	C2/c	Int. Channel	25 / 4
BINAP•2(24LUT)	2,4-Lutidine	1:2	C2/c	Int. Channel	25 / 4
BINAP•35LUT	3,5-Lutidine	1:1	$P\bar{1}$	Channel	25 / 4
BINAP•35X	3,5-xylidine	1:1	$P\bar{1}$	Channel	25 / 4
BINAP•2(26X)	2,6-xylidine	1:2	C2/c	Int. Channel	25 / 4
BINAP•3(23X)	2,3-xylidine	1:3	Pbca	Int. Channel	25 / 4
BINAP•1.5DOX	1,4-Dioxane	1:1.5	$P2_1/c$	Int. Channel	60
BINAP•3.5DOX	1,4-Dioxane	1:3.5	$P\bar{1}$	Int. Channel	25 / 4
BINAP•DMSO	DMSO	1:1	$P2_1/n$	Int. Cage	60
BINAP•2DMSO	DMSO	1:2	$P2_1/c$	Int. Channel	25 / 4
BINAP•1.5(MOP)(I)	Morpholine	1:1.5	$P2_1/c$	Int. Channel	60
BINAP•1.5(MOP)(II)	Morpholine	1:1.5	$P2_1/n$	Int. Channel	4
BINAP•1.5(THF)	THF	1:1.5	Fdd2	Int. Cage	60 / 25 / 4
BINAP•ACT	Acetone	1:1	$P2_1/n$	Channel	60 / 25 / 4

Note: 'Cryst. temp.' is abbreviated for 'Crystallisation temperature'.

'Int.' is abbreviated for 'interconnected'.

the separation of 1,4-dioxane and morpholine by **BINAP**. As discussed in the previous chapters, the guest, which forms an inclusion compound with the highest thermal stability in term of T_{on} - T_b and the most negative lattice energy, is always preferentially enclathrated by the host in the competition experiments.

In this study lattice energies were calculated and compared for the inclusion compounds of the same stoichiometries with isomeric guests. The lattice energy of an inclusion compound characterises the overall strength of the intermolecular interactions in the host-guest system and represents the overall stability of the compound. When the lattice energies differ substantially the competition results could be readily predicted. When the difference in the lattice energy values (ΔE) was small, the competition results either show selectivity is concentration dependent related to ΔE, *e.g.* separation of 3,5- and 3,4-xylidine by **DHPC** [$\Delta E_{DHPC\cdot35X\text{-}DHPC\cdot34X}$ = 8.1 kJ mol^{-1}, selectivity parameter $Q_{35X:34X}$ = 0.68], 2- and 4-picoline by **BINAP** [$\Delta E_{BINAP\cdot2(2PIC)\text{-}BINAP\cdot2(4PIC)}$ = 3.2 kJ mol^{-1}, $Q_{2PIC:4PIC}$ = 0.61], 2,6- and 2,4-lutidine by **BINAP** [$\Delta E_{BINAP\cdot2(26LUT)\text{-}BINAP\cdot2(24LUT)}$ = 1.3 kJ mol^{-1}, $Q_{26LUT:24LUT}$ = 0.50], or no selectivity, *e.g.* 3- and 4-picoline by **DHPC** [$\Delta E_{DHPC\cdot3PIC\text{-}DHPC\cdot4PIC}$ = 0.1 kJ mol^{-1}] (Caira *et al.* 1997). In these situations kinetic effects may play a part during the dynamic inclusion processes.

However the situation was different in the case of the separation of xylidines by **BINAP**, where the host:guest ratios of the host with 3,5-, 2,6- and 2,3-xylidine were 1:1, 1:2 and 1:3 respectively. Lattice energy values are dependent on the summation of atom-pair potentials, and are only comparable in cases where the stoichiometries are the same. Therefore, no lattice energy calculations were carried out for these inclusion compounds and there is also no direct correlation between the selectivity results and the thermal stabilities and results from structural analysis, as discussed in **Chapter 5**. This indicates that selective lattice inclusion is not only subject to thermodynamic and kinetic factors but is also influenced by stoichiometry. Since the stoichiometry changes with the crystallisation temperatures, further work needs to be done to carry out competition experiments at different temperatures, in order to estimate how the stoichiometry affects the selectivity.

The separation of xylidine isomers was attempted by employing both hosts **DHPC** and **BINAP**. For the 2,3-, 2,6- and 3,5-substitued isomers of xylidine, either host compound exhibits a different selectivity trend as follows:

Host **DHPC**: 3,5-xylidine ≥ 2,3-xylidine >> 2,6-xylidine

Host **BINAP**: 2,6-xylidine > 2,3-xylidine ≈ 3,5-xylidine

The observed selectivity trend in each case is almost reversed, particularly with regard to the 2,6- and 3,5-isomers. Both the host compounds possess chemically identical functionality [the hydroxyl (-OH) group]. In the host-guest systems of **DHPC** with xylidines, the steric hindrance of the methyl substituents at 2 and 6 positions around the functional $-NH_2$ group of the guest impedes the formation of hydrogen bonds. This was discussed in **Chapter 5**. However this is not the case in the host-guest systems of **BINAP** with xylidines. The (**BINAP**)O-H···N(xylidine) hydrogen bonding distance is, in fact, shorter with 2,6-xylidine than that with 3,5-xylidine [2.814(3)Å versus 2.837(2)Å]. Therefore the reverse selectivity trends might be attributed to the different molecular shapes of the host compounds. The host **DHPC** preferably forms layer type inclusion structures with xylidines, whereas the host **BINAP** preferably forms channel type inclusion structures, due to the same reasons. This implies that separation of isomers could be achieved as well as the separation efficiency could be improved by the choice of the host compound.

The kinetics of desolvation of a variety of inclusion compounds were investigated in this study. The kinetic mechanisms were established from TG experiments. All the desolvation reactions showed Arrhenius behaviour. The kinetic models and Arrhenius parameters obtained for the desolvations of selected inclusion compounds are summarised in **Table 8.2**.

The highest activation energy was obtained for the desolvation of **DHPC•0.5(23X)** [177(2) kJ mol^{-1}]. This is the only inclusion compound in this study in which the guest is located in closed cages. Among the rest of the inclusion compounds, the activation energies for those containing earth-metal salts (**MGDAME** and **CADAME**) are in the range 128(10) to 133(6) kJ mol^{-1}, while for those containing diol host the activation energies are in the range 61(6) to 108(8) kJ mol^{-1}. Apparently the desolvation energies for the former inclusion compounds of earth-metal salts are higher. This is expected since the guests in these structures are coordinated to the earth-metal ion and the desolvation of guest requires breaking of coordination bonds in addition to the hydrogen bonds, as opposed to the purely organic inclusion compounds that do not display metal-ligand coordination.

Table 8.2 Kinetic models and Arrhenius parameters for the desolvations of the inclusion compounds investigated in this study.

Inclusion Compound	Kinetic model	*ln A*	E_a (kJ mol^{-1})
MGDAME	F1	38(4)	128(10)
CADAME	R3	35.9(2)	133(6)
DHPC•35X	R2	32(2)	108(5)
DHPC•2(23X)*	N / A	N / A	64(6)-75(6)
DHPC•0.5(23X)*	F2	N / A	177(2)
BINAP•2(2PIC)	R2	25(2)	86(4)
BINAP•2(3PIC)	R2	26(2)	82(6)
BINAP•2(4PIC)	R2	25(2)	84(7)
BINAP•2(26LUT)	R2	24(1)	80(4)
BINAP•2(24LUT)	R2	27(2)	92(3)
BINAP•35LUT	A3	28(2)	101(7)
BINAP•35X	R2	29(3)	106(8)
BINAP•2(26X)	R2	24(1)	88(4)
BINAP•3(23X)	A2	35(3)	108(8)
BINAP•3.5DOX —1st step	R2	21(2)	61(6)
— 2nd step	R2	19(3)	63(8)
BINAP•1.5DOX	R2	27(1)	86(2)
BINAP•2DMSO — 1st step	R2	23(2)	79(5)
— 2nd step	R2	22(1)	85(5)
BINAP•DMSO	R2	24(1)	94(3)
BINAP•ACT	A2	28(1)	85(4)

*Their kinetics of desolvation were measured using non-isothermal TG methods, while all the others were studied using isothermal TG technique.

Deceleratory α-time curves were observed for the majority of reactions. These accounts for the first and second order mechanisms F1 and F2, and the geometrical models R2 and R3. The order of the reactions studied here does not have the same significance as in homogeneous reactions. For the R2 or R3 mechanisms, the rate-determining step is the growth of the product interface two- or three- dimensionally according to the simple cylindrical or spherical particles. The contracting area kinetic model R2 was predominantly observed for the desolvations of the inclusion compounds of the host **BINAP** (13 out of 16 structures). The structures of these inclusion

compounds are predominantly of the channel type, with the interconnected cage structure of **BINAP•DMSO** being an exception. In the channel type structures there is no sturdy physical barrier to the diffusion of guest out of the host framework. Sigmoidal α-time curves were obtained for the desolvations of three of the inclusion compounds of the host **BINAP**. The desolvation reactions followed the Avrami-Erofe'ev kinetic mechanisms (A2 and A3). Both A2 and A3 rate laws are derived to account for mechanisms dominated by growth of nuclei of the product phase.

As pointed out in **Chapter 1**, one has to be cautious when attempting to interpret the kinetic rate law followed by a reaction (Bamford and Tipper, 1980). Since thermogravimetry measures only the mass loss of gaseous guest products, the concomitant thermal events, *e.g.* phase changes, occur upon guest loss were not taken into account. The seemingly simple α-time curve, from which the rate law was derived and mechanism inferred, may not reflect the true mechanism of desolvation at a molecular level. Further work will need to be done for the kinetic identification of kinetic models using more powerful microscopy other than hot stage microscopy. A larger database of desolvation kinetic parameters will have to be built in order to draw conclusive correlations between kinetic models, the topologies of inclusion and magnitudes of activation energies.

When $ln\ A$ is plotted against E_a for those inclusion compounds containing the same host **BINAP**, an approximate linear relationship between the two Arrhenius parameters is observed, as shown in **Figure 8.1**. This phenomenon is the so-called kinetic compensation effect. Generally it occurs in a group of related reactions, for which the influence of changes in A on reaction rate is accompanied by a change in E_a:

$$ln\ A = BE_a + C$$

where B and C are constants (Zsako *et al.* 1975; Galway, 1977).

The compensation effect has been observed for both heterogeneous and homogeneous reactions (Brown *et al.* 1980). No satisfactory theoretical interpretations have yet been made for this phenomenon (Agrawal, 1989; Koga and Šesták, 1991). However, Zsako *et al.* (1975) have suggested that, the constant B may characterise the strength of the bond to be broken, and C be related to the structure of, and defects in, the starting reactant. Coetzee (1996) has also observed this phenomenon for a number of groups of related inclusion compounds. These inclusion compounds comprise the same host compounds. Their structures were mainly stabilised by hydrogen bonds formed between host and guest. In each case guest desolvation was accompanied by a rearrangement of the host crystalline network. The existence of the compensation

effect confirms that the desolvation reactions were similar with respect to the same type of bonds being broken and the same kind of conformational changes that occur.

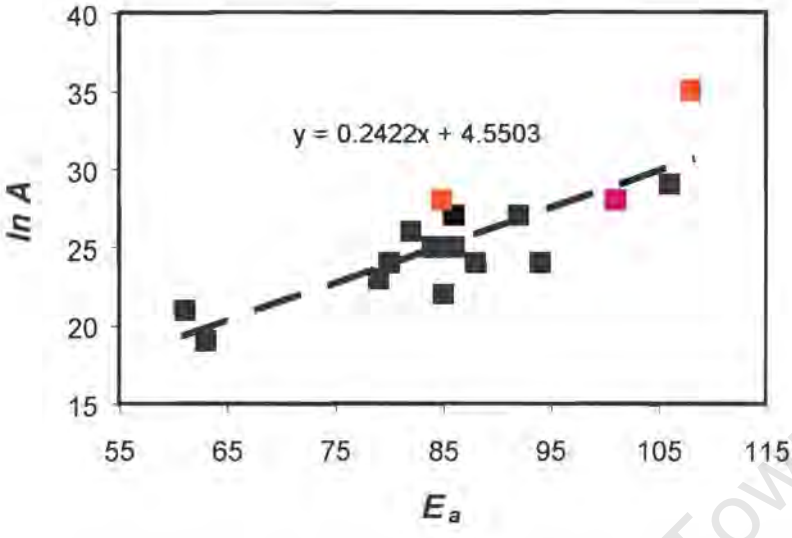

Figure 8.1 Compensation behaviour for the sixteen desolvation reactions of the inclusion compounds of the host **BINAP**. The black square points are for desolvation reactions that followed the kinetic model R2, the orange points are for model A2 and the pink is for model A3.

References for Chapters 2 – 8

Agrawal, R. K. (1989). *J. Therm. Anal.*, 35, 909.

Allen, F. H., Kennard, O., Watson, D. G., Brammer, L., Orpen, A. G. and Taylor, R. (1992). International Tables For Crystallography, Vol. C, edited by Wilson, A. J. C., Kluwer Academic publishers, Dordrecht.

Anwar, J., Tarling, S. E. and Barnes, P. (1989). *J. Pharmaceutical Sciences*, Vol. 78, No. 4, 337-342.

Avrami, A. (1939). J. Cem. Phys., 7, 1103.

Badger, R. M. and Bauer, S. H. (1937). *J. Chem. Phys.*, 5, 839.

Barbour, L. J. (1994). KINETIC programme, PhD thesis, University of Cape Town.

Barbour, L. J. (1999a). X-seed, a graphical interface for the SHELX program, University of Missouri-Columbia, USA.

Barbour, L. J. (1999b). Layer, a computer program for the graphic display of intensity data as simulated procession photographs, *J. Appl. Cryst.* 32, 351.

Barbour, L. J. (1999c). Section, a computer program for the graphic display of cross sections through a unit cell, *J. Appl. Cryst.* 32, 353.

Barmford, C. H. and Tipper, C. F. H. (eds) (1980). 'Compreshensive Chemical Kinetics', Vol. 22, Elsevier, Aqmsterdam.

Borchardt, H. J. and Daniels, F. (1957). *J. Am. Chem. Soc.*, 79, 41.

Bourne, S., Kilkenny, M. L. and Nassimbeni, L. R. (2001). *J. Chem. Soc.*, Dalton Transactions, 1176.

Brown, D. W., Floyd, A. J. and Sainsbury, M. (1998). 'Organic Spectroscopy', John Wiley & Sons, Chapter 3.

Brown, M. E. (1988). 'Introduction to Thermal Analysis - Techniques and Applications', Chapter 13, Chapman and Hall, London.

Brown, M. E. (1997). *J. Chem. Anal.* 49, 17.

Brown, M. E., Dollimore, D. and Galwey, A. K. (1980). 'Comprehensive Chemical Kinetics', Vol. 22, 'Reaction In The Solid State', Elsevier, Amsterdam.

Byrn, S. R., Pfeiffer R. R. and Stowell, J. G. (1999). 'Solid-state Chemistry of Drugs', 2nd Ed, SSCI, West Lafayette, Chapter 21.

Caira, M. R., Horne, A., Nassimbeni, L. R. and Toda, F. (1997). *J. Mater. Chem.*, 7, 2145-2149.

Caira, M. R., Horne, A., Nassimbeni, L. R. and Toda, F. (1998). *Supermol. Chem.*, 9, 231.

Caira, M. R., Nassimbeni, L. R. (1996) 'Comprehensive Supramolecular Chemistry', Vol. 6, 'Solid-state Supramolecular Chemistry: Crystal Engineering', Volume editor: MacNicol, D. D., Toda, F. and Bishop, R., Chapter 25.

Caira, M. R., Nassimbeni, L. R., Toda, F. and Vujovic, D. (1999b). *J. Chem. Soc. Perkin Trans* 2, 2681.

Caira, M. R., Nassimbeni, L. R., Toda, F. and Vujovic, D. (2000). *J. Phys. Org. Chem.*, Vol.13, 75.

Caira, M. R., Nassimbeni, L. R., Vujovic, D., Weber, E. and Wierig, A. (1999a). *Structural Chem.*, 10, 205.

Charles J. Pouchert (1990). The Aldrich Library of Infrared Spectra, 3rd Ed., Aldrich Chemical Company, Inc.

Coetzee, A. (1996). PhD thesis, University of Cape Town.

COLLECT, data collection software, Nonius, Delft, Netherlands, 1999.

ConQuest, a program for search CSD, version 1.3, © CCDC 2001.

Cremer, D. and Pople, J. A. (1975). *J. Am. Chem. Soc.*, 97, 1354.

CSD (2001), the Cambridge Structural Database System, Version 5.22, the Cambridge Crystallographic Data Centre, University Chemical Laboratory, Cambridge, England.

DELTA: Delta chromatography Data System for Windows, Version 5.0, © 1995-1998.

Duax, W. L. and Norton, D. A. (1975). 'Altas of Steroid Structure', Vol.1, Editor: Norton, D. A., Plenum Press, London.

Erofe'ev, B. V. and Dokl, C. R. (1946). Acad. Sci. URSS, 52, 551.

Flynn, J. H. and Wall, L. A. (1966). *Polym. Lett.*, 4, 323.

Galway, A. K. (1977). *Catal. Rev.*, 26, 247.

Galway, A. K. and Brown, M. E. (1998). 'Handbook of Thermal Analysis and Calorimetry', Vol. 1, Elsevier, Amsterdam, Chapter 3.

Gavezotti, A. (1983). *J. Am. Chem. Soc.*, 16, 105.

Gavezzotti, A. (1998). *Cryst. Rev.* 7, 5-21.

Gordon, A. J. and Ford, R A. (1972). 'A Chemist's Companion', John Wiley & Sons, New York.

Gridunova, G. V., Furmanova, N. G., Shklover, V. E., Struchkov, T. Yu and Ezhkova, Z. I. (1982). *Kristallografiya*, 27, 477-484.

Ibragimov, B. (1999). *J. Incl. Phenom. And Macrocyclic Chemistry,* 34, 345-353.

Koga, N. and Šesták, J. (1991). *Thermochim. Acta*, 182, 201.

Lindoy, L. F. and Atkinson, I. M. (2000), 'Self-Assembly in Supramolecular Systems', Series Editor: Fraser Stoddart, J., Royal Society of Chemistry, Cambridge University Press, Cambridge, UK.

Makhkamov, K., Ibragimov, B. T., Weber, E. and Beketov, K. M. (1999). *J. Phys. Org. chem.* 12, 157-164.

McGreal, M. E., Niederl, V. and Niederl, J. B. (1939). *J. Am. Chem. Soc.*, 61, 345.

Mori, K., Masuda, Y. and Kashino, S. (1993). *Acta Cryst. C*, 49, 1224-1227.

Mravik, Z. Bocskei, Z. Katona, Imre Markovits and Elemer Fogassy. (1997). *Angew. Chem. Int. Ed. Engl.*, 36, 1534.

Nash-Gifford, K. (1998). PhD thesis, University of Cape Town.

Nieger, M. (1999). REFCODE BIRKOCO3 in CSD (version 5.22). Private communication, contribution from Department of Inorganic Chemistry, University of Bonn, Germany.

Olovsson, I. and Jönsson, P. (1975). 'The Hydrogen Bonds - Structure and Spectroscopy', Editor: Schuster, P., Zundel, G. and Sarderfy, C., North-Holland Publishing Company, USA.

Otwinowski, Z. and Minor, W. (1997). 'Methods in Enzymology, Macromolecular Crystallography', Part A, 307-326, Vol. 276, Editor: Carter, C. W. Jr and Sweet, R. M., Academic Press.

P. W. Atkins, Physical Chemistry, 6th Ed. Oxford University Press, Oxford, 1998, p485.

Pivotar, A. M., Holman, K. T. and Ward, M. D. (2001). *Chem. Mater.*, 13, 3018.

PovRay for Windows, Version 3.1e. watcom.win32, the persistence of vision development team, © 1991 - 1999.

Sheldrick, G. M. (1985). SHELX-86: Crystallographic Computing, Vol. 3, Editor: Sheldrick, G. M., Kruger, C. and Goddard, R., Oxford University Press, Oxford, UK.

Sheldrick, G. M. (1997). SHELX-97: Program for Crystal Structure Determination. University of Göttingen, Germany.

Soft Imaging System GmbH: Digital Solutions for Imaging and Microscopy, Version 3.1 for Windows.

Spek, A. L. (1990). PLATON, a multipurpose crystallographic tool, Acta Cryst., A46, C-34. Vol. 2.

Toda, F., Tanaka, K., Miyamoto, H., Koshima, H., Miyahara, I. and Hirotsu, K. (1997). *J. Chem. Soc. Perkin Trans. 2*, 1877-1885.

Toyota, S., Sawa, H., Asakura, M., Hirano, S. and Toda, F. (2001). *Crsyt. Eng. Comm*, 7.

Vedani, A. and Dunitz, J. D. (1985). *J. Am. Chem. Soc.* 107, 7653-7658.

Williams, D. E. (1999). MPA: Molecular Packing Analysis, Version 2. Department of Chemistry, University of Louisville, Louisville, KY 40292.

XPrep, Data Preparation & Reciprocal Space Group Exploration, version 5.1/NT, ©1997, Bruker Analytical X-ray Systems.

Yvon, K., Jeitschko, W. and Parthe, E. (1977). *J. Appl. Cryst.*, 10, 73.

Zsako, J., Varhelyi, Cs. and Szilagyi, K. (1975). *J. Therm. Anal.*, 7, 41.

Appendices

Supplementary materials can be found on the CD-ROM attached. Three files are included for each of the structure elucidated in this thesis, namely:

- **Filename.SFT**: This file contains tables of observed and calculated structure factors as F_o and F_c.
- **Filename.TEX**: This file contains tables of crystal data and structure refinement, atomic coordinates, isotropic and anisotropic displacement parameters, bond lengths and angles, torsion angles and hydrogen bonding details.
- **Filename.CIF**: This file is the Crystallographic Information File. It can be used for visualising molecular structure and packing features through appropriate programmes, *e.g.* X-Seed, Platon, Ortep etc.

All the files are text files and can be viewed in an editor, under any of the following operating systems:
DOS
WINDOWS 3.1
WINDOWS 95
OS/2
APPLE MAC
UNIX
VMS
Linux

For each structure, the **.SFT**, **.TEX** and **.CIF** files were grouped into a subdirectory bearing the same name as the filename. The filename for each structure is not the same as the compound code name used in the text. The subdirectory names (or filenames) for all the structures described in this thesis are given in **Table A**.

Table A Subdirectory names and filenames used in the attached CD-ROM for the crystal structures studied in this thesis.

Structures	Host	Guest	H:G	Subdirectory / File name
MGDAME	**DBTAM (M = Mg)**	2-Methoxyethanol /Ethanol/H_2O	1:1:1:1	**MGDAME**
CADAME	**DBTAM (M = Ca)**	2-Methoxyethanol /H_2O	1:2:1	**CADAME**
SRDAME	**DBTAM (M = Sr)**	2-Methoxyethanol /H_2O	1:2:1	**SRDAME**
DHPC•26X	**DHPC**	2,6-Xylidine	1:1	**DC26X**
DHPC•1.5(26X)	**DHPC**	2,6-Xylidine	1:1.5	**DC1526X**
DHPC•2.5(26X)	**DHPC**	2,6-Xylidine	1:2.5	**DC2526X**
DHPC•3(26X)	**DHPC**	2,6-Xylidine	1:3	**DC326X**
DHPC•0.5(23X)	**DHPC**	2,3-Xylidine	1:0.5	**DC0523X**
DHPC•2(23X)	**DHPC**	2,3-Xylidine	1:2	**DC223X**
DHPC•0.5(34X)•H_2O	**DHPC**	3,4-Xylidine/H_2O	1:0.5:1	**DC0534X**
DHPC•34X	**DHPC**	3,4-Xylidine	1:1	**DC34X**
DHPC•35X	**DHPC**	3,5-Xylidine	1:1	**DC35X**
BINAP•2(2PIC)	**BINAP**	2-Picoline	1:2	**BP2PIC**
BINAP•2(3PIC)	**BINAP**	3-Picoline	1:2	**BP3PIC**
BINAP•2(4PIC)	**BINAP**	4-Picoline	1:2	**BP4PIC**
BINAP•2(26LUT)	**BINAP**	2,6-Lutidine	1:2	**BP26LUT**
BINAP•2(24LUT)	**BINAP**	2,4-Lutidine	1:2	**BP24LUT**
BINAP•35LUT	**BINAP**	3,5-Lutidine	1:1	**BP35LUT**
BINAP•35X	**BINAP**	3,5-xylidine	1:1	**BP35X**
BINAP•2(26X)	**BINAP**	2,6-xylidine	1:2	**BP26X**
BINAP•3(23X)	**BINAP**	2,3-xylidine	1:3	**BP23X**
BINAP•1.5DOX	**BINAP**	1,4-Dioxane	1:1.5	**BP15DOX**
BINAP•3.5DOX	**BINAP**	1,4-Dioxane	1:3.5	**BP35DOX**
BINAP•DMSO	**BINAP**	DMSO	1:1	**BPDMSO**
BINAP•2DMSO	**BINAP**	DMSO	1:2	**BP2DMSO**
BINAP•1.5(MOP)(I)	**BINAP**	Morpholine	1:1.5	**BPMOP1**
BINAP•1.5(MOP)(II)	**BINAP**	Morpholine	1:1.5	**BPMOP2**
BINAP•1.5(THF)	**BINAP**	THF	1:1.5	**BP15THF**
BINAP•ACT	**BINAP**	Acetone	1:1	**BPACT**
BINAP	-	-	-	**BINAP**